BioMed Research International

New Paradigms in Orthodontics

Lead Guest Editor: Mohammad Khursheed Alam
Guest Editors: Shivam Mehta and Nafij Bin Jamayet

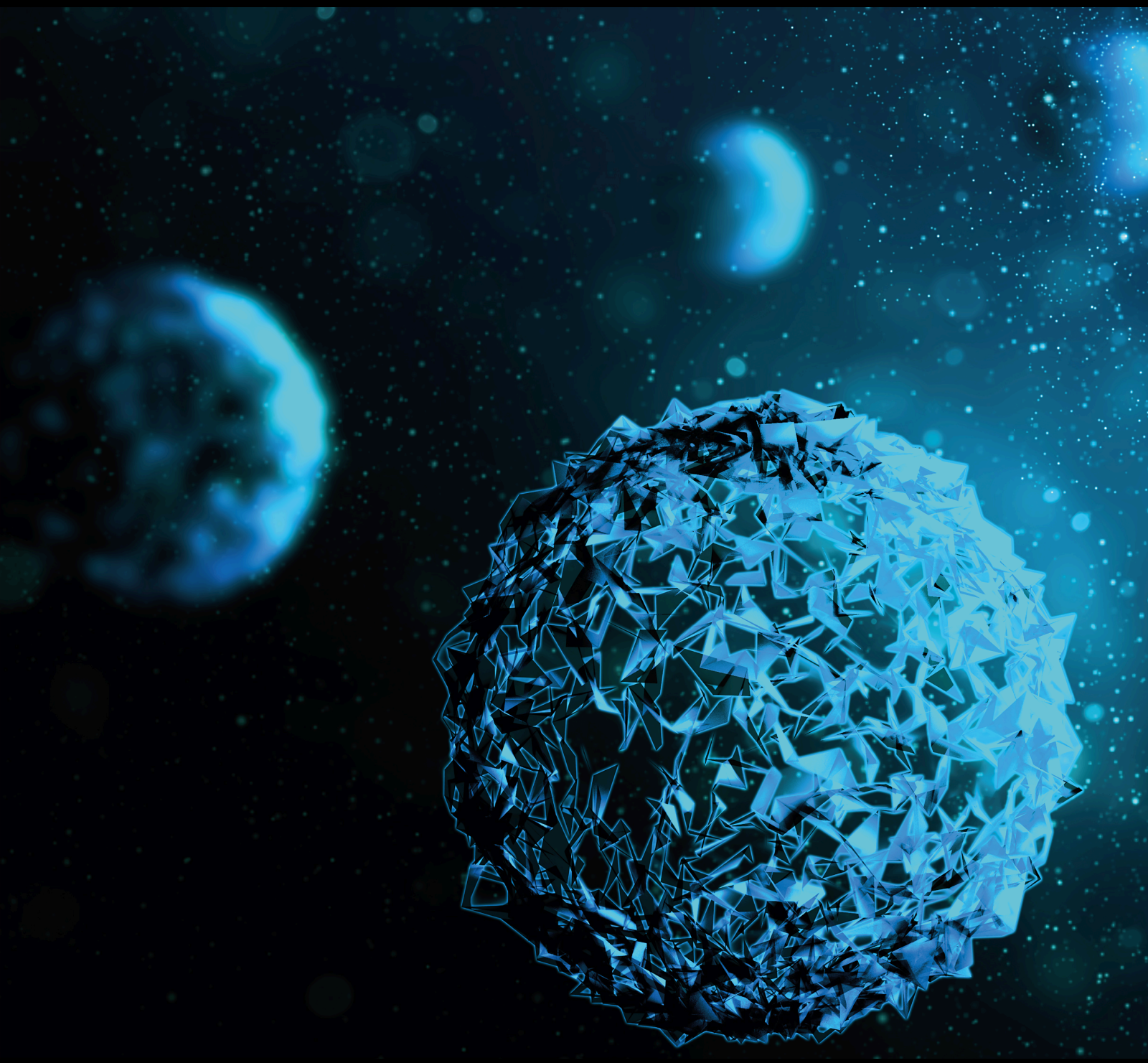

New Paradigms in Orthodontics

BioMed Research International

New Paradigms in Orthodontics

Lead Guest Editor: Mohammad Khursheed Alam
Guest Editors: Shivam Mehta and Nafij Bin Jamayet

Section Editors

Penny A. Asbell, USA
David Bernardo, Spain
Gerald Brandacher, USA
Kim Bridle, Australia
Laura Chronopoulou, Italy
Gerald A. Colvin, USA
Aaron S. Dumont, USA
Pierfrancesco Franco, Italy
Raj P. Kandpal, USA
Fabrizio Montecucco, Italy
Mangesh S. Pednekar, India
Letterio S. Politi, USA
Jinsong Ren, China
William B. Rodgers, USA
Harry W. Schroeder, USA
Andrea Scribante, Italy
Germán Vicente-Rodriguez, Spain
Momiao Xiong, USA
Hui Zhang, China

Academic Editors

Dentistry

Ali I. Abdalla, Egypt
Carlos M. Ardila, Colombia
Nicola Cirillo, Australia
Fernanda Faot, Brazil
Luca Fiorillo, Italy
Flavia Gonçalves, Brazil
Vincenzo Grassia, Italy
Yeliz Guven, Turkey
Heng Bo Jiang, China
Saber Khazaei, Iran
H. Y. Kim, USA
Carlo Medina-Solis, Mexico
Nenad Mitrović, Serbia
Pablo G. Moreno, Spain
Piero Papi, Italy
Romeo Patini, Italy
Giorgio Pompa, Italy
Joao Paulo Mendes Tribst, The Netherlands
Giuseppe Varvara, Italy
Li Wu Zheng, Hong Kong

Contents

Hindawi
BioMed Research International
Volume 2022, Article ID 4714347, 33 pages
https://doi.org/10.1155/2022/4714347

Research Article

Effects of Rigid and Nonrigid Connections between the Miniscrew and Anchorage Tooth on Dynamics, Efficacy, and Adverse Effects of Maxillary Second Molar Protraction: A Finite Element Analysis

Marzieh Mazhari[1], **Mehrnaz Moradinejad**[1], **Mohsen Mazhary**[2], **Atefe Rekabi**[1] and **Vahid Rakhshan**[3]

[1]*Department of Orthodontics, School of Dentistry, Ahvaz Jundishapur University of Medical Sciences, Ahvaz, Iran*
[2]*Department of Civil and Environmental Engineering, ACECR Institute for Higher Education, Ahvaz, Iran*
[3]*Department of Anatomy, Dental School, Azad University of Medical Sciences, Tehran, Iran*

Correspondence should be addressed to Atefe Rekabi; rekabi.at72@gmail.com

Received 22 January 2022; Revised 18 September 2022; Accepted 26 September 2022; Published 14 October 2022

Academic Editor: Shivam Mehta

Introduction. Direct, rigid indirect, and nonrigid indirect absolute anchorages using temporary anchorage devices (TADs, mini-implants/miniscrews) can provide promising opportunities for challenging, yet common, orthodontic tooth movements such as molar protraction. Rigid rectangular wire and ligature wire are the most common methods of attaching a tooth to a miniscrew in indirect anchorages. We aimed to provide a comparison of the rigidity of the connecting wire in terms of stress on the miniscrew, the anchorage loss, and the risk of root resorption using finite element analysis (FEA). *Methods*. The maxillary right second molar was protracted into the proximal space at a 150 g load (1) using direct absolute anchorage with a tapered miniscrew implanted between the premolar roots and using indirect absolute anchorage with the second premolar reinforced by the miniscrew through (2) a rigid stainless steel (SS) wire or (3) a nonrigid SS ligature wire (4) at different elastic moduli. Stresses and displacements of 4 models' elements were measured. The risk of external root resorption was evaluated. *Results*. Connecting the tooth to the miniscrew using rigid full-size wire (model 2) compared to ligature (model 3) can give better control of the anchorage (using the ligature wire, the anchorage loss is 1.5 times larger than the rectangular wire) and may reduce the risk of root resorption of the anchorage unit. However, the risk of miniscrew failure increases with a rigid connection, although it is still lower than with direct anchorage. The miniscrew stress when using a ligature is approximately 30% of the rigid model using the rectangular wire. The miniscrew stress using the rectangular wire is approximately 82.4% of the miniscrew stress in the direct model. Parametric analysis shows that the higher the elastic modulus of the miniscrew-tooth connecting wire in the indirect anchorage, the less the anchorage loss/palatal rotation of the premolars/and the risk of root resorption of the anchorage teeth and instead the stress on the miniscrew increases. *Conclusions*. Direct anchorage (followed by rigid indirect anchorage but not nonrigid) might be recommended when the premolars should not be moved or premolar root resorption is a concern. Miniscrew loosening risk might be the highest in direct anchorage and lowest in nonrigid indirect anchorage (which might be recommended for poor bone densities).

1. Introduction

In orthodontics, the first permanent molar is the key to occlusion [1]. This tooth appears in the mouth at the age of 6 and is claimed to be the most commonly missing tooth in adults [2]. Losing this tooth will cause numerous problems such as the disruption of arch symmetry, drifting of the neighboring teeth into its space, malocclusion, and temporomandibular joint problems [3]. There are several solutions to restore the function of this missing tooth,

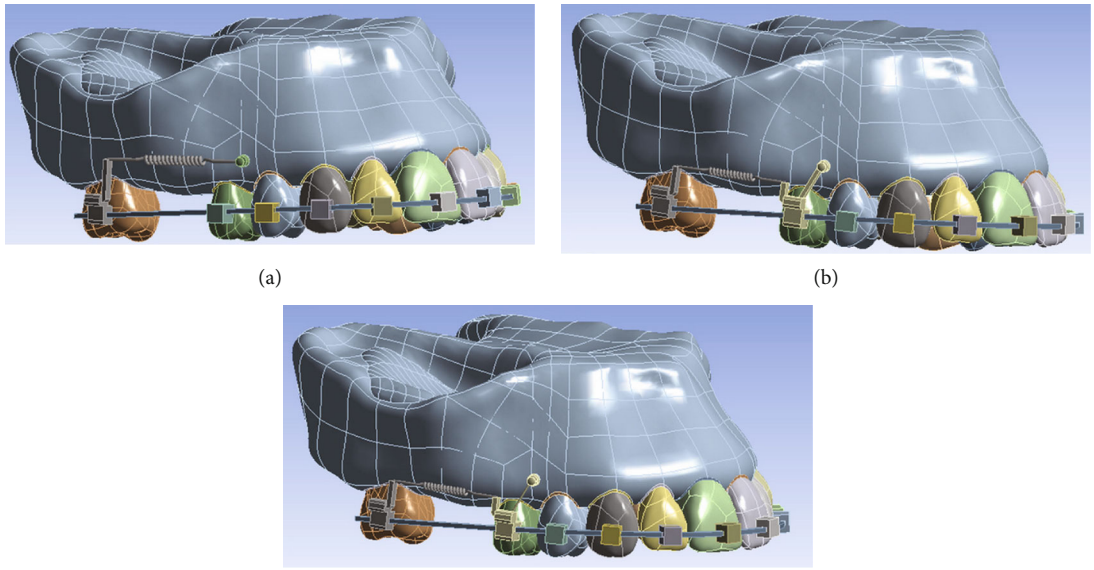

(a) (b)

(c)

Figure 1: The three different models used in this study: (a) model 1 with direct anchorage; (b) model 2 with rigid indirect anchorage; (c) model 3 with nonrigid indirect anchorage.

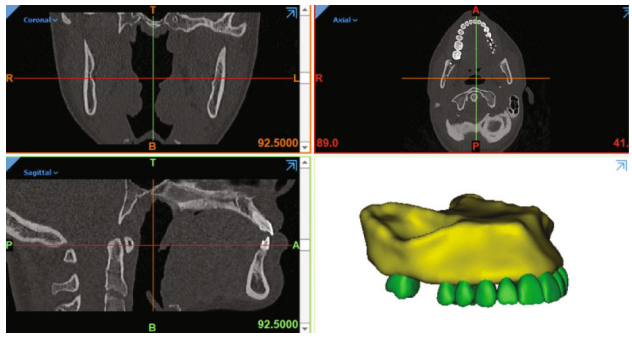

Figure 2: Creating the 3D model of the maxilla.

including fixed partial dentures, dental implants, or orthodontic replacement with a second molar if sufficient anchorage is available [4]. Molar protraction and proper anchorage may be needed also in other clinical conditions such as the unforeseen residual space after aligning the teeth, the congenital missing of the second premolars, and the extraction of hopeless teeth [5]. Therefore, various techniques have been proposed for obtaining proper anchorages for molar protraction.

Anchorage is a critical part and a prerequisite of orthodontic treatments [6–8]; and anchorage loss is a serious complication [9, 10]. When the anchorage unit consists of only teeth, it faces limitations and conditions similar to the movement unit and may move like an active unit under the influence of force; therefore, the orthodontist should strengthen the anchorage unit [11–13]. Different methods and appliances have been proposed for strengthening the anchorage unit, such as extraoral anchorages or cortical anchorages [5, 14, 15]. The use of nondental structures as anchorage units allows therapeutic movements or growth modifications to be performed without side effects [5]. It has been proven that implants can be a reliable and effective tool as orthodontic anchorage and have created a new pattern of anchorage called absolute anchorage [5, 16, 17]. A common form of absolute anchorages is utilizing mini-implants/miniscrews [18].

Miniscrews are gaining ever-increasing popularity among orthodontists, as their use as an anchorage unit dramatically improves the balance between the active unit and the anchorage unit, and can have significant therapeutic benefits [18]. Miniscrews can provide two types of absolute anchorage: direct anchorage and indirect anchorage. In the direct anchorage method, the force from the miniscrew is directly applied to the teeth of the active unit [19–22]. In the indirect absolute anchorage, the anchorage unit is consisted of teeth and the orthodontic force is applied from the teeth in the anchorage unit to the active unit; however, the teeth in the anchorage unit are reinforced and immobilized using a miniscrew [22–25]. In this method, the miniscrew can be placed either in the interradicular space or somewhere else such as the palate or retromolar area in the mandible, depending on the available space, the used materials, and the dynamics of orthodontic force [23]. Indirect anchorage allows the miniscrew to be placed in a variety of positions and reduces the risk of root trauma; other advantages of this type of anchorage include the use of standard orthodontic methods in the application of force, which provides reliable control over tooth movement [19, 22, 26, 27].

In the indirect absolute anchorage method, anchorage unit teeth can be fixed with rigid components such as stainless steel (SS) wires or nonrigid components such as SS ligatures [23, 28]. In the use of rigid components such as SS wires, the miniscrew can be placed in any location regardless of the direction of force, because this structure can act as a tie and strut, and there is more freedom in choosing the

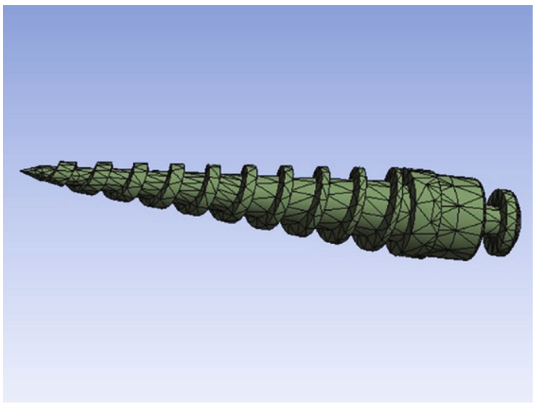

Figure 3: The miniscrew in use.

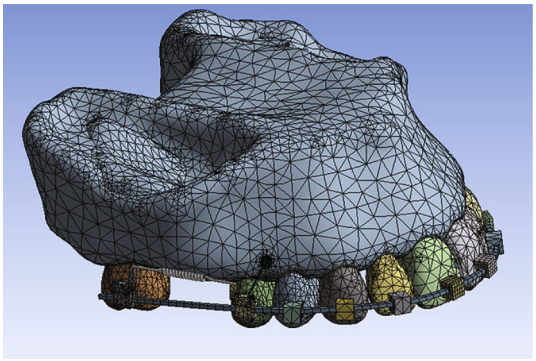

Figure 4: An example of meshing.

Table 1: Material properties.

Material	Elastic modulus (MPa)	Poisson's ratio
Cortical bone [41]	1000	0.3
Cancellous bone [41]	500	0.3
Dentine [41]	18600	0.3
PDL [42]	0.15	0.45
Stainless steel [43]	200000	0.3
Miniscrew titanium G5 [44]	115000	0.33
Ligature (dead soft wire) [45]	8500	0.3

location of the miniscrew, and hence, the operator can focus more on choosing the ideal anatomical location of the implant [23].

Failure rate of miniscrews may be rather high (about 15% to 20%) in the direct absolute anchorage method [29], but may be lower in the indirect method with lower miniscrew loads [26]. Direct anchorage can have more side effects than indirect anchorage in challenging clinical situations such as molar protraction (for example, mesial rotation during molar protraction) due to the torsional moment caused by laterally exerted force [30]. Despite numerous benefits of indirect anchorage, the risk of anchorage loss in this method is unknown [30, 31].

In spite of the increasing use of miniscrews, there is still insufficient knowledge about the optimal placement patterns, safety, and mini-implant anchorage characteristics in relation to the surrounding bone. This lack of information can lead to a high failure rate of this device and be a major deterrent to their use [31]. There are different methods for molar protraction using interradicular miniscrews, and the use of each of these methods may lead to different results (in terms of miniscrew stability and the amount and type of tooth movement). However, the role of the type of wire connecting the miniscrew to the anchorage unit teeth in indirect anchorage has not been investigated until now.

Rigid rectangular wire or ligature wire are the most common methods of attaching a tooth to a miniscrew in indirect anchorage. Moreover, as stated above, it seems that no study has assessed the effects of rigidity of the tooth-implant connecting wire in terms of the stress exerted on the miniscrew, the amount of anchorage loss, and the risk of root resorption (which can be caused by orthodontic tooth movement [32]). Therefore, we compared the connection of the anchorage tooth with the miniscrew using the full-size rectangular rigid, with a third model (direct anchorage method) serving as the gold standard or control model. We measured the effects of the type of connector wire on the stability of the miniscrew and the movement of the anchorage unit. In this way, it is possible to choose the most appropriate technique for each clinical situation, depending on the characteristics of occlusion and bone quality.

2. Materials and Methods

This was a 4-phase experimental in silico simulation study. The model designed in this study was a simulation of the clinical protraction of the right maxillary second molar into the extraction space of the right first molar. A titanium square-threaded tapered miniscrew with dimensions of 8×1.6 mm with a head length of 2 mm [4] was placed in the buccal and distal sides of the first premolar perpendicular to the bone surface.

A stainless steel (SS) archwire $0.019' \times 0.025'$ was simulated as the base archwire in all models. The connection between the miniscrew and the bone was defined as a tight tie in all models. A protractive force of 150 g was applied within each model. The spring type used in this study was SS closed-coil [33] with wire diameter, lumen size, initial length range, estimated stiffness of 0.010 (inch), 0.030 (inch), 4-10 (mm), and 1 (N/Sq·mm), respectively.

2.1. Study Models. Based on the above model, four models (three main models and one extension) were prepared with some differences (Figure 1).

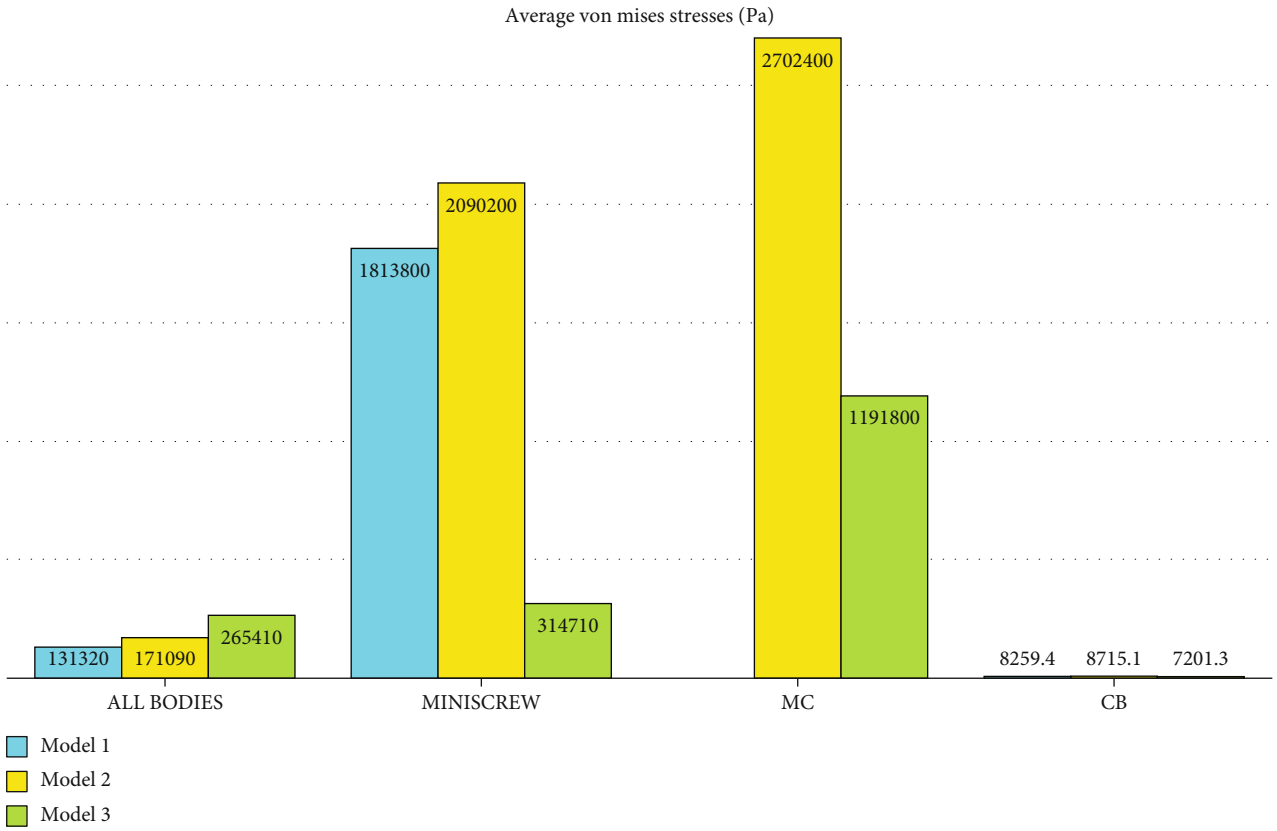

Figure 5: Average stresses exerted to different components in different models. MC: miniscrew+connections; CB: cancellous bone. Model 1 has direct anchorage; model 2 has rigid indirect anchorage; model 3 has nonrigid indirect anchorage.

2.1.1. Model 1 (Direct Absolute Anchorage). Model 1 is the model with direct connection between the second molar and the miniscrew using a spring between the power arm of the molar tooth and the mini screw.

2.1.2. Model 2 (Rigid Indirect Absolute Anchorage). In this model, a spring was used to connect the second molar to the second premolar; using a rectangular $0.021' \times 0.025'$ stainless steel (SS) wire, the second premolar was engaged with the miniscrew (rigid connection).

2.1.3. Model 3 (Nonrigid Indirect Absolute Anchorage). In this model, again a spring was used to connect the second molar to the second premolar; however, the second premolar was engaged with the miniscrew using a 0.5 mm SS ligature wire as the nonrigid connection (which had a smaller elastic modulus and yield stress compared to the SS rectangular wire used in model 2). In the direct anchorage model (model 1), a force of 150 g [4] was applied parallel with the occlusal plane using a spring between the center of the miniscrew head and the 8 mm long SS power arm of the molar band. In the two indirect anchorage models (models 2 and 3), the second premolar and miniscrew were attached using a $0.021' \times 0.025'$ SS wire (in the rigid indirect model [model 2]) and a 0.5 mm SS ligature (in the nonrigid indirect model [model 3]). In both the indirect models, a protraction force of 150 g was applied to the second molar using a spring between the molar's hook and the second premolar's hook (Figure 1).

2.1.4. Model 4 (Parametric Extensions of Model 3). Since various elastic moduli had been stated for the ligature wire in the literature [34–40], we also simulated a range of elastic moduli in model 3 and reported the effects of parametric changes in the ligature wire rigidity on stresses and displacements of model elements.

The bone, tooth, and PDL models were modeled in Mimics 3D image processing software (Mimics Research 21; Materialise NV; Brussels, Belgium) and 3-Matic (Materialise). First, 16-bit monochrome CT scan images of a young man with a distance of 1 mm between the slices and a resolution of 768×768 (NewTom VGi; Finland) were entered into Mimics. Using segmentation tools, masks for the maxilla, PDLs, teeth, and bones were created, and then a 3D model of these components was created using the Calculate 3D command (Figure 2). Then, all the parts were exported in the ".stl" format from these softwares. The miniscrews were designed with the help of Helix and Revolution commands in Solidworks software (version 2018, Dassault Systemes; Paris, France), and the brackets and orthodontic wires were designed in ANSYS software (ANSYS Workbench 2021, ANSYS Inc., Canonsburg, Pennsylvania, USA). The components were assembled together in ANSYS (Figure 3). Parts exported in the ".stl" format from Mimics and 3-Matic softwares (Materialise) in Geomagic software

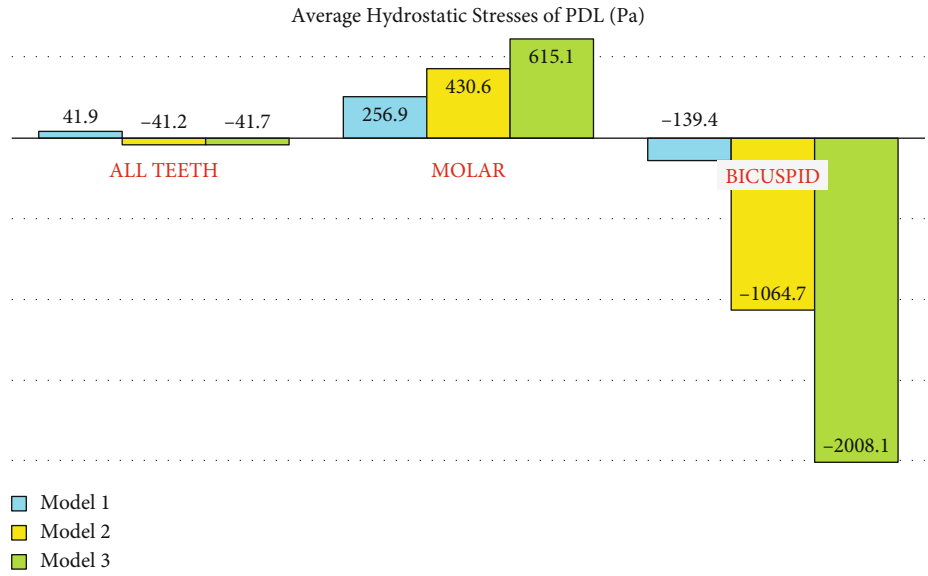

Figure 6: Average hydrostatic pressures exerted to the PDLs in different models. Positive values are tensile stresses, and negative values are compressive pressures. Model 1 has direct anchorage; model 2 has rigid indirect anchorage; model 3 has nonrigid indirect anchorage.

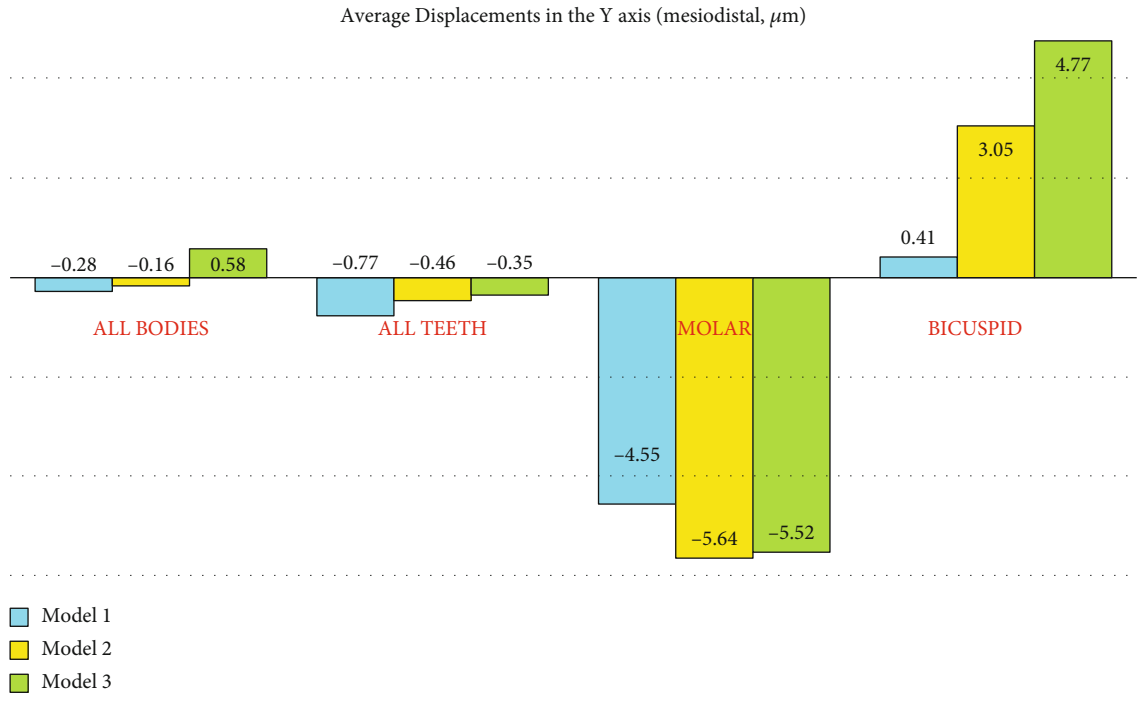

Figure 7: Average displacements in the Y-axis (the mesiodistal direction, μm) in different models. Model 1 has direct anchorage; model 2 has rigid indirect anchorage; model 3 has nonrigid indirect anchorage. Positive values indicate distalization while negative values indicate mesialization.

(3D Systems, Morrisville, North Carolina, United States) became "parts" in the ".stp" format. After converting all geometries to the ".stp" format, these geometries were entered into Ansys Workbench 2021 (ANSYS Inc) for analysis. The maxilla was fixed at its upper surface. There were 487540 nodes, 227394 contact elements, 254167 solid elements, and 481564 total elements (Figure 4). The finite element approximation was of higher order (quadratic functions were used). Materials in the 3 models were assigned the properties in Table 1 [41–45].

2.2. Outcomes. The created and loaded models were compared in terms of von Mises stresses, hydrostatic stresses, and movements of all the involved elements. If the PDL hydrostatic pressure surpasses the capillary pressure in the area, the risk of root resorption will increase owing to the

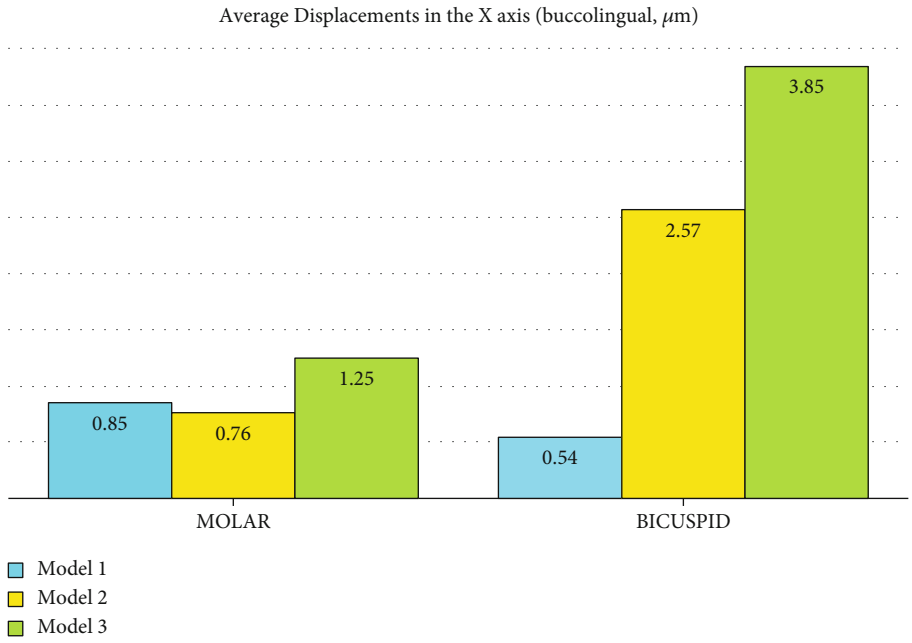

Figure 8: Average displacements in the X-axis (the buccolingual direction, μm) in different models. Model 1 has direct anchorage; model 2 has rigid indirect anchorage; model 3 has nonrigid indirect anchorage. Negative values indicate buccal movement, while positive values indicate palatalization.

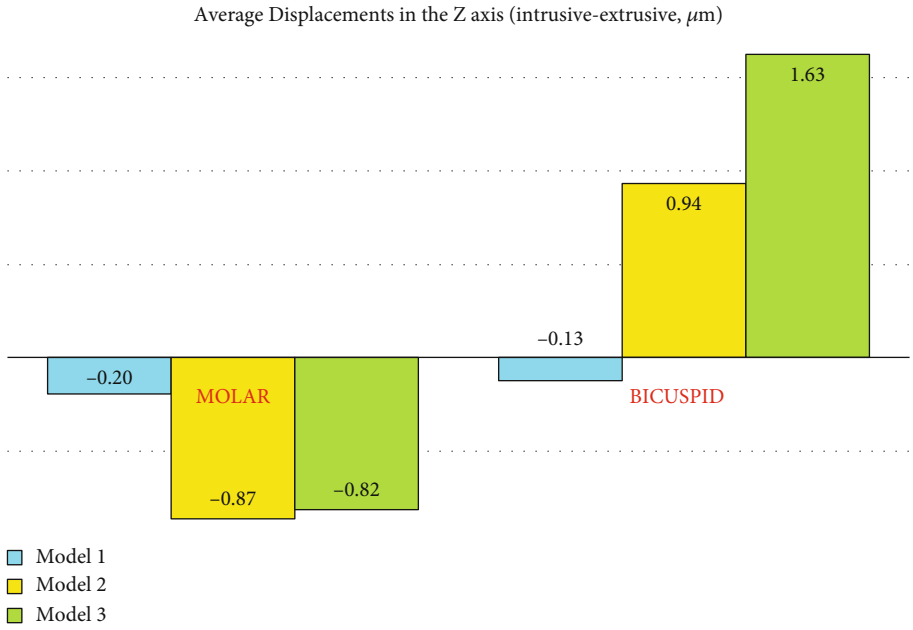

Figure 9: Average displacements in the Z-axis (the intrusive-extrusive direction, μm) in different models. Model 1 has direct anchorage; model 2 has rigid indirect anchorage; model 3 has nonrigid indirect anchorage. Positive values mean intrusive movement, while negative values mean extrusion.

impaired blood flow. PDL capillary pressure might be about 0.002 to 0.005 MPa [46]. Also, compressive hydrostatic stresses at the PDLs were compared with 0.0047 MPa as a threshold for significant increase of the risk of external root resorption [46, 47].

3. Results

3.1. Model Stresses. Overall, the stress was distributed mostly in the molar band's power arm followed by the buccal surface of the molar, around the miniscrew, and the buccal

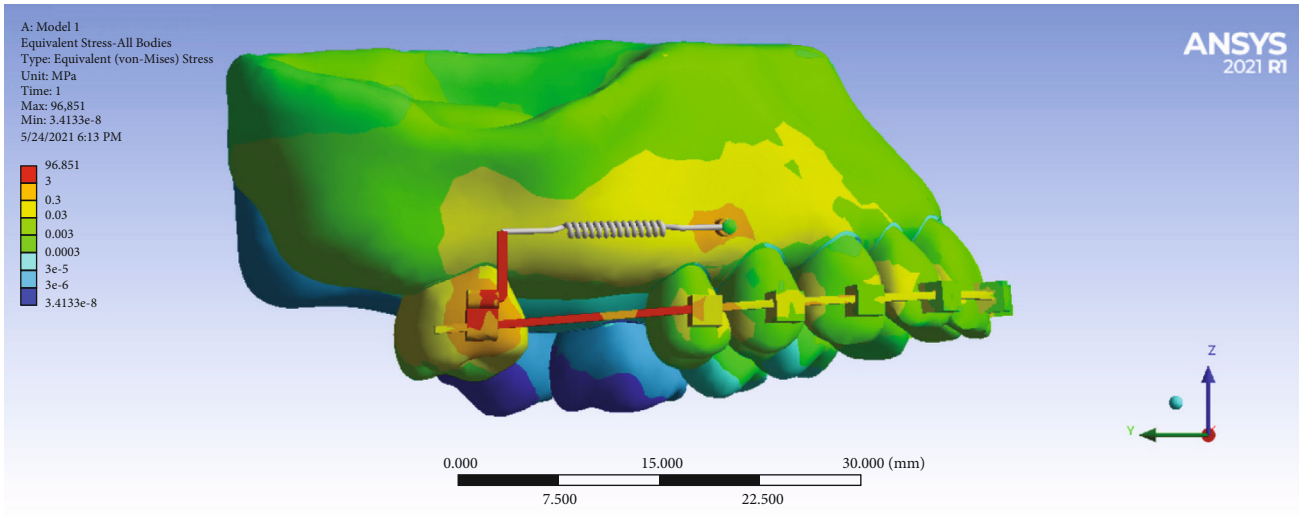

(a)

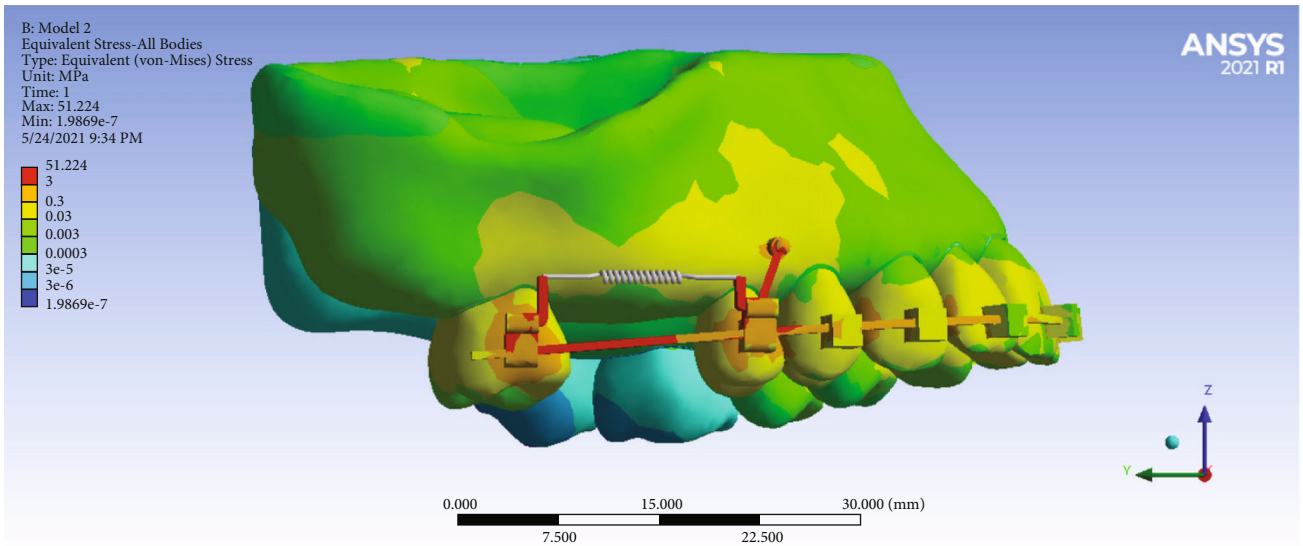

(b)

Figure 10: Continued.

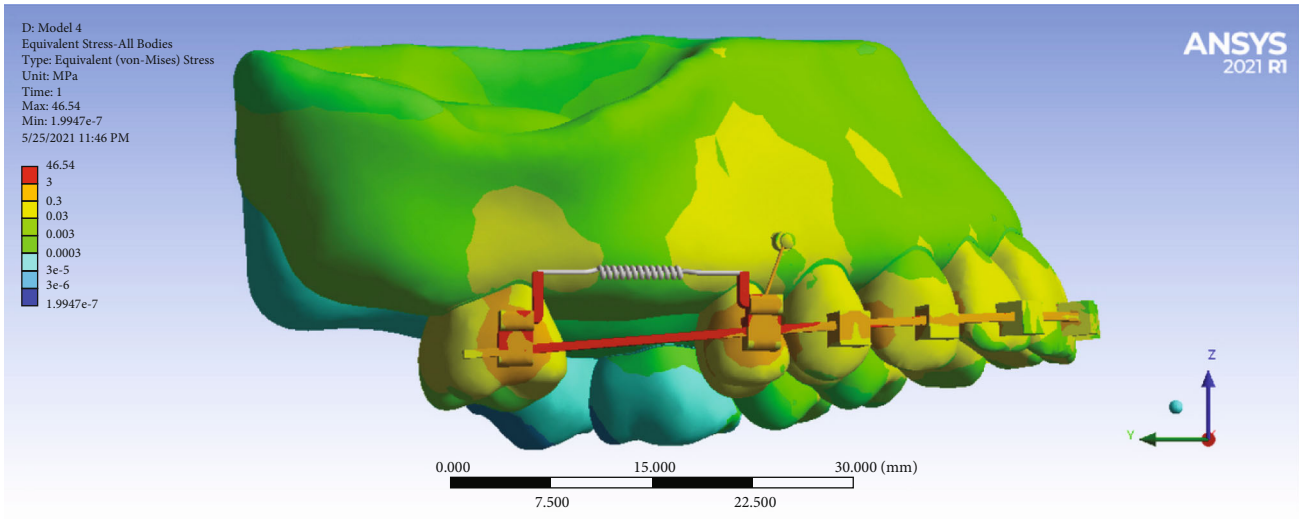

(c)

Figure 10: Stresses of the model parts in different models: (a) model 1 with direct anchorage; (b) model 2 with rigid indirect anchorage; (c) model 3 with nonrigid indirect anchorage.

Table 2: Simulation results.

Property	Scope	Model 1			Model 2			Model 3		
		Minimum	Maximum	Average	Minimum	Maximum	Average	Minimum	Maximum	Average
Von Mises stress (Pa)	All bodies	0.034133	96851000	131320	0.19869	51224000	171090	0.19947	46540000	265410
	Miniscrew	84.003	10916000	1813800	136130	32146000	2090200	3188.4	20948000	314710
	MC				36528	33983000	2702400	2129.3	39577000	1191800
	CB	1.3817	214350	8259.4	7.7935	129060	8715.1	6.921	107600	7201.3
Hydrostatic stress (Pa) of PDL	All teeth	-18550	19086	41.912	-22380	20448	-41.21	-21616	19891	-41.715
	Molar	-18550	19086	256.85	-22380	20448	430.59	-21616	19891	615.05
	Bicuspid	-1593.4	3491.4	-139.38	-8594.6	7366	-1064.7	-14919	12599	-2008.1
Displacement-Y (μm)	All bodies	-29.86	7.8788	-0.27785	-22.776	9.2276	-0.16363	-23.173	12.898	0.58086
	All teeth	-15.046	7.8788	-0.76672	-18.853	9.2276	-0.46188	-18.982	9.5846	-0.35065
	Molar	-15.046	7.8788	-4.5531	-18.853	9.2276	-5.6413	-18.982	9.5846	-5.5237
	Bicuspid	-0.047037	0.93044	0.41375	0.023664	5.7812	3.0526	-0.14605	9.1463	4.7655
Displacement-X (μm)	Molar	-8.0563	10.925	0.85247	-7.2972	11.676	0.76299	-7.0894	12.648	1.2485
	Bicuspid	-0.071982	1.1741	0.54464	0.53623	5.4207	2.5706	0.68342	8.6448	3.8454
Displacement-Z (μm)	Molar	-1.7501	1.3832	-0.19644	-3.1339	2.3739	-0.86759	-3.0095	2.1798	-0.81859
	Bicuspid	-0.47873	0.13339	-0.12516	-0.30058	1.8392	0.93506	-0.19574	3.1345	1.6291

surface of premolars and the buccal palate of the alveolar bone of the molars, premolars, and canine (Figures 5–10). The pattern of stress differed between Model 1 (direct anchorage) with Models 2 and 3 (indirect anchorages), in a way that the stress of premolars was considerably greater in the indirect anchorage models (Figures 5–10). The extents of the maximum stress were much greater in the direct anchorage model than the two indirect anchorage models (Table 2). The average stress of the whole system was greater in Model 3 followed by Models 2 and 1 (Table 2).

MC: miniscrew+connections; CB: cancellous bone.

3.2. Miniscrew Stresses. The miniscrew stress when using a ligature is approximately 30% of the rigid model using the rectangular wire. The miniscrew stress using the rectangular wire is approximately 82.4% of the miniscrew stress in the direct model. As seen in Figure 11(a), the highest amount of stress in the body of the miniscrew was created in the direct anchorage model and its magnitude was 10.916 MPa. Figure 11(b) shows the miniscrew in the rigid indirect anchorage model. The maximum stress in the body of the miniscrew in this model was 9 MPa and in the cervical half of this miniscrew. Figure 11(c) shows the miniscrew in the

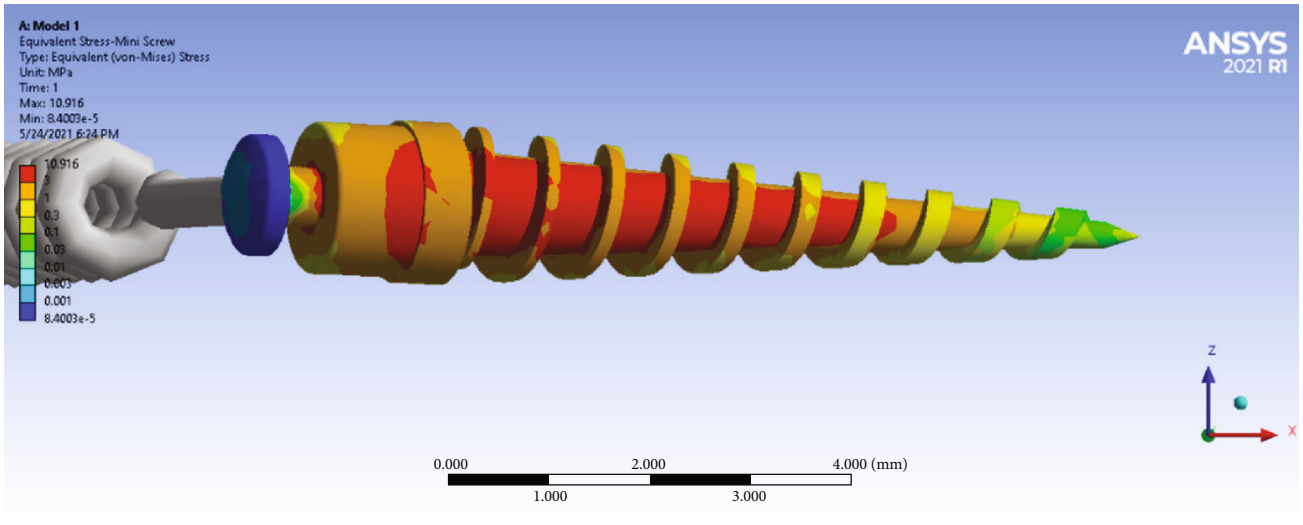

(a)

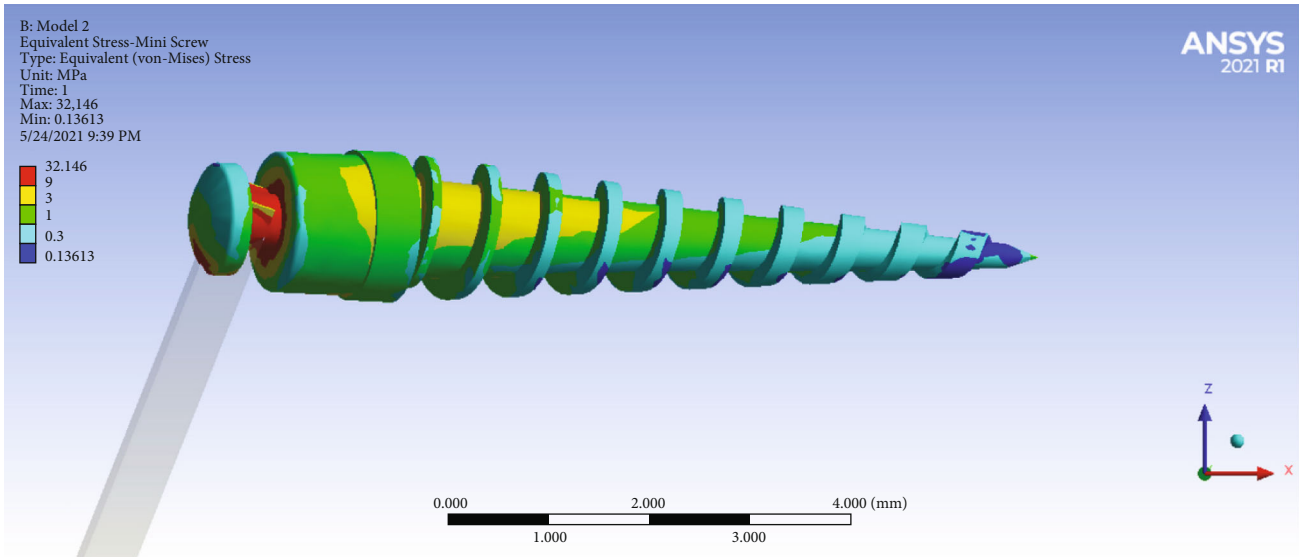

(b)

Figure 11: Continued.

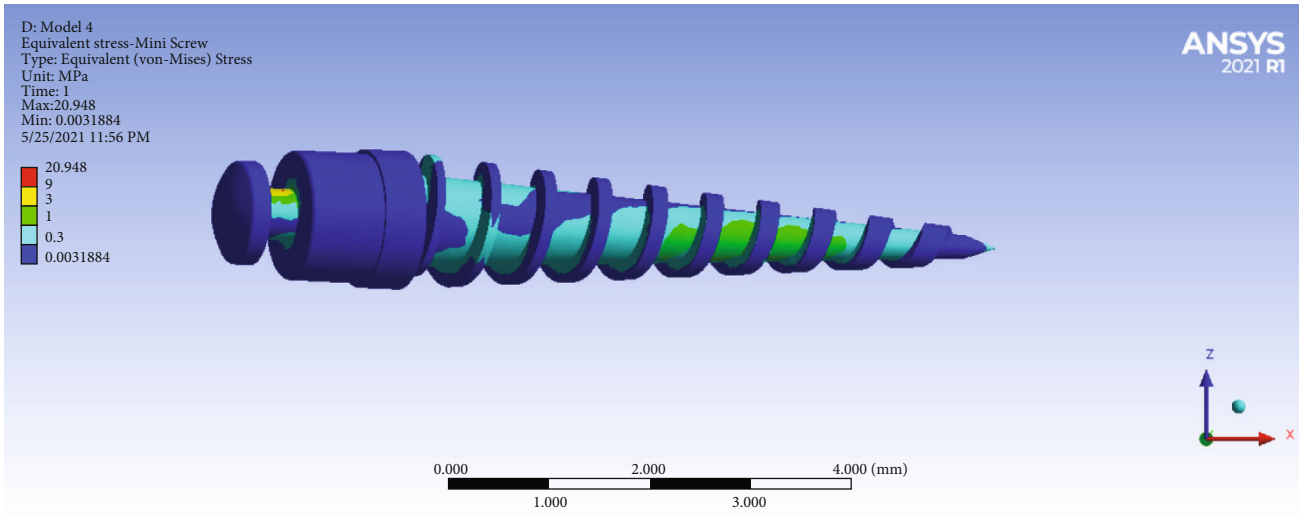

(c)

Figure 11: Stresses of the miniscrew in different models: (a) model 1 with direct anchorage; (b) model 2 with rigid indirect anchorage; (c) model 3 with nonrigid indirect anchorage.

nonrigid indirect anchorage model. The maximum stress in the body of the miniscrew in this model was 3 MPa (green color spectrum). According to the above results, the highest stress was applied to the screw in the direct anchorage model, and the lowest stress was applied in the indirect nonrigid anchorage model (Table 2).

3.3. Cancellous Bone Stresses. The stress on the spongy bone was almost halved in the rigid model (0.12906 MPa) and the nonrigid model (0.1076 MPa) compared to the direct model (0.21435 MPa). In Figure 12(a), the stress exerted to the spongy bone is shown in the direct anchorage model. At the location of the miniscrew socket, the color is red, which indicates the maximum stress created on the spongy bone (with a magnitude of 0.21435 MPa) due to the application of force. Figure 12(b) shows the stress on the spongy bone mostly around the second premolar and second molar roots in the rigid indirect anchorage model. The maximum stress reported in this model was 0.12906 MPa. Figure 12(c) shows the equivalent stress on the spongy bone in the nonrigid indirect anchorage model. The maximum stress reported in this model was 0.1076 MPa which would be observed around the second premolar and second molar roots. As can be seen from the Table 2, the highest amount of stress in the spongy bone was created in the direct anchorage model (Figure 12(a)) and was in the miniscrew hole followed by the bone surrounding the second premolar root, while the lowest amount of stress was seen in the spongy bone in the indirect nonrigid anchorage model 3 (Figure 12(c), Table 2).

3.4. Hydrostatic Pressure at the Premolar PDL. Using a ligature wire, more root resorption was observed in the anchorage unit. Figure 13(a) shows the hydrostatic stress in the PDL of the premolars in the direct anchorage model. The red color spectrum indicates the highest amount of tensile hydrostatic stress created in the PDL of cervical third of the distobuccal side of the root of the first premolar at 0.0035 MPa. The maximum tensile strength is seen over a small area close to the miniscrew and may be caused by the tension caused by the traction of miniscrew to the distal side. Figure 13(b) shows the hydrostatic stress in the PDL of premolars in the rigid indirect anchorage model. The red color spectrum in the PDL of the second premolar root indicates the maximum tensile stress created at 0.007366 MPa on the buccal side extending to the mesial side through the cervical to the apical areas. The maximum tensile hydrostatic stress was as well seen on the buccal side of the PDL of the first premolar root. Figure 13(c) shows the hydrostatic stress in the PDL of premolars in the nonrigid indirect anchorage model. Similar to the pattern of the tensile strength observed in model 2, the maximum amount of tensile stress is created at 0.012599 MPa in the root of the second premolar over the buccal and mesial sides from the cervical to the apical areas. Unlike model 2, in this model, the tensile hydrostatic stress is much less in the first premolar PDL. In the comparison of these three models, the lowest amount of tensile hydrostatic stress in the premolars was related to the direct anchorage model, while the highest hydrostatic pressure was seen in the nonrigid indirect anchorage model (0.012599 MPa). In the two indirect anchorage models, the compressive hydrostatic pressure (shown by the color blue) is seen on the distal sides of the roots, and is considerably greater in the nonrigid indirect model (model 3). In the direct anchorage model (model 1), the compressive hydrostatic pressure (blue) was observed in the mesial surface of the second premolar root, right beside the miniscrew hole, suggesting that it is the miniscrew that is exerting the compressive force over the root of the second premolar (Figure 13, Table 2).

3.5. Hydrostatic Stress in the Second Molar PDL. In the rigid model, using the rectangular wire, the maximum compressive stress was observed in the molar. The reason for the slight difference with the nonrigid model seems to be the

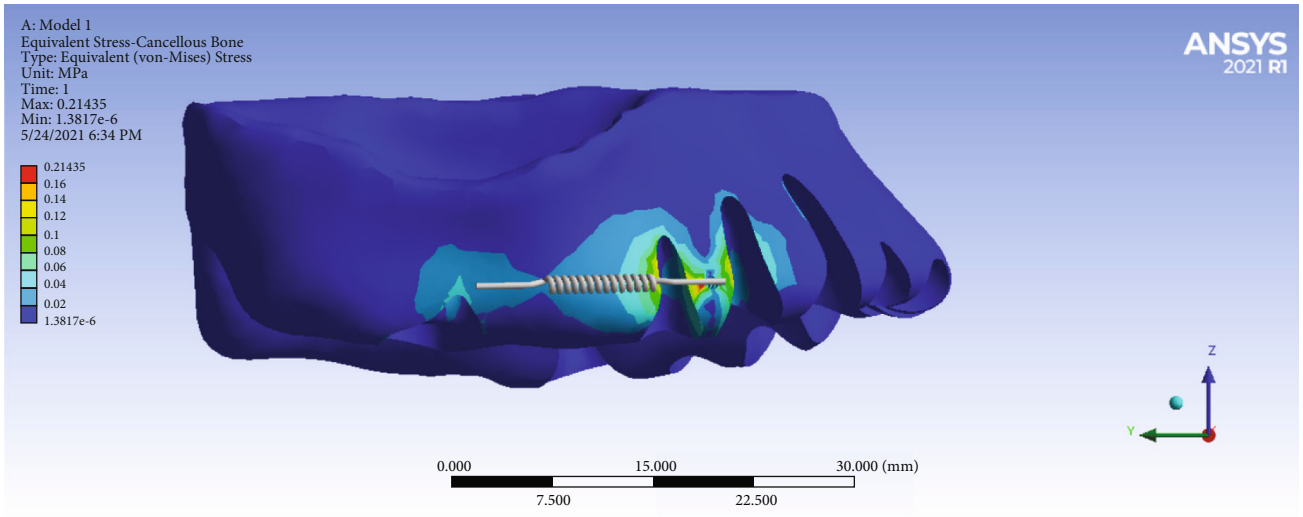

(a)

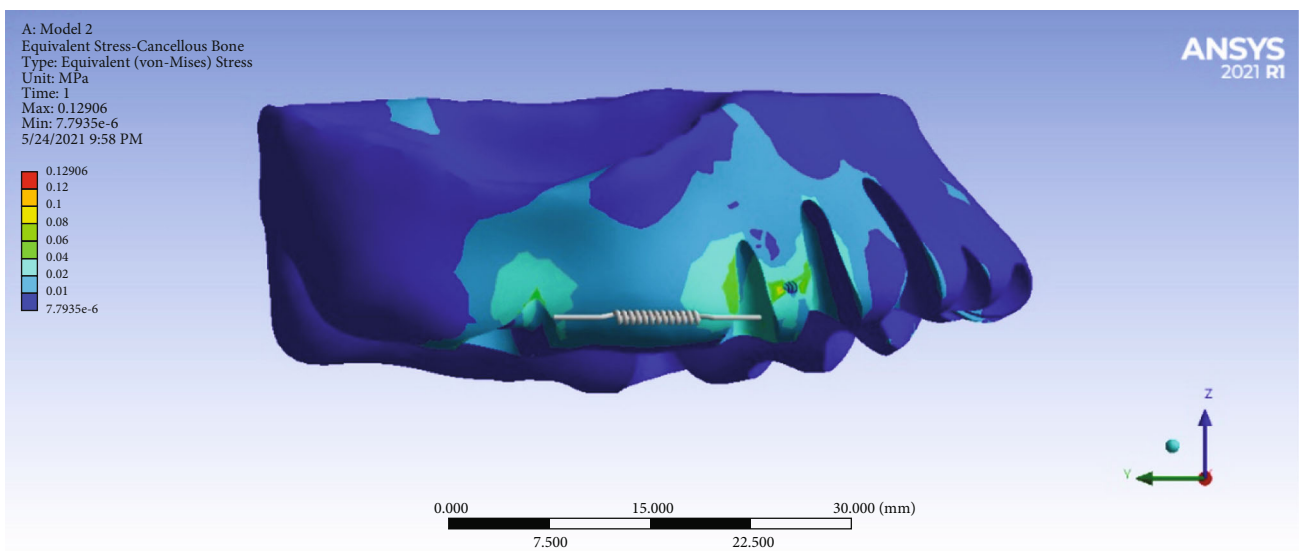

(b)

Figure 12: Continued.

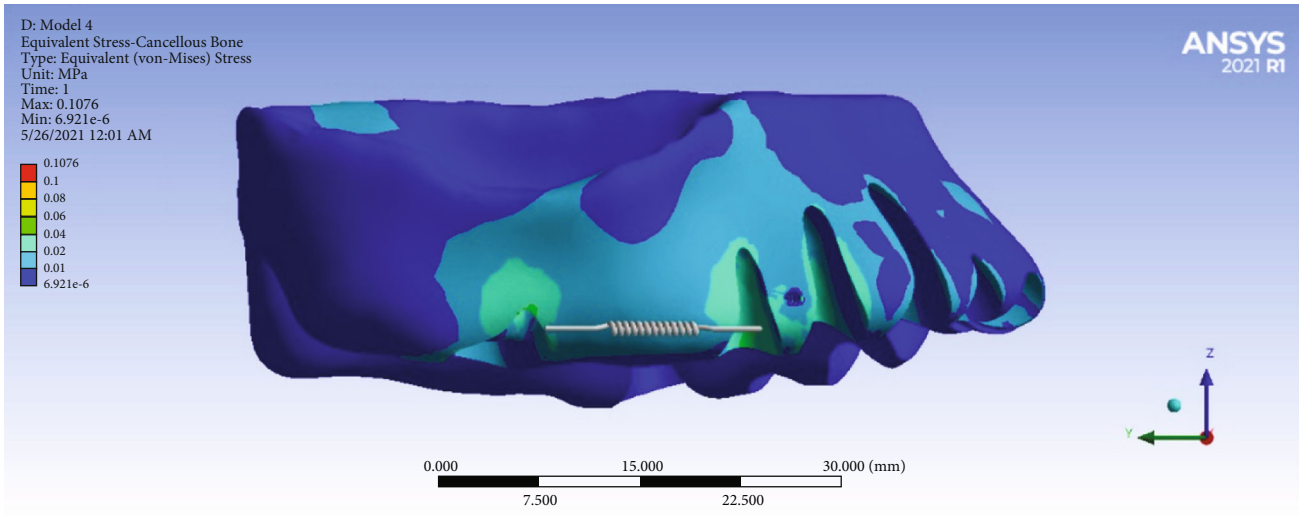

(c)

Figure 12: Stresses of the bone in different models: (a) model 1 with direct anchorage; (b) model 2 with rigid indirect anchorage; (c) model 3 with nonrigid indirect anchorage.

greater extent of distal movement of the premolars. In fact, with more movement of the premolars in the distal direction in the third model (nonrigid) compared to the second one (rigid), the spring closes and the force decreases.

The patterns of hydrostatic pressure distribution in the molar root PDLs were similar in the three models, with the tensile stress (warm colors) being higher in the distal sides of the mesiobuccal and distobuccal roots and the mesial side of the palatal root (which may be due to a mesial-in rotation). The amounts of the maximum tensile stress were rather similar among the models (0.019086, 0.020448, and 0.019891 MPa, respectively, in models 1, 2, and 3). On the other hand, the compressive hydrostatic pressure (blue color spectrum) was seen on the mesial sides of the buccal roots, on the mesial side of the root trunk, and on the distal side of the palatal root, reinforcing the "mesial-in rotation" idea. The compressive stress was the greatest in model 2 and the smallest in model 1 (Figure 14, Table 2).

3.6. Displacement through the Y-Axis (Mesiodistal)

3.6.1. The Premolars. Using the ligature wire, the anchorage loss was 1.5 times the amount of anchorage loss using the rectangular wire. The patterns of displacement in the mesiodistal direction were similar among the models (especially between models 1 and 2). Positive values indicate distal movement while negative values indicate mesial movement. The most extent of distal displacement was seen in the buccal side of the crown of the first premolar followed by the crown of the second premolar. Apical areas displaced less than the coronal areas, indicating tipping of these teeth. Also, palatal sides moved less than buccal sides, indicating some degree of rotation as well. The maximum displacement extents were the highest in model 3 and the lowest in model 1. Comparing the extents of movement in the distal direction, the displacement of the premolars in the nonrigid indirect anchorage model was the highest extent (highest anchorage loss) and it had the lowest extent in the direct anchorage model (the lowest anchorage loss) (Figure 15, Table 2).

3.6.2. The Second Molar. In the direct model, the force is applied close to the center of resistance of the molar, which leads to a uniform distribution of stress throughout the tooth. Therefore, the movement will be bodily, and compared to models 2 and 3 (in which the force is applied at a distance from the center of resistance and tipping is done), less movement is observed in the direct model. In the nonrigid model using the ligature wire, more distal movement of the premolars is observed compared to the second model (in which, the movement of the premolars is inhibited using the rectangular wire); the more distal movement of the premolars leads to spring closure and reduced force. Thus, using the ligature wire, the molar's displacement is slightly reduced (second model: 0.00564 mm, third model: 0.00552 mm).

The pattern of second molar mesialization was similar in all three models, with the buccal side being mesialized more than the palatal side, which indicates a "mesial-in" rotation of the tooth during protraction. Also, the coronal mesialization was greater than apical movement (which became slightly distalized), indicating an uncontrolled tipping movement. The amounts of maximum mesialization were similar for the indirect anchorage models (-0.018853 and -0.018982 mm, respectively, in models 2 and 3), both being greater than the extent of mesialization in the direct model (model 1, -0.015046 mm). The same pattern was also seen in the amounts of the average mesialization (Figure 16, Table 2).

3.7. Displacement on the X-Axis (Buccolingual)

3.7.1. The Premolars. In all the three models, both the premolar teeth moved in the palatal direction (the positive

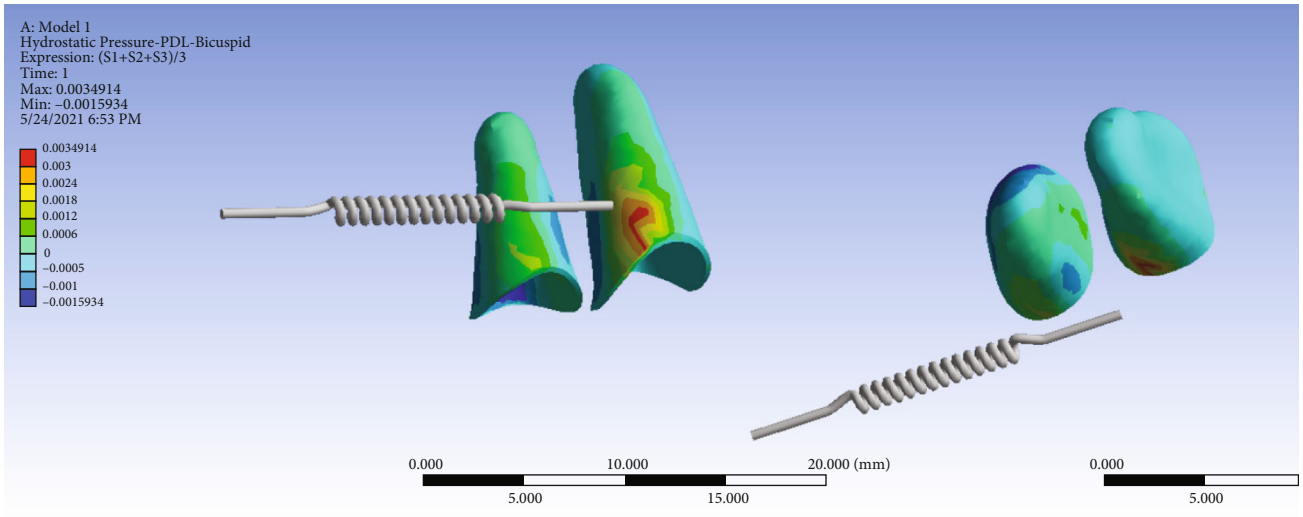

(a)

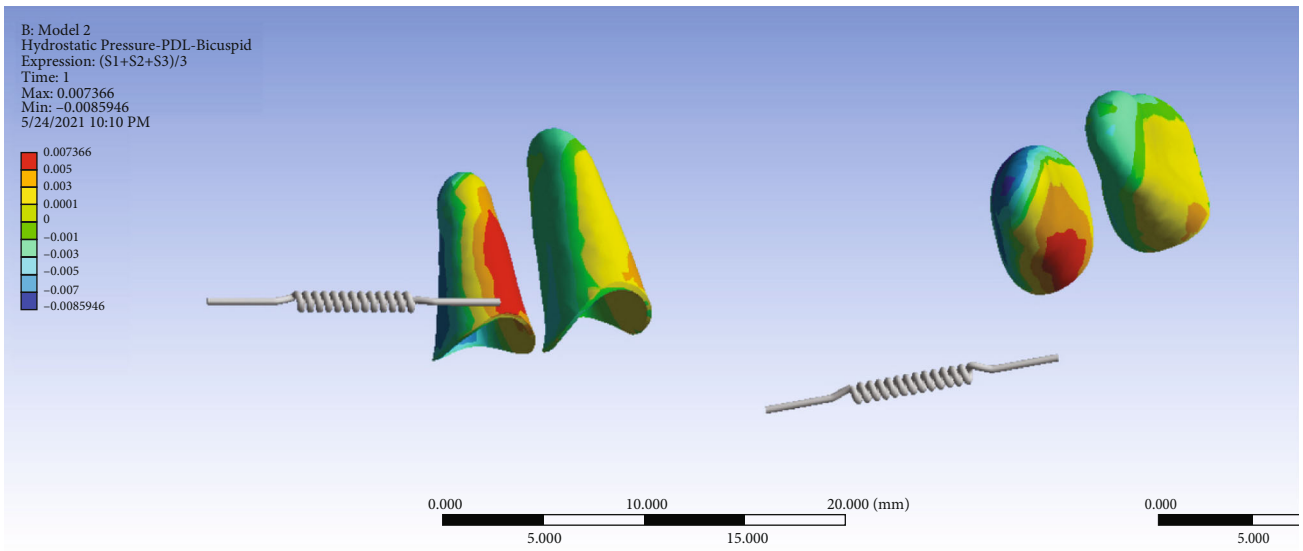

(b)

Figure 13: Continued.

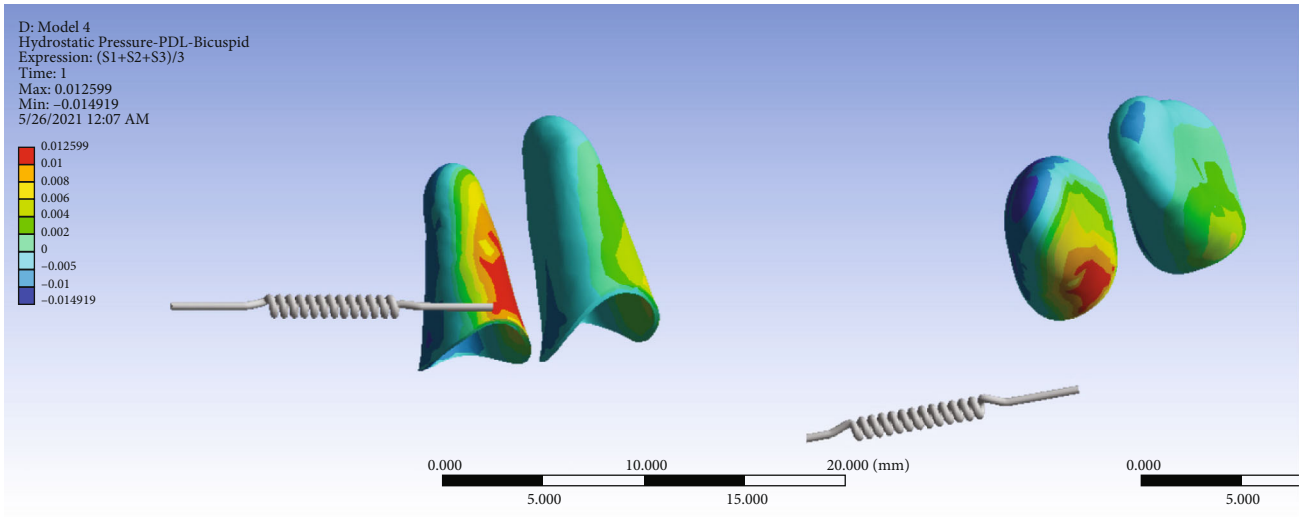

(c)

Figure 13: Hydrostatic stresses in the PDL of the premolars in different models: (a) model 1 with direct anchorage; (b) model 2 with rigid indirect anchorage; (c) model 3 with nonrigid indirect anchorage. Negative values indicate compressive stresses, and positive values indicate tensile ones. Negative values smaller than -0.0047 MPa pose a significantly higher external root resorption risk. The spring shows the force direction. The pair of root PDLs on the right side of each subimage is exactly the same pair of root PDLs on the left side, only from a different angle of view (apical view).

values on the *X*-axis). This lingualization reduces from the posterior to the anterior segments. Also, it reduces from the coronal tip to the apical area. The extent of palatalization is much less in model 1 compared to the lingualization extents seen in the indirect anchorage models. Between the two indirect anchorage models, the maximum and average lingualizations of model 3 (nonrigid indirect anchorage) were considerably greater than those of model 2 (rigid indirect anchorage), which might imply a higher risk of anchorage loss in model 3 (Figure 17, Table 2).

3.7.2. The Second Molar. The displacement of the second molar in the *X*-axis was positive (towards the palate) on the mesial side and negative (towards the buccal) on the distal side, indicating a "mesial-in" rotation of the tooth with the axis of rotation almost passing through the long axis of the tooth. The extent of this rotation was quite similar throughout the vertical dimension of the tooth, i.e., from the coronal tip to the root apices. This pattern was observed in all models. And the extents of the maximum and minimum *X*-axis displacements were rather similar among the three models. The average *X*-axis movement was somehow similar in models 1 and 2 (model 1 slightly larger); however, the average *X*-axis displacement was considerably greater in model 3 (Figure 18, Table 2).

3.8. Displacement on the Z-Axis (Intrusive or Extrusive)

3.8.1. The Premolars. The positive values show intrusive motion while negative values show extrusion. In all the models, the buccal side of the crown was extruded while the buccal side of the root was intruded, and this intrusive motion was more vivid towards the apical area. The palatal parts of the crowns and roots underwent intrusive displacement. These indicated a simultaneous buccal root torque and palatal crown tipping, as in uncontrolled tipping. Root and palatal tooth intrusive movements were much greater in the indirect anchorage models (2 and 3) compared to the direct anchorage model (#1). And between the two indirect anchorage models, it was greater in the nonrigid one (model 3). On the other hand, the extrusive movement of the buccal side of the crowns was greater in the direct anchorage model (1) followed by models 2 and 3 (Figure 19, Table 2).

3.8.2. The Second Molar. In model 1, the force is applied close to the center of resistance of the molar; hence, less tipping is created compared to the second and third models. In the second model, the rigid wire holds the base arch in place (in fact, it has inhibited the distortion of the base wire as a result of applying the force). Therefore, less intrusion is observed compared to the third model; in other words, the molar's unwanted movement is reduced.

The patterns of *Z*-axis displacements of the second molar differed between the direct anchorage model (model 1) and the two indirect anchorage models (models 2 and 3). In the indirect anchorage models (2 and 3), the mesial side of the tooth (equally from the coronal to the apical areas) tended to have intrusive displacements, while the distal side (again both coronal and radicular areas equally) tended to become extruded; the long axis of the tooth tended to have almost no movement in the *Z*-axis. The maximum intrusive movement was slightly smaller than the maximum extrusive movement, in both models. Overall, the two indirect anchorage models tended to mesially tip the crown of the second molar while at the same time, distally torque its root (both movements around somewhere close to the center

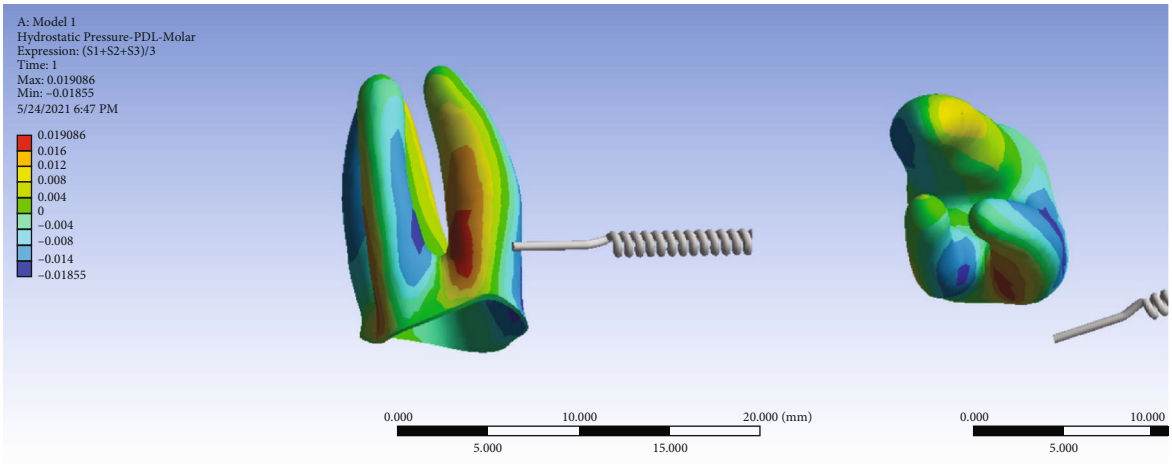

(a)

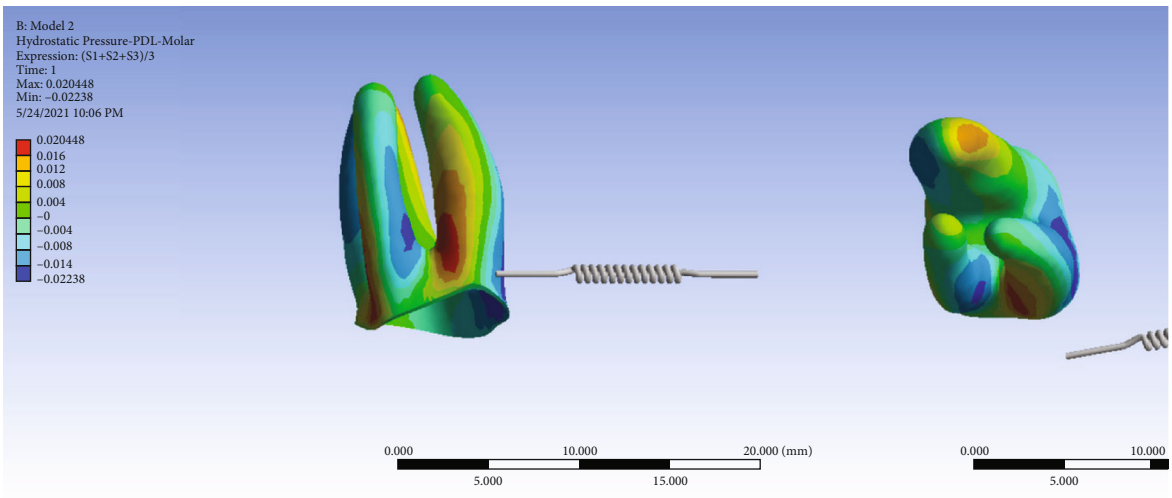

(b)

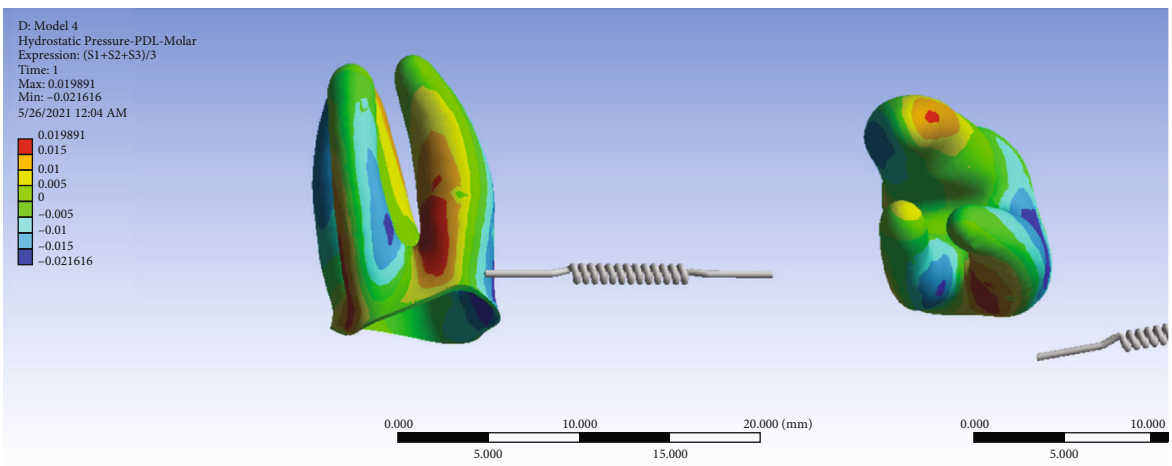

(c)

Figure 14: Hydrostatic stresses in the PDL of the second molar in different models: (a) model 1 with direct anchorage; (b) model 2 with rigid indirect anchorage; (c) model 3 with nonrigid indirect anchorage. Negative values indicate compressive stresses; positive values indicate tensile stresses. Negative values smaller than -0.0047 MPa pose a considerably higher risk for root resorption. The spring shows the force direction. The root PDLs on the right side of each subimage are exactly the same PDLs on the left side, only from a different angle of view (apical view).

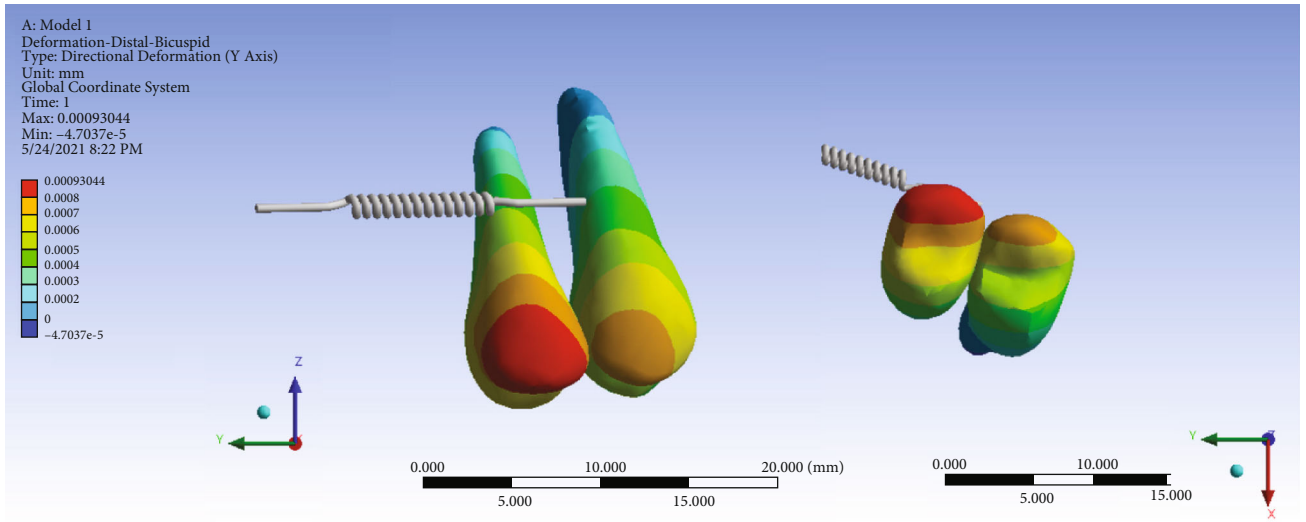

(a)

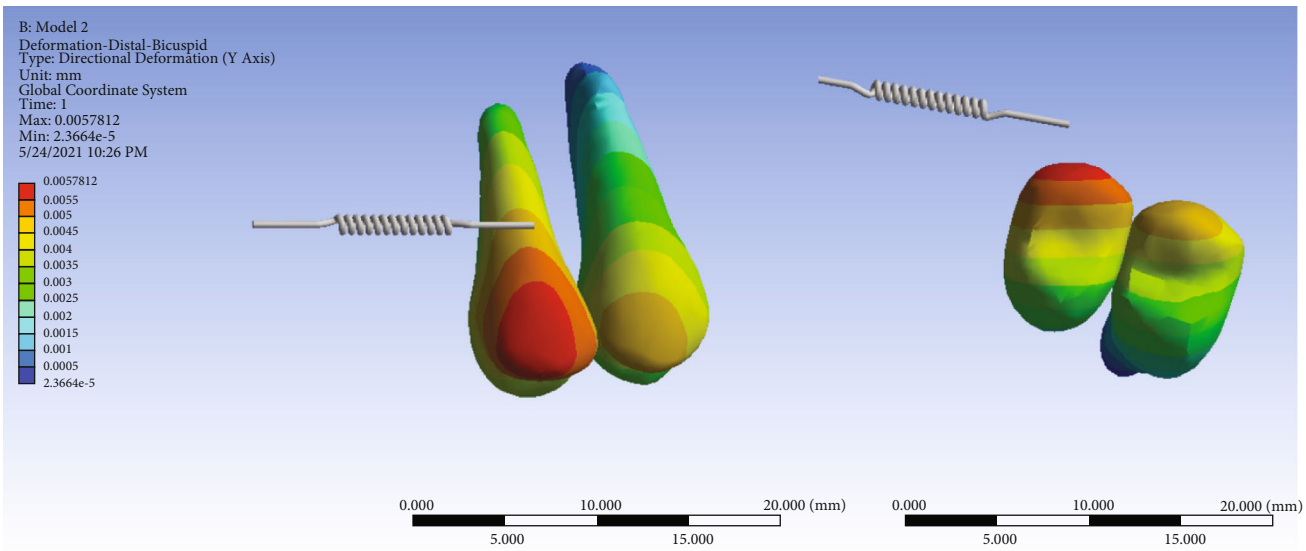

(b)

Figure 15: Continued.

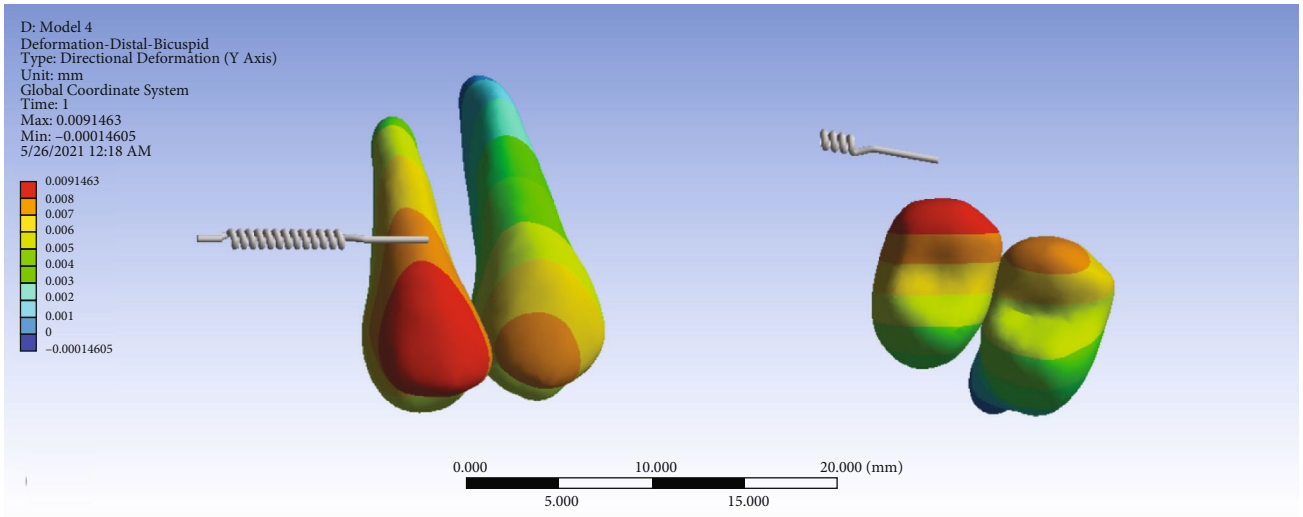

(c)

Figure 15: Displacements of the premolars through the *Y*-axis (the mesiodistal direction) in different models: (a) model 1 with direct anchorage; (b) model 2 with rigid indirect anchorage; (c) model 3 with nonrigid indirect anchorage. Positive values indicate distalization; negative values mean mesialization. The spring shows the force direction.

of resistance) again causing an uncontrolled tipping (Figure 20, Table 2).

However, the direction of *Z*-axis displacement in the first model differed: instead of the mesial side, the mesiobuccal side (mostly buccal with a small mesial extension) tended to have the maximum intrusive displacement (almost similar for the crown and root), while at the same time, instead of the distal side of the tooth, the distopalatal side (mostly palatal with a small distal extension) of the palatal root followed by the distopalatal side (again mostly palatal with a small distal extension) of the crown had the most extrusive displacement. Again, the long axis had almost no *Z*-axis displacement. The extents of the maximum intrusive and extrusive movements were similar. All of this indicated an uncontrolled tipping with mesiobuccal (more buccal than mesial) tipping of the crown and a distopalatal (mostly palatal) torque of the root around the center of resistance of the tooth (Figure 20, Table 2).

The magnitudes of the maximum intrusion were quite similar between the two indirect anchorage models (2 and 3). They were twice as larger than that in model 1. Similarly, the magnitudes of the maximum extrusions observed were as well similar between models 2 and 3, each being greater than the first model. The "average" *Z*-axis displacements were negative (extrusive) in all the three models; these were very similar in the indirect anchorage models (2 and 3), both being much greater than the rather subtle average (extrusive) movement seen in model 1 (Figure 20, Table 2).

3.9. Parametric Assessment of ligature's Elastic Modulus Alterations. The simulation was repeated with different elastic moduli for the ligature in model 3 (nonrigid indirect anchorage); the effects of such parametric changes on stresses and displacements were assessed. It was shown that the diagram of changes in von Mises stresses would reach a rather steady slope at some elastic moduli (Figure 21, Supplementary Table 1). A similar pattern was observed for the PDL hydrostatic pressures, although with a less remarkable overall change in hydrostatic pressures as a function of increasing the modulus of elasticity. In this regard, the minimum hydrostatic pressure remained below the critical value of -0.0047 MPa (as the threshold for root resorption risk), meaning that there was a risk of root resorption at all different moduli of elasticity (Figure 22, Supplementary Table 2).

3.9.1. Displacements in the Y-Axis (Mesiodistal). By increasing the elastic modulus of the wire, the distal movement of the premolars decreased, which means strengthening the anchorage and more resistance to anchorage loss (Figure 23, Supplementary Table 3).

3.9.2. Displacements in the X-Axis (Buccolingual). With increasing the elastic modulus of the wire, a slight decrease in premolar displacement in the buccolingual axis was observed (Figure 24, Supplementary Table 4). As the rigidity of the wire increases, its resistance to the buccolingual displacement increases and prevents the palatal movement of the teeth.

3.9.3. Movements in the Z-Axis (Intrusive/Extrusive). By increasing the rigidity of the ligature wire, a slight increase in the intrusive movement of the premolars in the vertical axis was observed, while the extrusive motion of the molar was reduced (Figure 25, Supplementary Table 5). The force vector from the ligature wire on the premolar tooth is mesioapical. With increasing the rigidity, the intrusive component also increases, and the intrusive movement of the premolar increases.

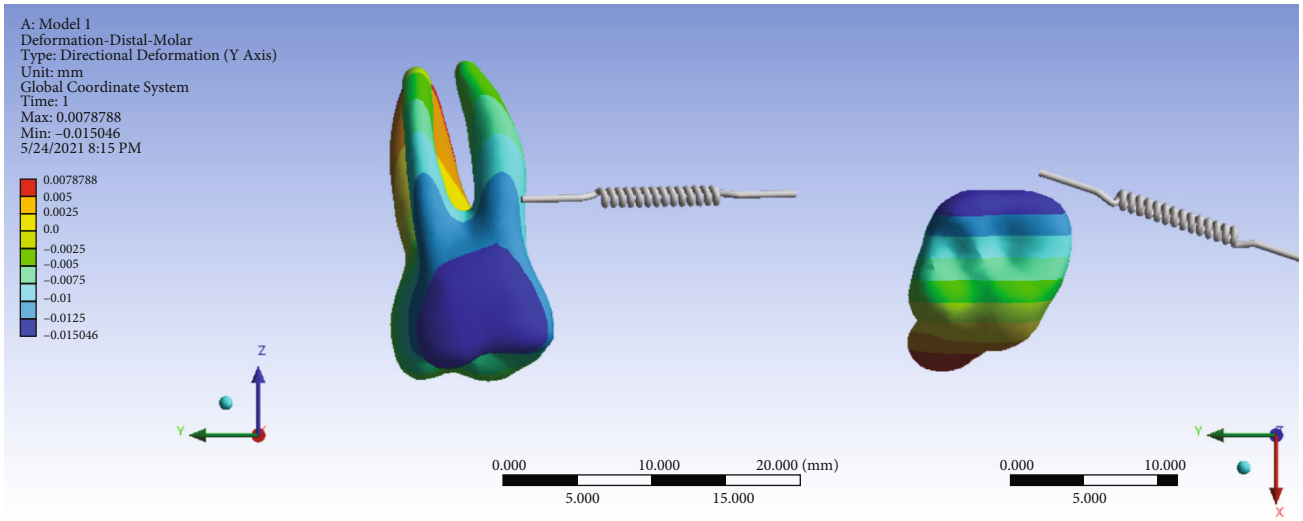

(a)

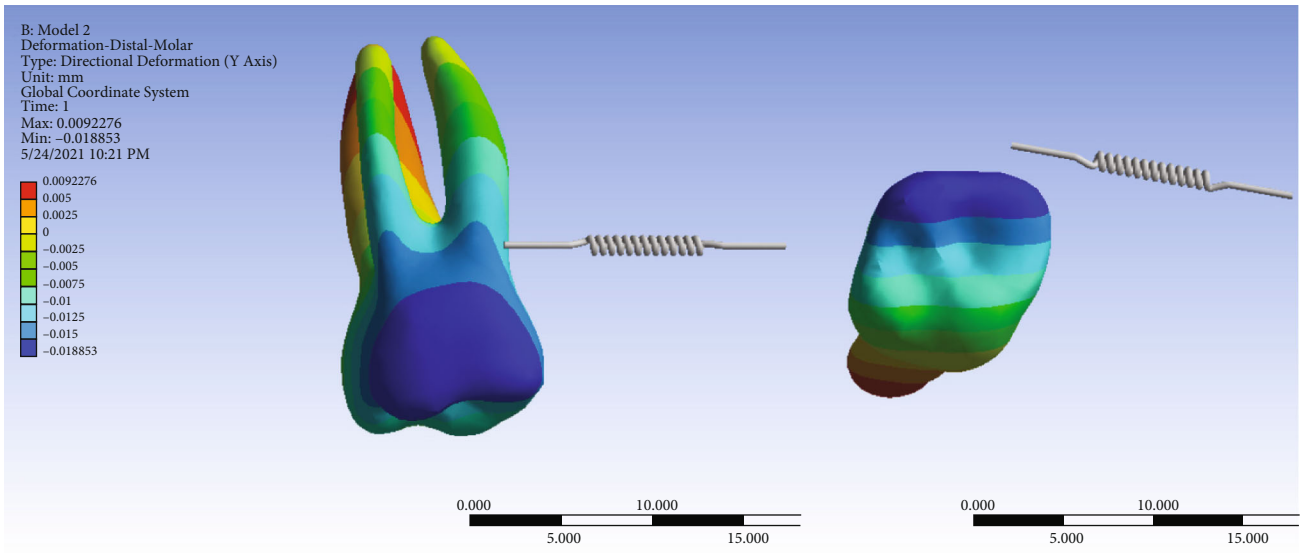

(b)

Figure 16: Continued.

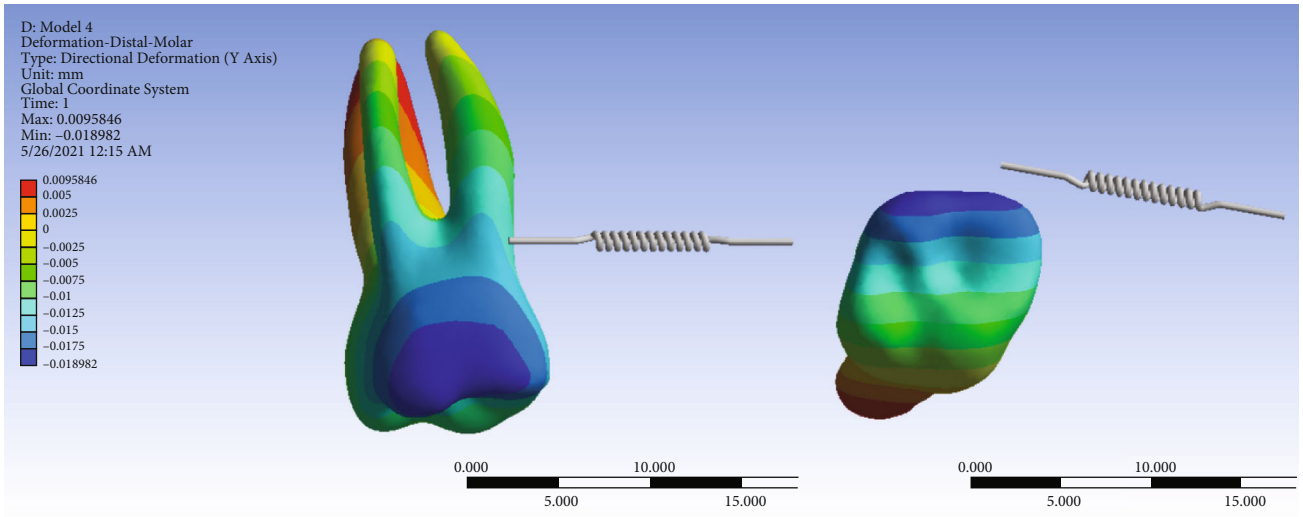

(c)

Figure 16: Displacements of the second molar on the *Y*-axis (the mesiodistal direction) in different models: (a) model 1 with direct anchorage; (b) model 2 with rigid indirect anchorage; (c) model 3 with nonrigid indirect anchorage. Negative values indicate mesialization. The spring shows the force direction.

4. Discussion

Effective management of the space of missing posterior teeth is a major challenge in orthodontic treatment. Posterior edentulous spaces are commonly seen in adult maxillary arches, the most common of which is the loss of the first molars due to caries [4]. The greater the amount of tooth displacement, the more difficult it is to control for side effects. In molar protraction, due to the large mesiodistal dimensions of the tooth, even with temporary skeletal anchorages, controlling the transverse, vertical, and horizontal dimensions is not easy [48]. Three models were considered to investigate the stress distribution. The miniscrews simulated in this study were 1.6 mm in diameter and 8 mm long and were placed vertically in the interdental space of the first and second premolars. According to previous studies, the vertical angle of miniscrew placement reduces stress concentration and increases the likelihood of miniscrew stability [49]. In all models of the present study, a force of 150 g was applied according to previous studies [4]. In the direct anchorage model, the force was applied from the miniscrew to the power arm of the second molar. In the indirect anchorage models, direct and indirect forces were applied from the hook of the second premolars to the second molars, and the teeth of the anchorage unit were fixed using a stainless-steel wire and a ligature steel. In the present study, the average second molar displacement in all 3 models was mesially, palatally, and extrusive. In previous studies, it has been mentioned that there is an increase in the possibility of molar tooth extrusion and subsequently creating an anterior open bite, which emphasizes the importance of controlling the vertical dimension [50].

Our findings had some clinical implications. In the direct anchorage method, there is the lowest possibility of anchorage loss and at the same time the highest risk of failure and loosening of the miniscrew. The stress created in the bone around the miniscrew is almost double compared to the indirect model. In situations where it may not be suitable due to certain factors (such as the young age of the patient or in low-density bones such as the maxillary alveolar process), we should provide measures to improve the stability of the miniscrew. For example, we should remove the force from the miniscrew and use indirect anchorages; this reduces the risk of miniscrew failure. Rigid or nonrigid connection can be used for indirect anchorage (in indirect anchorage, the stress in spongy bone was halved). But indirect anchorage increases the amount of anchorage loss. In the nonrigid indirect anchorage model—using ligature wire—compared to the rigid one—using full-size steel wire, the extent of anchorage loss was about 1.5 times greater. But the advantage of using ligature wire was the less stress created in the miniscrew and its surrounding bone: i.e., about 70% stress reduction was observed in the miniscrew body. In the nonrigid method, the least amount of stress was created in the miniscrew and its surrounding bone; this allows us to use a smaller diameter and length of the miniscrew. This can be useful in some cases such as choosing miniscrews in the interdental area where the space is more limited such as between premolars [51]; in less dense bones like the maxilla; and or in the younger patients who have a lower bone density.

Some studies have shown that there is a need for high anchorage control in molar protraction; according to them, with insufficient anchorage, there is a possibility of tipping of the molar and root resorption [52]. In an earlier research [53], in general, placing the miniscrew in the buccal area (due to the passage of the force through the buccal side of the center of resistance) could lead to unwanted expansion, while placing the miniscrew in the palatal area will reduce the width of the arch [53]. However, in the present study, despite the buccal placement of the miniscrew, the average displacement of molars and premolars was palatally. The

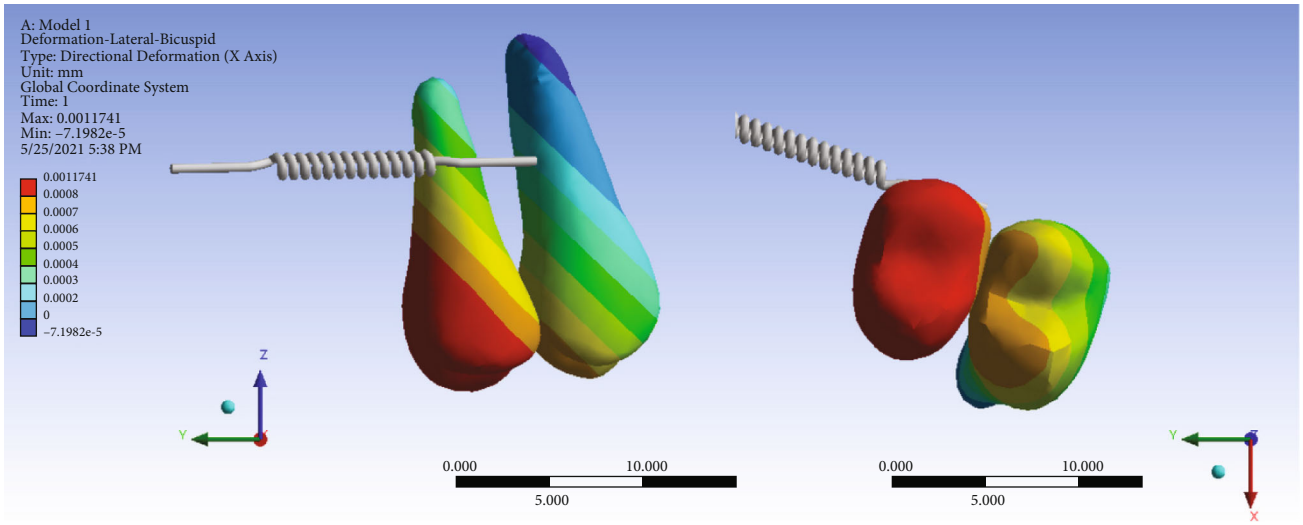

(a)

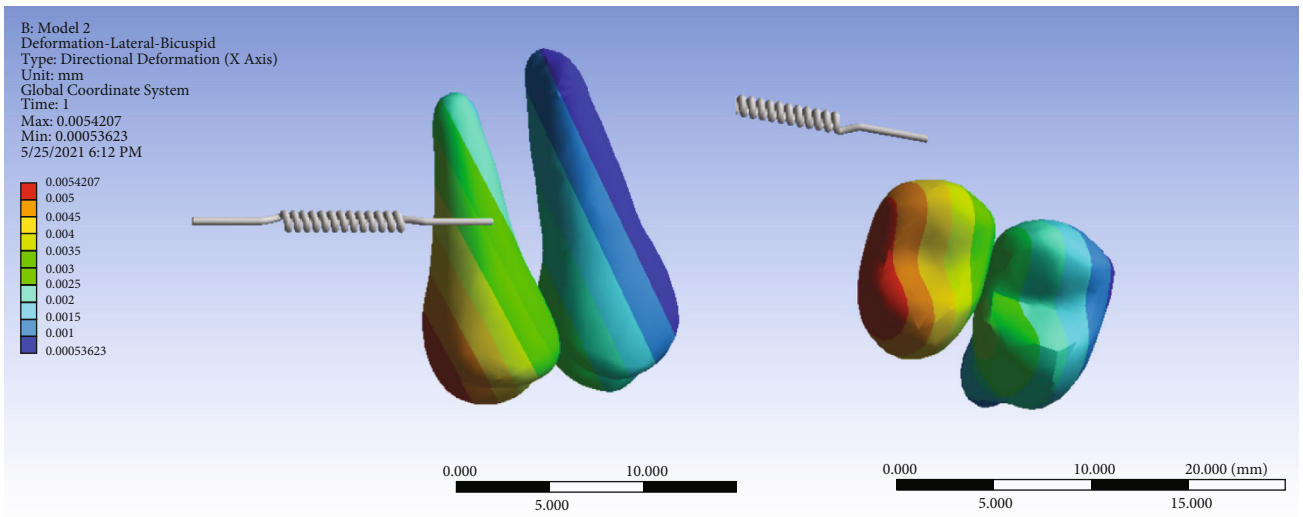

(b)

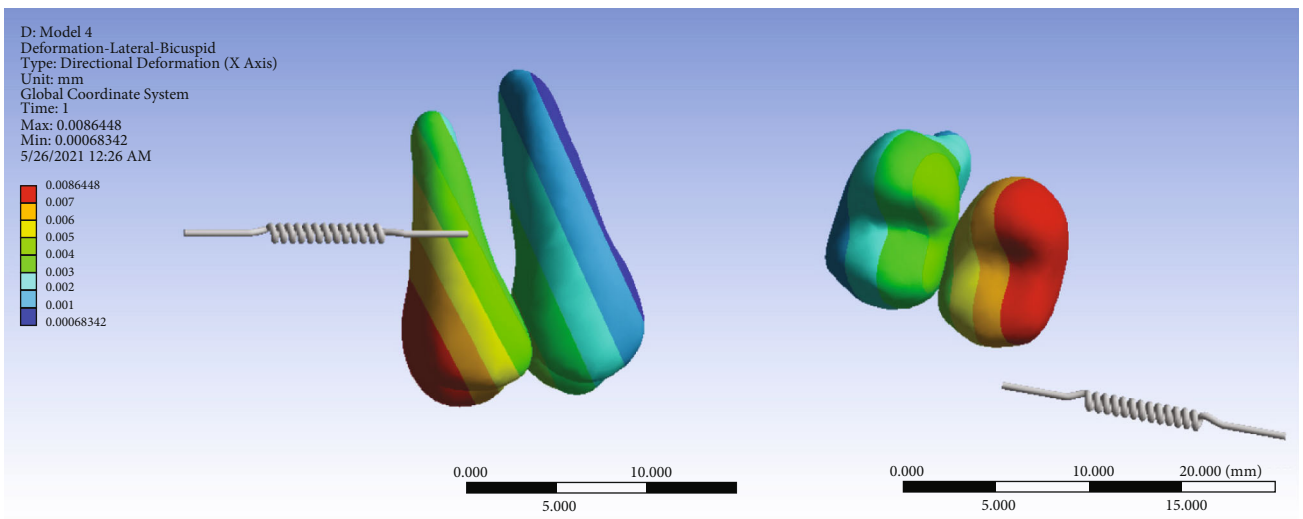

(c)

Figure 17: Displacements of the premolars on the X-axis (the buccolingual direction) in different models: (a) model 1 with direct anchorage; (b) model 2 with rigid indirect anchorage; (c) model 3 with nonrigid indirect anchorage. Positive values indicate palatalization; negative values indicate buccal movements. The spring shows the force direction.

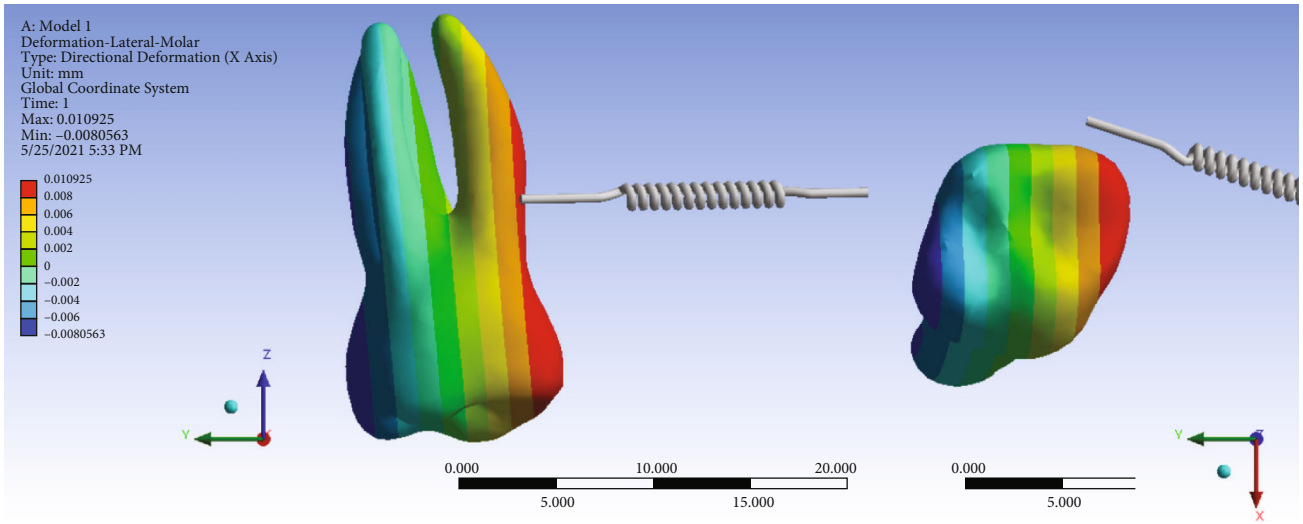

(a)

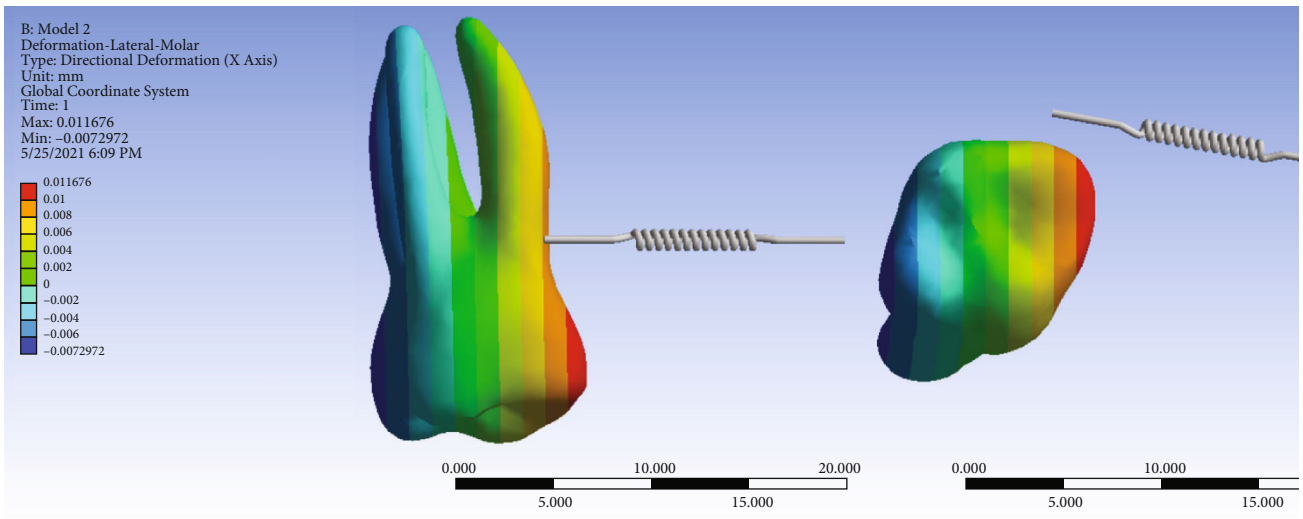

(b)

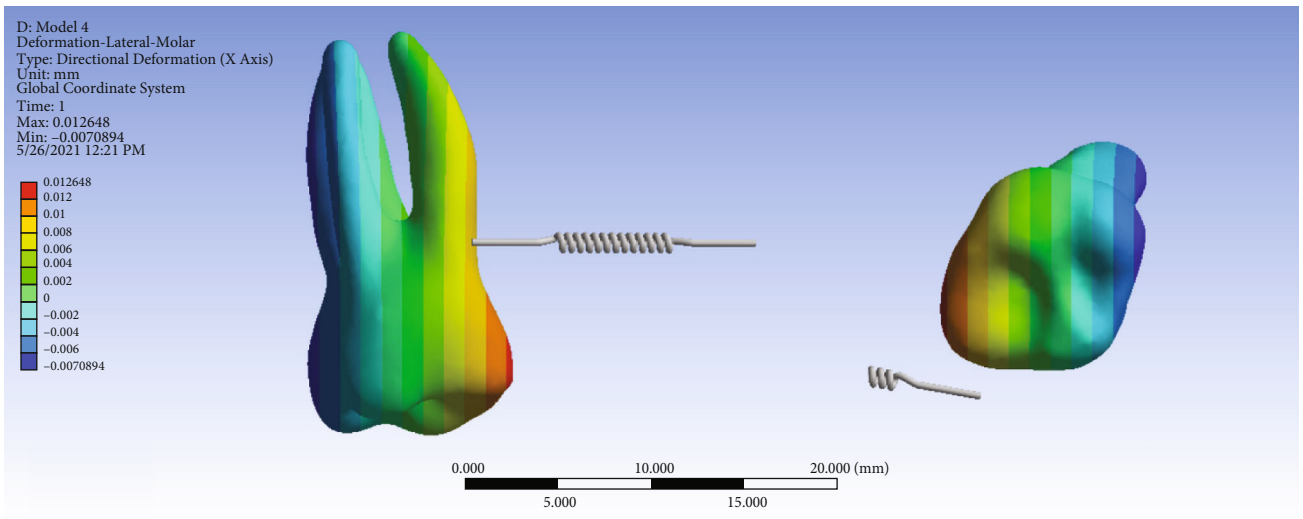

(c)

Figure 18: Movements of the second molar in the X-axis (the buccolingual direction) in different models: (a) model 1 with direct anchorage; (b) model 2 with rigid indirect anchorage; (c) model 3 with nonrigid indirect anchorage. Positive values indicate lingualization. The spring shows the force direction.

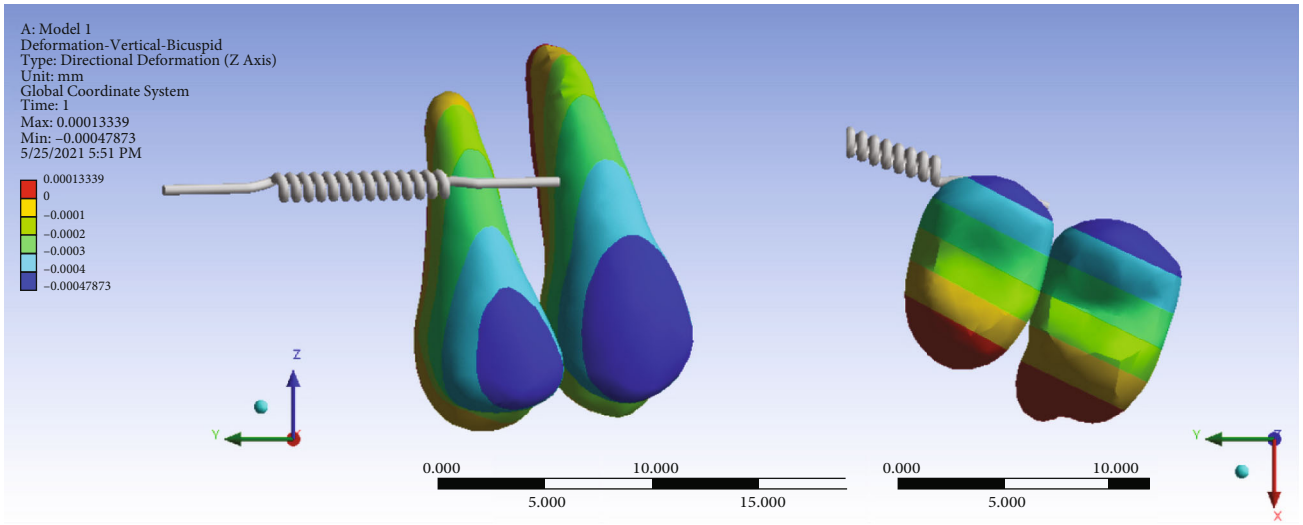

(a)

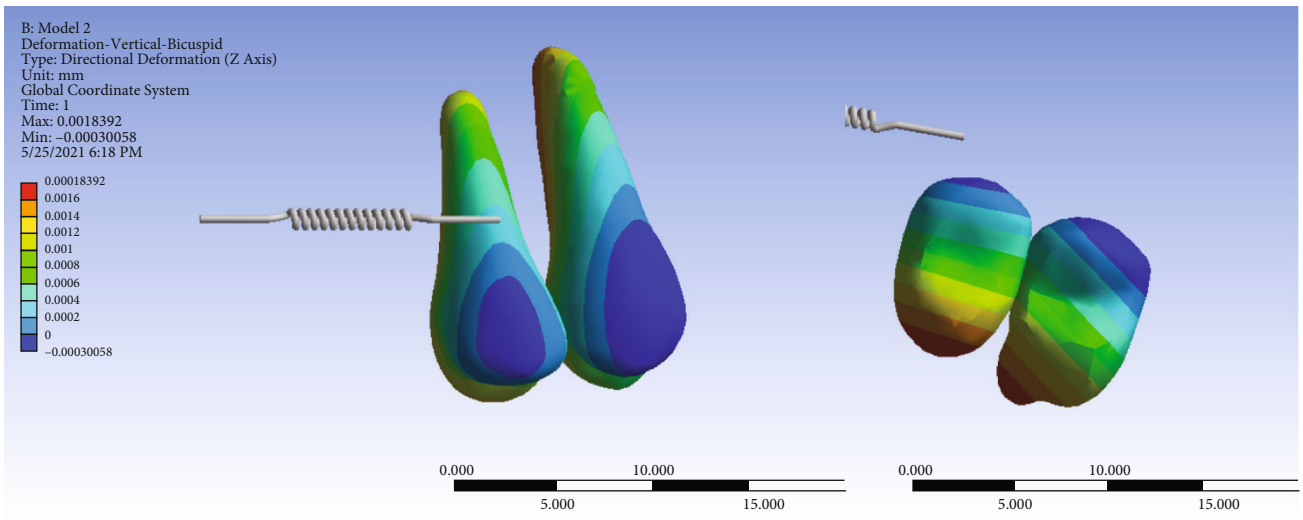

(b)

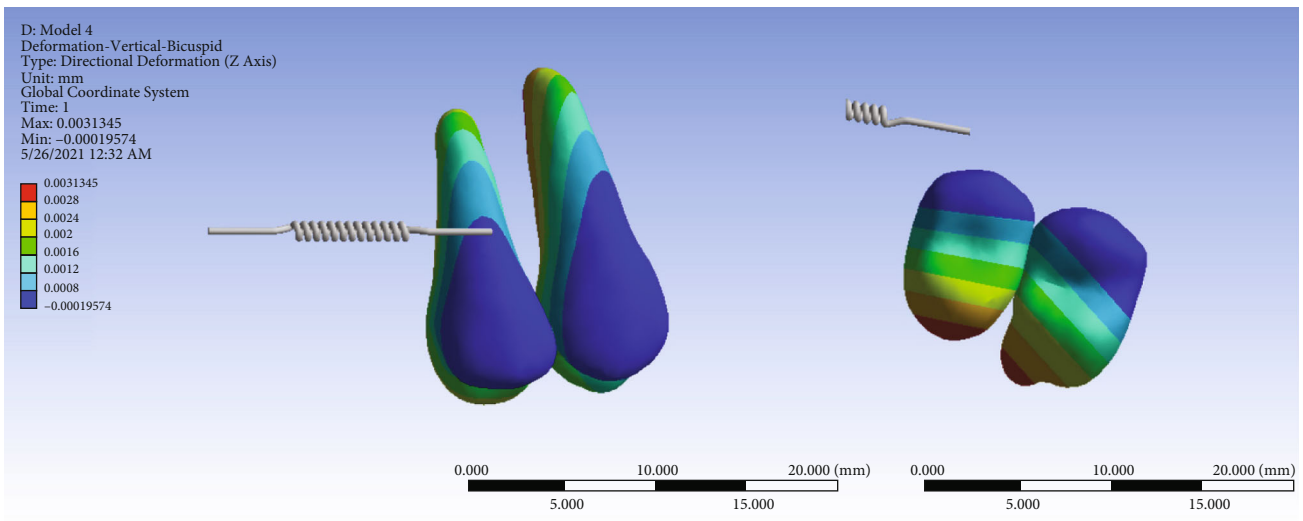

(c)

Figure 19: Displacements of the premolars on the Z-axis (the intrusive-extrusive direction) in different models: (a) model 1 with direct anchorage; (b) model 2 with rigid indirect anchorage; (c) model 3 with nonrigid indirect anchorage. Positive values indicate intrusion; negative values indicate extrusion. The spring shows the force direction.

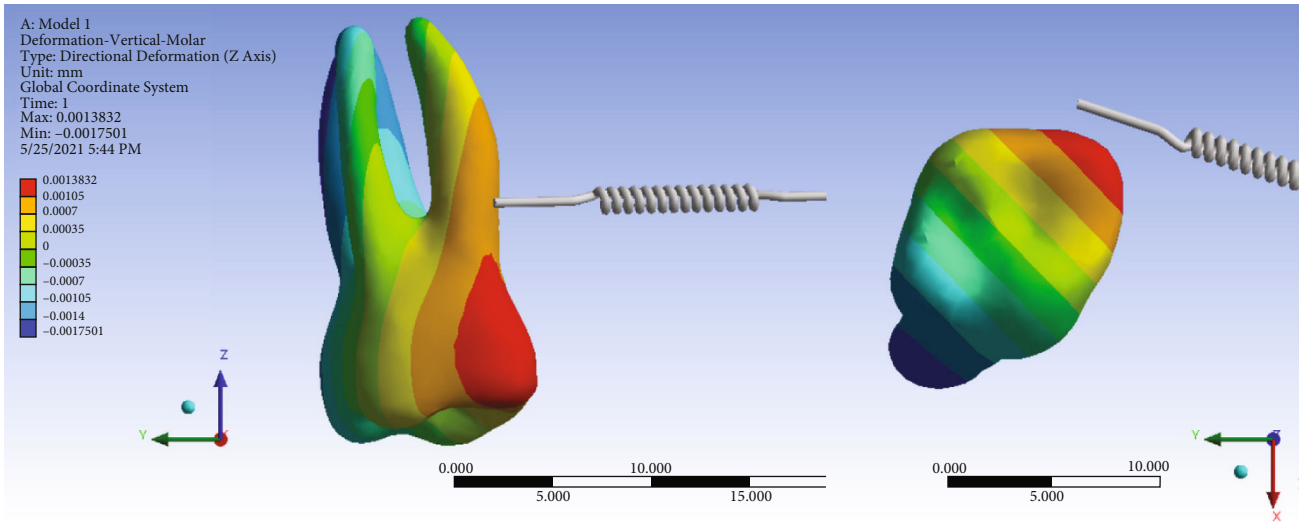

(a)

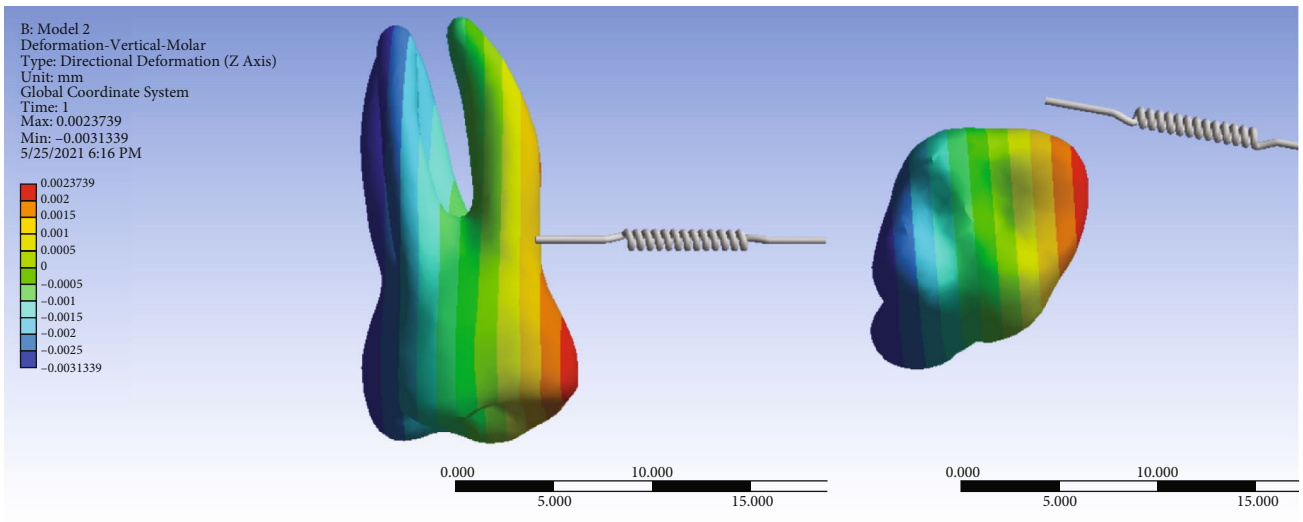

(b)

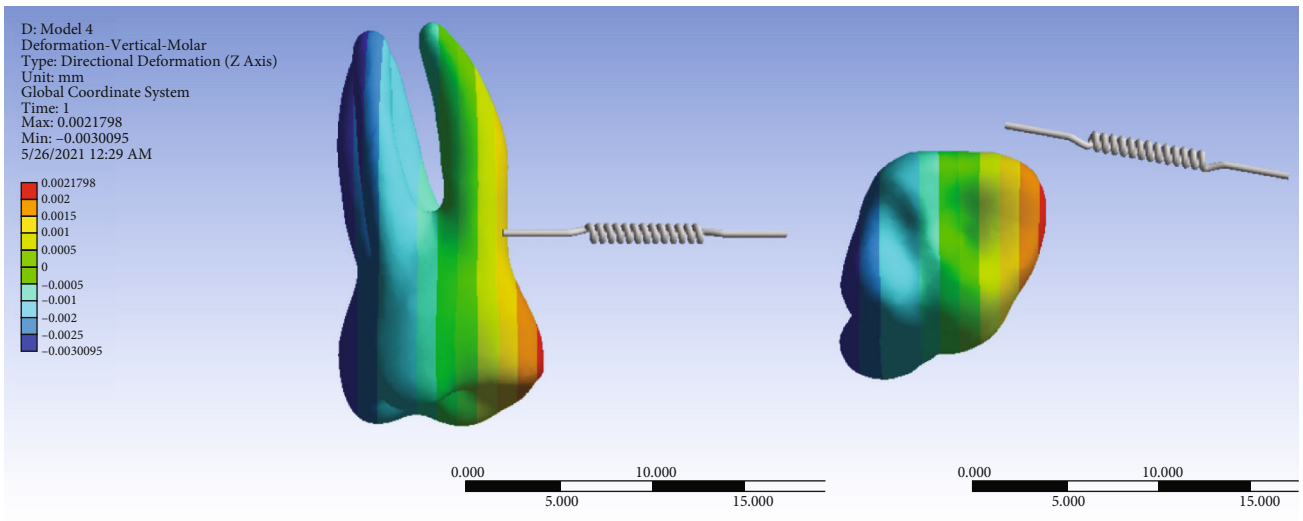

(c)

Figure 20: Displacements of the second molar through the Z-axis (the intrusive-extrusive direction) in different models: (a) model 1 with direct anchorage; (b) model 2 with rigid indirect anchorage; (c) model 3 with nonrigid indirect anchorage. Negative values indicate extrusion. The spring shows the force direction.

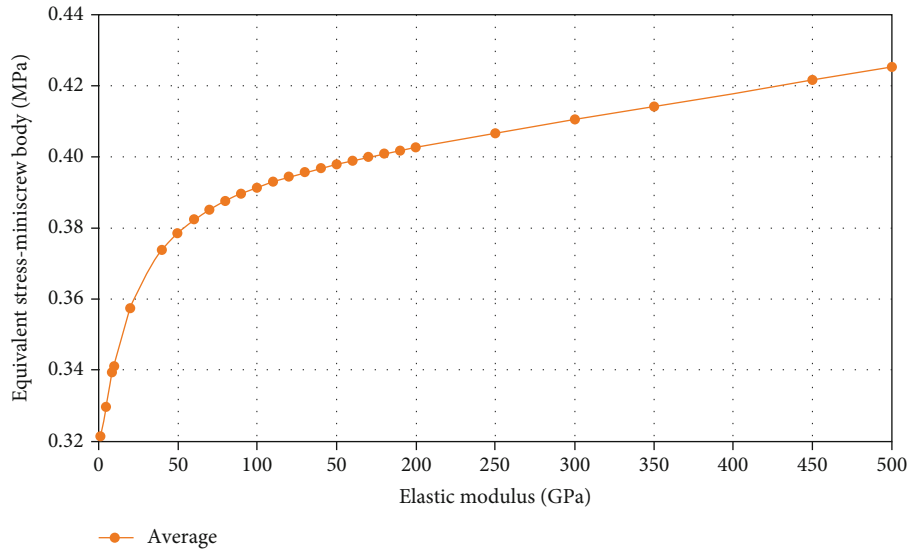

(a)

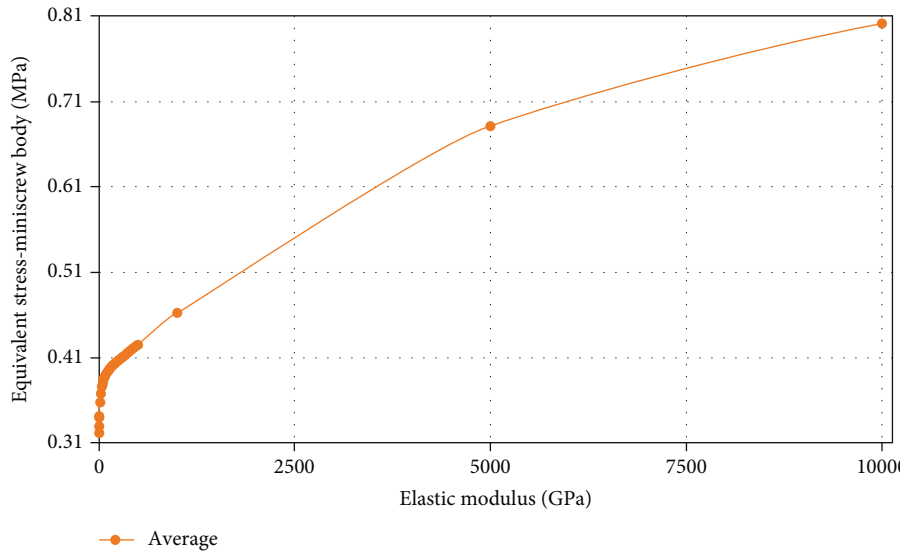

(b)

Figure 21: Continued.

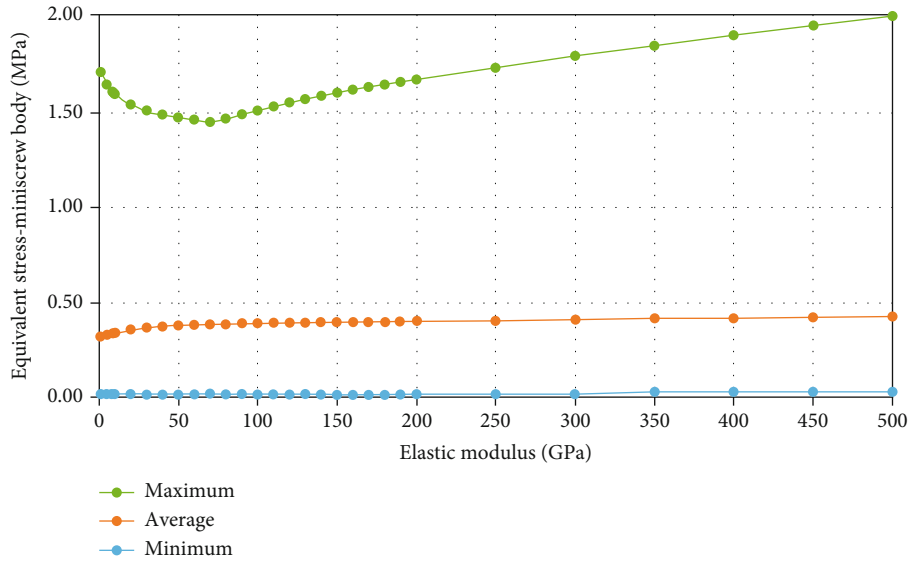

(c)

Figure 21: Parametric assessment of the miniscrew stresses (MPa) by increasing the elastic modulus of the ligature wire (GPa). Average changes up to 500 GPa (a); average changes up to 10000 GPa (b); minimum, maximum, and average changes (c).

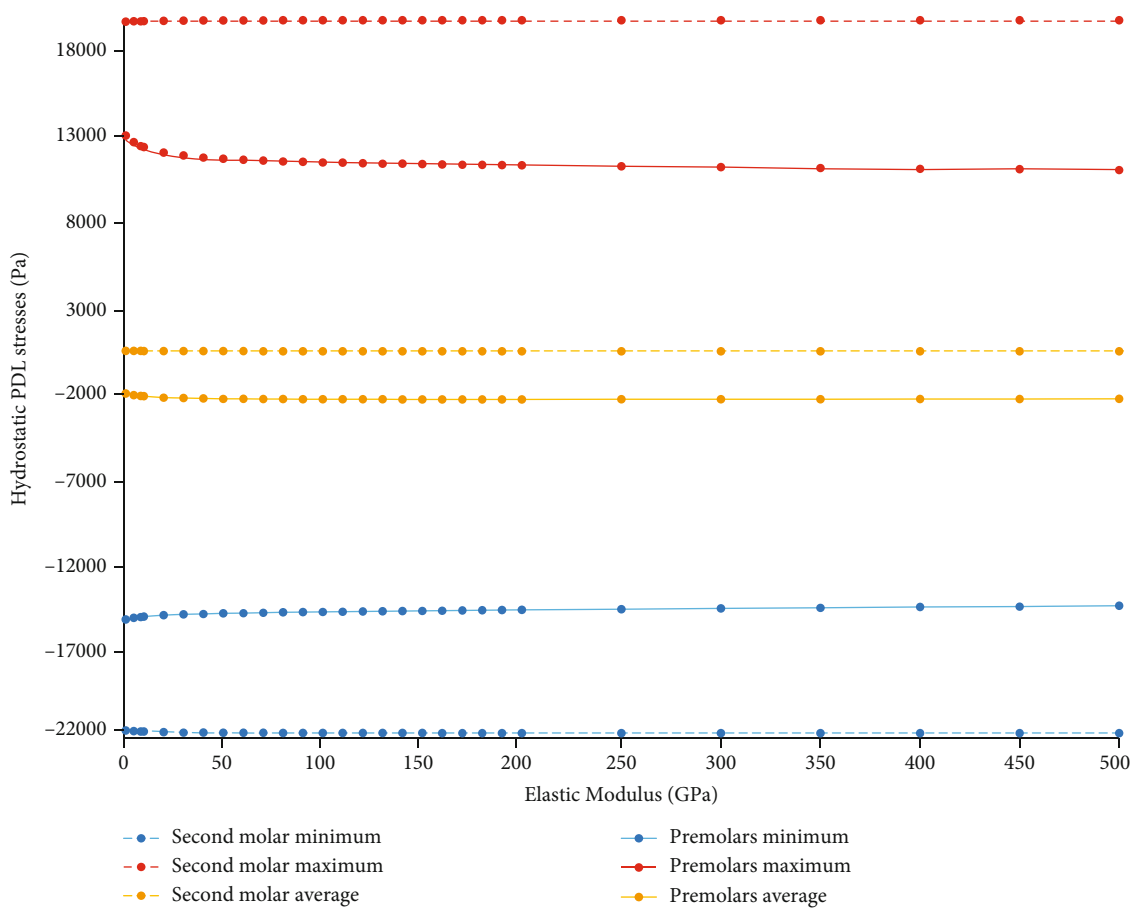

Figure 22: Parametric evaluations of the hydrostatic stresses (Pa) in the PDLs of model 3 at different elastic moduli up to 500 GPa. Negative stresses mean compressive hydrostatic pressure, while positive values mean tensile stress. The minimum stresses (negative values) smaller than -4700 Pa pose an external root resorption risk. Molar stresses are shown using dashed lines. Min: minimum; Max: maximum; Avg: average.

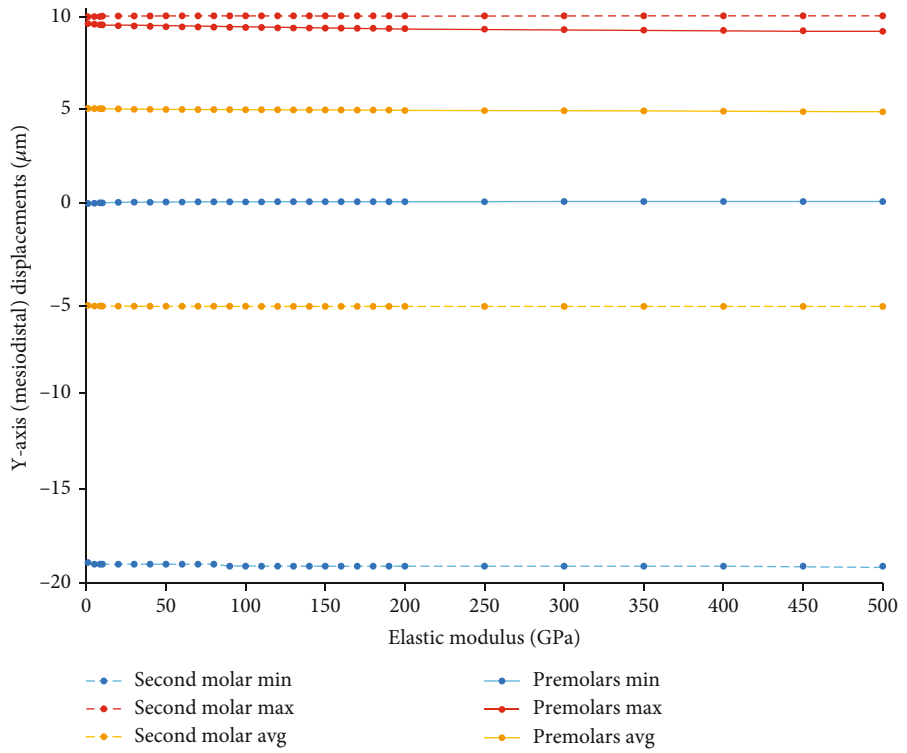

Figure 23: Changes in the extent of Y-axis (mesiodistal) displacements of the anchorage and active unit teeth (μm) in model 3 by increasing the elastic modulus of the ligature wire up to 500 GPa. Positive values indicate distalization while negative values indicate mesialization. Molar movements are shown using dashed lines. Min: minimum; Max: maximum; Avg: average.

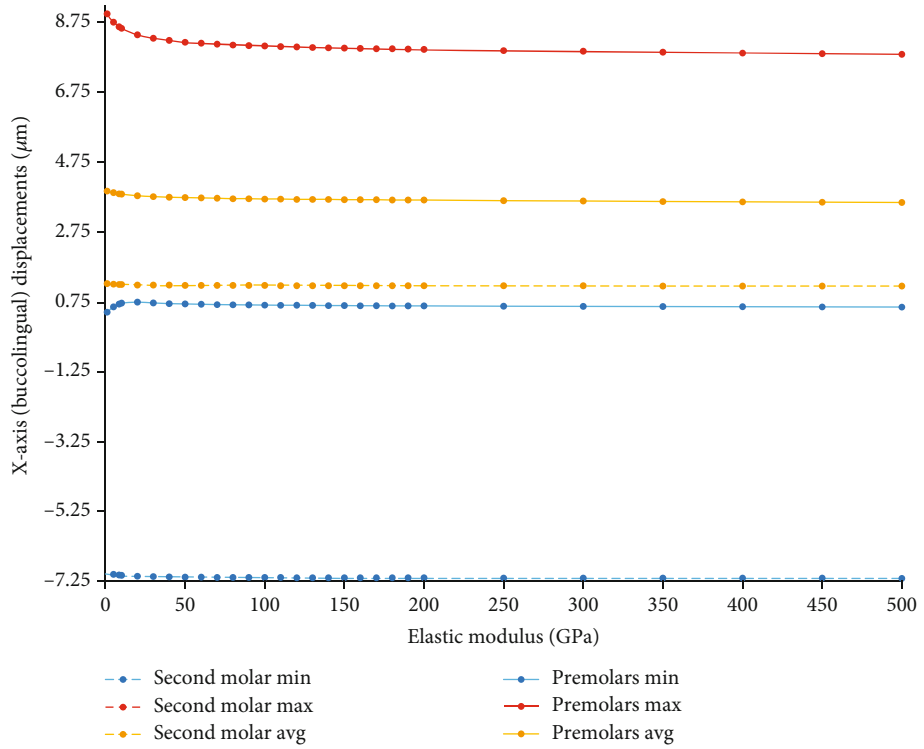

Figure 24: Changes in the extent of X-axis (buccolingual) displacements of the anchorage and active unit teeth (μm) in model 3 by increasing the elastic modulus of the ligature wire up to 500 GPa. Negative values indicate buccal movement, while positive values indicate palatalization. Molar movements are shown using dashed lines. Min: minimum; Max: maximum; Avg: average.

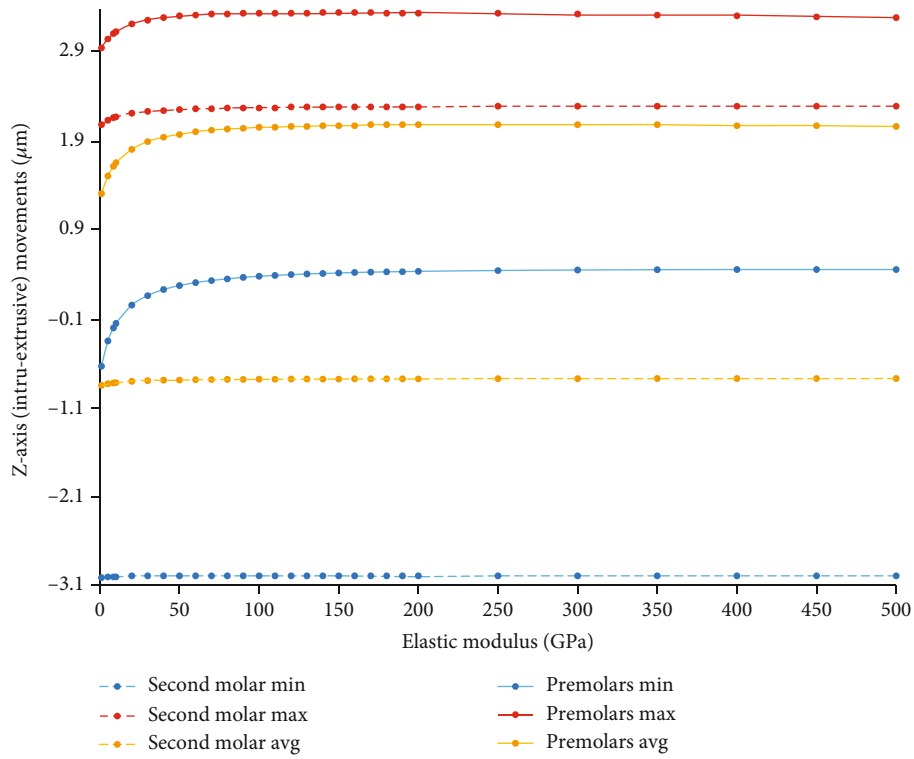

FIGURE 25: Alterations in the extent of Z-axis (intrusive-extrusive) displacements of the teeth (μm) in the nonrigid indirect anchorage model by increasing the elastic modulus of the ligature wire up to 500 GPa. Positive values mean intrusive movement, while negative values mean extrusion. Molar movements are shown using dashed lines. Min: minimum; Max: maximum; Avg: average.

direction of the force components will determine the direction of displacement. In our study, the miniscrew was placed in the buccal side. However, due to the shape of the arch being narrower at the location of the miniscrew (between the premolars) compared to the location of the second molar, the components of the force will be mesially and lingually; probably because of this, the movement of the tooth had finally become palatally. In other studies, the unwanted side effects of molar protraction were a buccal force, tipping of adjacent teeth, mesial rotation and buccalization of molar teeth, and crossbite [50]. In the study of Marusamy et al. [52], during maxillary molar protraction, the archwire needs to be expanded at each visit to prevent crossbite due to tooth movement to a narrower arch area [52]. In the study of Holberg et al. [30], mandibular molar protraction was compared using dental anchorage and miniscrew. In the use of dental anchorage, high stresses were reported on the anchorage unit tooth, indicating the high potential of the anchorage loss. In their direct anchorage model, the loss of the anchorage (premolar movement) was effectively prevented, but the high stress around the miniscrew could lead to loosening or loss of the miniscrew. The main problem in this model was the mesial rotation of the molar. To offset this movement, it was recommended to apply force from the lingual to the molar tooth [30]. In the current study, the mesial rotation of the molar was seen in all three models, which is due to the application of force to the buccal side of the center of resistance of the molar tooth. The indirect anchorage model might be preferred by many clinicians because it provides freedom in choosing the location of the miniscrew, reduces the risk of damage to the tooth roots, and allows the use of appropriate biomechanics to control the teeth. In the indirect anchorage model, less displacement was observed on the second premolar tooth compared to the dental anchorage and more displacement was observed compared to the direct anchorage [30]. In our study, the highest displacement of the premolars was related to the indirect nonrigid anchorage model, which was seen in the distal and palatal directions; the lowest displacement of the premolars was related to the direct anchorage model, which in the mesiodistal axis was approximately one tenth of the maximum displacement in the nonrigid indirect anchorage model. The average movement of the premolars in the direct anchorage model was less than indirect models, which can be expected owing to the lack of force exerted onto the premolars in the first model. The results of this study were in line with other studies reporting that the rate of anchorage loss was higher in indirect anchorage models [4, 30]. The average movement of the premolars in the rigid indirect anchorage model of this study was less than that in the nonrigid one: due to the larger size and reduced elasticity of the wire connected to the miniscrew and the second premolar tooth, the movement of the teeth of the anchorage unit is more prevented; but the stress on the miniscrew and the surrounding bone increases, which increases the chance of the miniscrew failing. The results of this study showed that the highest amount of stress in the body of the miniscrew was created in the direct anchorage model (10.916 MPa) while the lowest amount of stress was in the indirect anchorage model (3 MPa). Previous studies have also shown that applying

force directly to the miniscrew creates excessive force on the bone around the miniscrew and increases the chances of loosening and failure [30, 54]. The results of our study showed that the stress level in the miniscrew and bone in the three models was lower than the yield stress of titanium (692 MPa) and bone (200 MPa) [55]. Therefore, the miniscrew had sufficient strength against the forces in three models.

Root resorption may occur during orthodontic treatment in the same areas where physiological root resorption begins as these areas are more sensitive to local changes [56]. In fact, orthodontic forces applied to the teeth cause stress distribution in the PDL. PDLs containing very small blood vessels are exposed to this stress. If the pressure is beyond capillary blood pressure, it causes collapse and dysfunction of blood vessels in supplying the blood [57]. According to Schwarz, there is a possibility of root resorption if pressure exceeds capillary blood pressure in the PDL [57–59]. Capillary blood pressure range has been reported between 15 and 35 mm of Hg (0.0020 to 0.0047 MPa) [46, 57, 60]. Mechanical stress can cause changes in blood flow, which is a factor in root resorption [61]. Therefore, hydrostatic pressure can be considered a key factor in assessing the risk of root resorption during orthodontic treatment [57]. The extent of the resorption also depends on the amount of force and torque applied [61–63]. In a recent study, no clear resorption was found in the traction region, which can suggest that odontoclasts do not respond to traction stimuli [64]. The pressure exerted by the tooth root on the bone and the surrounding PDL is the main factor determining the rate of tooth movement, not the force exerted on the tooth crown [65]. The optimal range of stress and force to induce the optimal rate of tooth movement should be between 0.015-0.026 N/mm^2 and 150-260 grams, and more than this amount will reduce tooth movement [65]. Therefore, the force used in this study was within the optimal range [65]. In all models of this study, this force caused the maximum compressive hydrostatic pressure points (with a value greater than 0.0047 MPa) in the PDL of the second molar, in the mesial sides of its buccal roots (especially over the coronal thirds) and its root trunk as well as the distal side of its palatal root (particularly at the middle and apical thirds). In the nonrigid and rigid indirect anchorage models (models 2 and 3), the highest compressive hydrostatic stress in the PDL was created in the distopalatal root of the premolars and its values were 0.0149 and 0.00859 MPa, respectively. If the compressive hydrostatic stress is greater than 0.0047 MPa, the risk of root resorption is largely increased [46, 47]. Therefore, in the nonrigid model, we expect more resorption in the teeth of the anchorage unit due to the greater movement and compression of these teeth against the bone. In the direct anchorage model, the maximum compressive hydrostatic stress was 0.0015 MPa in the premolars, which was less than the resorption threshold and well tolerated.

In the study of Nihara et al. [66], to determine the most desirable force system for the protraction of mandibular molars using a miniscrew in the interradicular area in the buccal side of the mandible, a power arm was used on the molars at different lengths (2 to 10 mm). The position of the miniscrew in different models was placed up to 8 mm more apical than the level of the gingival margin of the second molar (with vertical intervals of 2 mm). They concluded that mesiodistal tipping decreased with increasing the power arm length to 8 mm; at the 10 mm length, distal crown tipping occurred despite the mesial force, but the buccolingual displacement changed less and remained a buccal tipping [66]. In the direct anchorage model of our study, using a power arm, the force was applied near the center of resistance. In this model, the average and maximum movement in the mesial direction were less than other models in which the force was applied farther from the center of resistance of the molar.

In our study, the application of 150 g force in the rigid indirect anchorage model resulted in 0.129 MPa of stress in the spongy bone, and in the nonrigid indirect anchorage model resulted in 0.107 MPa of stress in the spongy bone; this higher stress in the rigid model can play a role in miniscrew failure. It was found that factors such as the connection of ligature wire or elastomeric chain increase the risk of miniscrew failure through plaque accumulation: plaque builds up around the elastomeric chain, leading to more inflammation around the miniscrew and more failure [67].

Besides root resorption, there is bone resorption risk as well. According to previous studies, increasing the level of stress and pressure can disrupt periosteal blood supply and lead to necrosis and bone resorption [68–70]. In this study, we preferred to calculate bone stresses rather than deformities. Since the model is considered having a linear elastic behavior, there is total reciprocity between strain (deformity) and stress; in other words, any strain level (that causes microdamage or other failure types caused by deformation) can be replaced with a corresponding stress level. Thus, we felt it would be more appropriate to calculate stresses (instead of deformities) for the sake of greater simplicity and comprehensibility of the outcomes and their interpretations. Moreover, there was no "stress or strain threshold" for the objective calculation of cancellous bone resorption in the literature. Therefore, we had to stick with the PDL pressure which has an objective threshold for root resorption and hence is examinable scientifically and objectively.

SS ligatures are very soft and malleable wires made from deadsoft wires [14]. In previous studies, different values were reported for the elastic modulus of this wire: it was reported 8500 MPa, 130000 MPa for 0.007-inch diameter, and 140000 MPa for 0.011-inch diameter [34]. In various FEA studies, different moduli of elasticity had been used, such as 160 gigapascals [35], 168 gigapascals [36], 176 gigapascals [37], 180 gigapascals [38], and 200 gigapascals [39, 40]. In the present study, with increasing ligature rigidity, the palatal and distal movements of the premolars decreased and their intrusive movement increased. In other words, with the increase in rigidity of the ligature wire, the resistance to anchorage loss was increased. The increase in the premolar intrusive displacement might seem to be caused due to the apical direction of the connection of the anchorage teeth to the miniscrew. As wire rigidity increased, the extrusion and palatal movement of the molar decreased as well, which

might be related to the increased resistance of the ligature wire to movements. Molar mesialization was slightly enhanced by increasing the wire rigidity. The increase in the ligature wire rigidity might not much reduce the risk of root resorption. No similar study was available to compare our results with.

In the first model, the distal movement of the root of the second premolar could be seen; it was very small and was caused by the spread of force and the stretching of the gingival fibers and hence not posing any serious anchorage loss risk. This distal movement was much smaller than the mesial movement of the root of the second molar. In the buccolingual axis (X-axis), the palatal displacement of the mesial half of the root of the second molar and the buccal displacement of the distal half of the root of the second molar can be seen. In fact, the rotation of the tooth took place around the vertical axis. But in the second premolar region, the palatal displacement of the root of the second premolar is observed, and the magnitude of this displacement is reduced towards the apical side. The amount of molar movement is more than the premolar. It seems that because the force is applied directly to the second molar, the greatest movement should be expected in it. In the vertical axis (Z-axis), an extrusive movement can be seen in the region of the root of the second premolar, which decreases toward the apical side. In the mesiobuccal root of the second molar, the movement is intrusive, while in the distobuccal and palatal roots of the second molar, the movement is extrusive. The average displacement of the second molar is greater than the second premolar.

In the second model, the distal displacement of the second premolar root and the mesial displacement of the molar root can be seen in the Y-axis. In both teeth, the magnitude of this displacement decreases towards the apical. It should be noted that the amount of molar root movement is greater than the amount of second premolar root movement. In this model, the lingual displacement of the second premolar root and the lingual displacement of the molar's mesiobuccal root and the buccal displacement of its distobuccal and palatal roots can be seen in the X-axis. The lingual displacement of the second premolar is less than that of the second molar, which seems reasonable considering the existence of a full-sized rigid wire that prevents the movement of the premolar. In the Z-axis, the intrusive movement of the premolar roots can be seen, which increases toward the apical end. In the second molar region, in the mesiobuccal root, the movement is mainly intrusive, and in the distobuccal and palatal roots, the movement is mainly extrusive. The amount of displacement of the molar root is greater than that of the premolar, which is due to the restraint caused by the rigid connecting wire between the miniscrew and the second premolar tooth.

In the third model, in the Y-axis, these movements were noted: the distal displacement of the root of the second premolar (toward the apical side, the magnitude of this displacement decreases); the mesial displacement of the buccal roots of the second molar; and the distal displacement of the palatal root of the second molar. In fact, the rotation of the second molar is observed around the vertical axis. Molar root movement is greater than premolar root movement. In X- and Z-axes, the displacement pattern observed is similar to the rigid model.

Hence, overall, it can be said that in direct anchorage, the highest amount of root displacement is observed in the second molar roots; in the premolars, the amount of displacement is very small, practically without anchorage loss. The total displacement of the root of the second premolar is distopalatal and extrusive, while the second molar roots are rotated around the vertical axis (i.e., the buccal roots were mesialized and the palatal root was distalized); furthermore, the mesiobuccal part of the second molar was intruded, while distobuccal and palatal parts were extrusion. In rigid anchorage and nonrigid anchorage, it is again observed that the root displacement of the second molar is greater than that of the premolar. In these two types of anchorage, the types of movements observed in the root area were similar to direct anchorage; with the difference that in premolar roots, the movement is intrusive (which seems to be due to the presence of a connecting wire between the tooth and the miniscrew).

One of the limitations of this finite element study is the simplification of modeling the complex tissues and structures. For example, bone properties are assumed to be isotropic and time-independent linear elastic, which differs from bone behavior in the clinic. In addition, FEA disregards numerous parameters such as various patients' sexes, ages, statures, or genetics. Anatomy and structural properties vary from person to person. This examination is essentially a static analysis which is hard to generalize to clinical situations; hence, its implementation and interpretation need cautious decision-making [71]. Furthermore, FEA may not simulate long-term kinetics of tooth movement, needing slow and quite complicated biological alterations in live tissues like remodeling of the PDL and bone [72]. Thus, future clinical studies are needed to assess our results. However, the finite element method is advantageous over clinical or even in vitro studies, as it can provide a very precise and detailed overview of the mechanics of the whole system and each of its parts, not possible with any other approach. Applying biologically comprehensible and multifaceted in silico simulations may allow the prediction of root resorption risk and also the clarification of some mechanisms underlying orthodontic tooth movement [73].

5. Conclusions

Within the limitations of this FEA simulation, the following could be concluded:

(1) The miniscrew stress and the spongy bone stress were much larger in the direct anchorage compared to the indirect anchorage models

(2) The lowest miniscrew and cancellous bone stresses were seen in the nonrigid indirect anchorage model

(3) Palatalization of the premolars in the nonrigid indirect anchorage model was considerably greater than the rigid one. Between the indirect anchorage

models, the nonrigid anchorage model had a greater root intrusion

(4) In the indirect models, there might be some risk of root resorption of the anchorage teeth, and this might be greater in the nonrigid indirect anchorage compared to the rigid one. In the direct model, the greatest compressive and tensile hydrostatic stresses were observed in the PDL parts around the miniscrew

(5) Hydrostatic pressure patterns of the molar PDLs might be rather similar in the three tested models, with the tensile stress concentrating in the distal sides of the mesiobuccal and distobuccal roots and the mesial side of the palatal root, and compressive hydrostatic pressures seen on the mesial sides of the buccal roots, on the mesial side of the root trunk, and on the distal side of the palatal root. The compressive stresses were the lowest and highest in the direct anchorage and rigid indirect anchorage models, respectively; however, extents of tensile stresses were similar

(6) The miniscrew load of 150 g might not break the titanium body of the implant in any of the three models. However, the miniscrew and bone stresses imply a higher risk of miniscrew loosening in the direct anchorage model and a lower one in the nonrigid indirect anchorage method. Therefore, it seems that when the bone quality around the mini-implant is not appropriate, shifting to the nonrigid indirect anchorage paradigm might be preferable to avoid a high risk of miniscrew failure

(7) Using ligature wire increases the risk of anchorage loss and root resorption in the anchorage unit

(8) Between the two indirect anchorage methods, the rigid one might provide a greater extent or rate of molar protraction

(9) The direct anchorage method is more likely to provide a bodily (but slower maximum) movement of the molar compared to the indirect anchorage methods

(10) Increasing the rigidity of the connecting wire in the nonrigid indirect anchorage method might slightly accelerate the mesialization of the second molar, while reducing the risk of anchorage loss

Data Availability

All data are presented as the article tables and figures.

Conflicts of Interest

The authors declare no conflict of interest.

Acknowledgments

The study was self-funded by the authors and their institutions. The authors express their sincere gratitude to Mr. Mojtaba Hasani for his contributions to FEA analyses.

Supplementary Materials

Supplementary Tables 1 to 5 present the details of parametric simulations. *(Supplementary Materials)*

References

[1] G. Risse, "The angulation of upper 1st permanent molars, the key to functional occlusion," *Artikel Fach Journal*, vol. 1, pp. 1–9, 2005.

[2] R. E. Moyers, *Handbook of orthodontics*, Year Book Medical Publishers, 1988.

[3] A. Hatami and C. Dreyer, "The extraction of first, second or third permanent molar teeth and its effect on the dentofacial complex," *Australian dental journal*, vol. 64, no. 4, pp. 302–311, 2019.

[4] M. A. Mohammed and K. M. Mohamed, "Three-dimensional stress analysis with two molar protraction techniques using finite element modeling," *Journal of the World Federation of Orthodontists*, vol. 7, no. 3, pp. 89–93, 2018.

[5] W. R. Proffit, H. W. Fields, and D. M. Sarver, *Contemporary Orthodontics*, Elsevier Health Sciences, 2006.

[6] S.-J. Cheng, I.-Y. Tseng, J.-J. Lee, and S.-H. Kok, "A prospective study of the risk factors associated with failure of mini-implants used for orthodontic anchorage," *International Journal of Oral & Maxillofacial Implants*, vol. 19, no. 1, pp. 100–106, 2004.

[7] K. Seung-Hyun, L. Jung-Ki, and P. Young-Chel, "The use of miniscrew as an anchorage for the orthodontic tooth movement," *Korean Journal of Orthodontics*, vol. 31, no. 4, pp. 415–424, 2001.

[8] H. Liu, X. Wu, L. Yang, and Y. Ding, "Safe zones for miniscrews in maxillary dentition distalization assessed with cone-beam computed tomography," *American Journal of Orthodontics and Dentofacial Orthopedics*, vol. 151, no. 3, pp. 500–506, 2017.

[9] W. A. J. Proffit, *Diagnosis and Treatment Planning Orthodontics: Current Principals and Treatment*, Mosby, St Louis MO, 1994.

[10] P. I. Brånemark, R. Adell, U. Breine, B. O. Hansson, J. Lindström, and A. Ohlsson, "Intra-osseous anchorage of dental prostheses. I. Experimental studies," *Scandinavian Journal of Plastic and Reconstructive Surgery*, vol. 3, no. 2, pp. 81–100, 1969.

[11] F. Celenza, "Implant-enhanced tooth movement: indirect absolute anchorage," *The International Journal of Periodontics & Restorative Dentistry*, vol. 23, no. 6, pp. 533–541, 2003.

[12] A. J. Haas, "Palatal expansion: just the beginning of dentofacial orthopedics," *American Journal of Orthodontics*, vol. 57, no. 3, pp. 219–255, 1970.

[13] C. Nishio, A. F. J. da Motta, C. N. Elias, and J. N. Mucha, "In vitro evaluation of frictional forces between archwires and ceramic brackets," *American journal of orthodontics and dentofacial orthopedics.*, vol. 125, no. 1, pp. 56–64, 2004.

[14] W. R. Proffit, H. W. Fields, D. M. Msd, B. Larson, and D. M. Sarver, "Contemporary Orthodontics," in *South Asia Edition-E-Book*, Elsevier India, 6th edition, 2019.

[15] M. K. Alam, *A to Z Orthodontics: Anchorage*, PPSP Publication, Kota Bharu, Malaysia, 2012.

[16] K. Rungcharassaeng, J. Kan, and J. M. Caruso, "Implants as absolute anchorage," *Journal of the California Dental Association*, vol. 33, no. 11, pp. 881–888, 2005.

[17] W. Tsui, H. Chua, and L. Cheung, "Bone anchor systems for orthodontic application: a systematic review," *International journal of oral and maxillofacial surgery*, vol. 41, no. 11, pp. 1427–1438, 2012.

[18] A. Alkadhimi and E. A. Al-Awadhi, "Miniscrews for orthodontic anchorage: a review of available systems," *Journal of Orthodontics*, vol. 45, no. 2, pp. 102–114, 2018.

[19] F. Janssens, G. Swennen, T. Dujardin, R. Glineur, and C. Malevez, "Use of an onplant as orthodontic anchorage," *American journal of orthodontics and dentofacial orthopedics*, vol. 122, no. 5, pp. 566–570, 2002.

[20] M. A. Papadopoulos and F. Tarawneh, "The use of miniscrew implants for temporary skeletal anchorage in orthodontics: a comprehensive review," *Oral Surgery, Oral Medicine, Oral Pathology, Oral Radiology, and Endodontology*, vol. 103, no. 5, pp. e6–e15, 2007.

[21] K. Becker, A. Pliska, C. Busch, B. Wilmes, M. Wolf, and D. Drescher, "Efficacy of orthodontic mini implants for en masse retraction in the maxilla: a systematic review and meta-analysis," *International journal of implant dentistry*, vol. 4, no. 1, pp. 1–12, 2018.

[22] Y. Chen, H. M. Kyung, W. T. Zhao, and W. J. Yu, "Critical factors for the success of orthodontic mini-implants: a systematic review," *American Journal of Orthodontics and Dentofacial Orthopedics*, vol. 135, no. 3, pp. 284–291, 2009.

[23] S. Baumgaertel, C. L. Jones, and M. Unal, "Miniscrew biomechanics: guidelines for the use of rigid indirect anchorage mechanics," *American Journal of Orthodontics and Dentofacial Orthopedics*, vol. 152, no. 3, pp. 413–419, 2017.

[24] C. Holberg, P. Winterhalder, N. Holberg, I. Rudzki-Janson, and A. Wichelhaus, "Direct versus indirect loading of orthodontic miniscrew implants—an FEM analysis," *Clinical oral investigations*, vol. 17, no. 8, pp. 1821–1827, 2013.

[25] M. Razavi, "Indirect anchorage using the palate: a unique application of the Unitek Temporary Anchorage Device," *Orthodontic Perspectives*, vol. 17, no. 2, pp. 6–9, 2010.

[26] U. Fritz, A. Ehmer, and P. Diedrich, "Clinical suitability of titanium microscrews for orthodontic anchorage—preliminary experiences," *Journal of Orofacial Orthopedics/Fortschritte der Kieferorthopädie*, vol. 65, no. 5, pp. 410–418, 2004.

[27] T. Eroğlu, B. Kaya, A. Çetinşahin, A. Arman, and S. Uçkan, "Success of zygomatic plate-screw anchorage system," *Journal of oral and maxillofacial surgery*, vol. 68, no. 3, pp. 602–605, 2010.

[28] J. Bird and C. Ross, *Mechanical engineering principles*, Routledge, 2014.

[29] A. G. Crismani, M. H. Bertl, A. G. Čelar, H.-P. Bantleon, and C. J. Burstone, "Miniscrews in orthodontic treatment: review and analysis of published clinical trials," *American Journal of Orthodontics and Dentofacial Orthopedics*, vol. 137, no. 1, pp. 108–113, 2010.

[30] C. Holberg, P. Winterhalder, N. Holberg, A. Wichelhaus, and I. Rudzki-Janson, "Indirect miniscrew anchorage: biomechanical loading of the dental anchorage during mandibular molar protraction—an FEM analysis," *Journal of Orofacial Orthopedics/Fortschritte der Kieferorthopädie*, vol. 75, no. 1, pp. 16–24, 2014.

[31] M. Alves Jr., C. Baratieri, and L. I. Nojima, "Assessment of mini-implant displacement using cone beam computed tomography," *Clinical oral implants research*, vol. 22, no. 10, pp. 1151–1156, 2011.

[32] L. Lo Russo, K. Zhurakivska, G. Montaruli et al., "Effects of crown movement on periodontal biotype: a digital analysis," *Odontology*, vol. 106, no. 4, pp. 414–421, 2018.

[33] D. K. Agarwal, A. Razdan, A. Agarwal, P. Bhattacharya, A. Gupta, and D. Kapoor, "A comparative study of orthodontic coil springs," *Journal of Indian Orthodontic Society*, vol. 45, no. 4, pp. 160–168, 2011.

[34] T. R. Katona and J. Chen, "Engineering and experimental analyses of the tensile loads applied during strength testing of direct bonded orthodontic brackets," *American Journal of Orthodontics and Dentofacial Orthopedics*, vol. 106, no. 2, pp. 167–174, 1994.

[35] R. Kothari, S. Gupta, E. Bhambri, S. Ahuja, and A. Bharadwaj, "Expression of torque and its effect on various biological structures caused by varying archwire material: a 3D FEM study," *Journal of Indian Orthodontic Society*, vol. 56, no. 1, pp. 63–70, 2022.

[36] J. Liu, D. Zhang, L. Xu et al., "Mechanical force system of double key loop with finite element analysis," *BMC Oral Health*, vol. 21, no. 1, pp. 1–10, 2021.

[37] Q. Xie and D. Li, "The cross-sectional effects of ribbon arch wires on class II malocclusion intermaxillary traction: a three-dimensional finite element analysis," *BMC Oral Health*, vol. 21, no. 1, pp. 1–9, 2021.

[38] S. Verma, A. K. Mathur, T. K. Balan, P. Keerthana, and P. Chitra, "Finite element analysis evaluation of forces generated with Damon Q and MBT conventional appliances," *Journal of Contemporary Orthodontics*, vol. 4, no. 2, pp. 16–24, 2020.

[39] S. J. Kim, Y. H. Kwon, and C. J. Hwang, "Biomechanical characteristics of self-ligating brackets in a vertically displaced canine model: a finite element analysis," *Orthodontics & craniofacial research*, vol. 19, no. 2, pp. 102–113, 2016.

[40] Y. Huang, L. Keilig, A. Rahimi et al., "Numeric modeling of torque capabilities of self-ligating and conventional brackets," *American Journal of Orthodontics and Dentofacial Orthopedics*, vol. 136, no. 5, pp. 638–643, 2009.

[41] A. Hohmann, C. Kober, P. Young et al., "Influence of different modeling strategies for the periodontal ligament on finite element simulation results," *American Journal of Orthodontics and Dentofacial Orthopedics*, vol. 139, no. 6, pp. 775–783, 2011.

[42] C. Dorow, N. Krstin, and F.-G. Sander, "Determination of the mechanical properties of the periodontal ligament in a uniaxial tensional experiment," *Journal of Orofacial Orthopedics/Fortschritte der Kieferorthopädie*, vol. 64, no. 2, pp. 100–107, 2003.

[43] Y. Kojima and H. Fukui, "A numerical simulation of tooth movement by wire bending," *American journal of orthodontics and dentofacial orthopedics*, vol. 130, no. 4, pp. 452–459, 2006.

[44] C. N. Elias, D. J. Fernandes, F. M. de Souza, M. E. dos Santos, and R. S. de Biasi, "Mechanical and clinical properties of

titanium and titanium-based alloys (Ti G2, Ti G4 cold worked nanostructured and Ti G5) for biomedical applications," *Journal of Materials Research and Technology*, vol. 8, no. 1, pp. 1060–1069, 2019.

[45] H. Kumar, *Evaluation of the shear bond strength of three types of retainer wires bonded with a composite adhesive: an in vitro study*, Rajiv Gandhi University of Health Sciences, Bengaluru, Karnataka, 2019.

[46] C. Dorow and F.-G. Sander, "Development of a model for the simulation of orthodontic load on lower first premolars using the finite element method," *Journal of Orofacial Orthopedics/Fortschritte der Kieferorthopädie*, vol. 66, no. 3, pp. 208–218, 2005.

[47] A. Hohmann, U. Wolfram, M. Geiger et al., "Periodontal ligament hydrostatic pressure with areas of root resorption after application of a continuous torquemMoment," *The Angle Orthodontist*, vol. 77, no. 4, pp. 653–659, 2007.

[48] S.-H. Kyung, J.-H. Choi, and Y.-C. Park, "Miniscrew anchorage used to protract lower second molars into first molar extraction sites," *Journal of clinical orthodontics: JCO*, vol. 37, no. 10, pp. 575–579, 2003.

[49] A. Ringane and R. Hattarki, "Comparison of stress distribution on bone and mini-implants during en-masse retraction of maxillary anterior teeth in labial and lingual orthodontics: a three-dimensional finite element analysis," *Indian Journal of Health Sciences and Biomedical Research*, vol. 11, pp. 130–135, 2018.

[50] U. B. Baik, "Molar Protraction: Orthodontic Substitution of Missing Posterior Teeth," in *Temporary skeletal anchorage devices: a guide to design and evidence-based solution*, K. B. Kim, Ed., pp. 119–160, Springer, Berlin, Heidelberg, 2014.

[51] M. Tepedino, M. A. Cornelis, C. Chimenti, and P. M. Cattaneo, "Correlation between tooth size-arch length discrepancy and interradicular distances measured on CBCT and panoramic radiograph: an evaluation for miniscrew insertion," *Journal of Orthodontics*, vol. 23, no. 5, p. 39.e1, 2018.

[52] K. O. Marusamy, S. Ramasamy, and O. Wali, "Molar protraction using miniscrews (temporary anchorage device) with simultaneous correction of lateral crossbite: an orthodontic case report," *Journal of International Society of Preventive & Community Dentistry*, vol. 8, no. 3, pp. 271–276, 2018.

[53] S. Hemmatpour, M. Oonchi, S. Karami, and G. Nahvi, "Temporary anchorage device as an innovative alternative for unilateral arch mesialization in medical application," *Biointerface Research in Applied Chemistry*, vol. 11, no. 2, pp. 8825–8835, 2020.

[54] G. Lemieux, A. Hart, C. Cheretakis et al., "Computed tomographic characterization of mini-implant placement pattern and maximum anchorage force in human cadavers," *American journal of orthodontics and dentofacial orthopedics*, vol. 140, no. 3, pp. 356–365, 2011.

[55] A. Jain, R. Hattarki, P. Patel, V. Khandelwal, and J. Sapre, "Comparison of stress distribution in bone and miniscrew and displacement pattern of maxillary anterior teeth by two methods of en-masse retraction: a 3-D finite element analysis," *Indian Journal of Orthodontics and Dentofacial Research*, vol. 3, no. 1, pp. 23–30, 2017.

[56] N. Brezniak and A. Wasserstein, "Root resorption after orthodontic treatment: part 1. Literature review," *American Journal of Orthodontics and Dentofacial Orthopedics*, vol. 103, no. 1, pp. 62–66, 1993.

[57] A. Hohmann, U. Wolfram, M. Geiger et al., "Correspondences of hydrostatic pressure in periodontal ligament with regions of root resorption: a clinical and a finite element study of the same human teeth," *Computer methods and programs in biomedicine*, vol. 93, no. 2, pp. 155–161, 2009.

[58] A. M. Schwarz, "Tissue changes incidental to orthodontic tooth movement," *International Journal of Orthodontia, Oral Surgery and Radiography*, vol. 18, no. 4, pp. 331–352, 1932.

[59] A. Schwarz, "Das biologische Verhalten orthodontisch beanspruchter Zähne," *Ztschr f zahnärztl Orthopaedie*, vol. 4, 1929.

[60] E. J. Speckmann, "Generation of field potentials in the brain," *The Journal of Clinical Pharmacology*, vol. 37, no. S1, pp. 8S–10S, 1997.

[61] R. Faltin, K. Faltin, F. Sander, and V. Arana-Chavez, "Ultrastructure of cementum and periodontal ligament after continuous intrusion in humans: a transmission electron microscopy study," *The European Journal of Orthodontics*, vol. 23, no. 1, pp. 35–49, 2001.

[62] R. M. Faltin, V. E. Arana-Chavez, K. Faltin, F.-G. Sander, and A. Wichelhaus, "Root resorptions in upper first premolars after application of continuous intrusive forces," *Journal of Orofacial Orthopedics/Fortschritte der Kieferorthopädie*, vol. 59, no. 4, pp. 208–219, 1998.

[63] M. A. Casa, R. M. Faltin, K. Faltin, F.-G. Sander, and V. E. Arana-Chavez, "Root resorptions in upper first premolars after application of continuous torque moment intra-individual study," *Journal of Orofacial Orthopedics/Fortschritte der Kieferorthopädie*, vol. 62, no. 4, pp. 285–295, 2001.

[64] J. Zhong, J. Chen, R. Weinkamer et al., "In vivo effects of different orthodontic loading on root resorption and correlation with mechanobiological stimulus in periodontal ligament," *Journal of the Royal Society Interface*, vol. 16, no. 154, p. 20190108, 2019.

[65] B. W. Lee, "Relationship between tooth-movement rate and estimated pressure applied," *Journal of dental research*, vol. 44, no. 5, p. 1053, 1965.

[66] J. Nihara, K. Gielo-Perczak, L. Cardinal, I. Saito, R. Nanda, and F. Uribe, "Finite element analysis of mandibular molar protraction mechanics using miniscrews," *European journal of orthodontics*, vol. 37, no. 1, pp. 95–100, 2015.

[67] R. Joshi, T. R. Shyagali, R. Jha, A. Gupta, A. Tiwari, and T. Tiwari, "Evaluation and comparison of the effect of elastomeric chain and stainless steel ligature wire on maxillary orthodontic miniscrew failure," *International Journal of Applied and Basic Medical Research*, vol. 11, no. 2, pp. 100–105, 2021.

[68] C. Misch, "Contemporary implant dentistry," *Implant Dentistry*, vol. 8, no. 1, p. 90, 1999.

[69] H. E. Lura, "Tissue reactions of bone upon mechanical stresses," *American Journal of Orthodontics*, vol. 38, no. 6, pp. 453–459, 1952.

[70] R. W. Treharne, "Review of Wolff's law and its proposed means of operation," *Orthopaedic Review*, vol. 10, pp. 35–47, 1981.

[71] Ç. Sakin and Ö. Aylikci, "Techniques to measure miniscrew implant stability," *Journal of Orthodontic Research*, vol. 1, no. 1, p. 5, 2013.

[72] M. Moradinejad, M. Yazdi, R. Chaharmahali, M. Araghbidikashani, S. Bagheri, and V. Rakhshan, "Efficiency and side effects of a novel method for maxillary central root torque (a horizontal box loop of round wire) in comparison with the conventional rectangular wire: a finite element study," *American Journal of Orthodontics and Dentofacial Orthopedics*, vol. 161, no. 2, pp. e172–e186, 2022.

[73] P. M. Cattaneo and M. A. Cornelis, "Orthodontic tooth movement studied by finite element analysis: an update. What can we learn from these simulations?," *Current Osteoporosis Reports*, vol. 19, no. 2, pp. 175–181, 2021.

Hindawi
BioMed Research International
Volume 2022, Article ID 6706392, 25 pages
https://doi.org/10.1155/2022/6706392

Research Article

Dynamics, Efficacies, and Adverse Effects of Maxillary Full-Arch Intrusion Using Temporary Anchorage Devices (Miniscrews): A Finite Element Analysis

Marzieh Mazhari,[1] **Mashallah Khanehmasjedi**,[1] **Mohsen Mazhary**,[2] **Nastaran Atashkar**,[1] **and Vahid Rakhshan**[3]

[1]*Department of Orthodontics, School of Dentistry, Ahvaz Jundishapur University of Medical Sciences, Ahvaz, Iran*
[2]*Department of Civil and Environmental Engineering, ACECR Institute for Higher Education, Ahvaz, Iran*
[3]*Department of Anatomy, Dental School, Azad University of Medical Sciences, Tehran, Iran*

Correspondence should be addressed to Nastaran Atashkar; atashkar.n@ajums.ac.ir

Received 3 April 2022; Revised 27 August 2022; Accepted 16 September 2022; Published 8 October 2022

Academic Editor: Shivam Mehta

Introduction. Absolute anchorages obtained from temporary anchorage devices (TADs, miniscrews) considerably facilitate dental movements and make some very difficult movements such as full-arch intrusions possible. Despite the significance of assessing strategies to fully intrude the arch using mini-implants, there is no study in this regard except a few case reports. Therefore, we simulated/tested 4 scenarios. *Methods*. Four maxilla models were created with different miniscrews/appliances: (1) two miniscrews were placed distal to laterals and one in the mid sagittal region. (2) Two mini-implants were inserted in mesial of canines and 2 others between bilateral first and second molars, plus another TAD in the midpalatal area, plus a transpalatal arch (TPA). (3) Two mini-implants were inserted between bilateral canines and first premolars and 2 others between bilateral first and second molars + TPA. (4) Two mini-implants were installed between lateral-and-canine and 2 miniscrews between second premolars and first molars + TPA. Intrusive forces (80 g anterior, 150 g posterior) were exerted using stainless-steel coil springs. Stresses/displacements were measured. Risk of external root resorption was evaluated. *Results*. The highest amounts of incisor/molar intrusion were seen in model 1. Model 2 had fewer intrusions, but its control over undesired movements was greater. Model 4 drastically reduced molar intrusion and considerably increased premolar intrusion. Overall amounts of intrusion were highest in the first 2 models, marking them as proper candidates for cases needing greater intrusion extents. Model 2 may be useful when miniscrew loosening/failure is a concern, while model 1 is recommended when fewer miniscrews are allowed. Overall, the highest and lowest root resorptions might occur in models 1 and 4, respectively. *Conclusions*. Each model showed certain efficacies/drawbacks and thus is recommended for a particular set of cases. Therefore, depending on the diagnosis and treatment plan, one or more of these scenarios might be desirable.

1. Introduction

Excessive gingival display, also known as "gummy smile," is an esthetic concern among dental patients, because it is generally considered unpleasant and causes many patients to seek treatment for this problem [1]. A gummy smile, in which more than 3 to 4 mm of gingival tissue is exposed when smiling, causes an esthetic disharmony. Anatomical landmarks that play a role in creating a gingival smile include the maxilla, lips, gingival structures, and teeth [1]. To achieve a beautiful smile, all these anatomical structures must be in harmony with each other [1]. The various causes of gummy smile are altered passive eruption of teeth, dentoalveolar extrusion, vertical maxillary excess, short or hyperactive muscles of the upper lip, or a combination of them [2].

Altered passive eruption can be corrected with crown lengthening surgery, which can be achieved through

gingivectomy or apically positioned flap. When the hyperactive upper lip is the main cause of gummy smile, surgical or nonsurgical methods (botulinum toxin injection) can be used for treatment [3].

However, gummy smiles caused by dentoalveolar and maxillary height etiologies are much more difficult to handle. In the past, dentoalveolar extrusion and increased maxillary height could only be corrected through orthognathic surgery, which is an invasive procedure [3]. However, with the advent of temporary skeletal anchorage devices (TADs), it has been reported that in some cases, gummy smiles caused by dentoalveolar extrusion and increased maxillary height can be corrected [3, 4]. Some case reports have shown that a miniscrew can achieve the same effect as maxillary impaction with Le Fort I surgery, and this way a gummy smile can be corrected with the full intrusion of the maxillary arch [5].

Dental intrusion is often an integral part of orthodontic treatment because it improves the sagittal and vertical relationships of the incisors, corrects the angle between the incisors and subsequently the gingival line, and restores the beauty of the smile [6]. Nikolai defines intrusion as a form of translational tooth movement that moves apically along the longitudinal axis of the tooth, while Burstone defines it as the apical movement of the geometric radicular center relative to the occlusal plane or a plane defined based on the long axis of the tooth [7–9].

Despite the significance of strategies to fully intrude the arch (and correct the gummy smile caused by dentoalveolar extrusion and vertical maxillary excess) using absolute anchorages provided by mini-implants, there is no study in this regard except a couple of case reports [3–5]. Therefore, we aimed to simulate, for the first time, four different strategies of full arch intrusion using TADs and study their dynamics, efficacies, and potential adverse effects (such as the risk of root resorption, indicated by an excessively high PDL hydrostatic pressure which can collapse the capillaries and impair blood flow [10, 11]).

2. Materials and Methods

This study was an experimental 4-phase in silico simulation. First, the models were created and then loaded.

2.1. Modeling in the Mimics and 3-Matic Programs. Models of the bones, teeth, and PDLs were modeled in Mimics 3D image processing program (Mimics Research 21; Materialise NV; Brussels, Belgium) and 3-Matic software (Materialise). For this purpose, CT scan slices with an interslice distance of 1 mm (NewTom VGi; Finland) were fed into Mimics. Segmentation tools were used to create masks for the teeth, bones, and PDLs. Afterwards, the Calculate 3D command was used to create a 3D model of these elements. Next, the export functions of these programs were used to create all these parts in the ".stl" format.

To design the mini-implants, the Helix and Revolution commands of the Solidworks program (version 2018, Dassault Systemes; Paris, France) were used. For designing the orthodontic wires and brackets, the ANSYS program (ANSYS Workbench 2021, ANSYS Inc., Canonsburg, Pennsylvania, USA) was used. Finally, the elements were assembled together in the ANSYS environment. The titanium miniscrews were self-drilling and conical square threaded.

2.2. Geometry Conversion in the Geomagic Program. The Geomagic program (3D Systems, Morrisville, North Carolina, United States) was used to convert the parts exported in the ".stl" format from the Mimics and 3-Matic programs (Materialise) into "parts" in the ".stp" format.

2.3. Analysis in the ANSYS Program. Following altering all components to the ".stp" format, they were opened by ANSYS Workbench 2021 (ANSYS Inc.) for simulations.

2.4. Simulation Models. All models designed in this study were a simulation of the full arch intrusion of maxillary teeth. The thickness of the periodontal ligament was assumed to be uniformly 0.25 mm, and the alveolar bone crest was constructed following the curvature of the cementoenamel junction (CEJ), 1 mm apical to the CEJ. Prescription brackets were designed based on the 0.022-inch-slot MBT system. The position of the brackets on the teeth was also based on this system. A stainless steel (SS) $0.019' \times 0.025'$ archwire was crated as the archwire in all models. The arch form was designed as oval. The midpoints of the incisal edge of the tips of the buccal cusps and the apex of the roots were used as landmarks to assess the extent of displacement. The occlusal plane was defined by connecting the midpoint of the central incisal edge and the mesiobuccal cusp of the first molar. The teeth, alveolar bone, brackets, periodontal ligament, and archwires were constructed using fine tetrahedron solid elements, and all isoparametric and linear elastic objects were assumed to be homogeneous. Owing to the displacement of the dentition within the basal bone, the model was limited to the nasal floor of the alveolar bone in all directions. The connection between the miniscrew and the bone was defined as a tight tie in all models. The miniscrew movements were negligible and thus were not reported.

Four different models were created with the above general descriptions and the following specifics (Figure 1). Two of them were inspired by two case reports [4, 12], but the other two were designed by the authors. In all models, the length of miniscrews were based on earlier references [4, 12, 13].

2.4.1. Model 1. This model was partly derived from a case report [4]. Two miniscrews with a diameter of 1.6 mm and a length of 6 mm were placed distally to the lateral teeth along with closed stainless-steel (SS) coil springs for the intrusion of the maxillary anterior teeth. For the intrusion of the incisors, 80 grams of force was applied on each side. A palatal TAD (6 mm long, 1.8 mm in diameter) was placed in the mid sagittal region, parallel to the palatal root of the first molar. For molar intrusion, 150 g of force was applied on each side (Figure 1).

2.4.2. Model 2. Four buccal miniscrews with a diameter of 1.6 and 6 mm were installed: two screws were placed in the

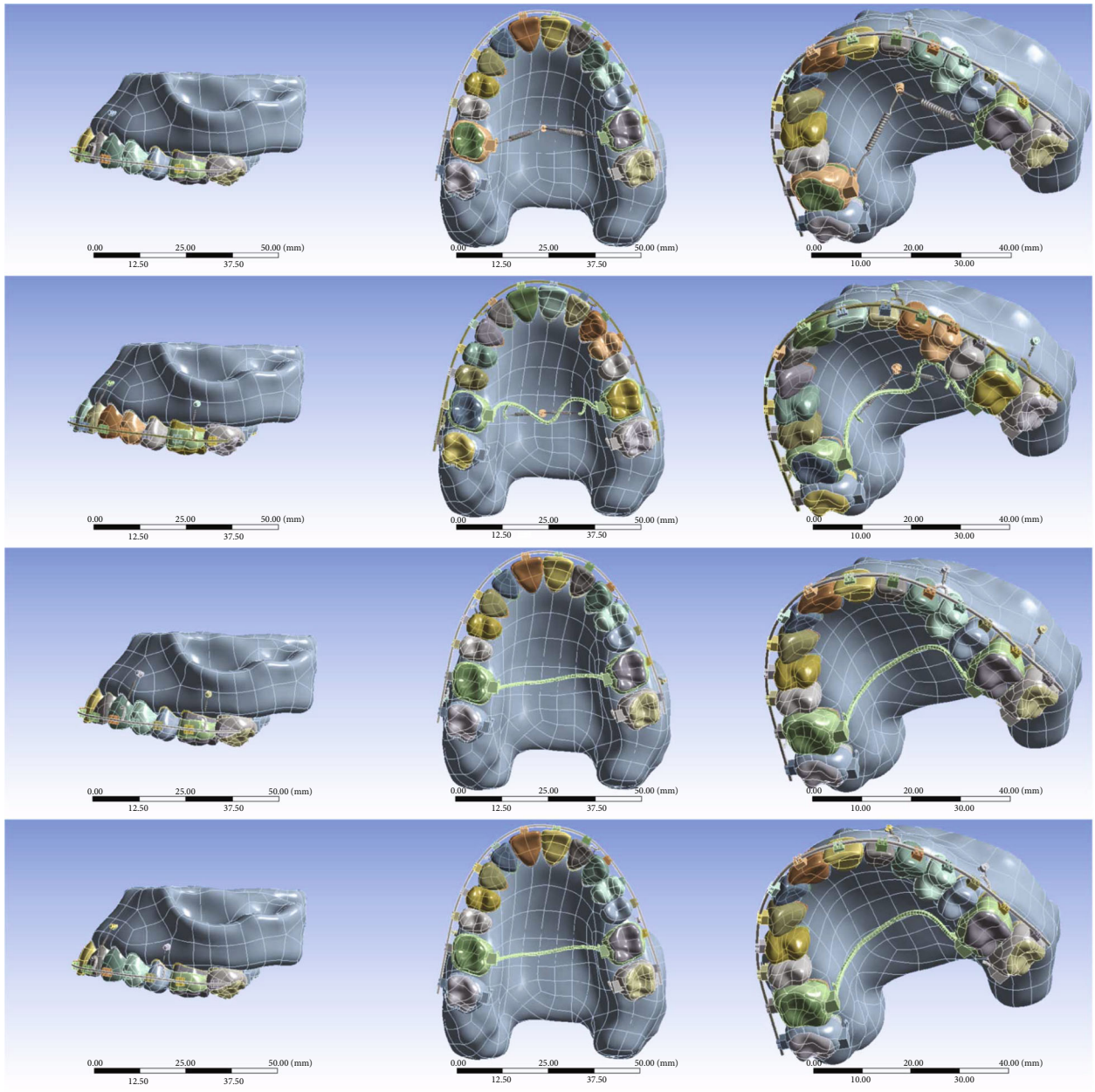

Figure 1: The models in use. From top to bottom: models 1, 2, 3, and 4.

mesial side of the canines and two screws between the first molar and the second molar. An 80 g force was exerted from each screw using SS closed coil springs. A mini-implant (with a diameter of 1.8 mm and a length of 5 mm) was inserted in the midpalatal; 80 grams of force was applied on each side of it with SS closed coil springs. A transpalatal arch (TPA) of 0.9′ wire was also placed (Figure 1).

2.4.3. Model 3. This model was inspired by a case report [12]. In this model, two miniscrews were placed between the maxillary canines and the first premolars on each side, and two other miniscrews were placed between the first and second maxillary molars (1.6 mm in diameter and 6 mm in length) on each side. Intrusive forces of 80 g in the anterior region and 150 g in the posterior region were applied vertically to the maxillary archwire from the miniscrews through SS closed coil springs. A TPA made of 0.9′ wire was applied as well (Figure 1).

2.4.4. Model 4. This model was rather similar to the 3rd model, apart from the locations of the mini-implants (1.6 mm in diameter and 6 mm in length): The anterior miniscrews were placed between the lateral and canine teeth on each side and between the second premolars and the first molars on each side. Intrusive forces of 80 g in the anterior region and 150 g in the posterior region were applied vertically using closed coil springs. The TPA in use was made of 0.9′ wire (Figure 1).

Table 1: Material properties.

Material	Elastic modulus (MPa)	Poisson ratio
Cortical bone [14]	1000	0.3
Cancellous bone [14]	500	0.3
Dentine [14]	18600	0.3
PDL [15]	0.15	0.45
Stainless steel [16]	200000	0.3
Miniscrew titanium G5 [17]	115000	0.33

2.5. Material Properties. Materials in the models were assigned the properties explained in Table 1 [14–17]. The simulated spring type was SS closed-coil [18] with the following characteristics: wire diameter of 0.010 inch, lumen size of 0.030 inch, initial length range of 4-10 mm, and estimated stiffness of 0.67 N/Sq.mm.

2.6. Meshing. After applying the properties of the components, their meshing, which is one of the main parts of finite element analysis, was performed. To do this, the model was divided into smaller three-dimensional parts called elements, which were made up of a number of nodes. The total number of elements in the model was 133161 tetrahedral elements, and the number of nodes was 252999.

2.7. Boundary Conditions. In the next step, boundary conditions were applied: in this step, the fixed parts of the model were identified and forces were applied to the model. The maxilla was immobilized at its upper surface (Figure 2).

2.8. Outcomes. The duration for finite element simulations was 1 second. The created and loaded models were compared regarding hydrostatic stresses of PDLs, von Mises stresses, and displacements of all the components. Several methods can be used to explain tooth displacement, two of which are used in this study. Tooth movement can be described based on the displacement of each tooth and its bracket, meaning that an axis of local coordinates is drawn at the location of the bracket. Another way is to use an external reference such as a global coordinate system [19]. We used both of these systems to illustrate the movements of the teeth in the 3D space. The global axes were defined as follows: The Y-axis was the posterior-anterior axis with positive values indicating posterior movements and negative values indicating anterior movements. The X-axis was the lateral movement (right-left) axis, with positive values indicating the displacement towards the patient's left side, while negative values indicating the movement towards the patient's right side. The Z-axis was for the vertical movement, with positive values indicating intrusion (upward movement) and negative values indicating extrusion (downward movement). The local axes were defined individually for each tooth: The vertical axis was defined as exactly the global Z (vertical) axis. The mesiodistal axis was defined as the axis pointing from the distal (negative) to the mesial (positive) of each tooth. The buccolingual (or buccopalatal) axis was defined as the axis pointing from the buccal (negative) to the palatal (positive) of each tooth.

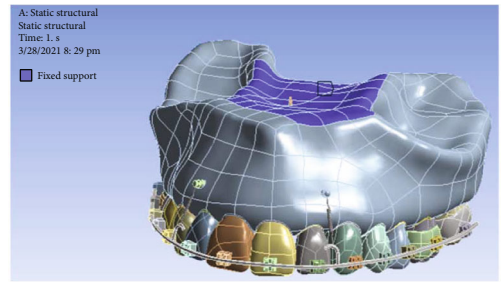

Figure 2: The fixed support of the maxilla.

It is suggested that if the PDL hydrostatic pressure exceeds the capillary pressure in the area, the vessels will collapse and blood flow to that area will be impaired, increasing the risk of root resorption. Capillary pressure in the PDL is estimated to be about 0.002 to 0.005 MPa [11]. Therefore, compressive hydrostatic stresses at the PDLs were compared with -0.0047 MPa as a threshold for a significant increase of the risk of external root resorption [10, 11].

3. Results

3.1. Miniscrew Stresses

3.1.1. Model 1. The palatal miniscrew endured more stresses than the two buccal miniscrews. The maximum stress in a great part of the buccal miniscrews was about 1 MPa. In the cervical and middle thirds of the buccal miniscrews, sections with a stress of up to 3 MPa were also seen. The minimum stress (up to 1 MPa) was seen in the head of the palatal miniscrew; the stress increased in the neck of the miniscrew and reached a maximum of 3 MPa. In the cervical and middle thirds of the threads, an increased stress and an approximate stress of 4-8 MPa was observed. In the apical part, like the head of the miniscrew, a little stress (up to 1 MPa) was seen (Figure 3, Table 2).

3.1.2. Model 2. In the second model, the stress distribution on the buccal and palatal miniscrews was relatively similar. In most parts of the palatal miniscrew (such as the head, neck, and apex), the maximum stress on the miniscrew was 1 MPa, but in some parts of the threads, the stress was 1-2 MPa. In parts of the buccal miniscrew neck, stress was seen up to a maximum of 2 MPa. Stresses of approximately 2-4 MPa were observed in parts of the threads of the cervical third of the buccal miniscrews (Figure 3, Table 2).

3.1.3. Model 3. In the third model, similar stresses were seen in the buccal miniscrews. In most of the neck of the miniscrews and their cervical half, a stress of 2-6 MPa was observed. At the head of the miniscrews and their apical parts, the maximum stress was 1 megapascal (Figure 3, Table 2).

3.1.4. Model 4. In the fourth model, the stress levels in the miniscrews were relatively similar. Stress was minimal in the head and apical parts of the miniscrews (maximum:

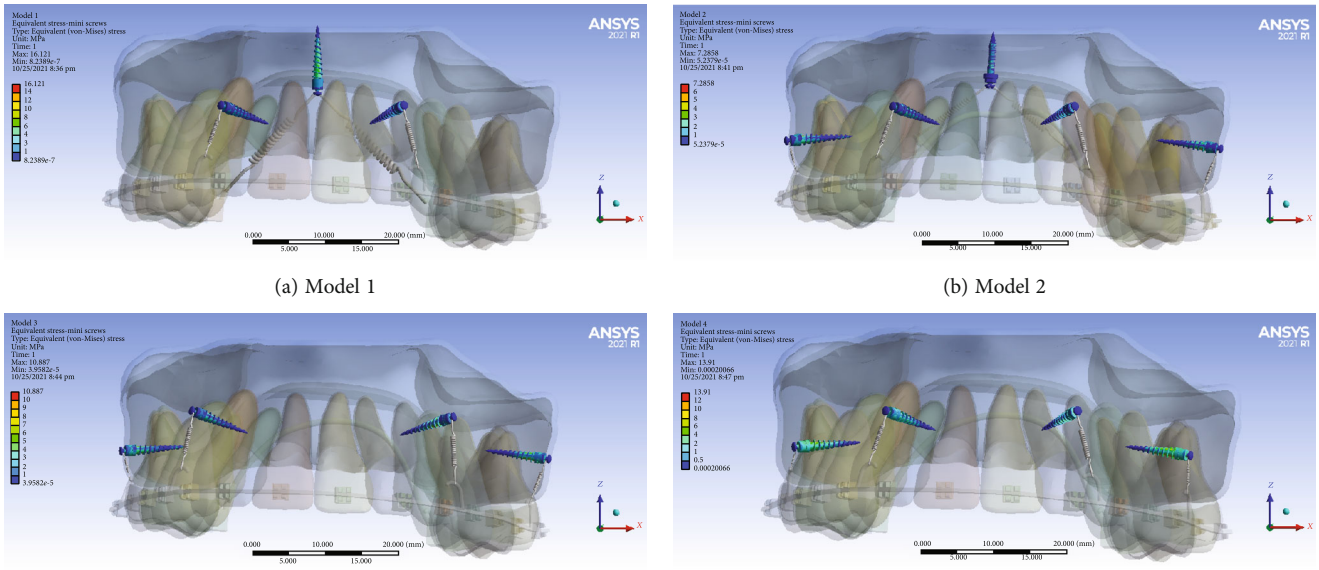

(a) Model 1

(b) Model 2

(c) Model 3

(d) Model 4

Figure 3: Mini-implant stresses (MPa). From top to bottom: models 1, 2, 3, and 4.

0.5 MPa). The stress on the neck of the miniscrew increased to 1-2 MPa. In most of the threads of the cervical half of the miniscrews, a stress of about 1-4 MPa was observed. In a small fraction of the cervical third of each miniscrew, an approximate stress of 4-6 MPa was observed (Figure 3, Table 2).

Palatal mini screw in model 1 tolerated the greatest stress. Buccal miniscrews in model 2 were less stressed than other models (Figure 3, Table 2).

3.2. PDL Hydrostatic Pressure

3.2.1. Model 1. In the anterior teeth and premolars and parts of the second molars such as the palatal root and the palatal part and most of the buccal parts of the buccal roots, periodontal ligament compression was observed at a maximum of 0.002 MPa. The maximum tension was 0.004 which was observed in parts of the second molars. In the cervical and middle parts of the buccal roots of the first molar teeth, tensions up to 0.008 MPa were observed. In the apical parts of the buccal roots, the furca region, and the palatal roots of the first molars, compression zones of about 0.012 MPa were observed. The maximum compressive stress was 0.020 MPa, which was seen in the apical parts of the palatal roots of the first molars. The areas with a high risk of root resorption were the apical parts of the palatal root of the first molars (Figure 4, Table 3).

3.2.2. Model 2. In most of the periodontal ligament of the anterior teeth and second premolars and molars, especially in the apical region and labial surfaces, mostly compression areas were observed. The maximum compressive hydrostatic pressure was 0.002 MPa and the maximum tensile hydrostatic stress was 0.001 MPa. In the mesiobuccal section of the mesiobuccal root of the first molars and the distal root of its distobuccal root, tension with a maximum value of 0.005 MPa was observed. Compression was seen in the cervicobuccal, furca and palatal roots of the first molars. The maximum compression extent was 0.0109 MPa. The cervicobuccal area, the furca, and the palatal root of the first molars were prone to external root resorption (Figure 4, Table 3).

3.2.3. Model 3. Tensile stresses were seen in parts of the periodontal ligament of the central and lateral teeth, and compressive pressures were seen in other parts of the anterior teeth and premolars. The maximum compression was 0.001 MPa, and the maximum tension extent was 0.001 MPa. Tensile stresses were observed in small parts of the second molar with a maximum of 0.001 MPa. But in the major parts of the periodontal ligament of this tooth, compressive pressures were seen. Maximum compression was observed in the cervicobuccal area which was about 0.006. Tensile stresses were observed in small parts of the mesiobuccal root of the first molar and parts of its distobuccal root, the maximum of which was 0.007 MPa. Compression areas were seen in the cervicobuccal, furca, and roots of the first molar. The maximum compressive pressure in the apical parts of the buccal roots was about 0.0152 MPa (Figure 4, Table 3).

3.2.4. Model 4. Tensile stresses were seen on the labial surfaces of the periodontal ligament of the incisors and distoapical sides of the premolars, and compression was seen in parts of the periodontal ligament of the anterior and first premolars and second molars. The maximum compression was 0.001 MPa, and the maximum traction was 0.001 MPa. In a small part of the second premolar periodontal ligament, tensile stresses were observed with a maximum of 0.0038 MPa. Compression of the second premolar periodontal ligament was observed in the cervicobuccal and apical parts, with a maximum value of 0.00501 MPa. In the first molar, tensile stresses were seen in parts of the distal and palatal roots. The cervicobuccal area of the second premolars

Table 2: Stresses of miniscrews (MPa).

Model	Miniscrew	Scope	Min.	Max.	Avg.
1	Palatal	Whole body	0.0000008	16.1210000	1.4865000
		Thread	0.0000008	16.1210000	1.9217000
	Left	Whole body	0.0001052	4.1372000	0.7149800
		Thread	0.0282100	4.1372000	0.7925700
	Right	Whole body	0.0001071	3.9836000	0.7328300
		Thread	0.0068716	3.9836000	0.8668500
2	Palatal	Whole body	0.0000524	7.2858000	0.6973300
		Thread	0.0000524	7.2858000	0.9712000
	Posterior-left	Whole body	0.0001009	5.8670000	0.8523300
		Thread	0.0527440	5.8670000	0.9218400
	Anterior-right	Whole body	0.0003064	4.4316000	0.7194800
		Thread	0.0194830	4.4316000	0.7812000
	Anterior-left	Whole body	0.0002860	4.4129000	0.7308100
		Thread	0.0095590	4.4129000	0.7899000
	Posterior-right	Whole body	0.0001355	5.9749000	0.8340100
		Thread	0.0100770	5.9749000	0.9612800
3	Posterior-left	Whole body	0.0001892	10.7130000	1.6071000
		Thread	0.1332100	10.7130000	1.7457000
	Anterior-right	Whole body	0.0000396	5.6620000	0.9710100
		Thread	0.0112180	5.6620000	1.0831000
	Anterior-left	Whole body	0.0000861	8.2548000	1.3595000
		Thread	0.0356900	8.2548000	1.6299000
	Posterior-right	Whole body	0.0002547	10.8870000	1.5293000
		Thread	0.0269770	10.8870000	1.7300000
4	Posterior-left	Whole body	0.0006735	10.5660000	1.5098000
		Thread	0.0356050	10.5660000	1.7541000
	Anterior-right	Whole body	0.0003839	5.5155000	0.8957400
		Thread	0.0321420	5.5155000	0.9818700
	Anterior-left	Whole body	0.0003572	5.5292000	0.9039300
		Thread	0.0199810	5.5292000	0.9948500
	Posterior-right	Whole body	0.0002007	13.9100000	1.8658000
		Thread	0.0229710	13.9100000	2.2215000

Min: minimum; Max: maximum; Avg: average.

and the apical areas of the buccal roots of the first molars were prone to external root resorption (Figure 4, Table 3).

The average stress of all models was negative and compressive. Model 1 had the greatest average (compressive) hydrostatic stress, while model 4 had the lowest average (compressive) stress. In model 3, the average stress was higher than that in model 2. The cervicobuccal and apical areas of the second premolars and the apical and cervicobuccal areas of the buccal roots of first molars were prone to external root resorption (Figure 4, Table 3).

3.3. Directional Displacements in the Global Y-Axis (Anterior-Posterior)

3.3.1. Model 1. The crowns of the anterior teeth were displaced anteriorly (buccalized) for -0.001 mm, and their roots were displaced posteriorly (palatalized, up to 0.001 mm). The crowns of the premolars were mesialized. Most of their roots were also mesialized, but some apical parts of the roots in the first premolars were distalized. The crown and roots of the second molars were displaced posteriorly (distalized, up to 0.001 mm). The palatal cusps of the first molar teeth were displaced anteriorly (mesially) by a maximum of -0.0044 mm. The buccal part of the first molars moved posteriorly (were distalized) up to 0.002 mm. The buccal roots of the first molar teeth were displaced posteriorly (distalized, up to 0.0036 mm), and the palatal roots were moved anteriorly (mesialized, up to -0.003 mm) (Figures 5 and 6, Table 4).

3.3.2. Model 2. The crowns of the first molar teeth moved posteriorly (distally) and their roots anteriorly (mesially).

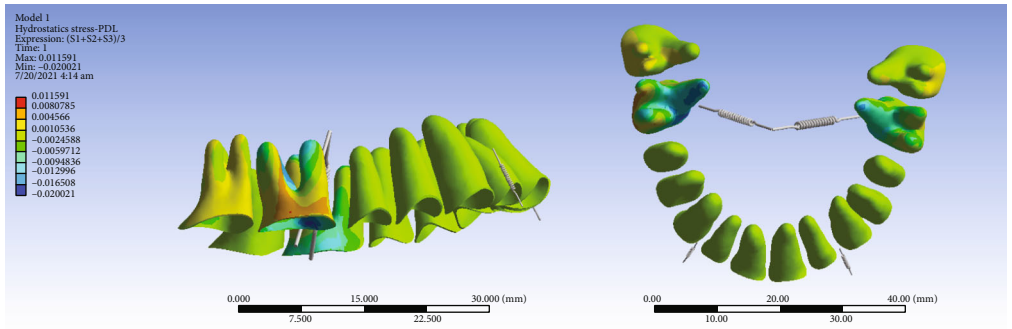

(a) Model 1

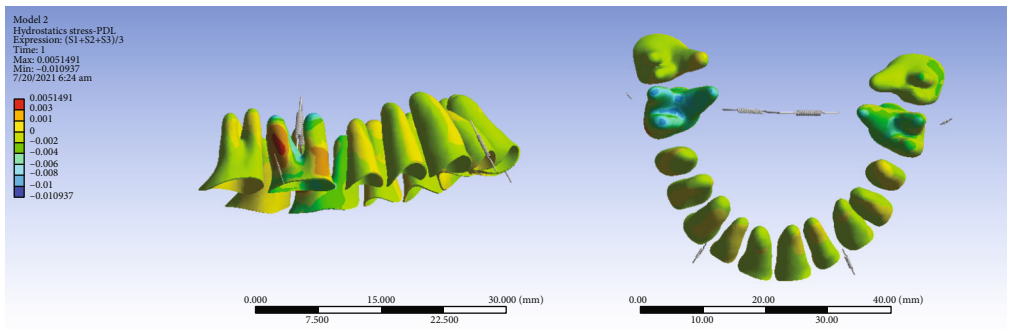

(b) Model 2

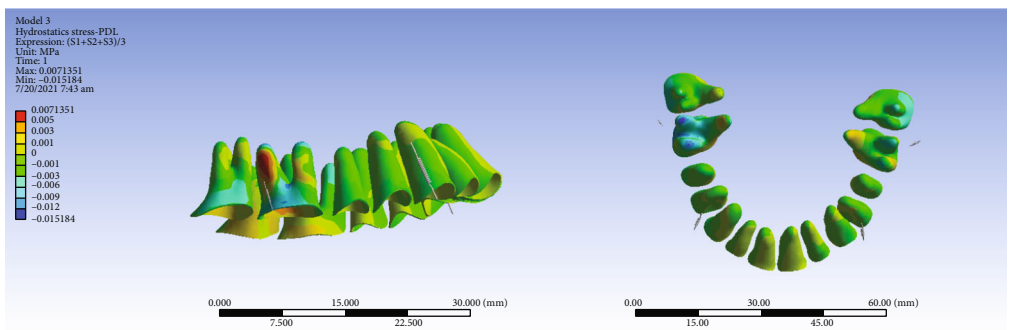

(c) Model 3

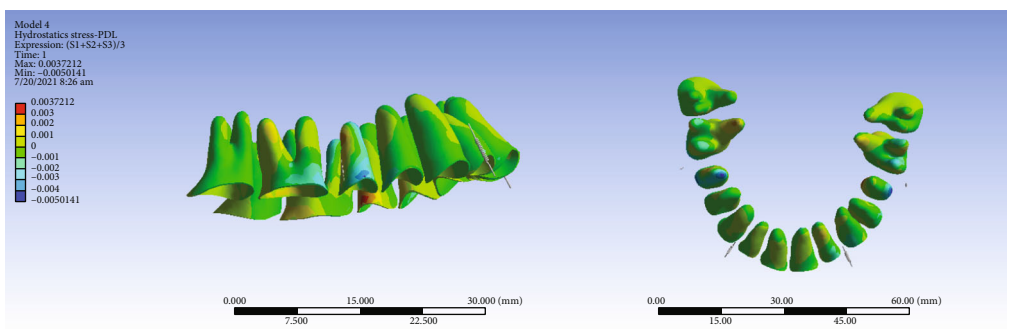

(d) Model 4

Figure 4: PDL hydrostatic stresses (MPa) from the lateral and occlusal views. From top to bottom: models 1, 2, 3, and 4. Positive values indicate tensile stresses while negative values show compressive pressures. Negative values below -0.0047 MPa (i.e., compressive pressures above 0.0047 MPa) pose a considerably higher external root resorption risk.

The maximum displacement was observed in the crown of the first molars (0.0012 mm). The roots of the right first molar were distalized, and the cervical and middle parts of the left first molar were distalized and the apical parts were mesialized. The crowns of the anterior teeth were palatalized for up to 0.0002 mm, and their roots were palatalized for 0.0002 to 0.0006 mm. The second molars were distalized up to 0.0004 mm (Figures 5 and 7, Table 4).

Table 3: Hydrostatic stresses of the PDL (kilopascal (kPa)). Positive values indicate tensile stresses while negative values show compressive pressures. Negative values below -4.7 kPa (i.e., compressive pressures above 0.0047 MPa) pose a considerably higher external root resorption risk.

N	Tooth	Model 1			Model 2			Model 3			Model 4		
		Min.	Max.	Avg.	Min.	Max.	Avg.	Min.	Max.	Avg.	Min.	Max.	Avg.
2	Right second molar	-3.071	3.965	0.635	-1.875	0.922	-0.282	-4.976	2.621	-0.692	-0.868	0.472	-0.105
3	Right first molar	-20.021	11.591	-2.794	-10.937	5.149	-2.378	-15.184	7.135	-2.154	-3.05	2.41	-0.04
4	Right second premolar	-0.769	0.996	0.043	-0.858	0.38	-0.174	-2.69	1.277	-0.657	-5.014	2.832	-0.829
5	Right first premolar	-0.459	0.22	0.003	-0.465	0.151	-0.067	-1.67	0.724	-0.331	-1.737	0.607	-0.248
6	Right canine	-0.926	0.576	-0.139	-0.76	0.663	-0.122	-2.285	0.533	-0.235	-1.21	0.72	-0.172
7	Right lateral	-1.046	0.524	-0.142	-1.066	0.432	-0.111	-0.84	0.593	-0.033	-1.49	0.826	-0.126
8	Right central	-0.913	0.687	-0.201	-0.91	0.372	-0.149	-0.613	0.607	0.007	-1.073	0.273	-0.158
9	Left central	-1.466	0.991	-0.237	-1.03	0.638	-0.187	-0.588	0.498	-0.049	-1.408	1.212	-0.223
10	Left lateral	-2.05	1.279	-0.217	-1.554	0.885	-0.16	-0.766	0.598	-0.047	-2.046	1.673	-0.188
11	Left canine	-1.589	0.415	-0.27	-1.288	0.357	-0.204	-1.811	0.741	-0.26	-2.173	1.09	-0.29
12	Left first premolar	-0.765	0.436	-0.097	-0.352	0.18	-0.069	-1.638	0.92	-0.151	-1.711	1.645	-0.117
13	Left second premolar	-0.492	0.428	-0.001	-0.284	0.121	-0.022	-0.463	0.148	-0.054	-4.752	3.721	-0.2
14	Left first molar	-16.417	7.337	-2.846	-6.945	3.349	-1.638	-6.16	3.527	-0.625	-3.207	2.113	-0.202
15	Left second molar	-1.984	1.832	-0.1	-2.811	0.928	-0.654	-5.56	2.691	-1.124	-0.932	0.779	-0.08

N: tooth number based on the Universal Dental Notation system; Min: minimum; Max: maximum; Avg: average.

3.3.3. Model 3. The anterior teeth and premolars moved slightly to the posterior (palatalized up to 0.004 mm). The premolars were distalized (maximum 0.004 mm). The greatest displacements were seen in the first molars. The roots of the first molars became mesialized (maximum root displacement: -0.0008 mm), and their crowns, especially the palatal cusps, became distalized (maximum crown displacement: 0.0016 mm). The crowns of the second molars were mesialized, and their roots were distalized (Figures 5 and 8, Table 4).

3.3.4. Model 4. The anterior teeth became palatalized: most displacements were at the root apex, and slight displacements were seen at the incisal edge. The highest amount of root palatalization was seen in the apical part of the lateral (up to 0.0009 mm). The crowns of the posterior teeth were mesialized, and their roots became distalized. The greatest displacements were observed in the first molar and premolars (up to 0.0016 mm) (Figures 5 and 9, Table 4).

In the anterior-posterior dimension, the second model and then the third model had the most displacements. The least displacement in this dimension was seen in the fourth model. The differences in displacements of the models 1 and 4 were very small (Figures 6–9, Table 4).

3.4. Displacements on the Global X-Axis (Left-Right)

3.4.1. Model 1. The anterior teeth were mesialized (up to 0.003 mm). The premolars were palatalized (up to 0.003 mm). The crowns of the first molars became palatalized (up to 0.015394 mm), while the apex of their roots became buccalized (up to 0.003 mm) (Figures 5 and 10, Table 5).

3.4.2. Model 2. The posterior teeth became palatalized. In the first molar teeth, the rate of palatalization was the greatest (0.002 mm). The anterior teeth were mesialized up to 0.006 mm (Figures 5 and 11, Table 5).

3.4.3. Model 3. The crowns and roots of the left anterior teeth became mesialized. The crown and root of the right central moved distally. The crown and the cervical and middle parts of the right lateral moved distally, while the apical part moved mesially. The right canine crown was distalized while its root was mesialized. The crowns and roots of the left premolars were palatalized up to 0.001 mm. The crown of the right premolars moved buccally, and their roots moved palatally. The greatest movement was observed in the first molars (maximum displacement: 0.0046 mm). The crowns of the first molars were buccalized up to 0.0046 mm. Their roots became palatalized up to 0.0036 mm. The crowns of the second molars moved towards buccal, and their roots moved palatally (Figures 5 and 12, Table 5).

3.4.4. Model 4. The left central and lateral were mesialized, while the other anterior teeth became distalized. The posterior teeth became buccalized. The displacement rate in most teeth was up to 0.0004 mm. The most extent of movement was observed in the second premolars at 0.00199 mm (Figures 5 and 13, Table 5).

In the X global axis, the highest displacement was seen in model 1, while the lowest displacement was seen in model 2 followed by model 4 (Figures 11–13, Table 5).

3.5. Displacements on the Global Z-Axis (Vertical, Intrusive-Extrusive)

3.5.1. Model 1. In this model, the intrusion was seen in all the teeth except the second molars, the second premolars, and the right first premolar. The second premolars, the right first premolar, and the second molars were extruded (maximum extrusion: 0.002 mm). The maximum average of extrusion

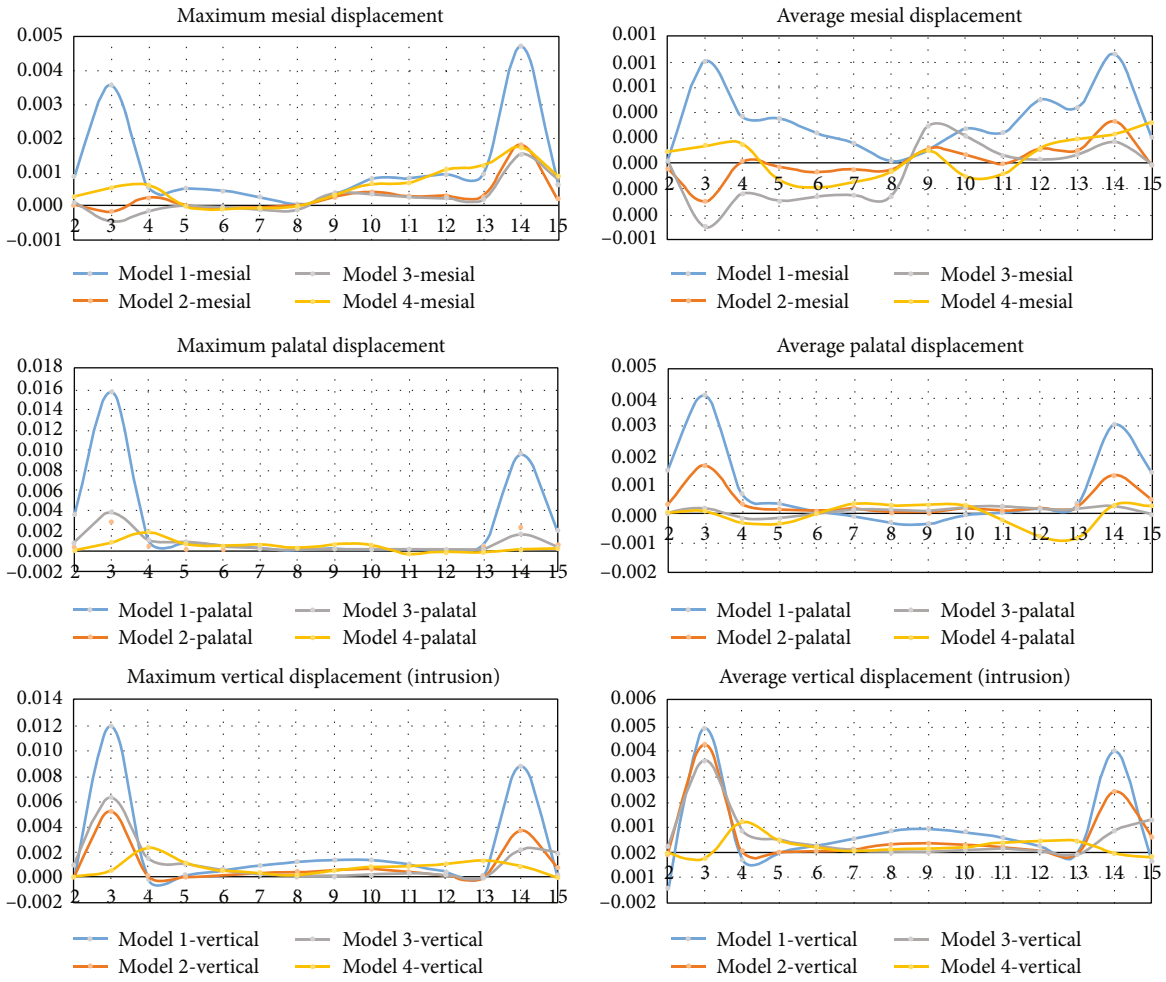

Figure 5: Maximum and average displacements of each of the 14 assessed teeth (mm), in each of the 4 models, in the local directions of mesial, distal, buccal, lingual, intrusive, and extrusive. The tooth numbers 2 to 15 represent the right second molar (#2) to the left second molar (#15), according to the *Universal Dental Notation* system (i.e., the molars are on the sides and the anterior teeth are in the center (the right central = #7, the left central = #8).

was seen in the second molars. The highest amount of intrusion was seen in the first molars. The maximum intrusion occurred in the palatal cusps of the first molars (maximum intrusion: 0.012 mm) (Figures 5 and 14, Table 6).

3.5.2. Model 2. The left second premolar and the second right molar were extruded, but the other teeth were intruded. The maximum amount of intrusion in the anterior teeth was 0.0005 mm. The first molar teeth were intruded more than other teeth, and the amount of intrusion was higher at the palatal surfaces (maximum intrusion: 0.0052 mm) (Figures 5 and 15, Table 6).

3.5.3. Model 3. The anterior teeth were intruded (maximum intrusion: 0.0005 mm). The highest amount of intrusion was observed in the right first molar (maximum displacement: 0.0052 mm). The second left molar showed the second maximum intrusion. Extrusion occurred in the right central and left second premolar (Figures 5 and 16, Table 6).

3.5.4. Model 4. In this model, all teeth except molars were intruded. The highest extent of intrusion was seen in the premolars, especially the second premolar (maximum intrusion: 0.0024 mm). Palatal roots and palatal cusps of the molars were extruded (maximum extrusion: 0.0011 mm, Figures 5 and 17, Table6).

In the vertical dimension, the highest amounts of intrusion were seen in model 1 followed by model 2. The least intrusion occurred in the fourth model (Figures 14–17, Table 6).

The maximum and average extents of movement of each tooth in each model in the local directions of mesial, distal, buccal, lingual, intrusive, and extrusive have been illustrated in Figure 5.

3.6. All Body Stresses

3.6.1. Model 1. The highest level of stress was seen in the archwire between the lateral and canine teeth and between the second premolars, first molars, and second molars. High

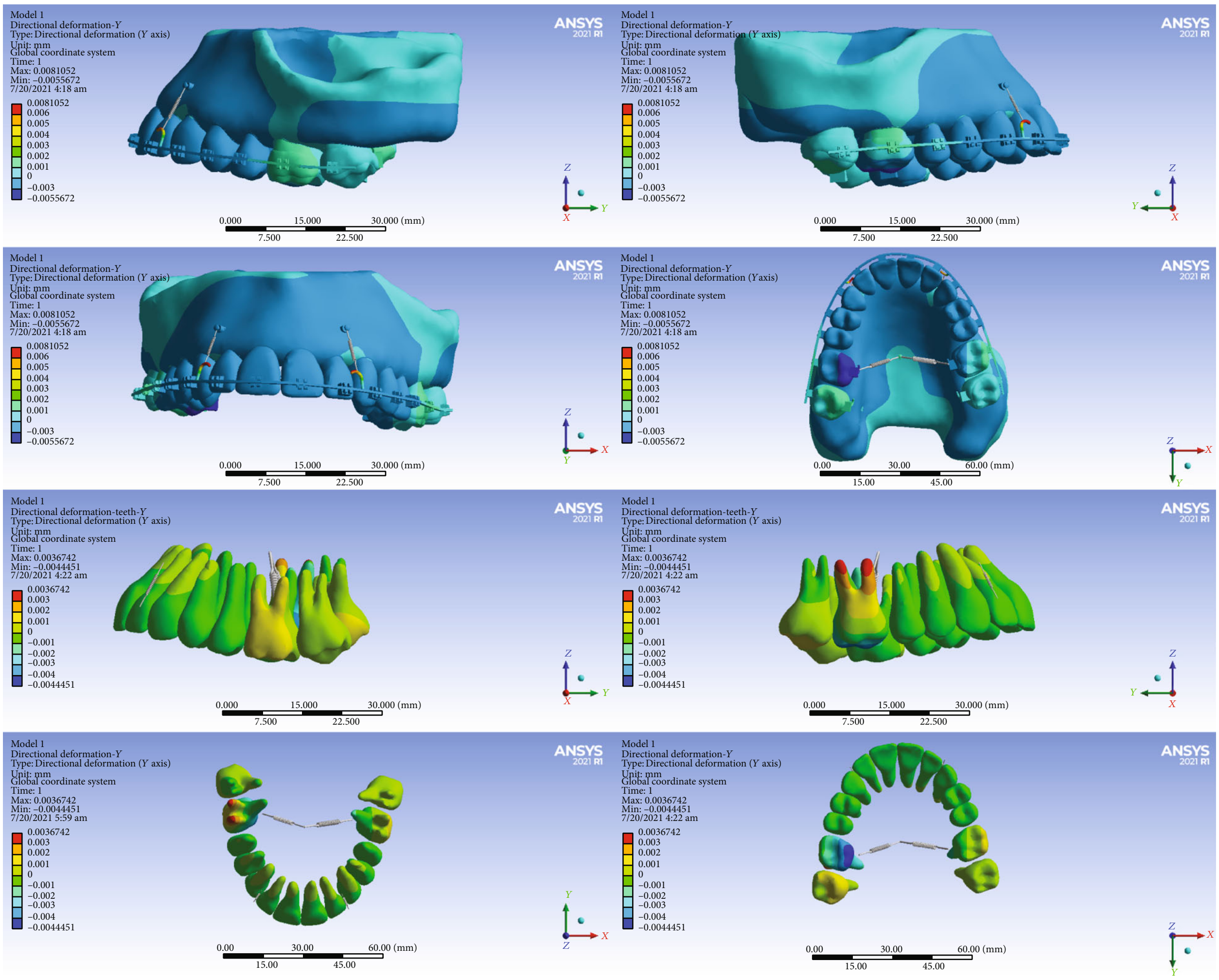

Figure 6: Displacements in the Y global direction (anterior-posterior) in model 1. Negative values indicate anterior movement, while positive values indicate posterior movement.

Table 4: Displacements (μm) in the global Y-axis (anterior-posterior). Positive values indicate posterior movement while negative values indicate anterior movement.

N	Tooth	Model 1			Model 2			Model 3			Model 4		
		Min.	Max.	Avg.	Min.	Max.	Avg.	Min.	Max.	Avg.	Min.	Max.	Avg.
2	Right second molar	-0.8561	1.6522	0.1938	-0.006	0.2233	0.085	-0.2819	0.1539	-0.0182	-0.2702	0.0491	-0.0825
3	Right first molar	-4.4451	3.6742	-0.0588	0.2849	0.94	0.5937	-0.3746	1.6572	0.5277	-0.7248	0.3685	-0.1214
4	Right second premolar	-0.4747	0.0126	-0.1977	-0.205	0.309	0.0653	-0.0903	0.4152	0.1971	-1.0682	0.4264	-0.2206
5	Right first premolar	-0.5514	0.0474	-0.2339	-0.0109	0.1846	0.0715	0.1904	0.2988	0.2404	-0.2016	0.2211	0.0305
6	Right canine	-0.5068	0.1192	-0.1744	-0.0133	0.2091	0.1092	0.1429	0.2944	0.2377	-0.0388	0.3484	0.1678
7	Right lateral	-0.6167	0.2064	-0.1417	-0.0709	0.3835	0.1894	0.1772	0.3291	0.2366	0.0551	0.612	0.3853
8	Right central	-0.7524	0.1524	-0.2853	-0.1219	0.2207	0.0678	0.0292	0.3392	0.1873	0.2208	0.3529	0.3163
9	Left central	-0.7967	0.2976	-0.3204	-0.1778	0.3577	0.0599	-0.0064	0.2915	0.1368	-0.0559	0.6699	0.3281
10	Left lateral	-0.7897	0.4918	-0.1663	-0.2357	0.5366	0.1476	0.0254	0.138	0.0788	-0.4363	0.9696	0.3074
11	Left canine	-0.7273	0.3051	-0.1662	-0.19	0.2689	0.0788	-0.0702	0.2477	0.1039	-0.6953	0.388	-0.0591
12	Left first premolar	-0.7138	0.0996	-0.3635	-0.161	0.1233	-0.0206	-0.1526	0.2661	0.0419	-0.9571	0.1787	-0.4609
13	Left second premolar	-0.6716	-0.0189	-0.2829	-0.1153	0.0619	-0.0012	-0.117	0.0747	0.0094	-1.1324	0.1277	-0.4888
14	Left first molar	-1.3722	1.465	0.1824	-0.9224	1.2803	0.1117	-0.885	1.0071	-0.0743	-1.6125	0.9381	-0.1241
15	Left second molar	0.0343	0.4685	0.2286	-0.004	0.3259	0.1628	-0.6031	0.4833	0.0001	-0.7531	0.1258	-0.2307

N: tooth number based on the Universal Dental Notation system; Min: minimum; Max: maximum; Avg: average.

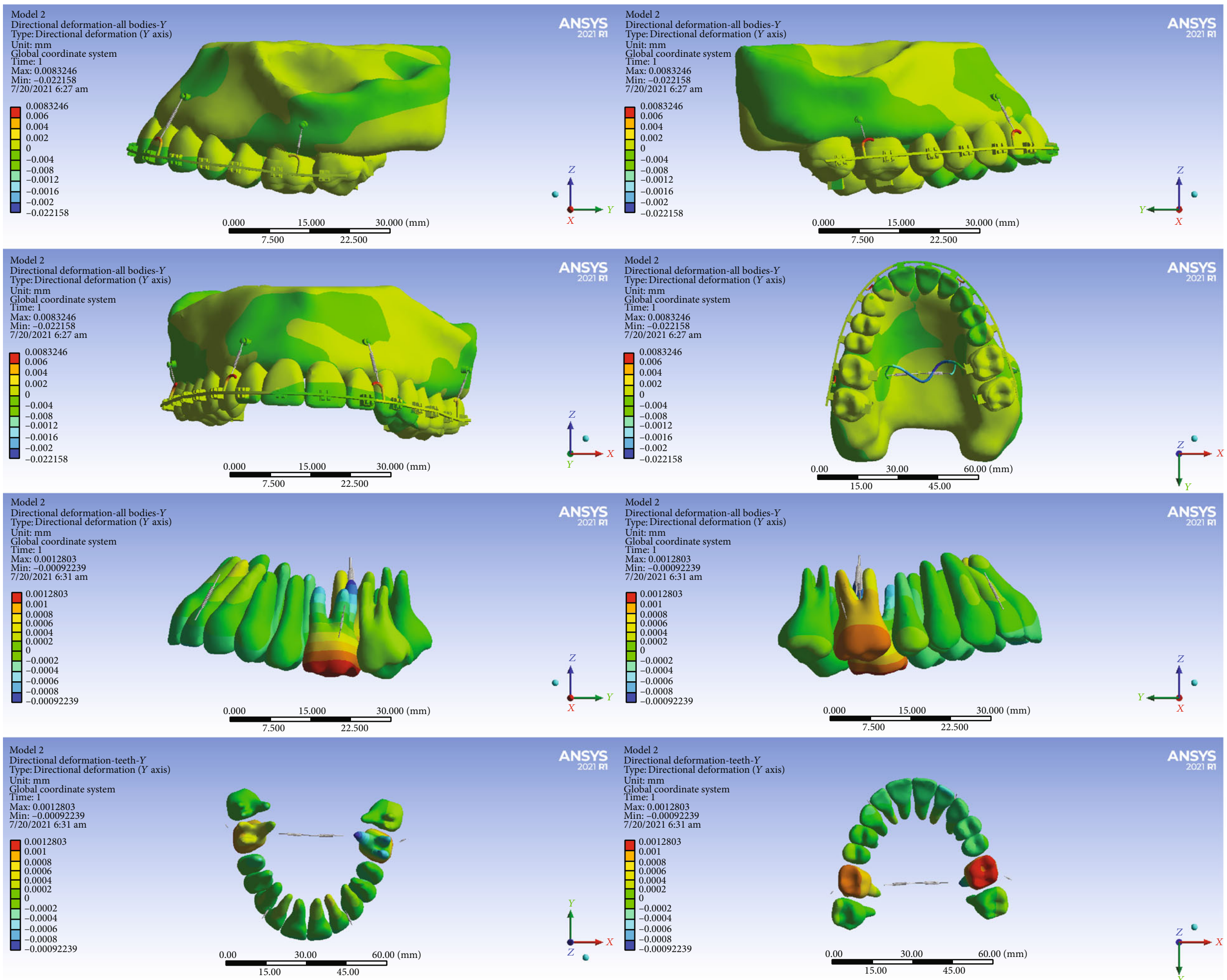

Figure 7: Displacements in the Y global direction (anterior-posterior) in model 2. Posterior movements are positive, while anterior movements are negative.

stresses were also seen in the lingual sheets of the first molar bands. The first and second molars, laterals, and canines tolerated the most stress among all teeth. A similarly high stress was observed in the bone around the miniscrew. Premolars received the least amount of stress (Figure 18).

3.6.2. Model 2. The highest stress was seen in the archwires in the area between the canine and lateral and between the first and second molars and the transpalatal arch. Less stress was exerted to the teeth. Small parts of the first and second molars were subjected to higher stress than other teeth (Figure 19).

3.6.3. Model 3. The highest amount of stress was seen mostly in the archwire between the second molar, first molar, and second molar and also between the canine and first premolar. Most teeth received similar stress levels except some parts of molars and canines that endured greater stresses (Figure 20).

3.6.4. Model 4. The highest stress extents were exerted to the archwire between the lateral and the first molar. The second premolars and first molars suffered the most amounts of stress (Figure 21).

4. Discussion

TADs (temporary anchorage devices) have increased orthodontic treatment capabilities by providing the desired movement of teeth in three dimensions, with their bone support. TADs are used in molar control, incisor segment control, molar distalization, and total arch displacement [19]. TADs are also used to treat skeletal problems. In patients with vertical maxillary excess who have excessive alveolar or gingival display, total arch intrusion is used [20–24]. In a recent review study, the use of miniscrews to reduce gingival appearance and improve gingival smile has been described as effective and practical [25]. The treatment of gingival hyperplasia using a miniscrew, with or without increasing the length of the periodontal crown, has advantages over orthognathic surgery such as lower risks, easier orthodontic biomechanics, less patient discomfort, increased cost-effectiveness, and not increasing the width of the alar base [26]. One of the main uses of TADs is the intrusion of the anterior

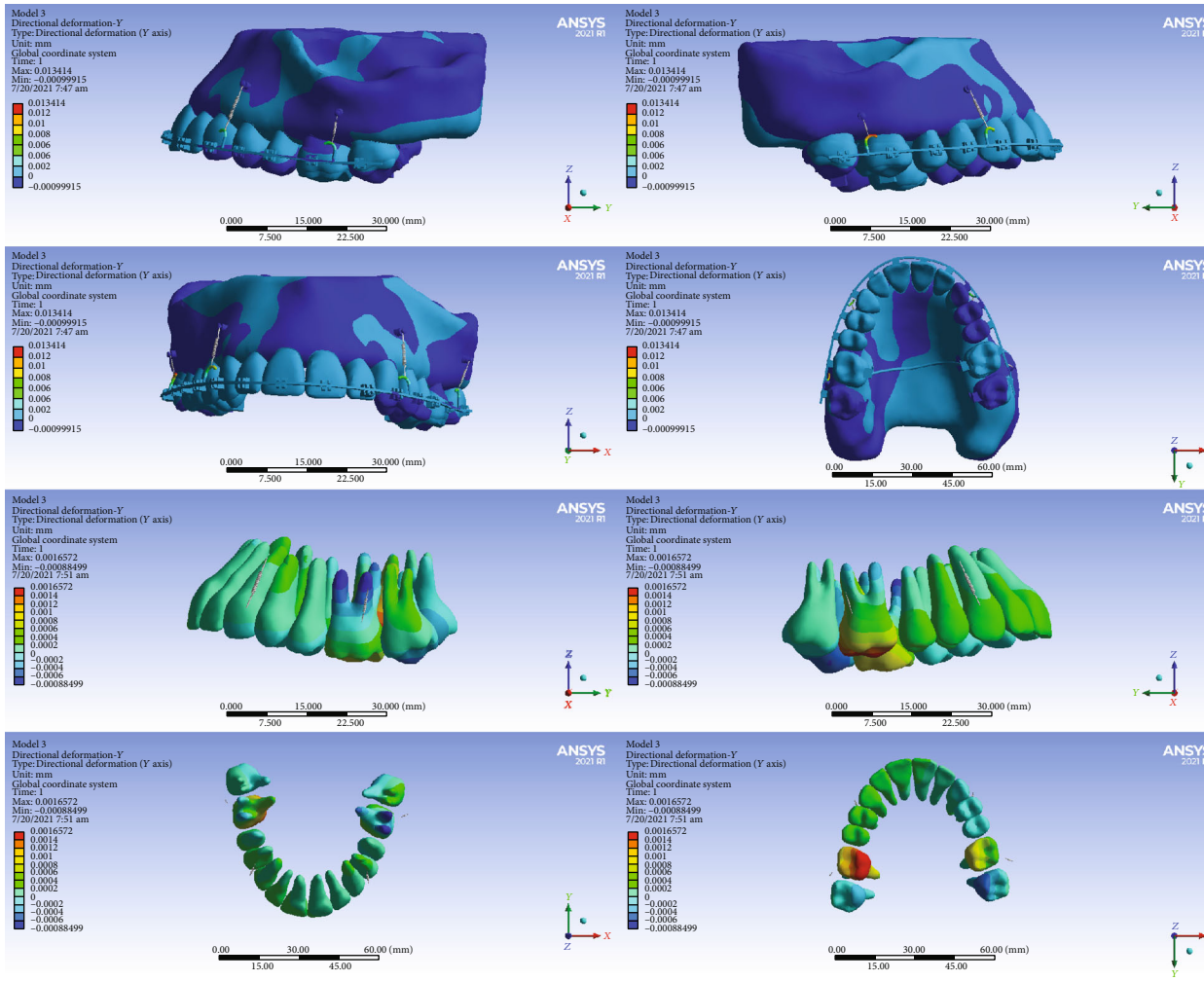

FIGURE 8: Displacements in the Y global direction (anterior-posterior) in model 3. Posterior and anterior displacements are positive and negative, respectively.

teeth in patients with gummy smile: One of the main challenges of orthodontic treatment is the deep overbite correction. In most cases, this correction is caused by extrusion of the posterior teeth or a combination of anterior intrusion with posterior extrusion, which is undesirable in patients with vertical growth. In such cases, absolute anterior intrusion is necessary, especially when there is excessive incisors with extruded teeth. In particular, in cases where orthodontic opening of the posterior teeth using a bite plate or cervical retainer is contraindicated or unsuccessful, deep bite correction is possible only with the intrusion of the anterior teeth. In order to improve esthetics, patients with class 2 malocclusion with increased overjet and short-face height (who show increased gingival exposure of the incisor teeth at rest of the lips) are considered suitable candidates for such intrusion [27].

Comparing the first and second models, it was observed that in the second model, two buccal mini-implants were added in the distal region of the first molars, as well as a TPA. The results show that the addition of buccal force in the molar region does not increase the amount of molar intrusion, and that the molar and incisor intrusions remain higher in the first model. But the side effects of intrusion are reduced in the second model such that the rotation of the molars towards the palatal is reduced and the general mesial movement of the maxillary teeth compared to the first model is well controlled. Additionally, the labial movement of the incisors in the anterior region is also inhibited. Interestingly, despite the similarity of the anterior settings of the two models (#1 and #2), with the addition of posterior miniscrews, the amount of anterior intrusion decreased (without an increase in posterior intrusion). This decrease in anterior intrusion is probably a reaction to the increase in intrusive force at the posterior end of the wire. Comparing the third and fourth models, In model 4, the TADs are placed more mesially than in model 3 (in the third model, the implants are placed in the distal of the canine and molar, while in the fourth model, they are located in the mesial of these teeth). Therefore, in the fourth model, a greater mesial movement is observed in the posterior teeth. The placement of the posterior miniscrews in the mesial of the first molars drastically reduces the amount of molar intrusion. Whereas, in the incisor region, there is no clear difference in the extent of intrusion between the two models. Instead, the more

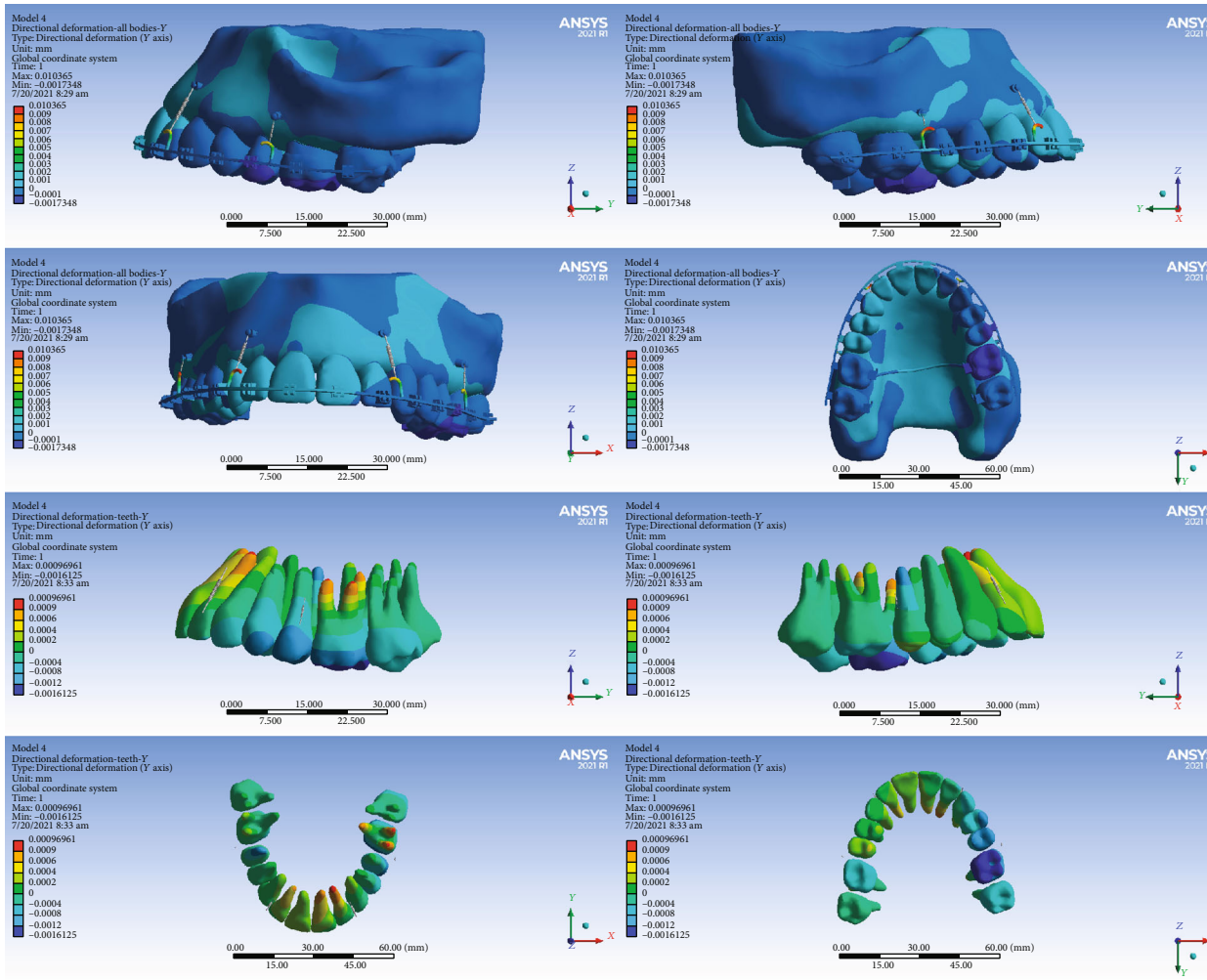

Figure 9: Displacements in the Y global direction (anterior-posterior) in model 4. The displacement to the posterior direction is positive, while anterior movements are negative.

mesial position of the posterior mini-implants in the third model has caused the highest amount of premolar intrusion in this model, in a way that unlike other models (which show the highest amount of dental arch intrusion in the molar area), in the third model, premolars are intruded more than any other tooth.

In this study, the palatal miniscrew in the first model (where a miniscrew was placed in the midpalatal between the first molars and two buccal miniscrews were placed between the laterals and canines) suffered the most stress. Buccal miniscrews in model 2 (which included a miniscrew in the midpalatal space between the first molars and four buccal miniscrews between the laterals and canines and between the molars) were less stressed than the other models. Therefore, it seems that in cases where the failure chance of the miniscrew is likely to be higher (due to the presence of patient-related factors such as younger age or poor oral hygiene [28]), the use of the second model is more useful. On the other hand, where it is necessary to use a smaller number of miniscrews and the stress on the miniscrew is not important, the first model that uses the least number of miniscrews is recommended. In the study of Gracco et al., the maximum stress was seen in the miniscrew head [29]. However, in the study of Fattahi et al. [30], the maximum stress was recorded in the lower parts of the miniscrew neck, which is in line with the present study. In another study [31], the pattern of stress distribution in miniscrews subjected to tooth intrusion was similar to our study. In the present study, the posterior miniscrews suffered more stress, which could be due to greater forces applied to them. The greatest stress among the models has been applied to the palatal miniscrew of the first model. By adding two buccal miniscrews in the second model, the stress of the palatal miniscrews has been reduced by almost half. And in this sense, it can be helpful in increasing the stability of palatal miniscrews.

Intrusion is a movement that makes the tooth prone to root resorption [32, 33]. If hydrostatic pressure exerted on the periodontal ligament is greater than the capillary pressure in the area, blood flow to that area will be impaired. Capillary pressure in the periodontal ligament is estimated to be around 0.002 to 0.005 MPa [11]. Based on the 0.0047-MPa threshold for compressive hydrostatic pressure as a risk factor for root resorption [10, 11], the followings

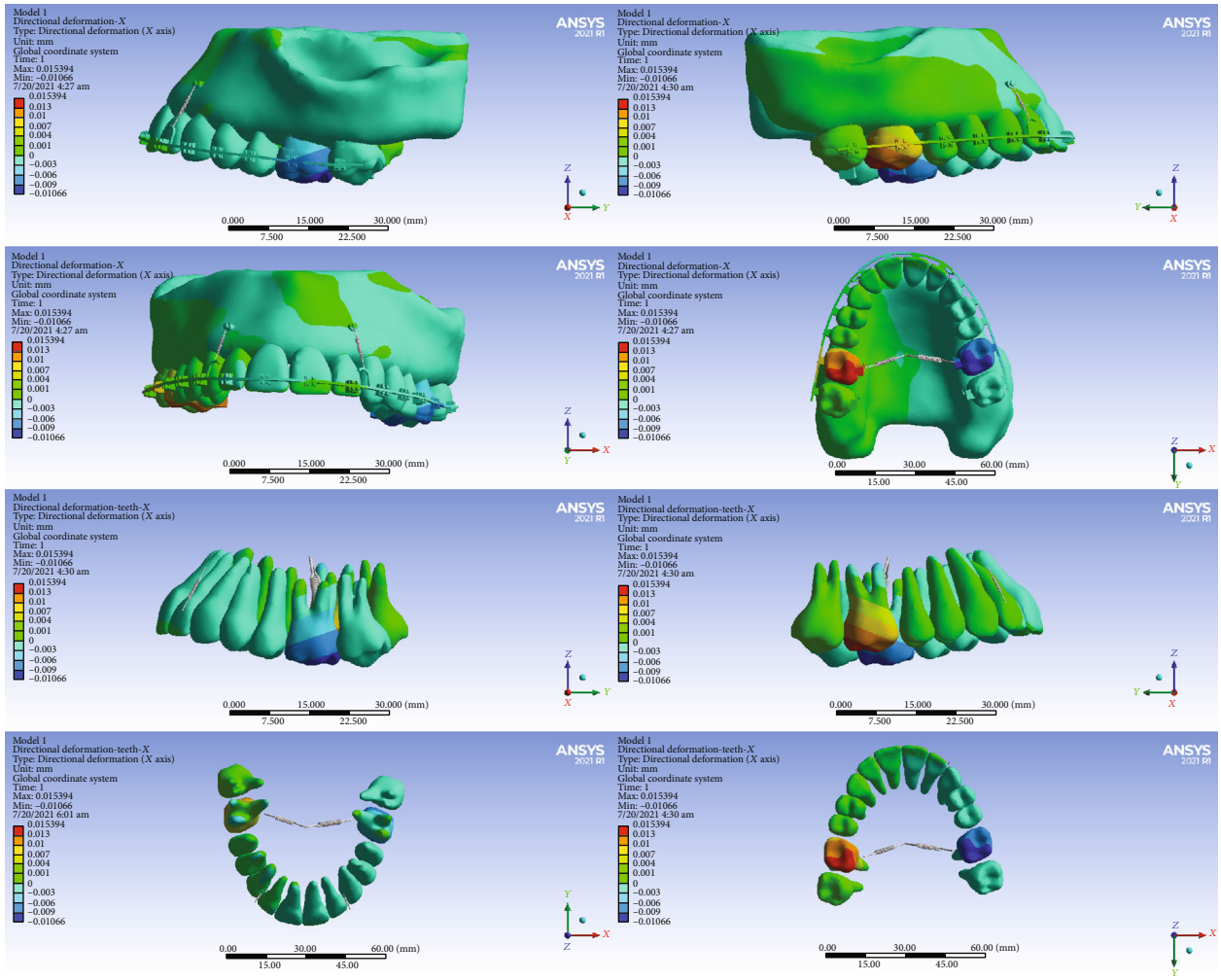

Figure 10: Displacements in the X global direction (left-right) in model 1. Positive values indicate movements to the patient's right side, while negative values indicate movements to the patient's left side.

were found to be areas prone to resorption: in model 1, the apical parts of the palatal root of the first molars; in model 2, the cervicobuccal area, the furca, and the palatal root of the first molars; in model 3, the cervicobuccal area of the second molars and the apical areas of the buccal roots of the first molars; and in model 4, the cervicobuccal and apical areas of the second molars and the apical areas and the cervicobuccal and apical areas of the buccal roots of first molars. In general, it seems that model 1 causes the highest compressive hydrostatic pressure in the periodontal ligament while model 4 causes the least stress, making it the most conservative one. According to Pizzo et al. [34], root resorption is an inflammatory process that leads to local ischemia of the periodontal ligament after applying force and is one of the most common complications of orthodontic treatment. The risk factors related to this complication include treatment-related factors such as the initial overjet size, amount of force, the direction of dental movement, and the method of applying force, treatment duration, and factors related to the patient, such as a person's sex, genetic predisposition, some systemic diseases, anomalies in root morphology, and dental trauma [34, 35]. Maxillary teeth may be more prone to root resorption than mandibular ones [36–39]. Among the maxillary teeth, the incisors are most prone to root resorption [37, 40]. In the maxillary arch, after the incisors, the molars are the next most prone to root resorption [38, 41]. In some studies, it has been stated that root resorption in premolars and molars may be trivial [36–38, 42]. In some studies, it has been reported that the intrusion movement has a great role in root resorption [33, 43–45]. This can be partially explained by the stress endured by the apex during intrusion [33, 46]. On the other hand, some studies did not show a relationship between intrusion and root resorption [33, 43, 47]. In a meta-analysis, it was asserted that the root resorption that occurs during intrusion is clinically within an acceptable range [33]. In the present study, the greatest risk for root resorption was seen in the first molars. In the fourth model, in addition to the first molars, the risk of root resorption was also seen in the second premolars. A higher amount of intrusion was seen in these teeth, which may be an associated with a greater probability of root resorption in these teeth. In an earlier study, the posterior intrusion was examined through the fine element method; they as well found the first molars to be

Table 5: Displacements (μm) in the global X axis (left-right). Positive values indicate displacements to the patient's left side while negative values indicate movements to the patient's right side.

N	Tooth	Model 1			Model 2			Model 3			Model 4		
		Min.	Max.	Avg.	Min.	Max.	Avg.	Min.	Max.	Avg.	Min.	Max.	Avg.
2	Right second molar	0.2216	3.4492	1.5025	0.15	0.4423	0.3237	-1.1963	0.8465	0.0108	0.0213	0.0939	0.0665
3	Right first molar	-4.4648	15.394	4.1755	0.6511	2.8208	1.585	-4.663	3.6657	0.1074	-0.9887	0.8839	0.1123
4	Right second premolar	0.3454	1.1381	0.7602	0.2028	0.4756	0.3382	-1.0895	1.0665	-0.2038	-1.7791	1.8821	-0.2537
5	Right first premolar	-0.0276	0.8414	0.4455	0.0832	0.2457	0.1504	-0.9842	0.9262	-0.2239	-1.1659	0.7048	-0.3645
6	Right canine	-0.0383	0.4762	0.1835	-0.0103	0.1161	0.0649	-0.7483	0.4497	-0.1082	-0.6504	0.4443	-0.0798
7	Right lateral	-0.0088	0.1921	0.1074	-0.08	0.1234	0.0391	-0.4353	0.0502	-0.1622	-0.279	0.2373	0.0282
8	Right central	-0.0831	0.0601	-0.0169	-0.0876	0.0127	-0.0439	-0.3611	-0.0764	-0.2397	-0.1023	0.0357	-0.0276
9	Left central	-0.3474	0.0597	-0.1256	-0.265	0.0096	-0.1182	-0.3741	-0.2147	-0.2896	-0.3244	0.1549	-0.0816
10	Left lateral	-0.4709	0.0706	-0.2204	-0.3466	0.0436	-0.1652	-0.4233	-0.1486	-0.2968	-0.496	0.3966	-0.0569
11	Left canine	-0.3997	-0.0361	-0.1876	-0.2218	-0.0204	-0.102	-0.3367	-0.0542	-0.2432	-0.212	0.805	0.218
12	Left first premolar	-0.6432	-0.0597	-0.3962	-0.3566	-0.0239	-0.2147	-0.199	-0.1038	-0.1569	-0.4772	1.3827	0.6526
13	Left second premolar	-0.8667	-0.1302	-0.4824	-0.4893	-0.0817	-0.2765	-0.2604	-0.1429	-0.2032	-0.3755	1.9971	0.7191
14	Left first molar	-10.66	2.3408	-3.2119	-2.8718	-0.229	-1.3595	-2.1271	2.1591	-0.3178	-0.6387	0.0659	-0.3545
15	Left second molar	-2.2129	-0.9151	-1.435	-0.6705	-0.153	-0.4767	-0.626	1.0607	0.0296	-0.5451	-0.2265	-0.3542

N: tooth number based on the Universal Dental Notation system; Min: minimum; Max: maximum; Avg: average.

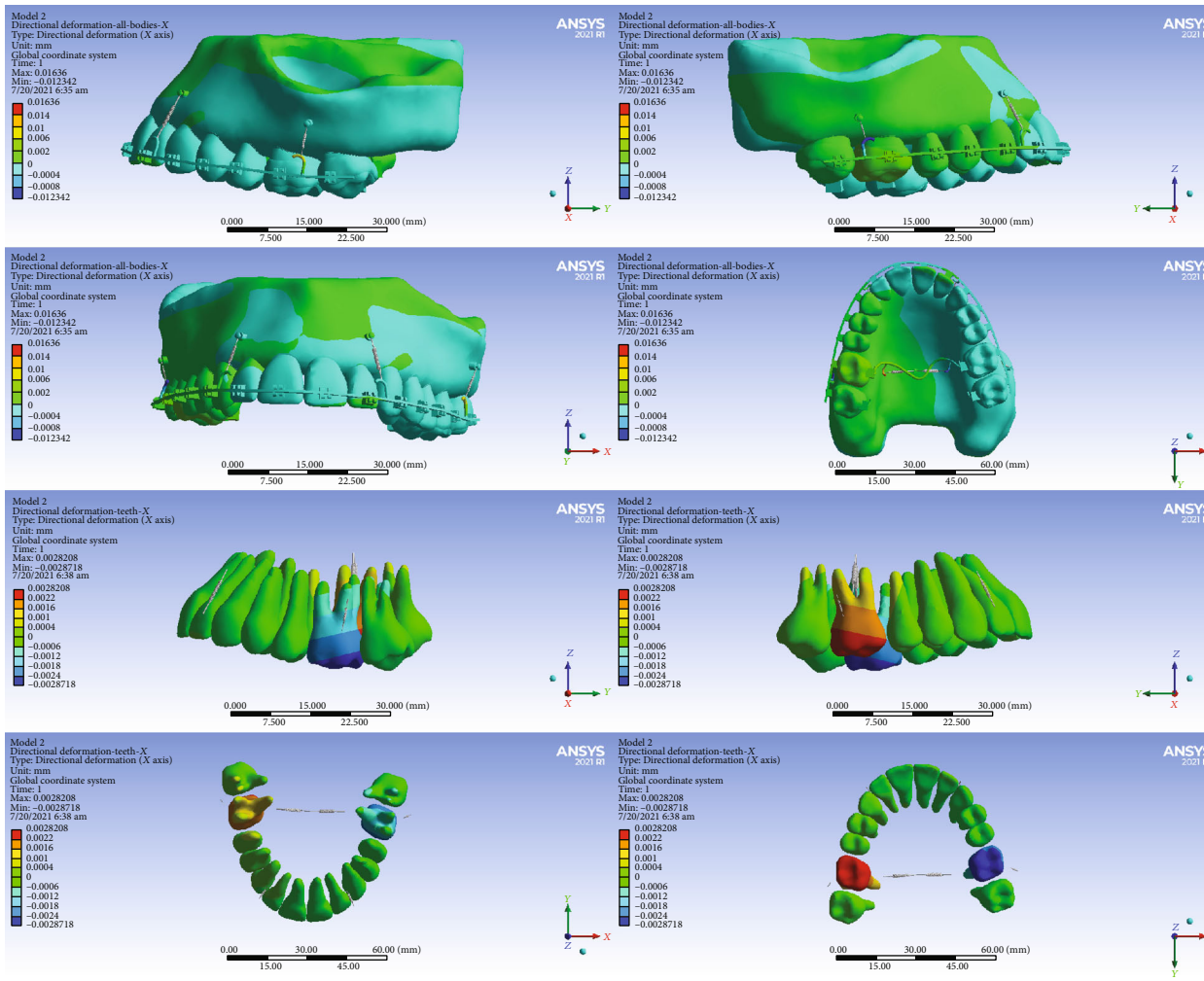

Figure 11: Displacements in the X global direction (left-right) in model 2. Positive and negative values indicate the movement towards the patient's right and left sides.

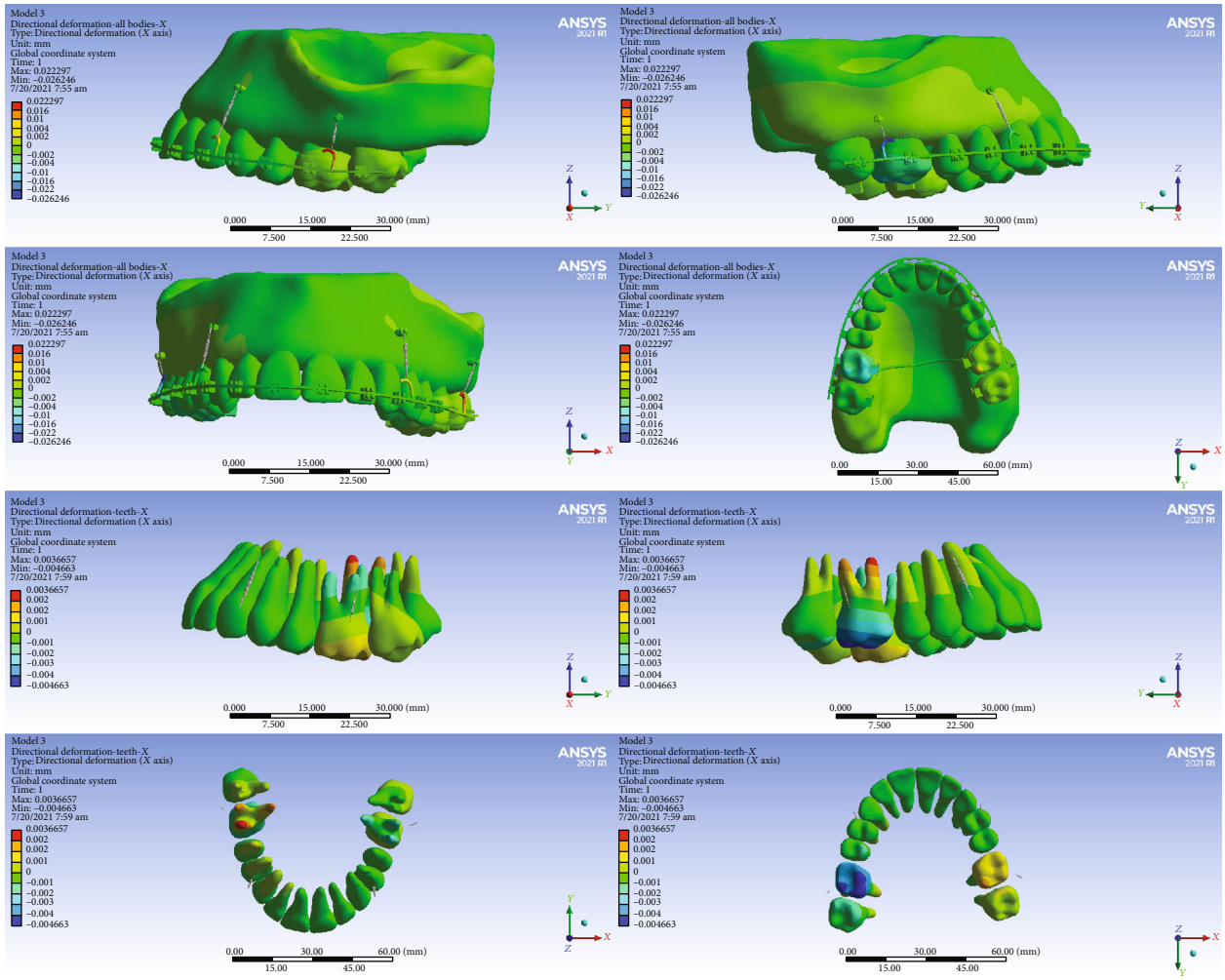

FIGURE 12: Displacements in the X global direction (left-right) in model 3. Positive values indicate movements to the patient's right side, while negative values indicate movements to the left side.

susceptible to root resorption [48]. In our study, in addition to the apex of the molars, the furca area was also susceptible to root resorption. This was in line with the results of another study finding the furca as the most susceptible area to resorption during intrusion [49].

In our first model, the crowns of the anterior teeth were displaced buccally while their roots moved palatally. If the buccal tipping movement is indicated, for example in class II div 2 patients, this method can be useful in correcting dental inclination [13, 19]. In other models, the anterior teeth became palatalized, which can be helpful in patients with dental protrusion or class II div 1 patients [13, 19]. In the first and second models, the posterior teeth were palatalized; thus, in cases where the teeth have a buccal inclination, the use of these models is preferable [13, 19]. On the other hand, in the third and fourth models, the posterior teeth became buccalized, so in cases where the palatal inclination of the posterior teeth is desired, this model can be used [13, 19].

In our first model, the crowns of the premolars were mesialized, the crowns and roots of the second molars were distalized, and the palatal portions of the first molars were displaced to the mesial and their buccal portions to the distal. In the second model, the crowns of the first and second molars were distalized. In the third model, the premolars were distalized, the roots of the first molars were mesialized, and their crowns, especially their palatal cusps, were distalized; and the crowns of the second molars were mesialized and their roots distalized. In the fourth model, the crown of posterior teeth became mesialized and their roots were distalized.

In the vertical dimension, the highest amount of intrusion was seen in our first model followed by the second one. Therefore, when the amount of intrusion is crucial, it seems more practical to use these two methods. The least amount of intrusion occurred in the fourth model. The maximum intrusion of the premolars was seen in the fourth model; hence, this method may be preferred when it is important to control the movements of the premolars. The maximum intrusion of the first molas was observed in the first model, whereas, in the fourth model, the first molars were extruded. In the second molars, the maximum intrusion occurred in the third model; but in the first and fourth models, extrusion was observed (more in the first model). Such extrusions might be due to wire deflection. Overall,

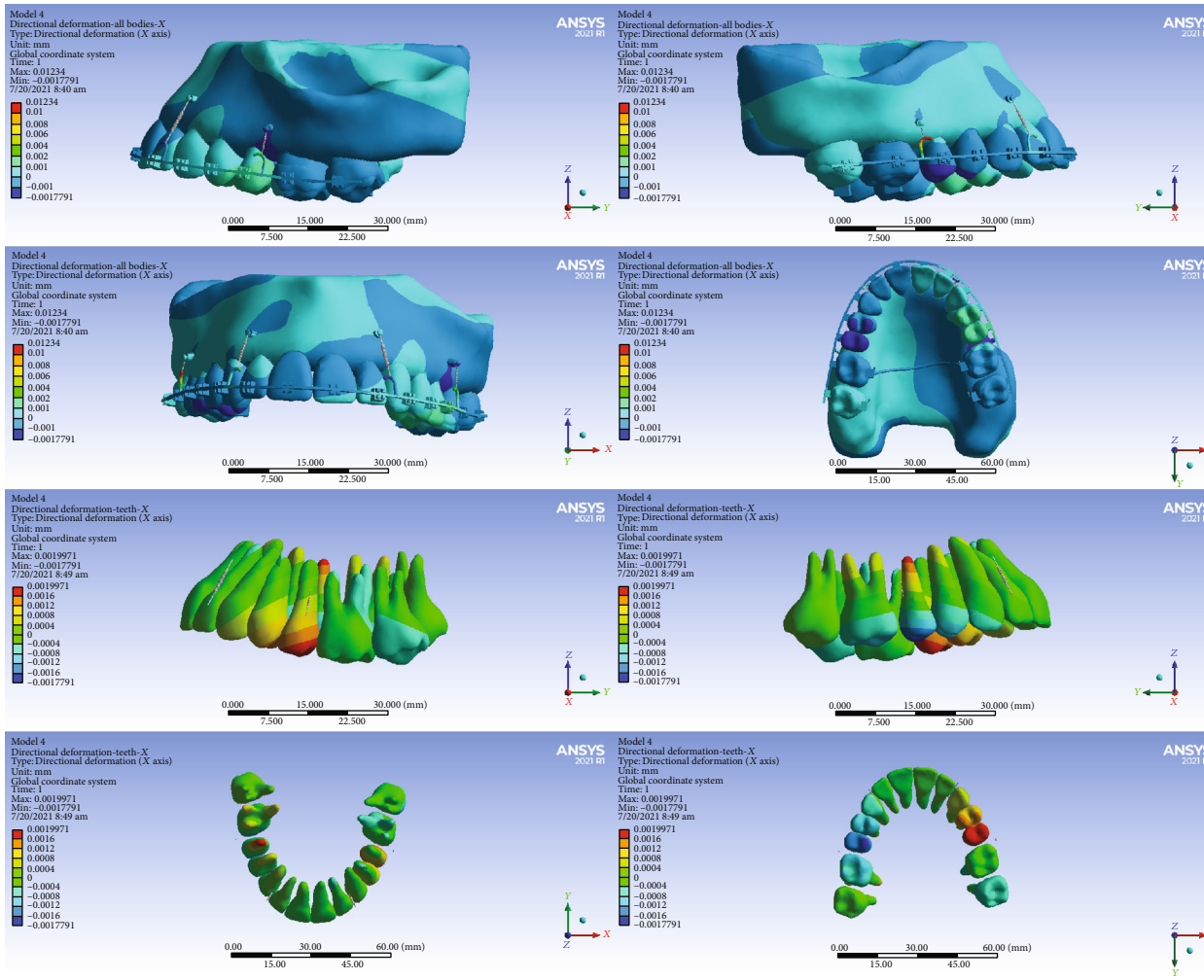

Figure 13: Displacements in the X global direction (left-right) in model 4. Positive values indicate movements to the patient's right side, while negative values indicate movements to the left side.

the fourth model does not seem to be successful in controlling the molar region. Few methods have been proposed in a few case reports for maxillary full-arch intrusion. However, the exact biomechanics of these methods, including the side effects of each of them on the anterior-posterior movement of the maxillary teeth (which can change the interarch relationship) or the resulting transverse dimensional changes, have not been systematically studied. Also in full-arch intrusion, the rotation of the occlusal plane during intrusion is very important. In patients with anterior open bite, a slight clockwise rotation during intrusion is desirable. While in patients with a long face with gummy smile, uniform intrusion in the anterior and posterior dental arch is preferred. Finite element analysis allows us to comprehensively evaluate the stress distribution and displacement of teeth in all three spatial dimensions for each model. In this study, we analyzed 4 models that at first glance seemed to effectively lead to uniform anterior and posterior maxillary intrusion, with minimal unwanted tooth movements in the anterior-posterior or transverse dimensions. However, this was not necessarily the case. Examination of our results shows that the first and second models cause a brief palatal movement of the crown of the posterior teeth, whereas, in the third and fourth models, these teeth move towards the buccal type. Therefore, the first two models should be used with caution in cases where there is a tendency for posterior crossbite before treatment or the roots of the posterior teeth are close to the buccal cortex. In the first and second models, where the posterior crowns became palatalized, the intrusive force was also applied from the palatal, but in the third and fourth models, despite the use of TPA, the teeth became buccalized. In the study of Kawamura et al. [50], it was reported that during posterior intrusion, buccal tipping of teeth occurred through buccal miniscrews, which recommended the use of TPA, which is stiffer, lingual constriction bend and lingual crown torque [50]. Only in the first model, the anterior teeth moved buccally, but in the other models, the anterior teeth became palatalized. The addition of two buccal miniscrews in the posterior side of the second, third, and fourth models may be effective in this regard. It is better not to use model 1 in cases where the anterior teeth are already in the buccal position and should not become more buccalized. In the first and second models (in which in addition to buccal miniscrews, there were also palatal

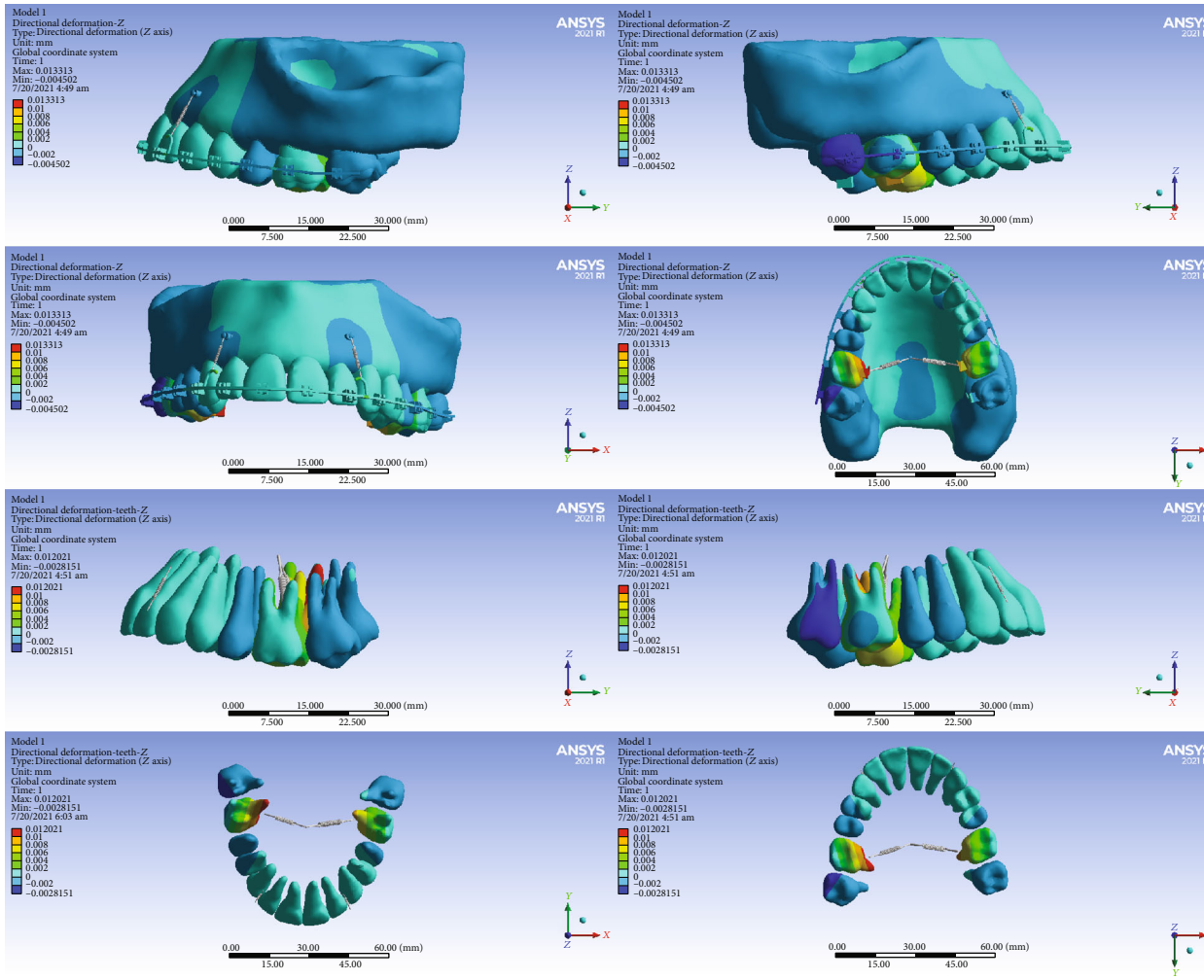

Figure 14: Displacements in the Z global direction (vertical) in model 1. Positive values indicate intrusion while negative values indicate extrusion.

Table 6: Movements (μm) in the global Z-axis (vertical, intrusive-extrusive). Positive values indicate intrusion while negative values indicate extrusion.

N	Tooth	Model 1			Model 2			Model 3			Model 4		
		Min.	Max.	Avg.	Min.	Max.	Avg.	Min.	Max.	Avg.	Min.	Max.	Avg.
2	Right second molar	-2.8151	0.0506	-1.4054	-0.1441	0.0638	-0.0647	-0.4464	0.9838	0.2346	-0.144	0.045	-0.0406
3	Right first molar	-1.1411	12.021	4.9139	3.5069	5.2231	4.283	0.2378	6.3665	3.6323	-1.1792	0.5967	-0.2499
4	Right second premolar	-0.5503	-0.0816	-0.2979	-0.011	0.1612	0.0766	0.2935	1.5269	0.8597	0.1987	2.3968	1.194
5	Right first premolar	-0.33	0.2424	-0.0198	-0.037	0.0497	0.0083	0.0107	1.0739	0.4913	-0.0636	1.1668	0.4724
6	Right canine	0.0664	0.5563	0.2918	0.0027	0.1988	0.0716	-0.0052	0.6591	0.2708	-0.1004	0.5573	0.2096
7	Right lateral	0.2236	0.9793	0.5303	-0.0596	0.3874	0.1351	-0.0172	0.2807	0.0796	-0.2476	0.4227	0.0484
8	Right central	0.4613	1.2538	0.8519	0.1715	0.4795	0.3102	-0.1311	0.1132	-0.0155	0.0652	0.2123	0.121
9	Left central	0.4476	1.3839	0.9419	0.1172	0.6051	0.3602	-0.1265	0.1143	0.0053	-0.1322	0.5661	0.1665
10	Left lateral	0.2897	1.3758	0.8061	-0.0127	0.6568	0.3034	0.0331	0.2269	0.1021	-0.3785	0.878	0.2107
11	Left canine	0.2745	1.0475	0.5943	0.1167	0.4656	0.2268	0.0341	0.3423	0.1519	-0.0428	0.888	0.3876
12	Left first premolar	0.0688	0.4701	0.2586	-0.0436	0.1596	0.0586	-0.0336	0.2173	0.0637	-0.103	1.0834	0.4485
13	Left second premolar	-0.2358	0.1752	-0.0433	-0.1499	0.0495	-0.0497	-0.1214	-0.0106	-0.0775	-0.2225	1.3321	0.455
14	Left first molar	0.373	8.8284	4.0164	1.2881	3.712	2.4076	-0.601	2.2099	0.8569	-0.7636	0.8948	-0.0348
15	Left second molar	-0.8398	0.167	-0.3456	0.4423	0.7901	0.6189	0.654	1.9433	1.2819	-0.5082	-0.0085	-0.1852

N: tooth number based on the Universal Dental Notation system; Min: minimum; Max: maximum; Avg: average.

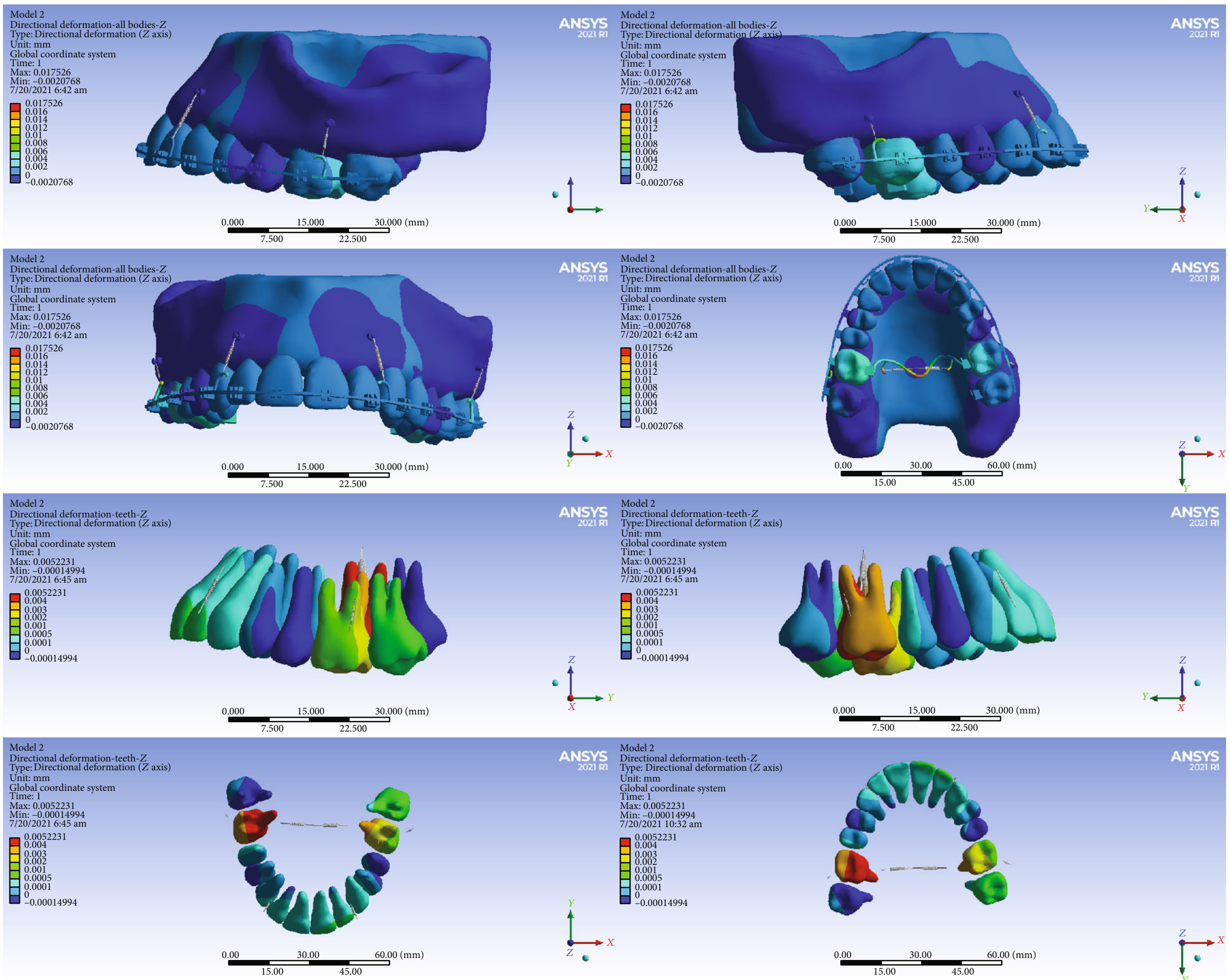

FIGURE 15: Displacements in the Z global direction (vertical) in model 2. Positive and negative values indicate intrusion and extrusion, respectively.

miniscrews), the highest amount of intrusion was seen; it can be concluded that in total intrusion, the use of palatal miniscrews contributes to more effective intrusion. In the study of Till et al. [51] (in which the degree of distalization was examined), by placing two miniscrews between the premolars in addition to the interradicular miniscrews (located between the second premolar and the first molar), the molar distallization and retraction and incisor intrusion were considerably higher than the group that included only interradicular miniscrews between the second premolar and the first molar [51]. Between the first and second models, the second model, which used the greatest number of miniscrews, intruded more teeth. In the fourth model, besides the lowest amount of intrusion that was observed, the vertical control on the molars was minimal and the highest amount of intrusion was in the premolar area, which can be justified by the more anterior position of the posterior miniscrews. This model is recommended in cases where the inclination of the occlusal plane is such that the need for intrusion in the premolars is the maximum. It seems that increasing the number of miniscrews has a positive effect on controlling the buccolingual dimension of the posterior teeth and the mesiodistal dimension of the anterior teeth, because, in the second model with the most miniscrews, the least dental displacements in the said dimensions were observed. On the other hand, the highest displacements were detected in the first model with the fewest miniscrews.

There is no FEA study on full-arch intrusion. Nevertheless, there are 3 finite element analyses examining intrusion of the anterior teeth. A 3D finite element model was created for six anterior teeth [52]. After adjusting the alveolar bone loss to 0, 2 or 4 mm, the positions of the miniscrews and hooks were changed. Then, the primary displacement of each tooth in three directions and the amount of labial tilt after applying 100 grams of intrusive force were measured. The findings showed that with the reduction of alveolar bone height, the amount of labial tilt increased under the same load. When a miniscrew was placed between two central teeth, the mediolateral and anterior-posterior displacements of the central incisor were significantly greater than other cases. In the case where the miniscrew was placed in the distal of canines (and the distal intrusion force was applied to the lateral incisors), the amount of labial tilting and displacement of the six anterior teeth was the lowest, and the

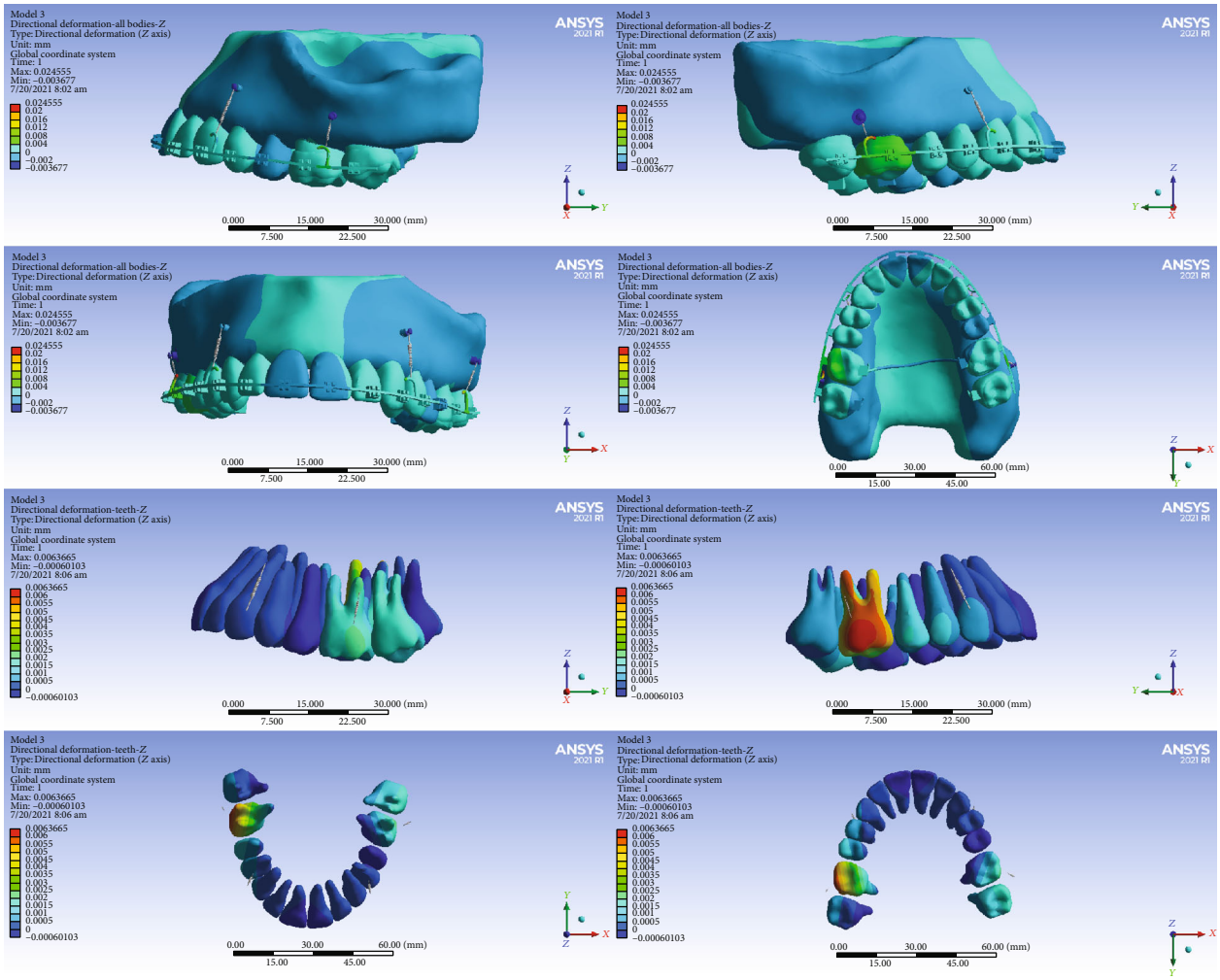

FIGURE 16: Displacements in the *Z* global direction (vertical) in model 3. Positive values indicate intrusion while negative values indicate extrusion.

maximum stress was uniformly distributed in all teeth [52]. In another study, intrusive loading of maxillary incisors was simulated [53]. The force application points were the following: the central area between the brackets of the central incisors, bilaterally between the brackets of the central and lateral incisors, at the distal of the brackets of the lateral incisors on both sides, and 7 mm distal to the center of the brackets of the lateral incisors on both sides. The results showed that the stress (regardless of the application point of the orthodontic force) was concentrated in the PDL of the root apex region. Four loading models showed different compressive stress values compared to the midsagittal reference line. Stress distributions in the central and lateral incisors were not the same in a similar loading model. When the force application point was in the distal of the brackets of the lateral incisors, a more balanced compressive stress distribution was seen [53]. In the third study, the finite element model was created from the central teeth to the maxillary first premolar [54]. Four different modes of intrusion mechanics were simulated with different placement locations for the miniscrews as well as different force application points. In each model, a force of 25 g was applied to the maxillary incisors. In all four models, there was an increase in stress values in the apical region of the lateral incisor. Proclination of maxillary incisors was also reported in all four models. The absolute minimum intrusion was observed when the miniscrew was placed between the lateral incisors and canines, and the force was applied at a right angle to the archwire (which is very common in clinical treatments). It seemed that the apical region of the lateral incisor was the most susceptible place for root resorption during the intrusion of anterior teeth. In clinical situations where minimum flaring of the maxillary incisors is required, it is suggested that miniscrews be placed between the roots of the lateral incisors and canines, and the force be applied between the central and lateral incisors. In order to achieve maximum absolute intrusion, it is recommended to place the miniscrew between the roots of the central and lateral incisors and apply the force at a right angle to the archwire between the two teeth [54].

This in silico simulation was limited by some factors. A limitation for finite element modeling is its theoretical

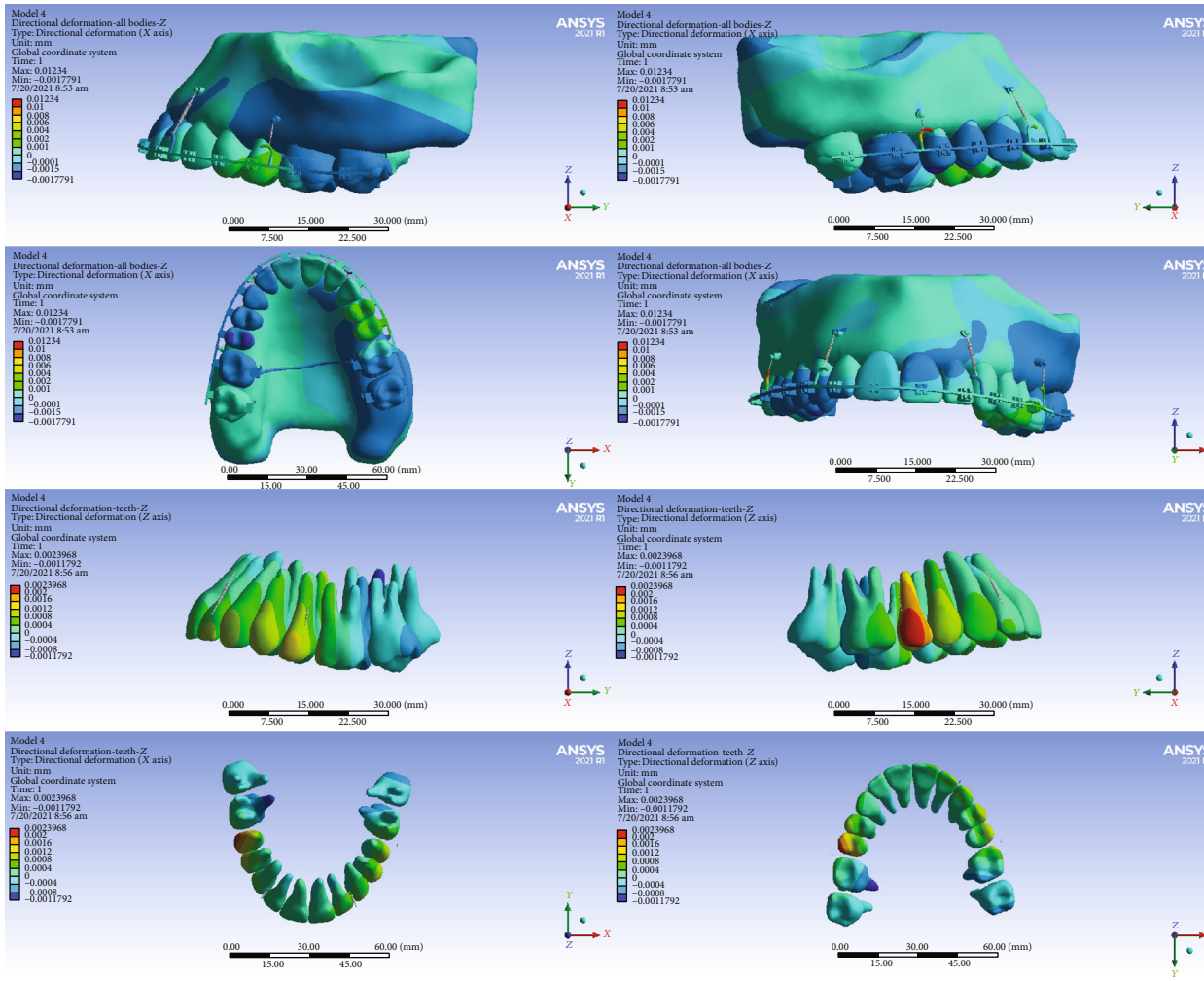

Figure 17: Displacements in the Z global direction (vertical) in model 4. Positive and negative values indicate intrusion and extrusion, respectively.

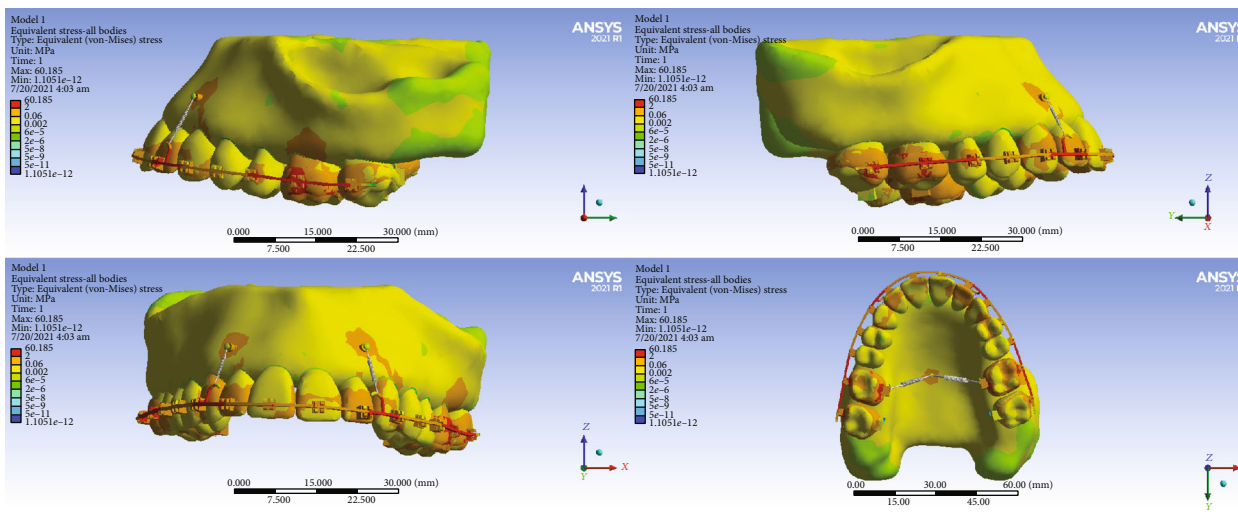

Figure 18: All body stresses (MPa) in model 1.

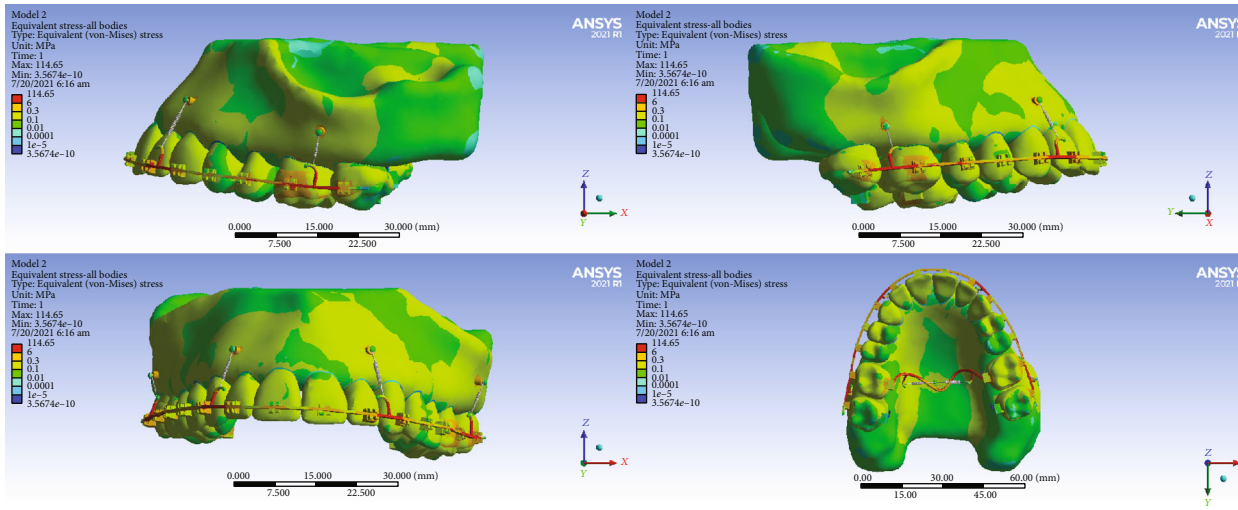

Figure 19: All body stresses (MPa) in model 2.

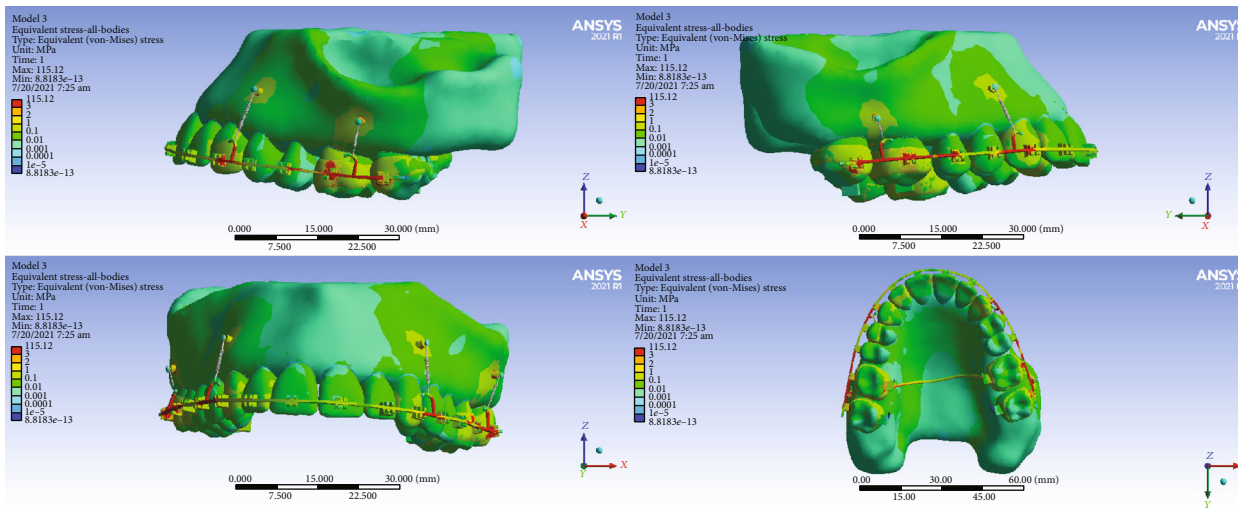

Figure 20: All body stresses (MPa) in model 3.

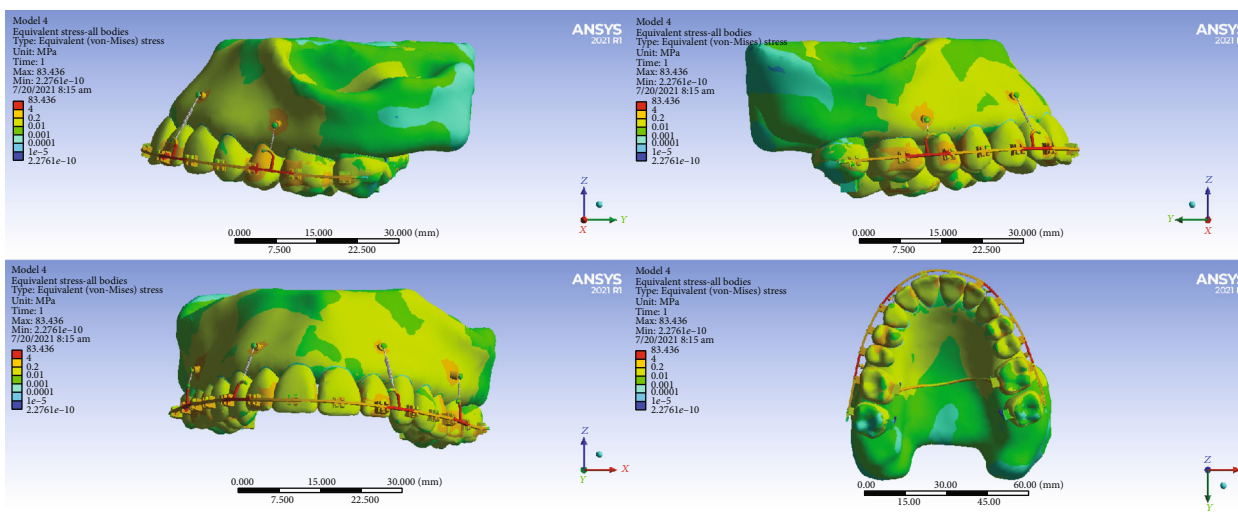

Figure 21: All body stresses (MPa) in model 4.

approach. Based on the hypotheses derived from the average properties of bone or teeth or other structures, this analysis is basically a static analysis that is difficult to apply in clinical conditions; thus, careful decisions must be made to realize its modeling and analysis [55]. Finite element studies only examine very short-lived and very fast and also static *mechanical* relationships. They do not and cannot examine the *biological* changes happening over a long period of time [56]. Root resorption has multiple potential mechanisms including the engagement of the root with the cortical bone. However, the movement of the roots towards the bone cortex and its engagement with the cortical bone happens over a long period of time and has biological mechanisms. Therefore, it is impossible for finite element studies to examine such dynamics which occur in long term and through biological mechanisms. Similarly, finite element studies cannot examine the biological changes happening in a very long time needed for the establishment of the secondary stability of miniscrews. However, since clinical examination of novel and unknown methods are not ethical in many situations, FEA simulations can act as a beginning point in a chain of research to be followed by later animal and clinical studies [56]. Therefore, future animal and clinical studies are needed to verify our results. Furthermore, future research should also examine zygomatic miniplates. They also should include in the "Mouse Trap" model, which is among the most widespread treatments for the solution of this clinical problem. The application of TAD in the palatal area at the height of the third palatine wrinkle can present significant biomechanical and biological advantages in this approach.

5. Conclusions

The following conclusions can be summarized: (1) The highest amounts of incisor and molar intrusion were seen in the first model. With the addition of buccal alveolar miniscrews in the posterior region in the second model (along with the TPA placement), the extents of incisor and molar intrusion were reduced compared to the first model, and at the same time, unwanted movements in other planes (such as palatal and mesial movements of molars and labial movements of incisors) were inhibited. (2) The more-mesial placement of the posterior miniscrews in the fourth model (in the mesial of the first molars) severely reduced the intrusion of the molars and instead increased the intrusion in the premolar area, so that the fourth model showed the highest premolar intrusion compared to other models. (3) In the first three models, the highest amount of intrusion occurred in the first molar region; in the fourth model, it was seen in the premolar area. The overall amounts of intrusion were highest in the first model followed by the second one; therefore, it seems that these might be more practical when a greater extent of intrusion is needed. (4) In general, it can be concluded that in model 1, compared to other models, the highest compressive hydrostatic stress is seen in the periodontal ligament, while in model 4, the least compressive stress is seen. Hence, it seems that the use of the fourth model is more conservative.

Data Availability

All data are presented as figures and tables.

Conflicts of Interest

The authors declare that they do not have any conflict of interest.

Authors' Contributions

Marzieh Mazhari conceived, designed, and financed the study, supervised the thesis, contributed to FEA analyses and validations, interpreted the findings, and revised the article. Mashallah Khanehmasjedi designed the study and contributed to interpretations. Mohsen Mazhary designed the study, performed and validated the FEA analyses, and provided the images and tables. Nastaran Atashkar designed the study, financed it, drafted the proposal and thesis, interpreted the findings, validated the findings, and revised the article. Vahid Rakhshan designed the study, supervised the thesis, validated and interpreted the FEA analyses and findings, suggested the analysis of local coordinates, drafted and revised the article, and edited the figures.

Acknowledgments

The study was self-funded by the authors. The authors express their gratitude to Mr. Mojtaba Hasani for his contributions to the FEA analyses.

References

[1] H. Dym and R. Pierre 2nd, "Diagnosis and treatment approaches to a "Gummy Smile"," *Dental Clinics of North America*, vol. 64, no. 2, pp. 341–349, 2020.

[2] D. Mostafa, "A successful management of sever gummy smile using gingivectomy and botulinum toxin injection: a case report," *International journal of surgery case reports*, vol. 42, pp. 169–174, 2018.

[3] M. P. Gibson and D. N. Tatakis, "Treatment of gummy smile of multifactorial etiology: a case report," *Clinical advances in periodontics*, vol. 7, no. 4, pp. 167–173, 2017.

[4] S. Uzuka, J.-M. Chae, K. Tai, T. Tsuchimochi, and J. H. Park, "Adult gummy smile correction with temporary skeletal anchorage devices," *Journal of the World Federation of Orthodontists*, vol. 7, no. 1, pp. 34–46, 2018.

[5] R.-K. Hong, S.-M. Lim, J.-M. Heo, and S.-H. Baek, "Orthodontic treatment of gummy smile by maxillary total intrusion with a midpalatal absolute anchorage system," *The Korean Journal of Orthodontics*, vol. 43, no. 3, pp. 147–158, 2013.

[6] C. Gioka and T. Eliades, "Orthodontic dental intrusion: indications, histological changes, biomechanical principles, possible side effects," *Hellenic Orthodontic Review*, vol. 6, pp. 129–146, 2003.

[7] N. M. Al-Zubair, "Orthodontic intrusion: a contemporary review," *Journal of Orthodontic Research*, vol. 2, no. 3, pp. 118–124, 2014.

[8] C. R. Burstone, "Deep overbite correction by intrusion," *American Journal of Orthodontics*, vol. 72, no. 1, pp. 1–22, 1977.

[9] R. Nikolai, "Response of dentition and periodontium to force," in *Bioengineering analysis of orthodontic mechanics*, pp. 146–193, Lea and Febinger, Philadelphia, 1985.

[10] A. Hohmann, U. Wolfram, M. Geiger et al., "Periodontal ligament hydrostatic pressure with areas of root resorption after application of a continuous torque moment," *The Angle Orthodontist*, vol. 77, no. 4, pp. 653–659, 2007.

[11] C. Dorow and F.-G. Sander, "Development of a model for the simulation of orthodontic load on lower first premolars using the finite element method," *Journal of Orofacial Orthopedics/Fortschritte der Kieferorthopädie*, vol. 66, no. 3, pp. 208–218, 2005.

[12] C. A. E. Tavares, S. Allgayer, and J. C. Dinato, "Mini-implants for the management of a gummy smile," *Journal of the World Federation of Orthodontists*, vol. 2, no. 2, pp. e99–e106, 2013.

[13] W. R. Proffit, H. W. Fields, D. M. Msd, B. Larson, and D. M. Sarver, *Contemporary Orthodontics*, Elsevier, Philadelphia, 6th edition, 2019.

[14] A. Hohmann, C. Kober, P. Young et al., "Influence of different modeling strategies for the periodontal ligament on finite element simulation results," *American Journal of Orthodontics and Dentofacial Orthopedics*, vol. 139, no. 6, pp. 775–783, 2011.

[15] C. Dorow, N. Krstin, and F.-G. Sander, "Determination of the mechanical properties of the periodontal ligament in a uniaxial tensional experiment," *Journal of Orofacial Orthopedics/Fortschritte der Kieferorthopädie*, vol. 64, no. 2, pp. 100–107, 2003.

[16] Y. Kojima and H. Fukui, "A numerical simulation of tooth movement by wire bending," *American Journal of Orthodontics and Dentofacial Orthopedics*, vol. 130, no. 4, pp. 452–459, 2006.

[17] C. N. Elias, D. J. Fernandes, F. M. de Souza, E. dos Santos Monteiro, and R. S. de Biasi, "Mechanical and clinical properties of titanium and titanium-based alloys (Ti G2, Ti G4 cold worked nanostructured and Ti G5) for biomedical applications," *Journal of Materials Research and Technology*, vol. 8, no. 1, pp. 1060–1069, 2019.

[18] D. K. Agarwal, A. Razdan, A. Agarwal, P. Bhattacharya, A. Gupta, and D. Kapoor, "A comparative study of orthodontic coil springs," *Journal of Indian Orthodontic Society*, vol. 45, no. 4, pp. 160–168, 2011.

[19] C. Burstone and K. Choy, "The biomechanical foundation of clinical orthodontics," Quintessence, Chicago, 2015.

[20] J. H. Choi, "TADs vs. Orthognathic Surgery," *Temporary Anchorage Devices in Clinical Orthodontics*, pp. 685–695, 2020.

[21] T.-T. Lai and M.-H. Chen, "Factors affecting the clinical success of orthodontic anchorage: experience with 266 temporary anchorage devices," *Journal of dental Sciences*, vol. 9, no. 1, pp. 49–55, 2014.

[22] M. K. McGuire, E. T. Scheyer, and R. L. Gallerano, "Temporary anchorage devices for tooth movement: a review and case reports," *Journal of Periodontology*, vol. 77, no. 10, pp. 1613–1624, 2006.

[23] C.-H. Paik, H.-S. Park, and H.-W. Ahn, "Treatment of vertical maxillary excess without open bite in a skeletal class II hyperdivergent patient," *The Angle Orthodontist*, vol. 87, no. 4, pp. 625–633, 2017.

[24] M. U. Sanap, A. Karandikar, and A. Jatania, "Temporary anchorage devices in orthodontics–a brief review," *Journal of Interdisciplinary Dental Sciences*, vol. 8, no. 1, pp. 10–14, 2019.

[25] D. Alshammery, N. Alqhtani, A. Alajmi et al., "Non-surgical correction of gummy smile using temporary skeletal miniscrew anchorage devices: a systematic review," *Journal of Clinical and Experimental Dentistry*, vol. 13, no. 7, pp. e717–e723, 2021.

[26] J. C. Lin, C. L. Yeh, E. J. Liou, and S. J. Bowman, "Treatment of skeletal-origin gummy smiles with miniscrew anchorage," *Journal of Clinical Orthodontics*, vol. 42, no. 5, pp. 285–296, 2008.

[27] H. Orton, D. Slattery, and S. Orton, "The treatment of severe 'gummy' Class II division 1 malocclusion using the maxillary intrusion splint," *The European Journal of Orthodontics*, vol. 14, no. 3, pp. 216–223, 1992.

[28] S. A. Aly, D. Alyan, M. S. Fayed, M. S. Alhammadi, and Y. A. Mostafa, "Success rates and factors associated with failure of temporary anchorage devices: a prospective clinical trial," *Journal of Investigative and Clinical Dentistry*, vol. 9, no. 3, article e12331, 2018.

[29] A. Gracco, A. Cirignaco, M. Cozzani, A. Boccaccio, C. Pappalettere, and G. Vitale, "Numerical/experimental analysis of the stress field around miniscrews for orthodontic anchorage," *The European Journal of Orthodontics*, vol. 31, no. 1, pp. 12–20, 2009.

[30] H. Fattahi, S. Ajami, and A. Nabavizadeh Rafsanjani, "The effects of different miniscrew thread designs and force directions on stress distribution by 3-dimensional finite element analysis," *J Dent (Shiraz)*, vol. 16, no. 4, pp. 341–348, 2015.

[31] G. Sivamurthy and S. Sundari, "Stress distribution patterns at mini-implant site during retraction and intrusion—a three-dimensional finite element study," *Progress in Orthodontics*, vol. 17, no. 1, pp. 1–11, 2016.

[32] H. E. Akl, A. R. El-Beialy, M. A. El-Ghafour, A. M. Abouelezz, and F. A. El Sharaby, "Root resorption associated with maxillary buccal segment intrusion using variable force magnitudes:," *The Angle Orthodontist*, vol. 91, no. 6, pp. 733–742, 2021.

[33] S. A. Bellini-Pereira, J. Almeida, A. Aliaga-Del Castillo, C. C. O. Dos Santos, J. F. C. Henriques, and G. Janson, "Evaluation of root resorption following orthodontic intrusion: a systematic review and meta-analysis," *European Journal of Orthodontics*, vol. 43, no. 4, pp. 432–441, 2021.

[34] G. Pizzo, M. Licata, R. Guiglia, and G. Giuliana, "Root resorption and orthodontic treatment. Review of the literature," *Minerva Stomatologica*, vol. 56, no. 1-2, pp. 31–44, 2007.

[35] V. Rakhshan, N. Nateghian, and M. Ordoubazari, "Risk factors associated with external apical root resorption of the maxillary incisors: a 15-year retrospective study," *Australian Orthodontic Journal*, vol. 28, no. 1, pp. 51–56, 2012.

[36] N. Brezniak and A. Wasserstein, "Root resorption after orthodontic treatment: part 2. Literature review," *American Journal of Orthodontics and Dentofacial Orthopedics*, vol. 103, no. 2, pp. 138–146, 1993.

[37] K. Lopatiene and A. Dumbravaite, "Risk factors of root resorption after orthodontic treatment," *Stomatologija*, vol. 10, no. 3, pp. 89–95, 2008.

[38] G. T. Sameshima and P. M. Sinclair, "Predicting and preventing root resorption: part I. diagnostic factors," *American Journal of Orthodontics and Dentofacial Orthopedics*, vol. 119, no. 5, pp. 505–510, 2001.

[39] H. Travess, D. Roberts-Harry, and J. Sandy, "Orthodontics. Part 6: risks in orthodontic treatment," *British Dental Journal*, vol. 196, no. 2, pp. 71–77, 2004.

[40] N. Fox, "Longer orthodontic treatment may result in greater external apical root resorption," *Evidence-Based Dentistry*, vol. 6, no. 1, p. 21, 2005.

[41] V. Krishnan, "Critical issues concerning root resorption: a contemporary review," *World Journal of Orthodontics*, vol. 6, no. 1, pp. 30–40, 2005.

[42] S. Apajalahti and J. S. Peltola, "Apical root resorption after orthodontic treatment—a retrospective study," *The European Journal of Orthodontics*, vol. 29, no. 4, pp. 408–412, 2007.

[43] G. Costopoulos and R. Nanda, "An evaluation of root resorption incident to orthodontic intrusion," *American Journal of Orthodontics and Dentofacial Orthopedics*, vol. 109, no. 5, pp. 543–548, 1996.

[44] G. Han, S. Huang, J. W. Von den Hoff, X. Zeng, and A. M. Kuijpers-Jagtman, "Root resorption after orthodontic intrusion and extrusion: an intraindividual study," *The Angle Orthodontist*, vol. 75, no. 6, pp. 912–918, 2005.

[45] R. J. Parker and E. F. Harris, "Directions of orthodontic tooth movements associated with external apical root resorption of the maxillary central incisor," *American Journal of Orthodontics and Dentofacial Orthopedics*, vol. 114, no. 6, pp. 677–683, 1998.

[46] B. Weltman, K. W. Vig, H. W. Fields, S. Shanker, and E. E. Kaizar, "Root resorption associated with orthodontic tooth movement: a systematic review," *American Journal of Orthodontics and Dentofacial Orthopedics*, vol. 137, no. 4, pp. 462–476, 2010.

[47] W. M. McFadden, C. Engstrom, H. Engstrom, and J. M. Anholm, "A study of the relationship between incisor intrusion and root shortening," *American Journal of Orthodontics and Dentofacial Orthopedics*, vol. 96, no. 5, pp. 390–396, 1989.

[48] M. Çifter and M. Saraç, "Maxillary posterior intrusion mechanics with mini-implant anchorage evaluated with the finite element method," *American Journal of Orthodontics and Dentofacial Orthopedics*, vol. 140, no. 5, pp. e233–e241, 2011.

[49] N. Dabla, T. S. Phull, P. N. Prasad, and N. Rawat, "Stress appraisal in periodontium of maxillary first molar using various intrusive forces: a finite element analysis study," *Journal of Orthodontic Research*, vol. 2, no. 2, p. 90, 2014.

[50] J. Kawamura, J. H. Park, N. Tamaya, J. H. Oh, and J. M. Chae, "Biomechanical analysis of the maxillary molar intrusion: a finite element study," *American Journal of Orthodontics and Dentofacial Orthopedics*, vol. 161, no. 6, pp. 775–782, 2022.

[51] T. E. Bechtold, J.-W. Kim, T.-H. Choi, Y.-C. Park, and K.-J. Lee, "Distalization pattern of the maxillary arch depending on the number of orthodontic miniscrews," *The Angle Orthodontist*, vol. 83, no. 2, pp. 266–273, 2013.

[52] S.-M. Cho, S.-H. Choi, S.-J. Sung, H.-S. Yu, and C.-J. Hwang, "The effects of alveolar bone loss and miniscrew position on initial tooth displacement during intrusion of the maxillary anterior teeth: finite element analysis," *The Korean Journal of Orthodontics*, vol. 46, no. 5, pp. 310–322, 2016.

[53] A. Y. Saga, H. Maruo, M. A. Argenta, I. T. Maruo, and O. M. Tanaka, "Orthodontic intrusion of maxillary incisors: a 3D finite element method study," *Dental press journal of orthodontics*, vol. 21, no. 1, p. 75, 2016.

[54] P. Salehi, A. Gerami, A. Najafi, and S. Torkan, "Evaluating stress distribution pattern in periodontal ligament of maxillary incisors during intrusion assessed by the finite element method," *J Dent (Shiraz)*, vol. 16, no. 4, pp. 314–322, 2015.

[55] Ç. Sakin and Ö. Aylikci, "Techniques to measure miniscrew implant stability," *Journal of Orthodontic Research*, vol. 1, no. 1, p. 5, 2013.

[56] M. Moradinejad, M. Yazdi, R. Chaharmahali, M. Araghbidikashani, S. Bagheri, and V. Rakhshan, "Efficiency and side effects of a novel method for maxillary central root torque (a horizontal box loop of round wire) in comparison with the conventional rectangular wire: a finite element study," *American Journal of Orthodontics and Dentofacial Orthopedics*, vol. 161, no. 2, pp. e172–e186, 2022.

Hindawi
BioMed Research International
Volume 2022, Article ID 5579243, 8 pages
https://doi.org/10.1155/2022/5579243

Research Article

Risk Prediction of Maxillary Canine Impaction among 9-10-Year-Old Malaysian Children: A Radiographic Study

Ahmad Faisal Ismail,[1] **Nur Farhana Auni Sharuddin**,[2] **Nur Hafizah Asha'ari**,[2] **Mohd Adli Md Ali**,[3] **Iswan Zuraidi Zainol**,[4] **Lamis Hejab Alotaibi**,[5] **and Sreekanth Kumar Mallineni**[6,7]

[1]*Department of Paediatric Dentistry and Dental Public Health, Kulliyyah of Dentistry, International Islamic University Malaysia, Malaysia*
[2]*Kulliyyah of Dentistry, International Islamic University Malaysia, Malaysia*
[3]*Kulliyyah of Science, International Islamic University Malaysia, Malaysia*
[4]*Department of Orthodontics, Kulliyyah of Dentistry, International Islamic University Malaysia, Malaysia*
[5]*Department of Preventive Dental Science, College of Dentistry, Majmaah University, Al Majmaah 11952, Saudi Arabia*
[6]*Center for Transdisciplinary Research (CFTR), Saveetha Institute of Medical and Technical Sciences, Saveetha Dental College, Saveetha University, Chennai, 600077 Tamil Nadu, India*
[7]*Division for Globalization Initiative, Liaison Center for Innovative Dentistry Graduate School of Dentistry, Tohoku University, Sendai, Japan*

Correspondence should be addressed to Ahmad Faisal Ismail; drfaisal@iium.edu.my

Received 17 March 2022; Revised 18 August 2022; Accepted 23 August 2022; Published 9 September 2022

Academic Editor: Mohammad Alam

Background. Early diagnosis and interceptive treatment of the maxillary canine impaction is crucial as it reduces treatment complexity and decreases complications and adverse outcomes. *Aim and Objectives*. To determine the mean maxillary canine position among 9-10-year-old children and predict the risk of impaction of the maxillary canines. *Methodology*. Panoramic radiographs (PANs) of 289 healthy children aged between 9 and 10 years were observed where the average position of maxillary canines was related to the lateral incisor, sector locations, and angulations to the bicondylar line were traced. The average position was obtained by using descriptive statistics. One sample Wilcoxon signed-rank test is done to predict the risk of canine impaction by comparing the data obtained to the average position from prior studies. *Results*. A total of 289 PANs (126 males and 163 females) were utilized for the analysis. The findings showed that the average position of the maxillary canines in our population was statistically different from the average position of nonimpacted canines in previous studies. However, on average, more than 85% of canines in our population were still located within the safe range of satisfactory position, with females showing slight predominance outside of the acceptable range. The mean scores of the angles between the right canine and lateral incisor were significantly higher among females than males ($p = 0.001$). Similarly, females had a significantly higher mean angle of the left canine than males ($p < 0.001$). In regard to the angles between the bicondylar line and permanent maxillary canine, the mean scores were not significantly different ($p > 0.05$) on both the left and right side. *Conclusion*. There is a low risk of impaction of maxillary canines in the Malaysian population. However, more retrospective studies using more radiographic and clinical indicators need to be done to confirm the risk of impaction further.

1. Introduction

Maxillary canines are considered the cornerstone of the maxillary arch since they serve a pivotal role in the smile's aesthetic appearance and the occlusion's functional aspect. It may be because it is the tooth with the longest root and has good bony support [1]. Besides that, its long path of eruption and the lengthy development period causes it to

be one of the last teeth to erupt. Though not as common as third molar impaction, the deleterious effects of late diagnosis of canine impaction make its early intervention an extremely crucial topic to be discussed [2]. Aside from creating aesthetic and functional problems, canine impaction can result in root resorption of neighboring teeth, necessitating surgical or orthodontic treatment for repositioning the impacted tooth to a favorable position. More complex displacements may pass unnoticed if not carefully evaluated and escape the time frame of early intervention [2, 3].

Mavreas and Athanasiou [4] reported that the analyzing factors responsible for the success of orthodontic treatment concluded that increased age and severity of impaction affect the complexity of treatment. Therefore, the most desirable approach for managing impacted canines is early diagnosis and the interception of potential impaction [5]. Palpation of the canine bulge in the buccal sulcus from 10 to 11 years is a well-established method for identifying canine impaction [6]. Nonetheless, various studies had been done to diagnose impacted canines early through panoramic radiographs and showed a notable degree of success [4–7]. Consequently, it has been reported that panoramic radiographs are a valuable tool for early prediction [7, 8]. The early observation of canine impaction through routine panoramic radiographs by general practitioners in Malaysia is not accustomed, considering the degree of seriousness of this disorder in the Malaysian community is not yet discussed. However, there are none of the studies reported on the investigation of maxillary canine position in the Malaysian population. Henceforth, the study is aimed at determining the mean maxillary canine position among 9-10 years old children and at predicting the risk of impaction of the maxillary canines.

2. Methodology

2.1. Study Design. This cross-sectional study was done according to a protocol that had been accepted and approved by the IIUM Human Research Ethics Committee (IREC) (ID no.: IREC 2021-006). All the data that were collected throughout this study will only be used for academic purposes. This study details would not be sold or reclaimed by other people without any permission, and all personal details of the child were protected to avoid misusage. This study was conducted at Polyclinic and Radiograph Unit (Kulliyyah of Dentistry, IIUM Kuantan). A convenience sampling method was used. The sample size was calculated using the following formula:

$$n = \frac{Z^2 P(1-P)}{d^2}, \quad (1)$$

where n is the sample size; Z value is the statistic for confidence level, 1.96 for 95% CI; P is the expected prevalence (estimated as 2%); d is the precision, where $d = 0.02$. The minimum sample size obtained was 188. Based on this value, a minimum of 188 panoramic radiographs (PANs) of children aged from 9 to 10 years, who attended Polyclinic Kulliyyah of Dentistry, Malaysia, were reviewed.

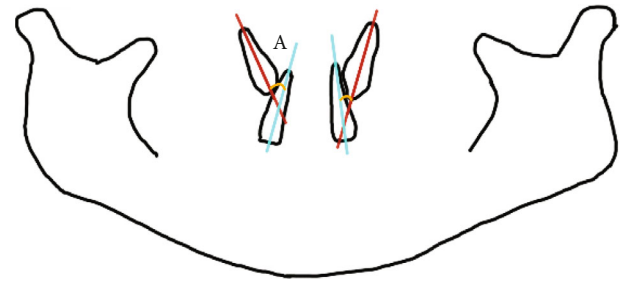

Figure 1: Parameter 1 (angle A): the angle between the axis of the unerupted canine and the lateral incisor (3^2).

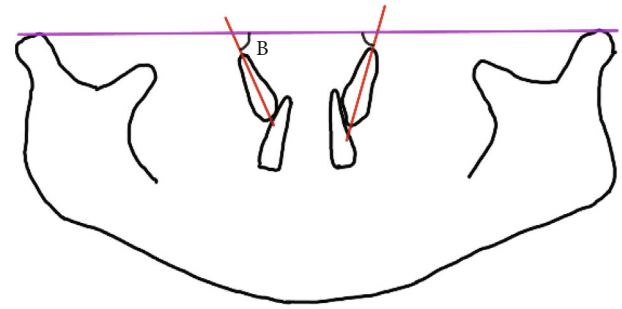

Figure 2: Parameter 2 (angle B): the angle between the bicondylar line and canine.

Children aged 9 to 10 years, who were fit and healthy and maxillary incisors, were fully erupted, with canines unerupted included in the study. Poor image quality and patients with pathology, such as syndromes, cleft lip, and palate, and severe abnormalities, and children with early extractions, orthodontic extrusion of the canine, or canines that are already erupted were excluded.

The average position of canines among children aged 9 to 10 years old was calculated as the average angulation between maxillary canines and the adjacent lateral incisors [9, 10] (3^2) (Figure 1). The position of unerupted maxillary canines and the adjacent lateral incisors, both left and right, was traced from 289 PANs. The angulations between the canines and the lateral incisors were then calculated using Python Programming. The average angulations were classified as either satisfactory or unsatisfactory based on the study by Almahdy et al. [11]. The average canine position is considered satisfactory if it is equal to or less than 30°. At more than 30°, the average canine position was classified as unsatisfactory. Next, the angulation and sector location of the canines were measured. The angular measurement was obtained in a manner; the most superior point of the condyle was selected as a landmark, and a bicondylar line was drawn as a horizontal reference line (Figure 2). The measurement was taken from the mesial angle formed between the constructed horizontal and the long axis of the unerupted canine, and the angles were then calculated using Python Programming. The position of the canine cusp tips was measured from the same tracing and classified into four sector locations as proposed by Lindauer et al. [12] as represented in Figure 3. Sector I represents the area distal to a line

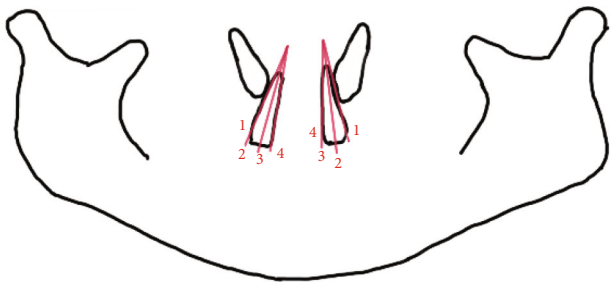

Figure 3: Parameter 3: the sector location of the canine—position of canine cusp tip in relation to the lateral incisors.

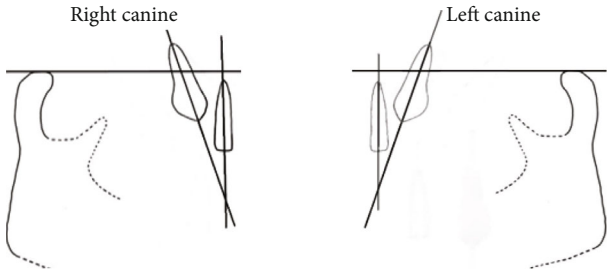

Figure 4: Average position of permanent canines among 9-10 years old children.

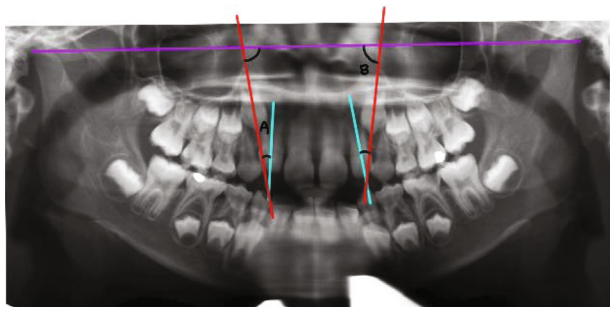

Figure 5: Showing parameters 1 and 2 traced on a panoramic radiograph.

tangent to distal heights of the contour of the lateral incisor crown and root. Sector II is mesial sector I but distal to the bisector of the lateral incisor's long axis. Sector III is mesial to sector II but distal to mesial heights of the contour of lateral incisor crown and root. Sector IV includes all areas mesial to sector III. Prediction of the risk of canine impaction was made according to the results from a study by Warford et al. [13] and Quadras et al. [14] as shown below

Mean angulations:

Below 65°: unsatisfactory.

Equal and above 65°: satisfactory.

Sector locations:

Sector I: satisfactory.

Sector II, III, and IV: unsatisfactory.

From Figure 4, it can be demonstrated that the average position of canines in 9-10 years old children in the Malaysian population based on the 3 parameters (Figures 5 and 6) recorded in this study was located within a good position,

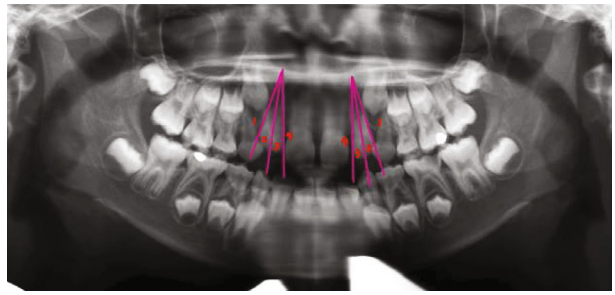

Figure 6: Showing parameter 3 traced on panoramic radiograph.

where they are not located in close proximity or overlapping with the lateral incisors, nor they are in a position that shows a concerning path of eruption.

2.2. Data Analysis. All the available PANs were analyzed to determine the average position, angular measurements, and sector locations of the unerupted maxillary canines. Cohen's kappa was used for intraexaminer reliability. The average position was calculated as average angles between axes of the unerupted canines and the lateral incisors (3^2). Descriptive statistics were then applied to the angulations and sector locations to obtain the mean, standard deviation, median, and range. Mann–Whitney U test was used to analyze the significant differences between male and female patients for each parameter with the significance (α) value set at 0.05. Wilcoxon signed-rank test was used to detect the significant differences between the median of the study and the hypothetical mean of the previous study to predict the risk of impaction of those canines. SPSS (IBM SPSS Statistics for Windows, Version 20.0. Armonk, NY: IBM Corp) was used to analyze all the data.

3. Results

A total of 289 PANs (126 males and 163 females) were utilized for the analysis. Hence, 578 canines were analyzed cumulatively with an equal number of left and right canines of 289. Assessment for good intraexaminer reliability with Cohen's kappa analysis yielded a result of $\kappa = 0.84$. Table 1 shows the descriptive statistics of the right and left maxillary canines. We can observe that both the mean and median of the angle between lateral incisor-canine and the angle between bicondylar line-canine are higher in the left canine compared to the right canine. Based on 3^2 angulation, higher mean and median were found in the female population compared to males. However, lower observed mean and median were found in the female population in terms of bicondylar angulation. The finding of our study indicates that the sector locations of unerupted canine cusp tips are primarily located in the sector I.

The frequency of the sector locations of the unerupted canine cusp tip in relation to the lateral incisor was summarized in Table 2. From the 289 PANs observed, the majority of both right and left canine cusp tips are located in sector I with a percentage of 90.7% and 86.5%, respectively, followed by sector II with a percentage of 7.3% on the right and 12.8%

Table 1: Descriptive details of right and left maxillary canines.

Parameter		3^2	Bicondylar	Sector
Right	Mean (SD)	19.204 (11.197) Male: 16.832 (10.637) Female: 20.919 (11.238)	69.654 (11.346) Male: 70.604 (10.612) Female: 68.919 (11.863)	
	Median (range)	17.598 (84.469) Male: 15.587 (84.469) Female: 19.358 (68.38)	70.391 (156.572) Male: 71.397 (72.905) Female: 69.385 (76.425)	1 (0)
Left	Mean (SD)	19.872 (9.991) Male: 17.622 (9.991) Female: 21.518 (9.624)	70.639 (10.671) Male: 71.640 (10.496) Female: 69.864 (10.773)	
	Median (range)	19.106 (74.916) Male: 17.095 (74.413) Female: 20.363 (55.810)	71.397 (161.899) Male: 72.402 (81.453) Female: 70.391 (67.745)	1 (0)

SD: standard deviation.

Table 2: Frequency data of sector location.

Sector	*n* (%)	
	Right	Left
I	262 (90.7%)	250 (86.5%)
II	21 (7.3%)	37 (12.8%)
III	5 (1.7%)	0
IV	1 (0.3%)	2 (0.7%)
Total	289	289

Table 3: Differences of radiographic parameters between males and females.

Parameters	*N*	3^2		Bicondylar	
		Mean (SD)	*p* values	Mean (SD)	*p* values
Right					
Male	126	16.832 (10.637)	0.001*	70.604 (10.612)	0.147
Female	163	20.919 (11.238)		68.919 (11.863)	
Left					
Male	126	17.622 (9.991)	0.000*	71.640 (10.496)	0.094
Female	163	21.518 (9.624)		69.864 (10.773)	

*$p < 0.05$; Mann–Whitney *U* test for two group comparison; SD: standard deviation.

on its left. Besides that, a total of 5 teeth were observed in sector III and three teeth in sector IV; however, none of them was found on the left side in sector III.

The female predilection (20.91 ± 11.238) was found higher for right side Li-C angle than their male (16.83 ± 10.63) counterparts ($p = 0.001$) as described in Table 3. Females had a significantly higher mean angle of the left canine than males ($p < 0.001$). In regard to the angles between the bicondylar line and permanent maxillary canine, the mean scores were not significantly different ($p > 0.05$) on both left and right sides. However, the mean is still higher in males compared to females.

Table 4: Differences of radiographic parameters between hypothetical mean and observed median values.

Parameters	*p* value
3^2 right	<0.001*
3^2 left	<0.001*
Bicondylar right	0.230
Bicondylar left	0.012*

*$p < 0.05$; Wilcoxon signed-rank test for two studies comparison.

Our findings in Table 4 show that the average position of the maxillary canines in our population based on the parameters recorded, with the exception of the bicondylar right angle, is statistically different from the theoretical mean values of nonimpacted canines in previous studies, with *p* values less than 0.05. However, based on Table 5, on average, at least 70% of canines in our population are still located within the safe range of satisfactory position. Therefore, this finding might suggest that the canine position in our population is not a high-risk position for impaction. From another perspective, in each of the recorded parameters, females show a higher percentage of being located outside of the satisfactory position than males. Apart from that, left canines also show a slightly higher percentage compared to right canines within the unsatisfactory range. Out of all the parameters recorded, the bicondylar angle shows the least percentage of canines that is located within the satisfactory range, followed by the 3^2 angle and sector location.

4. Discussion

Maxillary canines are the most commonly impacted teeth, excluding the third molars. Numerous studies have been done on various populations globally to identify its incidences, such as in South China, Japan, and Italy [15–17]. The results cumulatively showed a range of 1-3% [18–21]. Even though it might seem like it affects a relatively small proportion of people, it is speculated that in individual

Table 5: Prediction of the risk of canine impaction.

Parameter		Angle, *n* (%)	Gender, *n* (%)	Mean (SD)	Median (range)
3^2	Right	≤30: 249 (86.2%)	M: 117 (92.9%) F: 132 (81.0%)	15.900 (6.842)	16.089 (29.665)
		>30: 40 (13.8%)	M: 9 (7.1%) F: 31 (19.0%)	39.771 (11.160)	35.698 (54.302)
	Left	≤30: 248 (85.8%)	M: 117 (92.9%) F: 131 (80.4%)	17.101 (7.153)	17.095 (29.162)
		>30: 41 (14.2%)	M: 9 (7.1%) F: 32 (19.6%)	36.630 (8.205)	34.190 (45.251)
Bicondylar	Right	<65: 85 (29.4%)	M: 29 (23%) F: 56 (34.4%)	56.676 (10.267)	59.832 (47.765)
		≥65: 204 (70.6%)	M: 97 (77%) F: 107 (65.6%)	75.061 (6.254)	74.916 (28.156)
	Left	<65: 71 (24.6%)	M: 21 (16.7%) F: 50 (30.7%)	56.987 (9.081)	60.335 (49.777)
		≥65: 218 (75.4%)	M: 105 (83.3%) F: 113 (69.3%)	75.085 (6.611)	74.413 (32.682)
Sector	Right	I: 262 (90.7%)	M: 116 (92.1%) F: 146 (89.6%)		1 (0)
		II, III, IV: 27 (9.3%)	M: 10 (7.9%) F: 12 (10.4%)		2 (2)
	Left	I: 250 (86.5%)	M: 114 (90.5%) F: 136 (83.4%)		1 (0)
		II, III, IV: 39 (13.5%)	M: 12 (9.5%) F: 27 (16.6%)		2 (2)

n = 289; SD: standard deviation.

orthodontic practice, the incidence may be higher [22]. This anomaly also shows a female predominance in various studies published in the literature with the condition affecting female patients 2.3 to 3 times more frequently than males [23–26]. Prior studies [24, 27–29] also found that left maxillary canines are more frequently affected compared to right canines. The present study may reflect the findings of these previous studies, where the females and left canines in this study are more predominant within the unsatisfactory range of position compared to males and right canines, respectively.

Despite various prevalence figures mentioned above, the etiology of impacted maxillary canines remains uncertain. A single or exclusive cause cannot fully determine the maxillary permanent canine impaction's outcome and could be multifactorial [30]. The contributing factors can be either general or local [25]. Examples of general factors are if the patient has systemic diseases such as endocrine deficiencies, any febrile diseases, and if the patient has a history of radiation exposure. On the other hand, the local contributing factors that cause canine impaction include the discrepancies between tooth size and the arch length, any retained deciduous canine or failure of resorption of the primary canine root, and early loss of the deciduous canine. Peck et al. [31] reported that missing or peg-shaped lateral incisors and abnormal position of the tooth bud play a role in determining the impaction of permanent maxillary canine. Other anomalies such as the presence of alveolar cleft, ankylosis of the permanent canine, cystic or neoplastic formation, and dilacerations of the root also may cause disturbances to the eruption path, thus causing impaction of those canines. Along with it, evidence of genetic predisposition and familial occurrence of impacted canines were also found [32].

Prior studies [8–10, 17, 18, 20] investigated on impacted canines and reported that palatally displaced canines (PDC) and buccally displaced canines (BDC) have different etiopathogenesis. BDC is thought to be a result of crowding [29] and PDC, however, often occurs in patients with sufficient space in the maxillary arch for canine eruption [33]. The "guidance theory" refers to the lack of guidance by the adjacent teeth during the canine eruption, such as missing maxillary lateral incisors [34, 35]. The "genetic theory" explains that PDC is only one aspect of a general dental disorder that is genetic in origin and hereditary, which also causes other dental anomalies such as peg-shaped lateral incisors, cleft lip, and palate, and displaced premolars [17, 23, 24, 36–42]. In the present study, further analysis of the sample background and follow-up of the outcome of the canine position is either impacted buccally or palatally or not.

During patient history taking and examination, the dentist should suspect a potentially palatal impaction of permanent maxillary canine if the canine is not palpable in the buccal sulcus by the age of 10 to 11 years, and asymmetrical eruption pattern of canine is noted [6]. The early detection of signs of ectopic eruption of the canines will prevent

impaction and its potential sequelae. Ericson and Kurol [43] also suggested that an early diagnosis and treatment of the palatally ectopic canine is essential for a successful outcome. Based on the algorithm for management of the ectopic canine, radiographic investigations are indicated in patients ten years old and above with no canine bulge seen or palpable to detect any pathology or if there is a missing permanent tooth bud. Otherwise, if there is evidence of the canine presence and favorable for normal eruption, the child patient aged 10 to 13 years old might need an interceptive treatment and monitor their canine eruption for 12 months. Suppose, no permanent successor is present in the radiographic assessment. In that case, it is a sign that the patient might need a referral for specialist consultation and management and subsequent definitive orthodontic treatment if required. If not intercepted early, the impacted canine will cause several possible complications, such as root resorption of the adjacent teeth, formation of a dentigerous cyst, infection, and referred pain [26, 44–46]. Ravi et al. [47] reported that the sector classification, the angle formed by the long axis of the canine and the midline, an angle formed by the long axis of the canine and the lateral incisor, and the perpendicular distance between the canine cusp tip to the occlusal plane and to the midline and an angle formed by the long axis of the canine and the occlusal plane are commonly used predictors for maxillary impaction. The authors also reported that PANs are the best tools for the prediction of maxillary canine impaction. In the present study, PANs for the prediction of canine impaction are in the maxillary arch. Dadgar et al. [48] reported that the head and neck skeletal anomalies or variants could be used for the prediction of palatal canines. The present study was not explicitly focused on palatal canines, and PANs were used for the analysis.

The findings in the present study showed that the average position of unerupted canines in the Malaysian population is statistically different from the theoretical average value of unerupted nonimpacted canines from previous studies. This suggests that the average unerupted canine position in the Malaysian population is unsatisfactory. However, this is probably because the theoretical mean values that are used to compare with the means obtained in this study consist of the mean values of unerupted nonimpacted canines' position from a sample of a different population from the present article. The present study consists of the Southeast Asian population, while the previous studies used in this comparison consist of the United States and South Asian populations. More retrospective studies using more radiographic and clinical indicators in the Southeast Asian population need to be done to confirm the risk of impaction. Other than that, in the present study, all outliers are included within the data analysis, to prevent the exclusion of children that are actually at high risk for impaction. This may also bring about the difference of average in the present study to the theoretical value. Therefore, the percentage of canines within the satisfactory or unsatisfactory range provides more significance in determining whether the position of unerupted canines in the Malaysian population is within a satisfactory and low-risk position. The study sample size is very small, and the findings were confined only to the Malaysian population. The study sample was hospital-based. Nonetheless, a follow-up of the subsequent canine position from the sample population should be conducted to confirm whether the unsatisfactory range in this study foreshadows canine impaction. These are considered potential limitations of the present study. Various treatments might be suggested for an individual on a case-by-case basis.

5. Conclusion

The majority of the maxillary permanent canine buds of Malaysian children of 9 to 10 years of age are in an acceptable position. An early prediction of maxillary canine is beneficial for the dentist to develop an appropriate treatment plan to avoid potential complications.

(i) On average, more than 85% of canines in our population were still located within the safe range of satisfactory position, with females showing slight predominance outside of the acceptable range

(ii) The mean scores of the angles between the right canine and lateral incisor were significantly higher among females than males ($p = 0.001$), and females had a significantly higher mean angle of the left canine than males ($p < 0.001$)

Data Availability

The raw data supporting the conclusions of this article will be made available by the authors without undue reservation.

Ethical Approval

International Islamic University of Malaysia Human Research Ethics Committee approved the study under ID no: IREC 2021-006.

Conflicts of Interest

The authors declare that there is no conflicts of interest.

References

[1] Oral Health Division MOH Malaysia, *Clinical Practice Guidelines: Management of the Palatally Ectopic Canine*, CPG 2, 2nd edition, 2016.

[2] M. H. K. Motamedi and K. T. Talesh, "Management of extensive dentigerous cysts," *British Dental Journal*, vol. 198, no. 4, pp. 203–206, 2005.

[3] A. Alqerban, R. Jacobs, P. Lambrechts, G. Loozen, and G. Willems, "Root resorption of the maxillary lateral incisor caused by impacted canine: a literature review," *Clinical Oral Investigations*, vol. 13, no. 3, pp. 247–255, 2009.

[4] D. Mavreas and A. E. Athanasiou, "Factors affecting the duration of orthodontic treatment: a systematic review," *European Journal of Orthodontics*, vol. 30, no. 4, pp. 386–395, 2008.

[5] M. M. Bedoya and J. H. Park, "A review of the diagnosis and management of impacted maxillary canines," *The Journal of the American Dental Association*, vol. 140, no. 12, pp. 1485–1493, 2009.

[6] S. Ericson and J. Kurol, "Longitudinal study and analysis of clinical supervision of maxillary canine eruption," *Community Dentistry and Oral Epidemiology*, vol. 4, pp. 172–176, 1986.

[7] R. Margot, C. D. Maria, A. Ali, L. Annouschka, V. Anna, and W. Guy, "Prediction of maxillary canine impaction based on panoramic radiographs," *Clinical and Experimental Dental Research*, vol. 6, no. 1, pp. 44–50, 2020.

[8] F. Mehta, M. Jain, S. Verma et al., "Morphological comparison of the maxillary arch in buccal and palatal canine impaction among Asian population of Gujarati origin: a hospital-based study," *Healthcare*, vol. 10, no. 5, p. 939, 2022.

[9] A. Alqerban, A. S. Storms, M. Voet, S. Fieuws, and G. Willems, "Early prediction of maxillary canine impaction," *Dentomaxillofacial Radiology*, vol. 45, no. 3, 2016.

[10] A. K. Sajnani and N. M. King, "Early prediction of maxillary canine impaction from panoramic radiographs," *American Journal of Orthodontics and Dentofacial Orthopedics*, vol. 142, no. 1, pp. 45–51, 2012.

[11] A. Almahdy, A. Alqerban, O. Aljasir, Z. Alsaghir, and S. Alhammad, "Early radiographic features of maxillary canine impaction for orthodontically diagnosed children aged between 8-14 years old," *Journal of Clinical and Diagnostic Research*, vol. 12, no. 11, pp. 13–17, 2018.

[12] S. J. Lindauer, L. K. Rubenstein, W. M. Hang, W. C. Andersen, and R. J. Isaacson, "Canine impaction identified early with panoramic radiographs," *The Journal of the American Dental Association*, vol. 123, no. 3, pp. 91–97, 1992.

[13] J. H. Warford, R. K. Grandhi, and D. E. Tira, "Prediction of maxillary canine impaction using sectors and angular measurement," *American Journal of Orthodontics and Dentofacial Orthopedics*, vol. 124, no. 6, pp. 651–655, 2003.

[14] D. D. Quadras, U. S. Krishna Nayak, M. S. Ravi, and P. Pujari, "Early prediction of maxillary canine impaction using sectors and angular measurement-a radiographic study," *Manipal Journal of Dental Sciences*, vol. 2, no. 2, pp. 7–11, 2017.

[15] A. K. Sajnani and N. M. King, "Prevalence and characteristics of impacted maxillary canines in southern Chinese children and adolescents," *Journal of Investigative and Clinical Dentistry*, vol. 5, no. 1, pp. 38–44, 2014.

[16] Y. Takahama and Y. Aiyama, "Maxillary canine impaction as a possible microform of cleft lip and palate," *European Journal of Orthodontics*, vol. 4, no. 4, pp. 275–277, 1982.

[17] R. Sacerdoti and T. Baccetti, "Dentoskeletal features associated with unilateral or bilateral palatal displacement of maxillary canines," *Angle Orthodontics*, vol. 74, no. 6, pp. 723–730, 2004.

[18] S. E. Bishara, "Clinical management of impactedmaxillary canines," *Seminars in Orthodontics*, vol. 4, no. 2, pp. 87–98, 1998.

[19] S. Ericson and J. Kurol, "Radiographic examination of ectopically erupting maxillary canines," *American Journal of Orthodontics and Dentofacial Orthopedics*, vol. 91, no. 6, pp. 483–492, 1987.

[20] R. M. Kramer and A. C. Williams, "The incidence of impacted teeth," *Oral Surgery Oral Medicine Oral Pathology*, vol. 29, no. 2, pp. 237–241, 1970.

[21] B. Thilander and N. Myrberg, "The prevalence of malocclusion in Swedish schoolchildren," *European Journal of Oral Sciences*, vol. 81, no. 1, pp. 12–20, 1973.

[22] J. W. Ferguson, "Management of the unerupted maxillary canine," *British Dental Journal*, vol. 169, no. 1, pp. 11–17, 1990.

[23] A. Becker and S. Chaushu, "Etiology of maxillary canine impaction: a review," *American Journal of Orthodontics and Dentofacial Orthopedics*, vol. 148, no. 4, pp. 557–567, 2015.

[24] E. Mercuri, M. Cassetta, C. Cavallini, D. Vicari, R. Leonardi, and E. Barbato, "Dental anomalies and clinical features in patients with maxillary canine impaction," *The Angle Orthodontist*, vol. 83, no. 1, pp. 22–28, 2013.

[25] J. Cooke and H. L. Wang, "Canine impactions: incidence and management," *The International Journal of Periodontics & Restorative Dentistry*, vol. 26, no. 1, pp. 483–491, 2006.

[26] S. E. Bishara and D. Ortho, "Impacted maxillary canines: a review," *Am J Orthod Dentofacial Orthopaedics*, vol. 101, no. 2, pp. 159–171, 1992.

[27] M. Syrynska and A. Budzynska, "The incidence of uni- and bilateral impacted maxillary canines and their position in dental arch depending on gender and age," *Annales Academiae Medicae Stetinensis*, vol. 54, no. 1, pp. 132–137, 2008.

[28] S. Peck, L. Peck, and M. Kataja, "The palatally displaced canine as a dental anomaly of genetic origin," *The Angle Orthodontist*, vol. 64, no. 4, pp. 249–256, 1994.

[29] H. Jacoby, "The etiology of maxillary canine impactions," *American Journal of Orthodontics*, vol. 84, no. 2, pp. 125–132, 1983.

[30] A. Alqerban, R. Jacobs, S. Fieuws, and G. Willems, "Radiographic predictors for maxillary canine impaction," *American Journal of Orthodontics and Dentofacial Orthopedics*, vol. 147, no. 3, pp. 345–354, 2015.

[31] S. Peck, L. Peck, and M. Kataja, "Prevalence of tooth agenesis and peg-shaped maxillary lateral incisor associated with palatally displaced canine (PDC) anomaly," *American Journal of Orthodontics and Dentofacial Orthopedics*, vol. 110, no. 4, pp. 441–443, 1996.

[32] S. Camilleri, C. M. Lewis, and F. McDonald, "Ectopic maxillary canines: segregation analysis and a twin study," *Journal of Dental Research*, vol. 87, no. 6, pp. 580–583, 2008.

[33] E. Barbato, D. Proietti, and C. Malagola, "Evaluation of upper arch dimensions in subjects with palatally impacted canines," *Mondo Ortodontico*, vol. 15, no. 5, pp. 569–575, 1990.

[34] K. S. Al-Nimri and E. Bsoul, "Maxillary palatal canine impaction displacement in subjects with congenitally missing maxillary lateral incisors," *American Journal of Orthodontics and Dentofacial Orthopedics*, vol. 140, no. 1, pp. 81–86, 2011.

[35] A. Becker, S. Sharabi, and S. Chaushu, "Maxillary tooth size variation in dentitions with palatal canine displacement," *The European Journal of Orthodontics*, vol. 24, no. 3, pp. 313–318, 2002.

[36] S. K. Mallineni and J. Jayaraman, "A novel report of dental development pattern in a 3-year-old girl with three congenitally missing primary canines: a review of the literature and a case study," *Journal of the Indian Society of Pedodontics and Preventive Dentistry*, vol. 39, no. 3, pp. 321–324, 2021.

[37] T. Baccetti, M. Leonardi, and V. Giuntini, "Distally displaced premolars: a dental anomaly associated with palatally displaced canines," *American Journal of Orthodontics and Dentofacial Orthopedics*, vol. 138, no. 3, pp. 318–322, 2010.

[38] K. B. Becktor, K. Steiniche, and I. Kjaer, "Association between ectopic eruption of maxillary canines and first molars," *European Journal of Orthodontics*, vol. 27, no. 2, pp. 186–189, 2005.

[39] S. Camilleri, "Maxillary canine anomalies and tooth agenesis," *European Journal of Orthodontics*, vol. 27, no. 5, pp. 450–456, 2005.

[40] R. Leonardi, S. Peck, M. Caltabiano, and E. Barbato, "Palatally displaced canine anomaly in monozygotic twins," *Angle Orthodontics*, vol. 73, no. 4, pp. 466–470, 2003.

[41] S. Leifert and I. E. Jonas, "Dental anomalies as a microsymptom of palatal canine displacement," *Journal of Orofacial Orthopedics*, vol. 64, no. 2, pp. 108–120, 2003.

[42] S. Nirmala, S. K. Mallineni, and S. Nuvvula, "Pre-maxillary hypo-hyperdontia: report of a rare case," *Romanian Journal of Morphology and Embryology*, vol. 54, no. 2, pp. 443–445, 2013.

[43] S. Ericson and J. Kurol, "Early treatment of palatally erupting maxillary canines by extraction of the primary canines," *The European Journal of Orthodontics*, vol. 10, no. 1, pp. 283–295, 1988.

[44] S. Ericson and J. Kurol, "Resorption of maxillary lateral incisors caused by ectopic eruption of the canines. A clinical and radiographic analysis of predisposing factors," *American Journal of Orthodontics and Dentofacial Orthopedics*, vol. 94, no. 6, pp. 503–513, 1988.

[45] R. J. Rimes, C. N. T. Mitchell, and D. R. Willmot, "Maxillary incisor root resorption in relation to the ectopic canine: a review of 26 patients," *European Journal of Orthodontics*, vol. 19, no. 1, pp. 79–84, 1997.

[46] M. Laurenziello, G. Montaruli, C. Gallo et al., "Determinants of maxillary canine impaction: retrospective clinical and radiographic study," *Journal of Clinical and Experimental Dentistry*, vol. 9, no. 11, pp. e1304–e1309, 2017.

[47] I. Ravi, B. Srinivasan, and V. Kailasam, "Radiographic predictors of maxillary canine impaction in mixed and early permanent dentition–a systematic review and meta-analysis," *International Orthodontics*, vol. 19, no. 4, pp. 548–565, 2021.

[48] S. Dadgar, M. Alimohamadi, N. Rajabi, V. Rakhshan, and F. Sobouti, "Associations among palatal impaction of canine, sella turcica bridging, and ponticulus posticus (atlas arcuate foramen)," *Surgical and Radiologic Anatomy*, vol. 43, no. 1, pp. 93–99, 2021.

Hindawi
BioMed Research International
Volume 2022, Article ID 1880113, 9 pages
https://doi.org/10.1155/2022/1880113

Review Article

Cephalometric Analysis in Orthodontics Using Artificial Intelligence—A Comprehensive Review

Aravind Kumar Subramanian,[1] **Yong Chen**,[1,2] **Abdullah Almalki**,[3] **Gautham Sivamurthy**,[4] **and Dashrath Kafle**[5]

[1]*Department of Orthodontics, Saveetha Dental College and Hospital, Saveetha Institute of Medical and Technical Sciences, Saveetha University, Chennai 600077, India*
[2]*Department of Stomatology, School of Medicine, Xiamen University, 361005, China*
[3]*Orthodontics, Department of Preventive Dental Science, College of Dentistry, Majmaah University, Al Majmaah 11952, Saudi Arabia*
[4]*Dundee Dental School & Hospital, University of Dundee, Scotland, UK*
[5]*Department of Orthodontics, Kathmandu University School of Medical Sciences, Nepal*

Correspondence should be addressed to Dashrath Kafle; dashrath07@yahoo.com

Received 26 October 2021; Accepted 13 May 2022; Published 16 June 2022

Academic Editor: Mohammad Alam

Artificial intelligence (AI) is a branch of science concerned with developing programs and computers that can gather data, reason about it, and then translate it into intelligent actions. AI is a broad area that includes reasoning, typical linguistic dispensation, machine learning, and planning. In the area of medicine and dentistry, machine learning is currently the most widely used AI application. This narrative review is aimed at giving an outline of cephalometric analysis in orthodontics using AI. Latest algorithms are developing rapidly, and computational resources are increasing, resulting in increased efficiency, accuracy, and reliability. Current techniques for completely automatic identification of cephalometric landmarks have considerably improved efficiency and growth prospects for their regular use. The primary considerations for effective orthodontic treatment are an accurate diagnosis, exceptional treatment planning, and good prognosis estimation. The main objective of the AI technique is to make dentists' work more precise and accurate. AI is increasingly being used in the area of orthodontic treatment. It has been evidenced to be a time-saving and reliable tool in many ways. AI is a promising tool for facilitating cephalometric tracing in routine clinical practice and analyzing large databases for research purposes.

1. Introduction

The various applications used regularly, such as Siri and Alexa, have been introduced due to the rapid rise in science and technology. Artificial intelligence (AI) and its aspects serve as the foundation for these applications. The term "artificial intelligence" is usually related to robotics. It describes using technology to create software or a piece of equipment that can easily imitate intelligence and accomplish tasks [1]. The phrase artificial intelligence (AI) refers to a discipline of research involved with designing programs and computers that can collect data, reason about it, and then transform it into intelligent actions [2].

John McCarthy invented the term AI in 1955, and he is widely regarded as the father of AI. John McCarthy coined the word to describe machines' ability to execute tasks that are classified as intelligent [3]. Machine learning algorithms are being used more frequently in orthodontics. Data mining, automated diagnostics, and landmark detection are some of the most often used applications now available [4]. The field of artificial intelligence includes an important branch called expert system (ES). The ES is an information and knowledge processing computer program system that consists mainly of a base of knowledge and an inferential machine. It imitates expert decision-making and work procedures while solving real-world problems in a single field

[5]. AI allows for the organizing, investigation, categorization, and depiction of health data, and its influential design-obtaining and evaluated algorithms aid in the growth of science in general [6]. According to Morgan Stanley, the worldwide usage of AI in the medical sector might grow from $1.30 billion to $10 billion by 2024, a 40% annual growth rate [7].

Latest algorithms are developing rapidly, and computational resources are increasing, resulting in increased efficiency, accuracy, and reliability. Current techniques for completely automatic identification of cephalometric landmarks have established considerable efficiency improvements and increased prospects for their regular use [8, 9]. Deep learning, an advanced machine learning method, has recently gotten great attention. However, the primary move for implementing this newest technique to the automated system of cephalometric analysis was taken newly [10]. According to previous research, systems using the technique of random forest discovered 19 landmarks instantly. Computational performance is also essential when using automatic cephalometric in clinical practice, particularly when the procedure has to give out many landmarks to identify [9].

The primary considerations for effective orthodontic treatment are an accurate diagnosis, exceptional treatment planning, and good prognosis estimation. The AI technology has been used to determine if extractions are essential before the orthodontic treatment and the success of orthognathic surgeries [5, 11]. Arnett and Bergman stated in their article on face solutions in planning and diagnosis for orthodontic treatment that if the diagnosis is incorrect, the patient's aesthetics may deteriorate further, posing a considerable issue [12]. It implies that making diagnoses accurately by the dentist is an essential part of analyzing patients' problems. The main objective of the AI technique is to make dentists' work more precise and accurate. Image segmentation is vital in volumetric medical image analysis and automated or semi-automated computer-aided diagnosis systems. For decades, landmark identification in lateral cephalometric radiograph X-ray has been critical in diagnosis and treatment planning in orthodontic treatment [13]. Two hundred ninety-nine lateral cephalograms with 19 landmarks on X and Y coordinates were obtained from Colombian patients. The results showed that the selected mandibular variables were highly predictable and useful for craniofacial reconstruction [14].

Several studies investigated automated lateral cephalometric landmark identification [4, 15–18]. Arik et al. [8] used convolutional neural networks (CNN) to detect landmarks on lateral cephalogram automatically. Park and Hwang trained on 1028 cephalograms using the deep learning method. The transition from manual cephalometry to AI-based cephalogram is aimed at improving the diagnostic value of analysis by saving time and minimizing errors. Systematic and random errors are the most common types of errors in cephalometric analysis [19, 20]. A digital or scanned cephalometric image is saved in the database and added by software in automated cephalometric analysis. The identification of landmarks by software accomplishes the cephalometric dimensions automatically [21]. This narrative review is aimed at giving an outline of cephalometric analysis in orthodontics using AI.

2. Methodology

To select studies on AI in orthodontics, a narrative review was performed by utilizing Google Scholar, EMBASE, PubMed, MEDLINE, and Science Direct. An electronic literature search was conducted on August 10, 2021. The various search terminologies used were AI, machine learning, machine intelligence, deep learning, cognitive computing, radiomics, prediction machine cephalometric analysis, cephalometric prediction, cephalometric tracing, cephalometric landmarks, orthodontics, and dentistry. The literature search was restricted to the English language only and dated from 1980 to 2021. The significance of search results primarily assessed the articles depending on their abstract and title. After removing duplicate studies, two authors (AKS and YC) individually filtered the abstracts and titles of the citations obtained to eliminate nonqualified articles related to the study's qualifying keywords and criteria. The articles with abstracts or titles which are comprised of classified knowledge not relevant were excluded. The review included articles in the field of orthodontics that were AI-related. Only sufficient records of the data were used.

What about the reliability?

3. Results

The primary search strategy yielded 8420 records. About 135 articles were considered relevant to the reported electronic research. Seventy-one articles were omitted because they did not fulfill the eligibility criteria, and a manual reference search yielded no additional studies. Finally, the inclusion criteria resulted in 64 publications being considered for narrative review.

4. Discussion

4.1. History of AI in Orthodontics. The introduction of usage of AI in dentistry and orthodontics was to solve a variety of issues. The knowledge-based expert system was the first effort to use AI in the field of orthodontics and dentistry. These systems were designed primarily to assist dentists who were not specialists in developing proper diagnoses and successful treatment plans [22]. Research done by Alan Turing in 1950 began to investigate whether machines will have the same level of thinking ability as humans. Turing proposed a test that could be used to determine whether a machine is intelligent. The test is now regarded as a cornerstone of artificial intelligence. Professor Cahit Arf gave a talk at a conference in Turkey titled "Can Machines Think?" In 1958, he asked, "How does a machine think?" Professor Arf illustrated the idea of creating a machine that can think for itself, claiming that it is feasible [23].

After Alan Turing first proposed the "Turing test" to check the machine's ability to exhibit intelligent behaviour equivalent to human intelligence in 1950, John McCarthy provided the idea a name "Artificial Intelligence" in 1956.

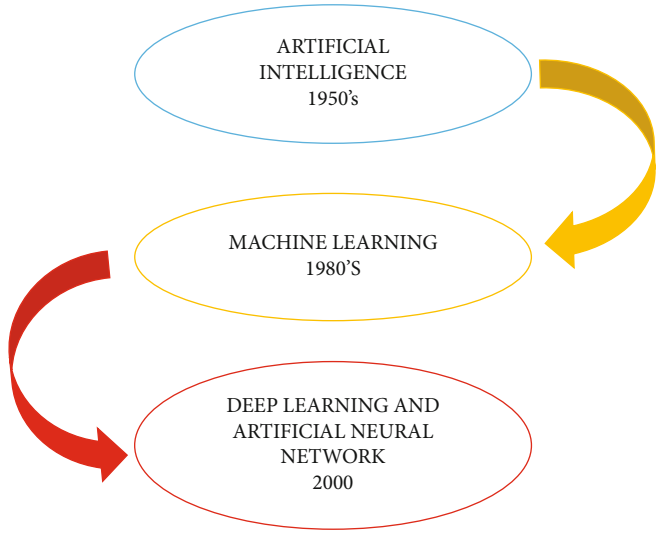

Figure 1: History of artificial intelligence.

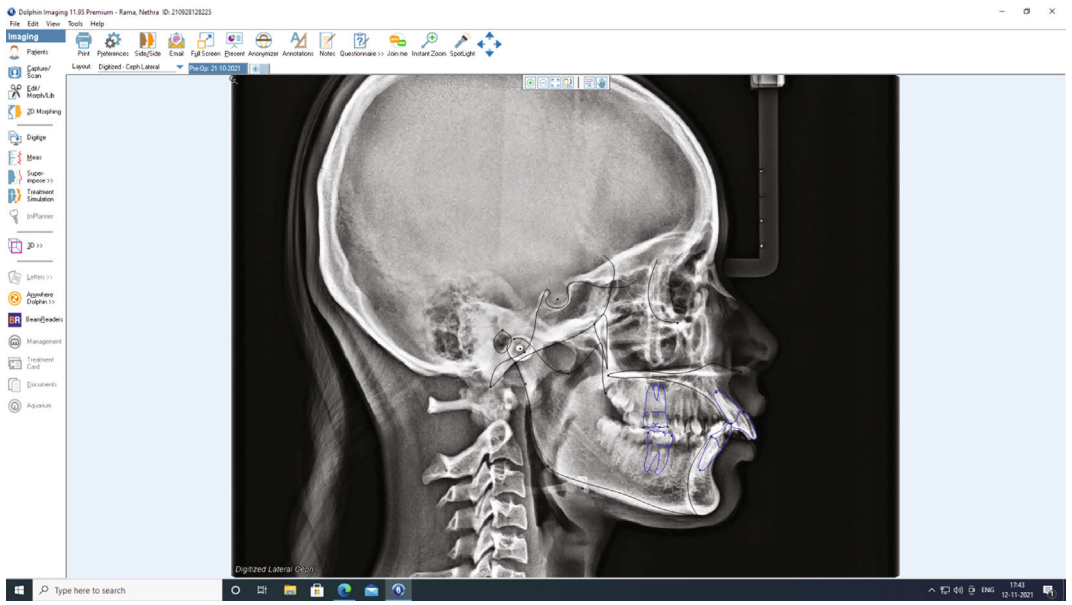

Figure 2: Cephalometric tracing done using Dolphin Imaging technology.

The development of stored-program electronic computers marks the beginning of modern AI. After seven decades, now we have an enormous set of AI-inspired applications, programs, and discoveries, with some of the most significant involvements coming from the orthodontics industry [20]. This discipline began when John McCarthy arranged a popular conference in 1956, an official AI-based research project. The conference ushered in a crucial period of AI research, which lasted from the 1950s to the 1970s [1].

Following the concept of artificial intelligence in the 1950s, the word "machine learning" was introduced in the 1980s, followed by the terms deep learning and artificial neural networks (Figure 1). To comprehend artificial intelligence, one must be familiar with terms such as machine learning, deep learning, and neural networks [23]. Cohen et al. made the first attempt at automated cephalogram landmarking in 1984 [24].

4.2. AI Used for Identification and Analysis of Cephalometric Landmarks. While artificial intelligence is essential in many fields, it is also becoming more prevalent in orthodontics. It has evolved into a valuable tool in orthodontics for correct diagnosis and proper management. The AI is primarily used to identify and analyze cephalometric landmarks, decision-making for tooth extraction, face analysis, tooth and mandible segmentation, bone age determination, prediction of orthognathic surgery, and temporomandibular bone segmentation [17, 18, 23]. Orthodontic diagnosis is a time-spending process that includes a dynamic

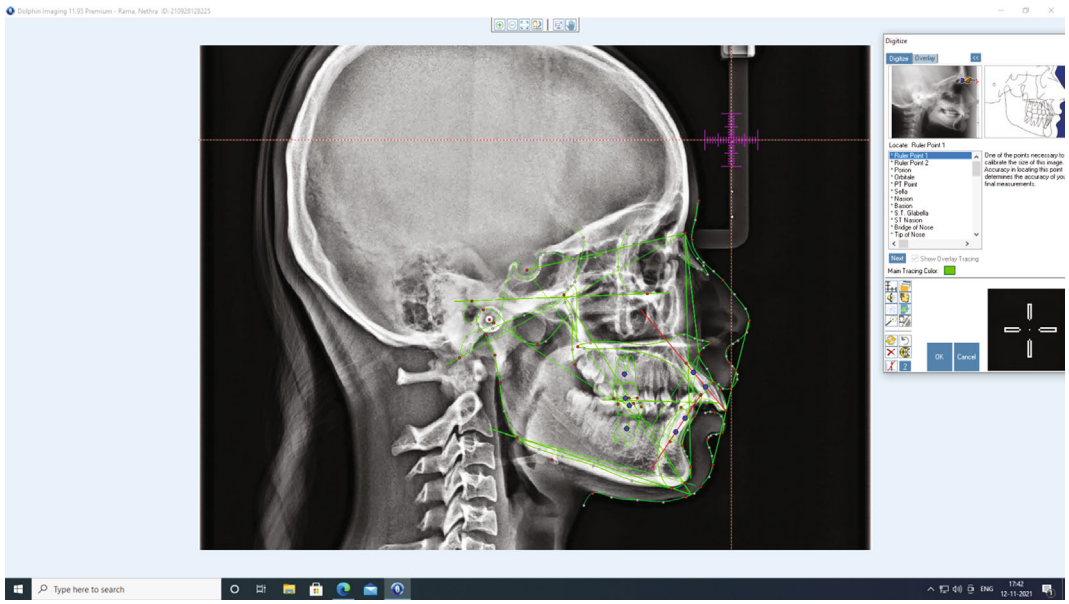

Figure 3: Prediction of cephalometric landmarks using artificial intelligence.

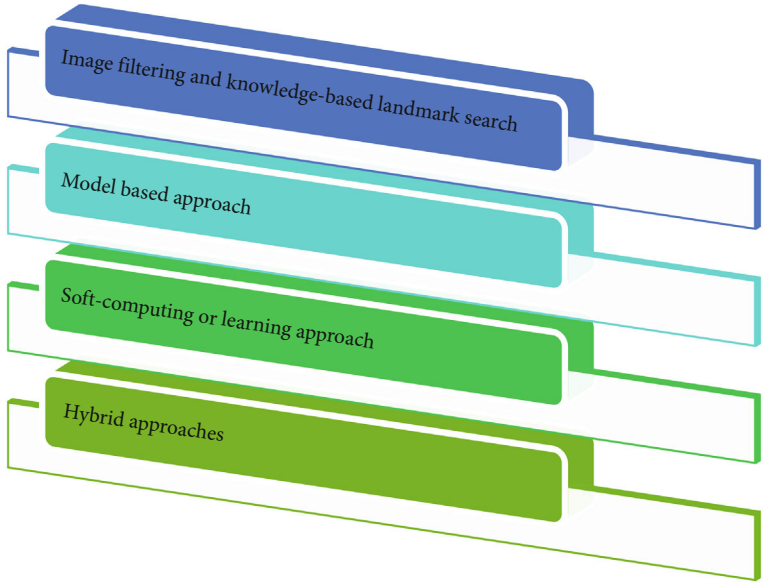

Figure 4: Artificial intelligence approaches to identify landmarks.

examination of the patient, the review and analysis of photographs and radiographic recordings, and model analyses. Different treatment plans may emerge as a result of this complex assessment process among orthodontists. As a result, the orthodontic diagnosis must be automated to improve speed, consistency, and accuracy [25].

Despite advancements and successful implementation of AI in clinical settings, AI applications in dentistry have remained a rarity until now. The first favourable efforts at automated dental decay identification on intraoral radiographs were made [26, 27]. Since Broadbent and Hofrath invented the cephalometer in 1931, it has aided in the assessment of malocclusion and proven to be a reliable diagnostic tool in orthodontic practice and research [21].

Table 1: Types of artificial intelligence used for cephalometric analysis.

S/no.	Types of artificial intelligence
1	Machine learning (ML)
2	Deep learning (DL)
3	Artificial neural network (ANN)
4	Convolutional neural network (CNN)
5	Planmeca Romexis Cephalometric Analysis Software
6	YOLOv3 algorithm
7	Automatic cephalon-diagnostic solutions (ACDS)
8	Web-based applications for automated cephalometric analysis

Table 2: Type of web-based applications and software.

S/no.	Type of web-based applications	Reference
1	CephX (ORCA dental AI, Las Vegas, NV, an artificial intelligence-based software that performs automatic, instant cephalometric analyses	[42]
2	WebCeph and AutoCAD software	[43]
3	Dolphin Imaging, Dentofacial Planner, Quick Ceph, and FACAD	[46]
4	AudaxCeph and OrisCeph Rx	[45]

The cephalometric radiograph assessment of sagittal and vertical skeletal structures introduced by Broadbent is used even now in orthodontic treatment planning. Cephalometric radiograph analysis relies on identifying radiographic landmarks and then measuring various distances, angles, and ratios [8]. The cephalometric analysis is mainly used for three reasons [23].

(1) Depending on the available standards, a sagittal evaluation of hard and soft tissues in the head and face is performed

(2) Changes identified during the reinforcement and treatment procedures

(3) Development and growth as a factor in determining changes

Manual tracing landmarks or AI approaches could be used to perform cephalometric analyses Figure 2. Manual tracing has been around for a long time and is a widely used method; moreover, it is time-consuming and liable to errors. Based on the orthodontists' experience, the cephalogram's quality, and several parameters to assess, manual tracing can take anywhere from 15-20 minutes to complete [26]. Upon tracing landmarks to be used in the design, automated cephalometric analysis transfers landmarks to a computer-attached digitizer; then, cephalometric analysis is completed via distances and angles measured by software after tracing landmarks. Artificial intelligence-assisted cephalometric studies minimize analysis time and enhance diagnostic value by reducing subjective errors [21, 28]. While the software is now generally used for cephalometric assessments, identifying the landmarks is still a routine task that requires the assistance of an orthodontic specialist. The level of quality of this analysis is primarily determined by the expert's experience [19]. Employing by means of improper identification of cephalometric landmarks can cause incorrect orthodontic treatment decisions, detecting completely automatic and accurate cephalometric landmarks is preferred, particularly for quality assurance [8]. This is where AI and machine learning can help orthodontists with their everyday activities. In a variety of ways, computer vision and AI techniques were used to detect cephalometric landmarks automatically Figure 3. Based on the methods used, or a combination of approaches, these approaches can be divided into four broad categories [21]. The approaches are explained in Figure 4.

4.3. Types of AI Programs or Software Used for Cephalometric Analysis

4.3.1. Artificial Intelligence. While AI is a broad topic with many categories, from a computational standpoint, there are two major types: symbolic AI and machine learning. Symbolic AI refers to a set of methods for constructing algorithms in a way that is understandable to humans. This categorization, identified as "good old-fashioned AI" (GOFAI), was the research framework of AI till the late 1980s [29]. The different aspects of artificial intelligence used for cephalometric analysis are illustrated in Table 1.

4.3.2. Machine Learning. The current paradigm is machine learning, a term coined by Arthur Samuel in 1952. The chief difference between symbolic AI and ML is that in ML, features acquire knowledge from explanations rather than from a system of rules devised by humans [6]. The purpose of machine learning is to make it simpler for machines to gain knowledge from records and find solutions without the assistance of humans. The most widely used ML techniques include the Bayesian Network classifier, verdict tree, reinforce path machine, random forest, logistic regression, fuzzified k-nearest neighbour, extreme learning machine, and convolution neural network [1, 30]. Depending on the algorithm's style of learning and the successful outcome, ML can be divided into three categories: organized learning (it is operated for prediction and classification based on an identified result), unorganized learning (it is used for finding designs and hidden configures with the unidentified result), and supported-learning (derived from previous versions, the machine creates a modified algorithm that enhances the intended remuneration) [31].

4.3.3. Deep Learning. Deep learning (DL) is a type of machine learning in which a computer recognizes features in data. The DL's initial version is an artificial intelligence system, which was developed in the 1900s. As computational technology and power have increased exponentially, scientists have created more difficult and deeper neural network models to resolve more challenging and complex problems. DL is the new name for the neural network [7].

4.3.4. Artificial Neural Network. The artificial neural network (ANN) is an algorithmic system that processes data in response to an external stimulus and is made up of artificial neurons, which are fully connected management elements. The artificial neuron is a simplified model that uses

Table 3: Studies related to the application of AI for cephalometric analysis.

Authors and year	Aim	Number of X-rays
Grau et al., 2001 [49]	Aims to identify the landmarks on lateral cephalogram	20
Kim et al., 2020 [41]	The objective of this paper was to create a fully automated cephalometric analysis method based on deep learning, as well as a web-based application that did not require high-end equipment.	2075
Kunz, et al., 2020 [19, 29, 48]	The goal of this study was to use a specialized AI technique to compute an automatic cephalometric X-ray analysis.	1792
Ma et al., 2020 [56]	The goal of the research is to build a suitable automatic landmarking method depending on real OMS data to help surgeons save time during cephalometric analysis.	66
Mario et al., 2010 [33]	To provide an analysis of the cephalometric variables, taking into consideration the system's unspecific, inconstant, and paracomplete data	120
Neelapu et al., 2018 [54]	The study suggested a method for automatically identifying cephalometric landmarks depending on 3D CBCT image data.	30
Nishimoto et al., 2019 [15]	The objective of this research was to create deep learning based automatic cephalometric analysis technique for a computer using cephalogram pictures found online.	219
Rudolph et al., 1998 [53]	This study's goal was to create and test a new computer-based technique for automatically detecting cephalometric landmarks.	14
Rueda and Alcaniz 2006 [50]	The goal of this research is to develop an automated system that uses active appearance models (AAMs)	83
Tanikawa et al., 2010 [25, 52, 55]	The focus of this research was to assess the reliability of the system in recognizing anatomic landmarks and surrounding structures on lateral cephalograms using landmark-specific eligibility criteria.	65
Tanikawa et al., 2010 [25, 52, 55]	To evaluate the system performance that automatically identifies dentoskeletal characteristics on preadolescent children's cephalograms, and to develop a system to do so.	859
Vučinić et al., 2010 [49]	The objective of this study was to assess an automatic method for cephalogram landmarking that relied on an active appearance model (AAM), which is a statistical method that represents both shape and texture variations in the model's coverage areas by analyzing the form and grey-level appearance of an interest point.	60
Yu et al., 2020 [42, 47]	Final analytic methods employ a neural network in each process with lateral cephalograms to provide a reliable and accurate skeletal detection algorithm.	5890
Ed-Dhahraouy et al., 2018 [57]	The purpose of this study was to create a new method for automatically detecting points of reference in 3D cephalometry to overcome some of the limitations of 2D cephalometric analysis.	5
Muraev et al., 2020 [58]	The objective of this study was to create a machine learning technique capable of effectively placing cephalometric positions on frontal cephs and relating it to human accuracy.	300
Park et al., 2019 [4, 42, 43]	The goal of this research was to compare the accuracy and efficiency of two latest deep learning techniques for automatic cephalometric landmark identification.	1028
Hutton et al., 2000 [59]	The goal of this research was to see how precise the active shaped methodology was at locating cephalometric landmarks automatically.	5
Liu et al., 2000 [60]	The goal of this study was to see how precise an edge-based method could make a computerized automatic landmark detection system.	10
Yue et al., 2006 [61]	Aims to analyze all craniofacial anatomical structures.	200
Wang, C.-W., et al., 2016	The goal of the research was to look into and relate different techniques for automatically detecting landmarks in cephalometric X-ray images.	300
Hwang et al., 2021 [9, 61]	To compare a conventional cephalometric assessment with a fully automated cephalometric evaluation using the most advanced deep learning method for identifying cephalometric landmarks.	1983
Lee et al., 2020 [43. 66]	The goal of the study was to use Bayesian convolutional neural networks to create a new framework for finding cephalometric landmarks with competence areas (BCNN).	400
Jeon et al., 2021 [64]	The rapid development of artificial intelligence technologies for medical imaging has recently enabled the automatic identification of anatomical landmarks on radiographs. The purpose of this study was to compare the results of an automatic cephalometric analysis using a convolutional neural network with those obtained by a conventional cephalometric approach.	35
Leonardi et al., 2008 [21, 65]	To describe the techniques used for automatic landmarking of cephalograms, highlighting the strengths and weaknesses of each one and reviewing the percentage of success in locating each cephalometric point.	118 articles

arithmetical structures to mimic the message assimilation and releasing behaviour of biological neural networks [32]. Artificial neurons are linked by interconnections that control data movement between them, just like their biological complements. Inhibitory or excitatory synapses or interconnections transmit stimulus from one processing element to another [33]. Neural networks have an advantage over traditional programmers. They can solve problems for which there is no computational solution or the existing solution is too complicated to find. The recognition and pattern prediction are examples of issues that ANNs are well suited to solving. ANNs have been used in the medical field for diagnosing, image and signal interpretation and analysis, and drug discovery [34, 35].

4.3.5. Convolutional Neural Network. The convolutional neural network uses a DL system that can start taking a record picture and allocate significance to various aspects of it while also distinguishing between them. DL refers to CNN's ability to learn different aspects of an image or to be expected to handle the image's elegance better than regular classification algorithms [36]. The CNN's function is to compact the pictures into a template that is simpler to manage while still retaining essential details. With a deeper understanding of dentistry, CNN can create programs to detect pathologies, automatically identify cephalometric landmarks, segment teeth, and other structures [37].

4.3.6. Planmeca Romexis Cephalometric Analysis Software. It allows for automatic cephalometric point detection and tracing in seconds; however, the software requires that a lateral radiograph be obtained only on the Planmeca cephalometric imaging unit, where it is automatically calibrated, resized, and oriented [38].

4.3.7. YOLOv3 Algorithm. Redmon et al. [39] created the YOLO (You Only Look Once) family of CNNs for fast object detection, which was first described in the article "You Only Look Once: Truly united, Actual Object Recognition" published in the year 2015. The method is divided into three versions: YOLOv1, YOLOv2, and YOLOv3. The first version developed a general framework, the second version sophisticated the design, and the third version further enhanced the network model and training method. For automated cephalometric landmark identification in orthodontic clinical practice, YOLOv3 appeared to be more promising [4].

4.3.8. Automatic Cephalon-Diagnostic Solutions. ACDS is an AI-based software that provides automatic cephalometric landmark detection, cephalometric tracing, measurements, and cephalometric analysis. After uploading thousands of cephalometric images to the computer database, the professor's group at Seoul National University Dental Hospital (SNUDH) developed the program. ACDS, according to the manufacturer, has a high level of accuracy in detecting cephalometric landmarks. Based on the evaluation of 80 landmarks in 253 consecutive digital lateral cephalometric radiographs, the error between the AI algorithm used in ACDS software and human examiners was 0.9 mm [40].

4.4. Web-Based Applications for Automated Cephalometric Analysis. The AI engine server performs the automatic cephalometric analysis. The user can also operate through the client webpage to correct the predicted landmarks. Operator information, cephalometric landmark locations, and cephalograms are all stored on the database server [41]. The types of web-based software are framed in Table 2 [42–45], and studies related to AI in the cephalometric analysis were summarised in Table 3 [4, 15, 19, 21, 32, 41, 46–63].

4.5. Conclusions and Future Perspectives. AI is increasingly being used in the area of orthodontic treatment. In many ways, it has been evidenced to be time-saving and a reliable tool. The AI is a promising tool for facilitating cephalometric tracing in routine clinical practice as well as analyzing large databases for research purposes. This review discusses the history, uses, and various methods of AI used for cephalometric assessment. The main objective of this narrative review was to assist clinicians and researchers in comprehending various features of this study area.

Conflicts of Interest

The authors declared there is no conflict of interest.

References

[1] S. B. Khanagar, A. Al-Ehaideb, P. C. Maganur et al., "Developments, application, and performance of artificial intelligence in dentistry - a systematic review," *Journal of Dental Sciences*, vol. 16, no. 1, pp. 508–522, 2021.

[2] S. Asiri, L. Tadlock, E. Schneiderman, and P. Buschang, "Applications of artificial intelligence and machine learning in orthodontics," *Progress in Orthodontics*, vol. 10, no. 1, pp. 17–24, 2020.

[3] V. Rajaraman, "JohnMcCarthy — father of artificial intelligence," *Resonance*, vol. 19, no. 3, pp. 198–207, 2014.

[4] J.-H. Park, H.-W. Hwang, J.-H. Moon et al., "Automated identification of cephalometric landmarks: part 1—comparisons between the latest deep-learning methods YOLOV3 and SSD," *The Angle Orthodontist*, vol. 89, no. 6, pp. 903–909, 2019.

[5] X. Xie, L. Wang, and A. Wang, "Artificial neural network modeling for deciding if extractions are necessary prior to orthodontic treatment," *The Angle Orthodontist*, vol. 80, no. 2, pp. 262–266, 2010.

[6] J. Faber, C. Faber, and P. Faber, "Artificial intelligence in orthodontics," *APOS Trends Orthod*, vol. 9, no. 4, pp. 201–205, 2019.

[7] Y. M. Bichu, I. Hansa, A. Y. Bichu, P. Premjani, C. Flores-Mir, and N. R. Vaid, "Applications of artificial intelligence and machine learning in orthodontics: a scoping review," *Progress in Orthodontics*, vol. 22, no. 1, pp. 1–11, 2021.

[8] S. Ö. Arik, B. Ibragimov, and L. Xing, "Fully automated quantitative cephalometry using convolutional neural networks," *Journal of Medical Imaging*, vol. 4, no. 1, p. 014501, 2017.

[9] C.-W. Wang, C.-T. Huang, J.-H. Lee et al., "A benchmark for comparison of dental radiography analysis algorithms," *Medical Image Analysis*, vol. 31, pp. 63–76, 2016.

[10] H. Dhillon, P. K. Chaudhari, K. Dhingra et al., "Current applications of artificial intelligence in cleft care: a scoping review," *Frontiers in Medicine*, vol. 8, article 676490, 2021.

[11] M. Mohamed, D. J. Ferguson, A. Venugopal, M. K. Alam, L. Makki, and N. R. Vaid, "An artificial intelligence based referral application to optimize orthodontic referrals in a public oral healthcare system," *Seminars in Orthodontics*, vol. 27, no. 2, pp. 157–163, 2021.

[12] G. W. Arnett and R. T. Bergman, "Facial keys to orthodontic diagnosis and treatment planning. Part I," *American Journal of Orthodontics and Dentofacial Orthopedics*, vol. 103, no. 4, pp. 299–312, 1993.

[13] B. H. Broadbent, "A new X-ray technique and its application to orthodontia: the introduction of cephalometric radiography," *The Angle Orthodontist*, vol. 51, no. 2, pp. 93–114, 1981.

[14] T. C. Niño-Sandoval, S. V. G. Pérez, F. A. González, R. A. Jaque, and C. Infante-Contreras, "Use of automated learning techniques for predicting mandibular morphology in skeletal class I, II and III," *Forensic science International*, vol. 281, pp. 187.e1–187.e7, 2017.

[15] S. Nishimoto, Y. Sotsuka, K. Kawai, H. Ishise, and M. Kakibuchi, "Personal computer-based cephalometric landmark detection with deep learning, using cephalograms on the internet," *Journal of Craniofacial Surgery*, vol. 30, no. 1, pp. 91–95, 2019.

[16] M. K. Alam, A. A. Alfawzan, S. Haque et al., "Sagittal jaw relationship of different types of cleft and non-cleft individuals," *Frontiers in Pediatrics*, vol. 9, article 651951, 2021.

[17] N. Ahmed, M. S. Abbasi, F. Zuberi et al., "Artificial intelligence techniques: analysis, application, and outcome in dentistry—a systematic review," *BioMed Research International*, vol. 2021, Article ID 9751564, 15 pages, 2021.

[18] S. Baumrind and D. M. Miller, "Computer-aided head film analysis: the University of California San Francisco method," *American Journal of Orthodontics*, vol. 78, no. 1, pp. 41–65, 1980.

[19] F. Kunz, A. Stellzig-Eisenhauer, F. Zeman, and J. Boldt, "Artificial intelligence in orthodontics," *Journal of Orofacial Orthopedics/Fortschritte der Kieferorthopädie*, vol. 81, no. 1, pp. 52–68, 2020.

[20] W. Houston, R. Maher, D. McElroy, and M. Sherriff, "Sources of error in measurements from cephalometric radiographs," *The European Journal of Orthodontics*, vol. 8, no. 3, pp. 149–151, 1986.

[21] R. Leonardi, D. Giordano, F. Maiorana, and C. Spampinato, "Automatic cephalometric analysis," *The Angle Orthodontist*, vol. 78, no. 1, pp. 145–151, 2008.

[22] V. Shetty, R. Rai, and K. Shetty, "Artificial intelligence and machine learning: the new paradigm in orthodontic practice," *International Journal of Orthodontic Rehabilitation*, vol. 11, no. 4, pp. 175–175, 2020.

[23] M. K. Alam and A. A. Alfawzan, "Evaluation of Sella Turcica bridging and morphology in different types of cleft patients," *Frontiers in Cell and Developmental Biology*, vol. 8, p. 656, 2020.

[24] A. Cohen, H.-S. Ip, and A. Linney, "A preliminary study of computer recognition and identification of skeletal landmarks as a new method of cephalometric analysis," *British Journal of Orthodontics*, vol. 11, no. 3, pp. 143–154, 1984.

[25] S. Murata, C. Lee, C. Tanikawa, and S. Date, "Towards a fully automated diagnostic system for orthodontic treatment in dentistry," *IEEE 13th International Conference on e-Science (e-Science)*, 2017, Auckland, New Zealand, October 2017, 2017.

[26] K. J. Dreyer and J. R. Geis, "When machines think: radiology's next frontier," *Radiology*, vol. 285, no. 3, pp. 713–718, 2017.

[27] J.-H. Lee, D.-H. Kim, S.-N. Jeong, and S.-H. Choi, "Detection and diagnosis of dental caries using a deep learning-based convolutional neural network algorithm," *Journal of Dentistry*, vol. 77, pp. 106–111, 2018.

[28] A. Richardson, "A comparison of traditional and computerized methods of cephalometric analysis," *The European Journal of Orthodontics*, vol. 3, no. 1, pp. 15–20, 1981.

[29] W. Michael and J. Haugeland, "Artificial intelligence: the very idea," *Technology and Culture*, vol. 28, no. 3, pp. 706–922, 1987.

[30] M. Jordan and T. Mitchell, "Machine learning: Trends, perspectives, and prospects," *Science*, vol. 349, no. 6245, pp. 255–260, 2015.

[31] C. M. Bishop and N. M. Nasrabadi, *Pattern recognition and machine learning*, springer, New York, 2006.

[32] M. C. Mario, J. M. Abe, N. R. Ortega, and M. Del Santo Jr, "Paraconsistent artificial neural network as auxiliary in cephalometric diagnosis," *Artificial Organs*, vol. 34, no. 7, pp. E215–E221, 2010.

[33] S. Haykin, "Redes Neurais: princípios e prática, 2ª edição, tradução: Paulo Martins Engel," *Editora: Bookman, Porto Alegre, Cap*, vol. 1, no. 2, p. 3, 2001.

[34] A. Subasi, M. K. Kiymik, A. Alkan, and E. Koklukaya, "Neural network classification of EEG signals by using AR with MLE preprocessing for epileptic seizure detection," *Mathematical and Computational Applications*, vol. 10, no. 1, pp. 57–70, 2005.

[35] W. G. Baxt, "Application of artificial neural networks to clinical medicine," *The Lancet*, vol. 346, no. 8983, pp. 1135–1138, 1995.

[36] J. Brownlee, "How do convolutional layers work in deep learning neural networks," *Machine Learning Mastery*, vol. 17, 2020.

[37] S. Talaat, A. Kaboudan, W. Talaat et al., "Improving the accuracy of publicly available search engines in recognizing and classifying dental visual assets using convolutional neural networks," *International Journal of Computerized Dentistry*, vol. 23, no. 3, pp. 211–218, 2020.

[38] G. V. Bulatova, B. Kusnoto, V. Grace, T. P. Tsay, D. M. Avenetti, and F. J. C. Sanchez, "Assessment of automatic cephalometric landmark identification using artificial intelligence," *Orthodontics & Craniofacial Research*, vol. 24, no. S2, pp. 37–42, 2021.

[39] J. Redmon, S. Divvala, R. Girshick, and A. Farhadi, "You only look once: unified, real-time object detection," in *Proceedings of the IEEE conference on computer vision and pattern recognition*, pp. 779–788, Las Vegas, NV, USA, 2016.

[40] H.-W. Hwang, J.-H. Park, J.-H. Moon et al., "Automated identification of cephalometric landmarks: part 2-might it be better than human," *The Angle Orthodontist*, vol. 90, no. 1, pp. 69–76, 2020.

[41] H. Kim, E. Shim, J. Park, Y.-J. Kim, U. Lee, and Y. Kim, "Web-based fully automated cephalometric analysis by deep learning," *Computer Methods and Programs in Biomedicine*, vol. 194, p. 105513, 2020.

[42] P. Meriç and J. Naoumova, "Web-based fully automated cephalometric analysis: comparisons between app-aided, computerized, and manual tracings," *Turkish Journal of Orthodontics*, vol. 33, no. 3, pp. 142–149, 2020.

[43] Y. A. Yassir, A. R. Salman, and S. A. Nabbat, "The accuracy and reliability of WebCeph for cephalometric analysis," *Journal of Taibah University Medical Sciences*, vol. 17, no. 1, pp. 57–66, 2022.

[44] H. Alqahtani, "Evaluation of an online website-based platform for cephalometric analysis," *Journal of Stomatology, Oral and Maxillofacial Surgery*, vol. 121, no. 1, pp. 53–57, 2020.

[45] M. Juneja, P. Garg, R. Kaur et al., "A review on cephalometric landmark detection techniques," *Biomedical Signal Processing and Control*, vol. 66, p. 102486, 2021.

[46] H. Yu, S. Cho, M. Kim, W. Kim, J. Kim, and J. Choi, "Automated skeletal classification with lateral cephalometry based on artificial intelligence," *Journal of Dental Research*, vol. 99, no. 3, pp. 249–256, 2020.

[47] P. Vučinić, Ž. Trpovski, and I. Šćepan, "Automatic landmarking of cephalograms using active appearance models," *The European Journal of Orthodontics*, vol. 32, no. 3, pp. 233–241, 2010.

[48] S. Rueda and M. Alcaniz, "An approach for the automatic cephalometric landmark detection using mathematical morphology and active appearance models," in *International Conference on Medical Image Computing and Computer-Assisted Intervention*, Springer, Berlin, Heidelberg, 2006.

[49] V. Grau, M. Alcaniz, M. Juan, C. Monserrat, and C. Knoll, "Automatic localization of cephalometric landmarks," *Journal of Biomedical Informatics*, vol. 34, no. 3, pp. 146–156, 2001.

[50] C. Tanikawa, M. Yagi, and K. Takada, "Automated cephalometry: system performance reliability using landmark-dependent criteria," *The Angle Orthodontist*, vol. 79, no. 6, pp. 1037–1046, 2009.

[51] D. Rudolph, P. Sinclair, and J. Coggins, "Automatic computerized radiographic identification of cephalometric landmarks," *American Journal of Orthodontics and Dentofacial Orthopedics*, vol. 113, no. 2, pp. 173–179, 1998.

[52] B. C. Neelapu, O. P. Kharbanda, V. Sardana et al., "Automatic localization of three-dimensional cephalometric landmarks on CBCT images by extracting symmetry features of the skull," *Dentomaxillofacial Radiology*, vol. 47, no. 2, p. 20170054, 2018.

[53] C. Tanikawa, T. Yamamoto, M. Yagi, and K. Takada, "Automatic recognition of anatomic features on cephalograms of preadolescent children," *The Angle Orthodontist*, vol. 80, no. 5, pp. 812–820, 2010.

[54] Q. Ma, E. Kobayashi, B. Fan et al., "Automatic 3D landmarking model using patch-based deep neural networks for CT image of oral and maxillofacial surgery," *International Journal of Medical Robotics and Computer Assisted Surgery*, vol. 16, no. 3, p. e2093, 2020.

[55] M. Ed-Dhahraouy, H. Riri, M. Ezzahmouly, F. Bourzgui, and A. El Moutaoukkil, "A new methodology for automatic detection of reference points in 3D cephalometry: a pilot study," *International Orthodontics*, vol. 16, no. 2, pp. 328–337, 2018.

[56] A. A. Muraev, P. Tsai, I. Kibardin et al., "Frontal cephalometric landmarking: humans vs artificial neural networks," *International Journal of Computerized Dentistry*, vol. 23, no. 2, pp. 139–148, 2020.

[57] T. J. Hutton, S. Cunningham, and P. Hammond, "An evaluation of active shape models for the automatic identification of cephalometric landmarks," *The European Journal of Orthodontics*, vol. 22, no. 5, pp. 499–508, 2000.

[58] J.-K. Liu, Y.-T. Chen, and K.-S. Cheng, "Accuracy of computerized automatic identification of cephalometric landmarks," *American Journal of Orthodontics and Dentofacial Orthopedics*, vol. 118, no. 5, pp. 535–540, 2000.

[59] W. Yue, D. Yin, C. Li, G. Wang, and T. Xu, "Automated 2-D cephalometric analysis on X-ray images by a model-based approach," *IEEE Transactions on Biomedical Engineering*, vol. 53, no. 8, pp. 1615–1623, 2006.

[60] C.-W. Wang, C.-T. Huang, M.-C. Hsieh et al., "Evaluation and comparison of anatomical landmark detection methods for cephalometric x-ray images: a grand challenge," *IEEE Transactions on Medical Imaging*, vol. 34, no. 9, pp. 1890–1900, 2015.

[61] H.-W. Hwang, J.-H. Moon, M.-G. Kim, R. E. Donatelli, and S.-J. Lee, "Evaluation of automated cephalometric analysis based on the latest deep learning method," *The Angle Orthodontist*, vol. 91, no. 3, pp. 329–335, 2021.

[62] J. H. Lee, H. J. Yu, M. J. Kim, J. W. Kim, and J. Choi, "Automated cephalometric landmark detection with confidence regions using Bayesian convolutional neural networks," *BMC Oral Health*, vol. 20, no. 1, pp. 1–10, 2020.

[63] S. Jeon and K. C. Lee, "Comparison of cephalometric measurements between conventional and automatic cephalometric analysis using convolutional neural network," *Progress in Orthodontics*, vol. 22, no. 1, pp. 1–8, 2021.

[64] A. Cash, S. Good, R. Curtis, and F. McDonald, "An evaluation of slot size in orthodontic brackets—are standards as expected?," *The Angle Orthodontist*, vol. 74, no. 4, pp. 450–453, 2004.

[65] J. N. Weinstein, K. W. Kohn, M. R. Grever et al., "Neural computing in cancer drug development: predicting mechanism of action," *Science*, vol. 258, no. 5081, pp. 447–451, 1992.

Hindawi
BioMed Research International
Volume 2022, Article ID 1503052, 7 pages
https://doi.org/10.1155/2022/1503052

Research Article

Transforming Growth Factor Beta Receptor 2 (TGFBR2) Promoter Region Polymorphisms May Be Involved in Mandibular Retrognathism

Margarita Kirschneck,[1] Nermien Zbidat,[1] Eva Paddenberg,[1] Caio Luiz Bitencourt Reis,[2] Isabela Ribeiro Madalena,[3,4,5] Maria Angélica Hueb de Menezes-Oliveira,[6] César Penazzo Lepri,[6] Peter Proff,[1] Christian Kirschneck,[1] and Erika Calvano Küchler[1]

[1]*Department of Orthodontics, University of Regensburg, Regensburg, Germany*
[2]*Department of Pediatric Dentistry, School of Dentistry of Ribeirão Preto, University of São Paulo, Ribeirão Preto, Brazil*
[3]*Department of Dentistry, University of Joinville Region, Joinville, Brazil*
[4]*School of Dentistry, Presidente Tancredo de Almeida Neves University Center, São João del Rei, Brazil*
[5]*Department of Restorative Dentistry, School of Dentistry, Federal University of Juiz de Fora, Juiz de Fora, Brazil*
[6]*Department Master's Program of Dentistry, School of Dentistry of Uberaba, Uberaba, Brazil*

Correspondence should be addressed to Erika Calvano Küchler; erikacalvano@gmail.com

Received 10 April 2022; Accepted 30 May 2022; Published 15 June 2022

Academic Editor: Mohammad Alam

Skeletal malocclusions are common phenotypes in humans and have a strong influence on genetic factors. Transforming growth factor beta (TGFβ) controls numerous functions of the human body, including cell proliferation, differentiation, and migration. Thus, this study is aimed at evaluating whether genetic polymorphisms in *TGFB1* and its receptor *TGFBR2* are associated with mandibular retrognathism in German children and adolescents. Children and teenagers older than 8 years in the mixed or permanent dentition were included in this study. Patients with syndromes and facial trauma and patients with congenital alterations were excluded. Digital cephalometric tracings were performed using the anatomical landmarks point A, point B, sella (S), and nasion (N). Patients that have a retrognathic mandible (SNB < 78°) were selected as case group, and the patients with an orthognathic mandible (SNB = 78° – 82°) were selected as the control group. Genomic deoxyribonucleic acid (DNA) from saliva was used to evaluate four genetic polymorphisms in *TGFB1* (rs1800469 and rs4803455) and *TGBR2* (rs3087465 and rs764522) using real-time PCR. Chi-square or Fisher exact tests were used to compare gender, genotype, and allele distribution among groups. Genotype distribution was calculated in an additive and recessive model. Haplotype analysis was also performed. The established alpha of this study was 5%. A total of 146 patients (age ranging from 8 to 18 years) were included in this epidemiological genetic study. The genetic polymorphism rs3087465 in *TGFBR2* was associated with mandibular retrognathism. Carrying the AA genotype in the rs3087465 polymorphism decreased the chance of having mandibular retrognathism (odds ratio = 0.25, confidence interval 95% = 0.06 to 0.94, $p = 0.045$). None of the haplotypes was associated with mandibular retrognathism ($p > 0.05$). In conclusion, we found that the genetic polymorphism rs3087465 in the promoter region of the *TGFBR2* was associated with mandibular retrognathism in Germans.

1. Introduction

There are a wide variety of skeletal malocclusions (dentofacial deformities) in humans [1], and the frequency of each dentofacial deformity ranges according to the studied population/ethnicity [2]. One of the most common dental facial deformities is mandibular retrognathism [3], which is a facial alteration of the skeletal jaw-cranial base relationship. Retrognathism is characterized by a retruded position of the mandible as a result of an anomaly of the skeletal jaw-cranial base relationship [4]. This condition has a strong genetic background and some genes have been associated with mandibular retrognathism in humans from different populations in past years [3–6]. Some previous studies associated mandibular retrognathism with genetic polymorphisms in genes encoding *Myosin IH* (*MYO1H*) [5], *Matrilin 1* (*MATN1*) [4], *bone morphogenetic protein 2* (*BMP2*) [7], *ADAM metallopeptidase with thrombospondin type 1 motif 9* (*ADAMTS9*) [6], and *parathyroid hormone* (*PTH*) and the vitamin-D-related genes: *vitamin D receptor* (*VDR*), *cytochrome P450 family 24 subfamily A member 1* (*CYP24A1*), and *cytochrome P450 family 27 subfamily B member 1* (*CYP27B1*) [8].

The transforming growth factor beta (TGFβ) family constitutes a group of three isoforms, TGFβ1, TGFβ2, and TGFβ3. Their structure is formed by interrelated dimeric polypeptide chains. Pleiotropic and redundant functions of the TGFβ family control several functions, such as cell proliferation, differentiation, and migration in all human tissues. The TGFβ family has numerous key roles in the bone tissue controlling physiological phenomena regarding maintenance of metabolic homeostasis [9]. TGFβ isoforms and their receptors, type I receptor (TGFβRI or ALK5) and type II receptor (TGFβRII or TGFBR2) play innumerous essential roles in endochondral and intramembranous ossification [10].

Several functional genetic polymorphisms were identified in TGFB1 (gene encoding TGFβ1) and TGFBR2 (gene encoding TGFβRII) and they were associated with higher serum or plasma level of TGFβ1 and enhanced transcriptional activity of TGFβRII [11]. It is possible that some of these functional genetic polymorphisms play a role in the establishment of maxillary and mandibular morphology leading to skeletal malocclusion phenotypes. Therefore, the present study evaluated if well-known functional genetic polymorphisms in *TGFB1* and its receptor *TGFBR2* are associated with mandibular retrognathism in Germans children and teenagers.

2. Materials and Methods

This study was approved by the Ethics Committee from the University of Regensburg (# 19-1549-101). Informed consent was obtained from all patients and/or their legal guardians (in the case of minors during the sample collection), and age-appropriate assent documents were also used for patients younger than 14 years. This project was made following the Helsinki Declaration. The Strengthening the Reporting of Genetic Association study (STREGA) statement checklist was followed to design the study and report the results. The chi-square test for sample size (power) calculation was performed by PASS 15 Power Analysis and Sample Size Software (NCSS, LLC. Kaysville, Utah, USA). Küchler et al.'s (2021) study was used to obtain the *W* effect size (0.225), with an alpha of 5% and power of 80% the test predicts 155 patients for this study.

This is a cross-sectional nested case-control study design. For this cross-sectional study, patients undergoing orthodontic treatment at private orthodontic practices in Regensburg-Germany and the University of Regensburg were screened. Children and teenagers of both sexes were recruited and they were consecutively included in this study from 2020 to 2021.

Patients with underling syndromes, adults (older than 18 years), patients with mandibular prognathism and congenital alterations including tooth agenesis (except for third molar agenesis), oral cleft patients, and patients with facial trauma were excluded. Only one patient per family was recruited. To minimize genetic and phenotypic variance and to maximize data interpretability, only patients with a Middle-European ancestry (at maximum one grandparent not from Middle Europe) were included. All patients included were children older than 8 years in the mixed or permanent dentition.

2.1. Retrognathic and Orthognathic Characterization. Digital lateral cephalograms from each patient's orthodontic record with the mandible in centric relationship were evaluated in this study.

The measurements were performed by two trained and calibrated examiners. Intraclass correlation coefficients (ICC) were used to calculate intra- and interexaminer reliability. Interexaminer reliability showed significant good agreement for both examiners (ICC, 0.98 - 0.95). Intraexaminer reliability also showed significant good agreement (ICC, 0.97 - 0.91).

Digital cephalometric were tracings performed using the software Ivoris® (Computer konkret AG, Falkenstein, Germany, version 8.2.15.110). The anatomical landmarks point A, point B, sella (S), and nasion (N) were determined manually using the cephalometric analysis software, and, subsequently, the angular measurements SNB and ANB were calculated (Figure 1).

Patients presenting a retrognathic mandible (SNB < 78°) were selected as a case group, while those presenting an orthognathic mandible (SNB = 78° – 82°) were selected as a control group. Patients having mandibular prognathism (SNB > 82°) were excluded.

2.2. Selection of Genetic Polymorphisms and Laboratorial Analysis. For the selection of the genetic polymorphisms, we searched the promoter, intronic, and coding genetic polymorphisms of the *TGFB1* and *TGFBR2* from the dbSNP database (http://www.ncbi.nlm.nih.gov/snp/). Only genetic polymorphisms with heterozygosity above 0.2 in the global population were considered. The classification of each genetic polymorphism as potentially functional (polymorphisms that can result in amino acid changes of the corresponding proteins or occurring in the promoter region of

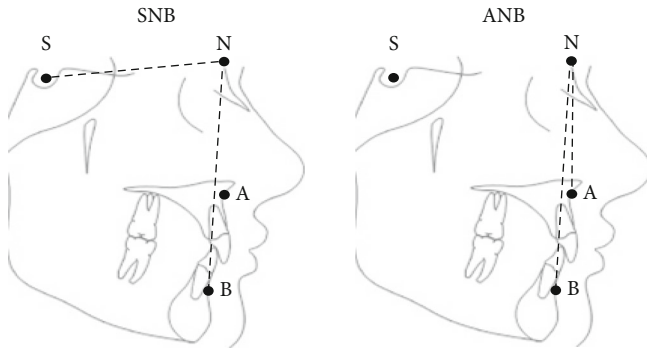

Figure 1: Lateral cephalometric landmarks and reference lines studied. Points: point A, point B, sella (S), and nasion (N).

Table 1: Characteristics of the studied genetic polymorphisms.

Gene	Polymorphism and base change	Comments
TGFB1 *Transforming growth factor beta 1*	rs1800469 (T/C)	Polymorphism rs1800469 is located in the promoter region of the TGFB1 gene and has the function of regulating expression levels of protein TGFβ1 (affects gene transcriptional activity and serum levels of TGFβ1) [19, 20].
	rs4803455 (C/A)	The polymorphism rs4803455 is located in intron 2 of TGFB1 gene and was associated with a variety of different conditions (https://www.ncbi.nlm.nih.gov/snp/rs4803455). Moreover, it was suggested as a potential genetic marker for growth response to recombinant human growth hormone (r-hGH) treatment [38].
TGFBR2 *Transforming growth factor beta receptor 2*	rs3087465(A/G)	Polymorphism rs3087465 is located in the promoter region of the gene and increases TGFβ type II receptor expression [26].
	rs764522 (G/C)	The polymorphism rs764522, which is located in 5 kb upstream in the promoter region of *TGFBR2* increases TGFβ type II receptor expression [26].

the gene and potentially affecting the expression of the gene or previously associated with other conditions and potentially clinically relevant) was also taken into consideration in the selection process. The characteristics and description of the genetic polymorphisms selected for this study are presented in Table 1.

For the genotyping analysis, we used genomic DNA that was isolated from buccal epithelial cells collected using two cytobrushes placed in extraction solution (Tris-HCl 10 mmol/L, pH 7.8; EDTA 5 mmol/L; SDS 0.5%, 1 mL). Briefly, proteinase K (100 ng/mL) were added to each tube. Ammonium acetate was added to eliminate nondigested proteins, and the liquid was then centrifuged. DNA was precipitated with isopropanol, washed with ethanol. The DNA was quantified by spectrophotometry (Nanodrop 1000; Thermo Scientific, Wilmington, DE, USA) [12].

The selected genetic polymorphisms, which were described in Table 1, were blindly genotyped via real-time polymerase chain reaction (PCR) using the Mastercycler® ep realplex-S thermocycler (Eppendorf AG, Hamburg, Germany). The TaqMan technology was used. Initial denaturation at 95°C for 30 seconds, followed by 40 cycles of denaturation at 92°C for 5 seconds and annealing/extension at 60°C for 20 seconds. The 3.125 μL reaction volume contained 1.5 μL Master Mix, 0.125 μM TaqMan probe, and 4 ng DNA in 1.5 μM nuclease-free water. Assays and reagents were supplied by Applied Biosystems (Foster City, CA, USA). A negative control template was included in each reaction (each 96-well plate), in which the reaction mixture contains the reagents, but not the DNA. Additionally, 10% of the samples were randomly selected in order to repeat the analysis and showed 99% concordance.

Patients with not enough DNA or DNA samples that failed to be genotyped in the PCR analysis were excluded from the further analyses.

2.3. Statistical Analysis. Chi-squared test estimated the Hardy-Weinberg equilibrium (HWE) for each studied polymorphism (https://wpcalc.com/en/equilibrium-hardy-weinberg/).

Chi-squared or Fisher's exact tests compared gender, genotype, and allele distribution among groups and genotype distribution was calculated in an additive model and recessive model. Haplotype analysis was also performed. PLINK version 1.06 (https://zzz.bwh.harvard.edu/plink/ld.shtml) was used for the analysis with an established alpha of 5% ($p < 0.05$). The odds ratio and confidence interval 95% was calculated to investigate the chance of presenting mandibular retrognathism for the associated genetic polymorphism.

3. Results

A total of 168 patients were screened, two patients were excluded due to biological relations to included patients (siblings), one due to oral cleft, 13 due to age older than 18 years,

Table 2: Comparison of cephalometric variables between mandibular retrognathism and orthognathic mandible.

Variables	Orthognathic mandible ($n = 50$)	Mandibular retrognathism ($n = 96$)	p value
Gender, n (%)			
Male	29 (58.0%)	45 (46.8%)	0.202
Female	21 (42.0%)	51 (53.2%)	
SNB (°)			
Mean (SD)	79.62 (SD 1.07)	78.32 (SD 2.67)	0.001∗
ANB (°)			
Mean (SD)	3.48 (SD 2.75)	4.26 (SD 2.27)	0.068

Note: SD: standard deviation; ∗statistically significant difference ($p < 0.05$); n: number of individuals; %: percent; °: degrees.

and six patients due to mandibular prognathism. Finally, 146 patients (age ranging from 8 to 18 years) were included in this epidemiological genetic study. The characteristics of the included sample are presented in Table 2. Mean age in the mandibular retrognathism group was 11.56 years (standard deviation = 2.05), while the mean age in the mandibular retrognathism group was 12.66 years (standard deviation = 2.2). The SNB angle was significantly lower in the mandibular retrognathism group (ranging from 66.0° to 77.9°) than in the control group (ranging from 78.1° to 81.9°) ($p = 0.0014$).

All the genetic polymorphisms assessed were within the Hardy-Weinberg equilibrium (chi-square$^{HWE} = 0.452$ for rs1800469, chi-square$^{HWE} = 0.309$ for rs4803455, chi-square$^{HWE} = 3.17$ for rs3087465, and chi-square$^{HWE} = 0.161$ for rs764522). For the rs1800469 (A/G), rs4803455 (C/A), rs3087465 (A/G), and rs764522 (G/C) polymorphisms, success rates of genotyping were 95.9%, 90.4%, 95.9%, and 91.8%, respectively.

Table 3 shows the genotype and allele distributions and the association results in the allele distribution and genotype distribution in additive and recessive models. The only significantly associated polymorphism was rs3087465 in *TGFBR2*. Patients that carry the AA genotype in the polymorphism rs3087465 had significantly decreased the chance to have mandibular retrognathism (odds ratio = 0.25, confidence interval = 0.06 to 0.94, $p = 0.045$).

The haplotype analysis for the polymorphisms in *TGFB1* (rs4803455-rs1800469) and *TGFBR2* (rs764522-rs3087465) is presented in Table 4. There was no statistically significant association ($p > 0.05$).

4. Discussion

Some studies evaluating dentofacial deformities via cephalometric images in different populations/ethnicities have been performed in the past decades to investigate the genetic contribution of different skeletal malocclusions. Literature reviews showed that many genes involved in a range of functions are associated with skeletal malocclusions [13, 14], especially genes encoding growth factors and growth factor receptors [8, 15–17]. Growth factors are found in all tissues; they regulate local cell-to-cell metabolism and mediate cellular effects of different hormones. Bone matrix is a large reservoir for numerous growth factors that are regulators of bone remodeling processes [18]. Therefore, we hypothesized that functional genetic polymorphisms in *TGFB1* and *TGFBR2* could be involved in the etiology of mandibular retrognathism in Germans.

In our study, we explored two well-known genetic polymorphisms in *TGFB1*. Several polymorphisms have been described in the coding and regulatory sequences of the *TGFB1* gene, including a promoter polymorphism involving a cytosine-to-thymine transition. The -509C/T functional promoter polymorphism (rs1800469) within the *TGFB1* gene has been extensively assessed in different genetic epidemiological studies. Moreover, a number of studies have attempted to investigate whether the polymorphic variants in *TGFB1* change TGFβ1 expression [19–21]. Another genetic polymorphism widely explored in different conditions is rs4803455 involving a C-to-A transition, which is located in intron 2 of *TGFB1* and was therefore selected in our study. Although both variants (rs1800469 and rs4803455) with a known role were hypothesized as potential candidates for mandibular retrognathism, none of these genetic polymorphisms were associated with the phenotype in our study. However, it is possible that other polymorphisms in these genes could be involved in mandibular retrognathism.

TGFB initially binds its receptor, which is TGFBR2 and later transactivates TGFBR1, leading to the formation of a heterotetrameric receptor complex. TGFBR1 and TGFBR2 are members of the serine-threonine protein kinase family. TGFBR2 is a constitutive kinase, while TGFBR1 kinase is only activated after the formation of the TGFB/TGFBR2 complex [22]. Recently, there have been several studies investigating the association between genetic polymorphisms in *TGFBR2* in various diseases, such as abdominal aortic aneurysm, papillary thyroid carcinoma, and end-stage renal disease, especially two promoter polymorphisms rs764522 (-1444C/G) and rs3087465 (-834A/G) [23–25]. Therefore, we decided to investigate these polymorphisms in our study. We observed that the AA genotype in polymorphism rs3087465 (-834A/G) acted as a protective factor for mandibular retrognathism. Interestingly, this genetic polymorphism located in a promoter region was previously associated with alterations in TGFβ type II receptor expression [26–28].

Although the sample size was a limitation that could lead to a type I error, our results raised a possibility of a novel candidate gene for mandibular retrognathism. It is interesting to mention that mutations in the *TGFBR2* gene are associated with Marfan syndrome [29] and Loeys-Deitz syndrome [30]. The craniofacial phenotypes of these both syndromes included mandibular retrognathism as a common trait observed [31–33], which clearly suggests the role of genetic polymorphisms in *TGFBR2* in nonsyndromic mandibular retrognathism. Also, studies with animal models

Table 3: Genotype distribution among group and p values.

Gene	rs	Genotype distribution and allele distributions, n (%)			p value^{Genotype}	p value^{Allele}	p value^{Recessive}
		Genotype	Orthognathic mandible	Mandibular retrognathism			
TGFB1	rs1800469	TT	5 (10.0)	4 (4.4)	0.310	0.525	0.199
		CT	18 (36.0)	41 (45.6)			
		CC	27 (54.0)	45 (50.0)			
		A	28 (28.0)	49 (27.2)			
		G	72 (72.0)	131 (72.8)			
	rs4803455	CC	10 (20.8)	18 (21.4)	0.740	0.692	0.478
		CA	27 (56.3)	42 (50.0)			
		AA	11 (22.9)	24 (28.6)			
		C	47 (48.0)	78 (46.4)			
		A	49 (52.0)	90 (57.3)			
TGFBR2	rs3087465	AA	6 (12.0)	3 (3.3)	0.098	0.603	0.045*
		AG	21 (42.0)	48 (53.3)			
		GG	23 (46.0)	39 (43.3)			
		A	33 (33.0)	54 (30.0)			
		G	67 (67.0)	126 (70.0)			
	rs764522	GG	0 (0.0)	2 (2.3)	0.575	0.525	0.302
		GC	11 (23.9)	22 (25.0)			
		CC	35 (76.1)	64 (72.7)			
		G	11 (12.0)	26 (14.8)			
		C	81 (88.0)	150 (85.2)			

Note: *means statistically significant difference; n: number of individuals; %: percent; rs: the code of polymorphisms; *TGFB1*: transforming growth factor beta 1; *TGFBR2*: transforming growth factor beta receptor 2; C: cytosine; A: adenine; T: thymine; G: guanine.

Table 4: Haplotype analysis of the studied genetic polymorphisms.

Gene	Haplotype		Frequency		p value
			Orthognathic mandible	Mandibular retrognathism	
TGFB1	rs4803455-rs1800469	CT	0.264	0.242	0.706
		AT	0.027	0.025	0.930
		CC	0.225	0.213	0.818
		AC	0.482	0.517	0.586
TGFBR2	rs764522-rs3087465	GA	0.084	0.103	0.610
		CA	0.252	0.208	0.407
		GG	0.035	0.049	0.602
		CG	0.627	0.639	0.855

Note: *TGFB1*: transforming growth factor beta 1; *TGFBR2*: transforming growth factor beta receptor 2; C: cytosine; A: adenine; T: thymine; G: guanine.

have demonstrated that TGFBR2 plays a critical role in the formation of the intramembranous bone and endochondral bone and that TGFBR2 is crucial for skeletal development [34, 35] including craniofacial development [34, 36, 37]. Deletion of *Tgfbr2* via Col2a1-Cre in mice caused several defects in the base of the skull [34]. Removal of TGFBR2 driven by Prx-Cre results in defects in the skull vault [37]. Mice with *Tgfbr2* conditional gene ablation in the cranial neural crest have craniofacial anomalies including defects in mandibular development resulting in a smaller mandible [36].

To the best of our knowledge, this is the first study to investigate genes involved in mandibular retrognathism in Germans; however, it is important to emphasize that these findings must be validated in independent larger cohorts. Another important aspect to be discussed is that we investigated children and teenagers. This approach was also performed before. The study from Sasaki et al. [15] investigated the association between a genetic polymorphism in the gene encoding growth hormone receptor (GHR) and mandibular prognathism in children aged 3 to 13 years. The authors concluded that P561T in GHR may affect mandibular growth during early childhood.

Briefly, our results add novel information regarding the genetic contribution to mandibular retrognathism etiology suggesting rs3087465 (-834A/G) in TGFBR2 as candidate

gene, additionally to the previously genes suggested in studies from different populations: *MYO1H* [5], *MATN1* [4], *BMP2* [7], *ADAMTS9* [6], *PTH*, *VDR*, *CYP24A1*, and *CYP27B1* [8]. Once our understanding of the nature of the genetic influences improves, we will be able to provide a clearer idea of how genes and environmental factors interact to influence mandibular retrognathism in humans.

5. Conclusion

The genetic polymorphism rs3087465 in the promoter region of the *TGFBR2* was associated with mandibular retrognathism in Germans. Determining the factors affecting mandibular growth will contribute to early diagnosis and treatment of mandibular retrognathism.

Data Availability

The data generated during the current study are available from the corresponding author on reasonable request.

Conflicts of Interest

The authors declare no conflict of interest.

Acknowledgments

The authors thank all participants of the study. This study was financed in part by the Alexander-von-Humboldt-Foundation (Küchler/Kirschneck accepted on July 4th, 2019) and by the Coordenação de Aperfeiçoamento de Pessoal de Nível Superior–Brasil (CAPES)–Finance Code 001.

References

[1] W. van den Braber, A. van der Bilt, H. van der Glas, T. Rosenberg, and R. Koole, "The influence of mandibular advancement surgery on oral function in retrognathic patients: a 5-year follow-up study," *Journal Oral and Maxillofacial Surgery*, vol. 64, no. 8, pp. 1237–1240, 2006.

[2] L. Kavitha and K. Karthik, "Comparison of cephalometric norms of caucasians and non-caucasians: a forensic aid in ethnic determination," *Journal of Forensic Dental Sciences*, vol. 4, no. 1, pp. 53–55, 2012.

[3] E. C. Küchler, C. L. B. Reis, J. Carelli et al., "Potential interactions among single nucleotide polymorphisms in bone- and cartilage-related genes in skeletal malocclusions," *Orthodontics & Craniofacial Research*, vol. 24, no. 2, pp. 277–287, 2021.

[4] P. B. Balkhande, B. V. K. S. Lakkakula, and A. B. Chitharanjan, "Relationship between matrilin-1 gene polymorphisms and mandibular retrognathism," *American Journal of Orthodontics and Dentofacial Orthopedics*, vol. 153, no. 2, pp. 255–261, 2018.

[5] R. M. Arun, B. V. Lakkakula, and A. B. Chitharanjan, "Role of myosin 1H gene polymorphisms in mandibular retrognathism," *Journal of Orthodontics and Dentofacial Orthopedics*, vol. 149, no. 5, pp. 699–704, 2016.

[6] C. Wang, Z. Ni, Y. Cai, Y. Zhou, and W. Chen, "Association of polymorphism rs67920064 in ADAMTS9 gene with mandibular retrognathism in a Chinese population," *Medical Science Monitor*, vol. 26, p. e925965, 2020.

[7] E. C. Küchler, N. D. Hannegraf, R. M. Lara et al., "Investigation of genetic polymorphisms in BMP2, BMP4, SMAD6, and RUNX2 and persistent apical periodontitis," *Journal of Endodontics*, vol. 47, no. 2, pp. 278–285, 2021.

[8] E. C. Küchler, C. L. B. Reis, G. Marañón-Vásquez et al., "Parathyroid hormone gene and genes involved in the maintenance of vitamin d levels association with mandibular retrognathism," *Journal of Personalized Medicine*, vol. 11, no. 5, p. 369, 2021.

[9] L. A. Poniatowski, P. Wojdasiewicz, R. Gasik, and R. Szukiewicz, "Transforming growth factor beta family: insight into the role of growth factors in regulation of fracture healing biology and potential clinical applications," *Mediators of Inflammation*, vol. 2015, Article ID 137823, 17 pages, 2015.

[10] G. Chen, C. Deng, and Y. P. Li, "TGF-beta and BMP signaling in osteoblast differentiation and bone formation," *International Journal of Biological Sciences*, vol. 8, no. 2, pp. 272–288, 2012.

[11] G. Jin, Y. Deng, R. Miao et al., "TGFB1 and TGFBR2 functional polymorphisms and risk of esophageal squamous cell carcinoma: a case-control analysis in a Chinese population," *Journal of Cancer Research and Clinical Oncology*, vol. 134, no. 3, pp. 345–351, 2008.

[12] E. C. Küchler, P. N. Tannure, P. Falagan-Lotsch, T. S. Lopes, J. M. Granjeiro, and L. M. F. Amorim, "Buccal cells DNA extraction to obtain high quality human genomic DNA suitable for polymorphism genotyping by PCR-RFLP and real-time PCR," *Journal of Applied Oral Science*, vol. 20, no. 4, pp. 467–471, 2012.

[13] L. M. M. Uribe and S. F. Miller, "Genetics of the dentofacial variation in human malocclusion," *Orthodontics & Craniofacial Research*, vol. 18, no. 1, pp. 91–99, 2015.

[14] A. Dehesa-Santos, P. Iber-Diaz, and A. Iglesias-Linares, "Genetic factors contributing to skeletal class III malocclusion: a systematic review and meta-analysis," *Clinical Oral Investigations*, vol. 25, no. 4, pp. 1587–1612, 2021.

[15] Y. Sasaki, K. Satoh, H. Hayasaki, S. Fukumoto, T. Fujiwara, and K. Nonaka, "The P561T polymorphism of the growth hormone receptor gene has an inhibitory effect on mandibular growth in young children," *European Journal of Orthodontics*, vol. 31, no. 5, pp. 536–541, 2009.

[16] Q. Jiang, L. Mei, Y. Zou et al., "Genetic polymorphisms in FGFR2 underlie skeletal malocclusion," *Journal of Dental Research*, vol. 98, no. 12, pp. 1340–1347, 2019.

[17] A. S. Rodrigues, E. C. Teixeira, L. S. Antunes et al., "Association between craniofacial morphological patterns and tooth agenesis-related genes," *Progress in Orthodontics*, vol. 21, no. 1, p. 9, 2020.

[18] M. Lind, "Growth factors: possible new clinical tools: a review," *Acta Orthopaedica Scandinavica*, vol. 67, no. 4, pp. 407–417, 1996.

[19] D. J. Grainger, K. Heathcote, M. Chiano et al., "Genetic control of the circulating concentration of transforming growth factor type beta1," *Human Molecular Genetics*, vol. 8, no. 1, pp. 93–97, 1999.

[20] D. J. Grainger, "TGF-beta and atherosclerosis in man," *Cardiovascular Research*, vol. 74, no. 2, pp. 213–222, 2007.

[21] L. Du, T. Gong, M. Yao, H. Dai, H. G. Ren, and H. Wang, "Contribution of the polymorphism rs1800469 of transforming growth factor β in the development of myocardial infarction: meta-analysis of 5460 cases and 8413 controls

(MOOSE-compliant article)," *Medicine*, vol. 98, no. 26, p. e15946, 2019.

[22] M. M. Rechtman, A. Nakaryakov, K. E. Shapira, M. Ehrlich, and Y. I. Henis, "Different domains regulate homomeric and heteromeric complex formation among type I and type II transforming growth factor-β receptors," *Journal of Biological Chemistry*, vol. 284, no. 12, pp. 7843–7852, 2009.

[23] E. Biros, P. E. Norman, G. T. Jones et al., "Meta-analysis of the association between single nucleotide polymorphisms in TGF-β receptor genes and abdominal aortic aneurysm," *Atherosclerosis*, vol. 219, no. 1, pp. 218–223, 2011.

[24] B. K. Choe, S. K. Kim, H. J. Park et al., "Polymorphisms of TGFBR2 contribute to the progression of papillary thyroid carcinoma," *Molecular & Cellular Toxicology*, vol. 8, no. 1, pp. 1–8, 2012.

[25] H. J. Ki, S. Y. Kim, S. H. Lee et al., "Transforming growth factor-β receptor 2 gene polymorphisms are associated with end-stage renal disease," *Kidney Research and Clinical Practice*, vol. 34, no. 2, pp. 93–97, 2015.

[26] G. A. F. Vitiello, M. K. Amarante, B. K. Banin-Hirata et al., "Transforming growth factor beta receptor II (TGFBR2) promoter region polymorphism in Brazilian breast cancer patients: association with susceptibility, clinicopathological features, and interaction with TGFB1 haplotypes," *Breast Cancer Research and Treatment*, vol. 178, no. 1, pp. 207–219, 2019.

[27] G. A. F. Vitiello, R. L. Guembarovski, B. K. B. Hirata et al., "Transforming growth factor beta 1 (TGFβ1) polymorphisms and haplotype structures have dual roles in breast cancer pathogenesis," *Journal of Cancer Research and Clinical Oncology*, vol. 144, no. 4, pp. 645–655, 2018.

[28] M. Hadj-Ahmed, R. M. Ghali, H. Bouaziz et al., "Transforming growth factor beta 1 polymorphisms and haplotypes associated with breast cancer susceptibility: a case-control study in Tunisian women," *Tumor Biology*, vol. 41, no. 8, p. 1010428319869096, 2019.

[29] T. Mizuguchi, G. Collod-Beroud, T. Akiyama et al., "Heterozygous TGFBR2 mutations in Marfan syndrome," *Nature Genetics*, vol. 36, no. 8, pp. 855–860, 2004.

[30] B. L. Loeys, J. Chen, E. R. Neptune et al., "A syndrome of altered cardiovascular, craniofacial, neurocognitive and skeletal development caused by mutations in TGFBR1 or TGFBR2," *Nature Genetics*, vol. 37, no. 3, pp. 275–281, 2005.

[31] P. Coster, G. Pauw, L. Martens, and A. Paepe, "Craniofacial structure in Marfan syndrome: a cephalometric study," *American Journal of Medical Genetics Part A*, vol. 131, no. 3, pp. 240–248, 2004.

[32] C. M. Johnson, B. Spruiell, C. Wiesen, L. A. Pimenta, W. Vann, and S. A. Frazier-Bowers, "Craniofacial characterization of Marfan syndrome," *Orthodontics & Craniofacial Research*, vol. 22, no. S1, pp. 56–61, 2019.

[33] K. Almpani, D. K. Liberton, P. Jani et al., "Loeys-Dietz and Shprintzen-Goldberg syndromes: analysis of TGF-β-opathies with craniofacial manifestations using an innovative multimodality method," *Journal of Medical Genetics*, vol. 2021, 107695 pages, 2021.

[34] M. M. Baffi, E. Slattery, P. Sohn, H. L. Moses, A. Chytil, and R. Serra, "Conditional deletion of the TGF-β type II receptor in Col2a expressing cells results in defects in the axial skeleton without alterations in chondrocyte differentiation or embryonic development of long bones," *Developmental Biology*, vol. 276, no. 1, pp. 124–142, 2004.

[35] H. S. Seo and R. Serra, "Deletion of Tgfbr2 in Prx1-cre expressing mesenchyme results in defects in development of the long bones and joints," *Developmental Biology*, vol. 310, no. 2, pp. 304–316, 2007.

[36] Y. Ito, J. Y. Yeo, A. Chytil et al., "Conditional inactivation of TGFBR2 in cranial neural crest causes cleft palate and calvaria defects," *Development*, vol. 130, no. 21, pp. 5269–5280, 2003.

[37] H. S. Seo and R. Serra, "Tgfbr2 is required for development of the skull vault," *Developmental Biology*, vol. 334, no. 2, pp. 481–490, 2009.

[38] P. Clayton, P. Chatelain, L. Tatò et al., "A pharmacogenomic approach to the treatment of children with GH deficiency or Turner syndrome," *European Journal of Endocrinology*, vol. 169, no. 3, pp. 277–289, 2013.

Hindawi
BioMed Research International
Volume 2022, Article ID 5310555, 7 pages
https://doi.org/10.1155/2022/5310555

Review Article

Efficacy of CAD/CAM Technology in Interventions Implemented in Orthodontics: A Scoping Review of Clinical Trials

Carlos M. Ardila[1], **Andrés Elorza-Durán**[1], **and Daniel Arrubla-Escobar**[1,2]

[1]*Biomedical Stomatology Research Group, Universidad de Antioquia, U de A, Medellín, Colombia*
[2]*Institución Universitaria Visión de Las Américas, Medellín, Colombia*

Correspondence should be addressed to Carlos M. Ardila; martin.ardila@udea.edu.co

Received 3 April 2022; Revised 22 April 2022; Accepted 18 May 2022; Published 2 June 2022

Academic Editor: Mohammad Alam

Objectives. To evaluate the efficacy of computer-aided design/computer-aided manufacturing (CAD/CAM) technology in interventions implemented in orthodontics. *Methods*. A scoping review of scientific evidence was accomplished, involving different databases. MesH terms and keywords were provided to examine clinical trials (CTs) in all languages. Exclusively CTs that fulfilled the eligibility criteria were admitted. *Results*. Eight CTs were chosen. These experiments evaluated 542 patients. Four CTs compared the computer-aided indirect bonding method versus the traditional direct bonding of orthodontic brackets. Three CTs compared CAD/CAM retainers with other types of retainers, and one CT compared the CAD/CAM group with multistranded stainless steel wires versus stainless steel wires. Regarding the efficacy of the interventions with CAD/CAM technology used in orthodontics, variable results were found. The indirect bonded customized CAD/CAM brackets presented just a slight effect on the treatment efficacy and therapy results. Two CTs showed that an indirect bonding self-ligating standard system had a similar quality of therapy in comparison with the CAD/CAM customized bracket system. Concerning the clinical failure rate, no differences were presented between the CAD/CAM retainer and other retainers. A CAD/CAM system had more loose brackets than a noncustomized system and was observed also a greater amount of immediate debonding with CAD/CAM indirect bonding than with direct bonding. CAD/CAM fixed retainers revealed inferior relapse and fewer failures than lab-based and conventional chairside retainers. No changes between treatment groups were observed regarding the total therapy time, amount of appointments, and quantity of archwire bends. *Conclusions*. In general terms, no greater efficacy of CAD/CAM technology was observed over traditional therapies used in orthodontics. However, it was found that gingival inflammation and the accumulation of bacterial plaque and dental calculus were lower when CAD/CAM retainers were used. When comparing interventions that include CAD/CAM systems with conventional therapies, no significant reduction in care times was found.

1. Introduction

The advent of computer-aided design/computer-aided manufacturing (CAD/CAM) technology has brought much innovation to dentistry. In orthodontics, this technology has been incorporated during diagnosis and treatment plans. CAD/CAM technology facilitates a fully digital workflow; moreover, various protocol studies have postulated clinical reliability, and it has been indicated that this technology produces very favorable feedback from patients [1, 2]. A retrospective study also proposed that CAD/CAM applications reduced treatment time [3].

Regarding fixed purposes, CAD/CAM technology may promote the accuracy of bracket placement, considering that its location significantly influences treatment effects [4]. Some fully individualized bracket systems incorporate virtual configurations to assume treatment outcomes, taking into account individual tooth surface and morphology, and custom archwires [5]. Furthermore, patients treated with CAD/CAM orthodontic systems, in a retrospective study,

required fewer appointments for archwire changes; besides, the treatment time was shorter and presented an inferior American Board of Orthodontics (ABO) score [6].

The CAD/CAM technology has also made it possible to develop retainers. The CAD/CAM lingual retainer is placed digitally, giving a particularly improved position, greater precision of fit, and interproximal adaptation. It causes less irritability of the tongue and prevents occlusal interferences. The rectangular nickel-titanium archwire offers better flexibility, improving the physiological movement of the teeth. Moreover, the wire is electropolished, making it smooth and corrosive resistant, reducing the growth of bacterial plaque [7].

Computer technology has also permitted novel methods of indirect bonding. The brackets are positioned in a virtual 3D dental model; then, this technology generates information on its location, and subsequently, this is indirectly transferred to the teeth. A prototype procedure indicated the reduction of the time of dental consultation and the improvement of precision [8].

Assessing the best available scientific evidence through clinical trials that compare CAD/CAM technologies with conventional therapies will allow clinicians to make better decisions in their practice. In this context, it is relevant to carry out a scoping review of clinical trials, which allows for evaluating the efficacy of CAD/CAM technology in interventions implemented in orthodontics. To achieve this objective, it was proposed to answer some questions related to the efficacy, treatment times, benefits, and/or adverse events of therapies using CAD/CAM in orthodontics.

2. Materials and Methods

This review of clinical trials was carried out considering the PRISMA (Preferred Reporting Items for Systematic Reviews and Meta-analyses) extension for scoping reviews [9]. The scoping structure involved different databases such as SCOPUS, PubMed/MEDLINE, SCIELO, and LILACS, including the gray literature. MesH terms and keywords were provided to examine clinical trials in humans in all languages, with no publication date range, including the terms computer-aided design, CAD/CAM system, 3D treatment planning, orthodontic, orthodontic treatment, customized brackets, retainer, digital orthodontics, intervention studies, and clinical trial. Trials comparing interventions between CAD/CAM groups were discarded. Exclusively clinical trials (CTs) that fulfilled the eligibility criteria were admitted. Research related to case reports, case series, duplicate studies, in vitro experiments, and animal studies were excluded.

2.1. Questions. This scoping review aims to answer the following questions: In which areas of orthodontics are CAD/CAM systems used for interventions? Do interventions with CAD/CAM technology show greater efficacy? Do interventions with CAD/CAM technology require less time? Do CAD/CAM interventions present benefits or adverse events?

2.2. Review Process. Two investigators reviewed the titles and abstracts and selected CTs to assess the full text for potential eligibility. In case of disagreement between authors, trial eligibility was made by consensus. The Kappa statistical test was used to assess the value of agreement between observers (>95).

2.3. Data Collection. A table was designed to incorporate the most relevant data from the selected CTs. This process was performed independently by each of the researchers. Subsequently, the data were compared. Recorded data included authors' names, date of publication, age and gender of participants, number of participants, intervention, and control, comparison between the groups (main studied variables), and treatment time.

2.4. Risk of Bias. The risk of bias and quality assessment of the included trials was performed following the Jadad scale for CTs [10], by two authors.

3. Results

The electronic search yielded 46 studies. After reviewing the titles and abstracts, 33 investigations were excluded. Reading the full text resulted in the exclusion of 5 additional trials. Finally, 8 CTs [5, 11–17] were included in this scoping review (Figure 1).

The characteristics of the included studies are presented in Table 1. Three CTs were randomized single-blind, controlled, and with parallel design [11, 12, 17]. Three CTs were randomized unblinded, controlled, and with parallel design [14–16], one CT was randomized unblinded, controlled, and with split-mouth design [13], and one CT was quasi-randomized, controlled, with parallel design [5]. One CT compared 4 groups [14], 2 CTs compared 3 groups [11, 12], and 5 CTs compared 2 groups [5, 13, 15–17]. These CTs were published between 2017 and 2022.

These trials assessed 542 patients with a minimum sample of 24 patients [15] and a maximum of 174 [16]. These experiments evaluated different interventions in orthodontics. Four studies compared the computer-aided indirect bonding method versus the traditional direct bonding of orthodontic brackets [5, 13, 15, 16]. Three studies compared CAD/CAM retainers with other types of retainers [12, 14, 17], and one CT compared CAD/CAM group with multistranded stainless steel wires versus stainless steel Ortho-FlexTech wires group (traditional group) and Lab group with multistranded stainless steel wires [11].

Variable results were found regarding the efficacy of interventions with CAD/CAM technology used in orthodontics. In contrast with a direct bonded self-ligating bracket system, the utilization of indirect bonded customized CAD/CAM brackets presented just a slight effect on treatment efficacy. Besides, after therapy, the ABO score in both interventions was diminished, without significant differences [5]. Likewise, an indirect bonding self-ligating standard system showed a similar quality of therapy in comparison with the CAD/CAM customized bracket system, and the final ABO score was similar [15]. Penning et al. [16] also showed that the treatment quality was equivalent between customized orthodontic systems and

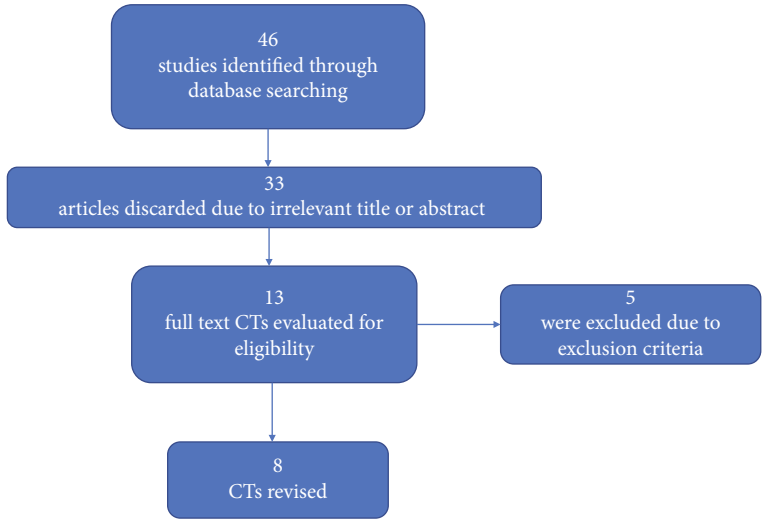

Figure 1: Flowchart of the CTs selection method.

noncustomized orthodontic systems. Concerning the clinical failure rate, no differences were presented between the CAD/CAM retainer and other retainers, admitting that CAD/CAM retainer has better fitting precision [12, 17]. Furthermore, the Little's irregularity index for CAD/CAM group was less than that of the other groups but similar to the stainless steel retainers [14, 17]. In contrast, a customized orthodontic system had more loose brackets than a noncustomized system [16] and was observed also a greater amount of immediate debonding with CAD/CAM indirect bonding than with direct bonding [13]. Regarding bonding fixed retainers, CAD/CAM fixed retainers revealed inferior relapse than lab-based and conventional chairside retainers. The CAD/CAM retainers also showed fewer failures than lab-based retainers [11].

Considering the time spent during the interventions, the results were also variable. It was founded that while CAD/CAM indirect bonding proved less chair time, the total bonding period, counting digital bracket position, was larger than for direct bonding [13]. It was also observed that the indirect bonding self-ligating standard system had a 26% longer total orthodontic therapy period, in comparison with the CAD/CAM customized bracket system [15]. Instead, Hegele et al. [5], Adanur et al. [14], and Penning et al. [16] did not find differences in treatment time between the analyzed groups.

Responding to the fourth question of this scoping review, it was found that gingival inflammation and the accumulation of bacterial plaque and dental calculus were lower when CAD/CAM retainers were used [12, 14]; however, Alrawas et al. [12] and Gelin et al. [17] did not show statistically significant differences between groups. On the other hand, two CTs revised here indicated that CAD/CAM indirect bonding was more expensive than direct bonding [13, 16]. Penning et al. [16] denoted that the patients in the customized group had more complaints. The rest of the clinical trials evaluated in this scoping review did not report adverse events with the use of CAD/CAM technology.

Two studies had a high risk of bias [5, 15], while the rest of the selected trials had a moderate risk of bias (Table 2).

4. Discussion

To the best of the authors' understanding, this scoping review is the first to compare the efficacy of CAD/CAM technology used in orthodontics with conventional therapies. Considering that the new CAD/CAM technologies propose novelties related to clinical interventions performed in orthodontics, it is essential to evaluate their clinical efficacy with the best available scientific evidence. Taking this aspect into account, in this review, answers were given to each of the four proposed questions.

In contrast with a direct bonded self-ligating bracket system, the utilization of indirect bonded customized CAD/CAM brackets presented just a slight effect on treatment efficacy and therapy results. Besides, after therapy, two trials revised here showed that the ABO score in both interventions was diminished, without significant differences [5, 15]. These findings corroborated previous results of a retrospective study that presented no changes between indirectly bonded CAD/CAM brackets, indirectly bonded custom brackets, and directly bonded custom brackets [3].

In this review, the study by Czolgoz et al. [13] showed that CAD/CAM indirect bonding presented more immediate bonding failures than conventional direct bonding. Comparable results were also documented by Penning et al. [16]. It has been postulated that indirect bonding failures may be caused by short periods of light-curing time [13].

Two CTS in this review showed that a customized orthodontic system had more loose brackets than a noncustomized system [16] and it was observed also a greater amount of immediate debonding with CAD/CAM indirect bonding than with direct bonding [13]. Even though it is

Table 1: Features of the CTs evaluated.

Authors Publication date	Participants	Mean Age	Female Male	Intervention control	Main outcomes	Treatment time
Shim et al. 2022	46	16 years	28/18	CAD/CAM group with multistranded stainless steel wires versus lab group with multistranded stainless steel wires versus a group with stainless steel Ortho-FlexTech wires (traditional group)	The CAD/CAM group experienced a less intercanine width decrease ($P < 0.05$). The CAD/CAM group experienced a less increase in Little's irregularity index ($P < 0.05$). Failures from greatest to least were experienced by the lab group (43.8%), the CAD/CAM group (25%), and the traditional group (14.3%)	6 months of bonding fixed retainers
Adanur-Atmaca et al. 2021	132	16 years	92/40	Lingual retainers with 0.016 3 0.022 in dead soft wire versus Lingual retainers with 0.0215 in 5 strand stainless steel wire versus lingual retainers with 0.014 3 0.014-in CAD/CAM nitinol versus lingual retainers with connected bonding pads	Gingival inflammation and calculus accumulation were the lowest in CAD/CAM group ($P < 0.05$). The Little's irregularity for CAD/CAM group and stainless steel retainers was less than that of the other groups. No clinically significant worsening of periodontal health or relapse was seen in any groups after 1 year	12 months
Hegele et al. 2021	38	14 years	23/15	Indirect bonded customized CAD/CAM brackets versus direct bonded self-ligating brackets	No differences between both treatment groups were found concerning overall treatment time, the number of appointments, and the number of archwire bends. Bonding failures occurred more often using the CAD/CAM system. Indirectly bonded brackets did not have to be repositioned as often as directly bonded brackets. Treatment results with both systems were similar concerning their effects on the reduction of ABO score. The number of the used archwires was higher in the CAD/CAM group	16.7 months
Jackers et al. 2021	24	23 years	17/7	CAD/CAM custom indirect bonding self-ligating system versus indirect bonding self-ligating standard system	The indirect bonding self-ligating standard system had a 26% longer overall orthodontic treatment time compared with the CAD/CAM customized bracket system ($P = 0.00002$). The indirect bonding self-ligating bracket system demonstrated the same quality of treatment. Patients showed a high level of acceptance and satisfaction with both techniques	393 days in the CAD/CAM group 497 days in the standard system
Alrawas et al. 2021	60	20 years	43/17	CAD/CAM NiTi retainer, multistranded stainless steel versus single-stranded nickel-free titanium retainer versus vacuum-formed removable group	All groups showed some relapse in the lower anterior teeth. No statistical significance was found intergroup in terms of all measured values. Less plaque accumulation and gingival inflammation were observed in the CAD/CAM NiTi retainer group but without statistical significance	6 months of follow-up
Czolgosz et al. 2020	27	17 years	15/12		Clinical chair time for bonding half a mouth was significantly shorter for	Not reported

Table 1: Continued.

Authors Publication date	Participants	Mean Age	Female Male	Intervention control	Main outcomes	Treatment time
				Computer-aided indirect bonding method versus traditional direct bonding of orthodontic brackets	computer-aided indirect bonding ($P < 0.001$). There was no single immediate debonding with the direct bonding method, while 14 brackets were lost with the indirect bonding method ($P = 0.0001$). Cost-minimization analysis showed that computer-aided indirect bonding was more expensive than direct bonding	
Gelin et al. 2020	41	17 years	43/18	To compare CAD/CAM customized nitinol retainers with standard stainless-steel fixed retainers	No significant difference between customized CAD/CAM nickel-titanium lingual retainers and standard stainless-steel lingual retainers in terms of dental anterior stability and retainer survival were observed. Both retainers eventually appeared to be equally effective in maintaining periodontal health	12 months
Penning et al. 2017	174	14 years	103/71	Customized orthodontic system versus non-customized orthodontic system	The customized group had more loose brackets, a longer planning time, and more complaints ($P < 0.05$). The customized orthodontic system was not associated with significantly reduced treatment duration, and treatment quality was comparable between the 2 systems	1.29 years in the customized system 1.24 years in the non-customized system

Table 2: Quality of the selected studies (Jadad et al. 1996).

Clinical trial	Randomization	Double blinding	Withdraw	Proper randomization	Proper double blinding	Score
Shim et al. (2022)	1	0	1	1	0	3
Adanur-Atmaca et al. (2021)	1	0	1	1	0	3
Hegele et al. (2021)	0	0	0	0	0	0
Jackers et al. (2021)	1	0	1	0	0	2
Alrawas et al. (2021)	1	0	1	1	0	3
Czolgosz et al. (2020)	1	0	1	1	0	3
Gelin et al. (2020)	1	0	1	1	0	3
Penning et al. (2017)	1	0	1	1	0	3

expected that a customized bracket has an ideal fit, the customized and the noncustomized system differ in the personally computed location of the bracket slot; then, the design of the personalized bracket is bigger, facilitating debonding [16]. Moreover, the customized brackets were indirectly bonded, characteristics that have also caused higher failure rates in a previous study [18].

The trial by Alrawas et al. [12] showed no differences between the CAD/CAM retainer and other retainers, which corresponds with the report of Geling et al. [17] and Attack et al. [19] and diverges with the research of Al-Moghrabi et al. [20], who established that the fixed retainers have higher efficacy, considering that patients are less collaborative over time with the use of removable retainers.

Regarding bonding fixed retainers, CAD/CAM fixed retainers revealed inferior relapse than lab-based and conventional chairside retainers. The CAD/CAM retainers also showed fewer failures than lab-based retainers. The CAD/CAM and lab groups utilized more rigid dentaflex wires; moreover, they are subject to constant deformation in comparison with Ortho-FlexTech wires that are flexible [11]. Similarly, thicker and rigid wires have been reported to better maintain intercanine width than flexible wires [21].

This review found that CAD/CAM indirect bonding (clinical chair time plus digital bracket location time) was

larger than direct bonding [13]. A comparative study also presented a greater total indirect bonding time [22]. However, retrospective studies with small simple sizes revealed a diminution in therapy time and quantity of appointments for the CAD/CAM systems [3, 6]. Similarly, Xiaolei et al. [23] indicated that the digital method was more effective in lingual retainer construction than the standard process. Moreover, it was more difficult to fabricate a lingual retainer for the maxilla than for the mandible; the standard technique cost two times to bend the lingual retainer for the maxilla of the time to bend the lingual retainer for the mandible. Instead, in this review, Hegele et al. [5], Adanur et al. [14], and Penning et al. [16] did not find differences in treatment time between the analyzed groups. These controversial results may have several explanations. Implementing a novel technique during clinical care is not constantly simple. The clinician's expertise with a new software increases with the passing of the practice, an aspect that can impact the results [13, 16]. On the other hand, the epidemiological design, the objectives, the interventions compared, the definition of chronological order, and the selection criteria of the studies may cause differences in the results [5].

Traditionally, it has been indicated that the indicators of bacterial plaque accumulation and gingival inflammation are higher with the use of stainless steel retainers [24]. The smoothness and polish of CAD/CAM retainers allow less plaque accumulation and therefore less inflammation, aspects that were corroborated in this review [12, 14].

A clinical trial selected in this review indicated that the costs of CAD/CAM technology are slightly higher than those of an orthodontist using conventional treatments [13]. Penning et al. [16] indicated that this is because CAD/CAM technology is more expensive due to laboratory costs. However, the costs of CAD/CAM technology present controversial results in other specialties of dentistry. Some studies indicate that the costs are similar to conventional treatments, while others indicate that the values are lower [25, 26]. More cost-effectiveness studies are required when using CAD/CAM systems in orthodontics to present more conclusive results in this regard.

In this scoping review, only one trial reported patient complaints related to the thickness of customized brackets [16]. Other studies have also described patient complaints in other areas of dentistry when this technology has been implemented [27, 28].

The main limitation of this scoping review is related to the moderate and high risk of bias of the CTs selected. Most of the biases in these studies were related to double-blinding. It has been reported that blinding the patient and the clinician in orthodontic interventions is difficult [5]. However, a greater number of CTs with a low risk of bias are required to allow more conclusive results. Other limitations of this review are related to missing keywords and other databases. However, two of the most important databases were used.

Finally, it is necessary to design clinical trials with longer follow-up times, higher scientific quality, and low risks of bias, to obtain more reliable results about CAD/CAM technologies used in orthodontics. Furthermore, the cost-benefit and patient satisfaction with the use of these technologies should also be investigated.

5. Conclusions

In general terms, no greater efficacy of CAD/CAM technology was observed over traditional therapies used in orthodontics. However, it was found that gingival inflammation and the accumulation of bacterial plaque and dental calculus were lower when CAD/CAM retainers were used. When comparing interventions that include CAD/CAM systems with conventional therapies, no significant reduction in care times was found.

Data Availability

Records were obtained from the included investigations.

Conflicts of Interest

The authors declare that there is no conflict of interest regarding the publication of this paper.

Acknowledgments

The authors acknowledge their employment relationship with the School of Dentistry, Universidad de Antioquia, Medellín, Colombia.

References

[1] M. F. Sfondrini, P. Gandini, M. Malfatto, F. Di Corato, F. Trovati, and A. Scribante, "Computerized casts for orthodontic purpose using powder-free intraoral scanners: accuracy, execution time, and patient feedback," *BioMed research international*, vol. 2018, Article ID 4103232, 8 pages, 2018.

[2] C. Xue, H. Xu, Y. Guo et al., "Accurate bracket placement using a computer-aided design and computer-aided manufacturing-guided bonding device: an in vivo study," *American Journal of Orthodontics and Dentofacial Orthopedics*, vol. 157, no. 2, pp. 269–277, 2020.

[3] M. W. Brown, L. Koroluk, C. C. Ko, K. Zhang, M. Chen, and T. Nguyen, "Effectiveness and efficiency of a CAD/CAM orthodontic bracket system," *American Journal of Orthodontics and Dentofacial Orthopedics: Official Publication of the American Association of Orthodontists, its constituent societies, and the American Board of Orthodontics*, vol. 148, no. 6, pp. 1067–1074, 2015.

[4] J. Kim, Y. S. Chun, and M. Kim, "Accuracy of bracket positions with a CAD/CAM indirect bonding system in posterior teeth with different cusp heights," *American journal of orthodontics and dentofacial orthopedics : official publication of the American Association of Orthodontists, its constituent societies, and the American Board of Orthodontics*, vol. 153, no. 2, pp. 298–307, 2018.

[5] J. Hegele, L. Seitz, C. Claussen, U. Baumert, H. Sabbagh, and A. Wichelhaus, "Clinical effects with customized brackets and CAD/CAM technology: a prospective controlled study," *Progress in Orthodontics*, vol. 22, no. 1, p. 40, 2021.

[6] D. J. Weber 2nd, L. D. Koroluk, C. Phillips, T. Nguyen, and W. R. Proffit, "Clinical effectiveness and efficiency of customized vs. conventional preadjusted bracket systems," *Journal of Clinical orthodontics: JCO*, vol. 47, no. 4, pp. 261–268, 2013.

[7] N. D. Kravitz, D. Grauer, P. Schumacher, and Y. M. Jo, "Memotain: a CAD/CAM nickel-titanium lingual retainer," *American journal of orthodontics and dentofacial orthopedics: official publication of the American Association of Orthodontists, its constituent societies, and the American Board of Orthodontics*, vol. 151, no. 4, pp. 812–815, 2017.

[8] F. Ciuffolo, E. Epifania, G. Duranti et al., "Rapid prototyping: a new method of preparing trays for indirect bonding," *American journal of orthodontics and dentofacial orthopedics: official publication of the American Association of Orthodontists, its constituent societies, and the American Board of Orthodontics*, vol. 129, no. 1, pp. 75–77, 2006.

[9] A. C. Tricco, E. Lillie, W. Zarin et al., "PRISMA extension for scoping reviews (PRISMA-ScR): checklist and explanation," *Annals of Internal Medicine*, vol. 169, no. 7, pp. 467–473, 2018.

[10] A. R. Jadad, R. A. Moore, D. Carroll et al., "Assessing the quality of reports of randomized clinical trials: is blinding necessary?," *Controlled Clinical Trials*, vol. 17, no. 1, pp. 1–12, 1996.

[11] H. Shim, P. Foley, B. Bankhead, and K. B. Kim, "Comparative assessment of relapse and failure between CAD/CAM stainless steel and standard stainless steel fixed retainers in orthodontic retention patients," *The Angle Orthodontist*, vol. 92, no. 1, pp. 87–94, 2022.

[12] M. B. Alrawas, Y. Kashoura, Ö. Tosun, and U. Öz, "Comparing the effects of CAD/CAM nickel-titanium lingual retainers on teeth stability and periodontal health with conventional fixed and removable retainers: a randomized clinical trial," *Orthodontics & Craniofacial Research*, vol. 24, no. 2, pp. 241–250, 2021.

[13] I. Czolgosz, P. M. Cattaneo, and M. A. Cornelis, "Computer-aided indirect bonding versus traditional direct bonding of orthodontic brackets: bonding time, immediate bonding failures, and cost-minimization. A randomized controlled trial," *European Journal of Orthodontics*, vol. 43, no. 2, pp. 144–151, 2021.

[14] R. Adanur-Atmaca, S. Çokakoğlu, and F. Öztürk, "Effects of different lingual retainers on periodontal health and stability," *The Angle Orthodontist*, vol. 91, no. 4, pp. 468–476, 2021.

[15] N. Jackers, N. Maes, F. Lambert, A. Albert, and C. Charavet, "Standard vs computer-aided design/computer-aided manufacturing customized self-ligating systems using indirect bonding with both," *The Angle Orthodontist*, vol. 91, no. 1, pp. 74–80, 2021.

[16] E. W. Penning, R. H. J. Peerlings, J. D. M. Govers et al., "Orthodontics with customized versus noncustomized appliances: a randomized controlled clinical trial," *Journal of Dental Research*, vol. 96, no. 13, pp. 1498–1504, 2017.

[17] E. Gelin, L. Seidel, A. Bruwier, A. Albert, and C. Charavet, "Innovative customized CAD/CAM nickel-titanium lingual retainer versus standard stainless-steel lingual retainer: a randomized controlled trial," *Korean Journal of Orthodontics*, vol. 50, no. 6, pp. 373–382, 2020.

[18] A. Menini, M. Cozzani, M. F. Sfondrini, A. Scribante, P. Cozzani, and P. Gandini, "A 15-month evaluation of bond failures of orthodontic brackets bonded with direct versus indirect bonding technique: a clinical trial," *Progress in Orthodontics*, vol. 15, no. 1, p. 70, 2014.

[19] N. Atack, N. Harradine, J. R. Sandy, and A. J. Ireland, "Which way forward? Fixed or removable lower retainers," *The Angle Orthodontist*, vol. 77, no. 6, pp. 954–959, 2007.

[20] D. Al-Moghrabi, A. Johal, N. O'Rourke et al., "Effects of fixed vs removable orthodontic retainers on stability and periodontal health: 4-year follow-up of a randomized controlled trial," *American Journal of Orthodontics and Dentofacial Orthopedics*, vol. 154, no. 2, pp. 167–174.e1, 2018.

[21] J. Butler and P. Dowling, "Orthodontic bonded retainers," *Journal of the Irish Dental Association*, vol. 51, no. 1, pp. 29–32, 2005.

[22] J. V. Bozelli, R. Bigliazzi, H. A. Barbosa, C. L. Ortolani, F. A. Bertoz, and J. K. Faltin, "Comparative study on direct and indirect bracket bonding techniques regarding time length and bracket detachment," *Journal of Orthodontics*, vol. 18, no. 6, pp. 51–57, 2013.

[23] X. Hu, J. Linga, and X. Wu, "The CAD/CAM method is more efficient and stable in fabricating of lingual retainer compared with the conventional method," *Biomedical Journal of Scientific & Technical Research*, vol. 18, no. 3, 2019.

[24] I. Knaup, Y. Wagner, J. Wego, U. Fritz, A. Jäger, and M. Wolf, "Potential impact of lingual retainers on oral health: comparison between conventional twistflex retainers and CAD/CAM fabricated nitinol retainers: a clinical in vitro and in vivo investigation," *Journal of Orofacial Orthopedics*, vol. 80, no. 2, pp. 88–96, 2019, English.

[25] S. Mühlemann, J. Hjerppe, C. H. F. Hämmerle, and D. S. Thoma, "Production time, effectiveness and costs of additive and subtractive computer- aided manufacturing (CAM) of implant prostheses: A systematic review," *Clinical Oral Implants Research*, vol. 32, Suppl 21, pp. 289–302, 2021.

[26] M. Srinivasan, P. Kamnoedboon, G. McKenna et al., "CAD-CAM removable complete dentures: a systematic review and meta-analysis of trueness of fit, biocompatibility, mechanical properties, surface characteristics, color stability, time-cost analysis, clinical and patient- reported outcomes," *Journal of Dentistry*, vol. 113, article 103777, 2021.

[27] S. Reich, L. Endres, C. Weber et al., "Three-unit CAD/CAM-generated lithium disilicate FDPs after a mean observation time of 46 months," *Clinical Oral Investigations*, vol. 18, no. 9, pp. 2171–2178, 2014.

[28] R. C. Mocelin, M. M. Penteado, F. Z. Pierre, A. C. V. Saraiva, E. S. Uemura, and J. M. F. da Silva, "Assessment of patient and dentist preference between conventional and digital diagnostic waxing," *The International Journal of Esthetic Dentistry*, vol. 16, no. 3, pp. 300–309, 2021.

Hindawi
BioMed Research International
Volume 2022, Article ID 1974467, 7 pages
https://doi.org/10.1155/2022/1974467

Research Article

Maxillary Expansion: A Comparison of Damon Self-Ligating Bracket Therapy with MARPE and PAOO

Eman Alsayegh[1], **Nasib Balut**[2,3], **Donald J. Ferguson**[1], **Laith Makki**[1], **Thomas Wilcko**[4], **Ismaeel Hansa**[1] and **Nikhilesh R. Vaid**[1]

[1]*Department of Orthodontics, European University College, Dubai, UAE*
[2]*Universidad Autónoma de Baja California, Mexicali, Mexico*
[3]*Universidad Del Valle, Cali, Colombia*
[4]*Department of Periodontology, Case Western Reserve University, Cleveland, USA*

Correspondence should be addressed to Ismaeel Hansa; ismaeel.hansa@gmail.com

Received 7 December 2021; Revised 22 February 2022; Accepted 14 March 2022; Published 9 May 2022

Academic Editor: Shivam Mehta

Purpose. The aim of this study was to investigate arch parameters and dentoalveolar changes from pretreatment to posttreatment by comparing the Miniscrew Assisted Rapid Palatal Expansion (MARPE), Periodontally Accelerated Osteogenic Orthodontics (PAOO), and Damon self-ligating bracket therapies. *Materials and Methods*. Seventy-nine patients underwent maxillary expansion followed by or in conjunction with Damon ($n = 23$), PAOO ($n = 28$), and MARPE ($n = 28$) therapies. Nine maxillary dental arch parameters were compared at pretreatment, posttreatment as well as, increments of treatment change. Measurements were made on STL study casts using 3Shape Ortho Analyzer 3D scanner software. *Results*. All groups showed significant posterior width increase in the molar area. The mean increase in inter-molar distance was more than 8X greater in MARPE group compared to Damon and more than 4X greater compared to PAOO. MARPE showed significantly greater increments of change in inter-molar width and palatal vault area *Conclusions*. All groups showed a significant width increase in the canine and molar area. MARPE showed the greatest increase in inter-molar width, followed by PAOO and Damon. MARPE was the only group to show a significant increase in palatal vault area.

1. Introduction

Transverse maxillary deficiency is a frequently occurring problem in patients presenting for orthodontic treatment. Approximately 9% of the US population have a transverse maxillary deficiency associated with a posterior crossbite [1]. Transverse maxillary deficiency is a skeletal deficiency and may also cause and influence the sagittal and occlusal dimensions, such as dental protrusion and crowding. Treatment of the transverse dimension therefore plays a vital part in resolving arch perimeter problems, especially when extractions are contraindicated [2].

Conventional rapid palatal expansion (RPE) has been used as a proven method for treating transverse maxillary deficiency in pre-pubertal children. Its usefulness in post-pubertal patients however is limited, as the circum-maxillary sutures fuse, resulting in little or no skeletal effects [3]. Due to the lack of skeletal expansion and the potential for damage to the periodontium, surgically assisted rapid palatal expansion (SARPE) has traditionally been the gold standard when treating transverse maxillary deficiency in the adult patient [4]. SARPE is an invasive procedure however, and the costs, risks, and morbidity associated to the surgery may discourage many patients, and orthodontists, from seeking correction through this procedure [5].

Much attention has been given recently to less invasive expansion procedures. The ability to resolve severe malocclusion without the need for surgical intervention has tremendous potential for benefit to the patient and orthodontist [6]. Lee et al. [7] introduced the Miniscrew Assisted Rapid Palatal Expansion (MARPE), in which miniscrews are used in conjunction with an expansion

appliance, and reported successful opening of the midpalatal suture. Despite the high success rate of MARPE, in older patients, where the sutures may be closely interdigitated, it may still be difficult to split the midpalatal and circummaxillary sutures despite utilizing cortical anchorage [8].

Wilcko et al. [9] introduced the Periodontally Accelerated Osteogenic Orthodontics (PAOO) which involves alveolar decortication with bone graft augmentation, combined with orthodontic treatment. PAOO has been shown to not only expand the scope of orthodontic tooth movement by 200 to 300% in most dimensions, but also hastens tooth movement due to the Regional Acceleratory Phenomenon (RAP) [10]. Ferguson et al. [10] demonstrated that up to 7 mm of inter-canine width was attained by expansion via the arch wires alone, following labial and lingual corticotomy and bone graft augmentation extending anteriorly between the two maxillary first molars.

The conventional notion was that once skeletal maturity had been reached, orthodontic treatment alone could not offer significant nor stable expansion of the maxilla for deficiencies greater than 5 mm [11]. Birnie [12] however claimed that the Damon System, which is a passive self-ligation system, has the ability to achieve significant posterior expansion without any need for auxiliary appliances such as RPE appliances. The Damon philosophy indicates that light forces do not overpower the musculature and periodontium, but rather the arch form aligns by posterior expansion due to the lesser resistance of the musculature.

To date, there have been no investigations of the treatment effects of expansion with Damon, MARPE, or PAOO. The aim of this study was to investigate arch parameters and dentoalveolar changes from pretreatment to posttreatment by comparing MARPE, PAOO, and Damon self-ligating bracket therapies. The null hypothesis tested was no significant difference in dentoalveolar changes when using Damon self-ligating non-extraction treatment compared to PAOO and MARPE therapies.

2. Materials and Methods

2.1. Sample. This retrospective cohort study evaluated the pretreatment and posttreatment STL study casts of adult patients treated with maxillary expansion using three different orthodontic treatment modalities. Inclusion criteria were as follows: (1) moderate to severe transverse skeletal discrepancy (5 mm or more); (2) patients greater than 16 years of age; (3) presence of a posterior unilateral or bilateral crossbite; (4) availability of pretreatment and final outcome study casts; (5) presence of all teeth anterior to, and including, the first molars; and (6) non-extraction orthodontic treatment. Exclusion criteria were as follows: (1) prior orthodontic treatment, (2) craniofacial congenital anomalies, and (3) taking any medication that might affect bone density.

2.2. Study Groups. A total of 79 patients fit the criteria: Damon ($n = 23$), MARPE ($n = 28$), and PAOO ($n = 28$). According to the orthodontic literature with a sample of approximately 26 subjects in each group, the study had a power of at least 80%, to detect a 1.25 standard deviation mean difference between the groups [13].

2.2.1. Damon. Maxillary expansion was obtained with arch wires only, following the Damon treatment philosophy with Damon brackets and Damon Cu-NiTi wide arch wires. All patients finished with .019x.025 TMA or stainless steel upper arch wires. The sample of 23 patients was obtained from a private clinic in Mexico treated between 2015 and 2018.

2.2.2. MARPE. Four self-drilled miniscrews with a length of 7 mm and a diameter of 1.8 mm (ORLUS, Ortholution, Seoul, Korea) were inserted in the palate following local anesthesia. The miniscrews were placed in the center of, and perpendicular to, the 4 mm diameter helical hooks attached to the MARPE appliance. The miniscrews were then connected to the helices using a light-cured resin (Transbond, 3 M Unitek, St Paul, MN, USA) to fix the miniscrews and MARPE appliance together, as well as reduce the potential for irritation to the tongue. The MARPE appliance was activated by a quarter of a turn (0.2 mm) every second day, and expansion was stopped when the palatal cusp of the maxillary first molars came in contact with the buccal cusp tips of the mandibular first molars. The MARPE appliance was then kept for 3 months after active expansion was ceased. Orthodontic treatment with a .022 x.028 inch edgewise straight wire appliances was then commenced. The MARPE sample of 28 patients was treated in Korea for transverse maxillary deficiency at the Department of Orthodontics, Yonsei Dental Hospital, Seoul, Korea, between 2004 and 2010.

2.2.3. PAOO. A full-thickness periosteal flap was reflected, and intentional scoring of both labial and lingual alveolar maxillary cortices was performed. Demineralized freeze-dried bone allograft (DFDBA) or bovine bone xenograft was used to augment the corticotomy sites. The surgical flap was sutured in place, and the patient was seen for orthodontic adjustments every second week after the surgical procedure. The surgical procedure was performed within one week of placement of the orthodontic brackets, and the arch wires were placed and ligated at the time of surgery. PAOO patients were treated with .022 x .028 inch edgewise straight wire appliances until the initial malocclusion was fully resolved. The PAOO adult sample of 28 patients were treated in the private practices of William and Thomas Wilcko (an orthodontist and periodontist, respectively) in Erie, Pennsylvania, USA.

2.3. Measurements. Measurements were made on digital STL models utilizing 3Shape Ortho Analyzer 3D scanner software (3Shape, Copenhagen, Denmark) for all 79 subjects in an identical manner. The 3Shape Ortho Analyzer software (3Shape, Copenhagen, Denmark) technique validity has been previously demonstrated [14].

2.3.1. Arch Width. The maxillary transverse arch width was recorded at the level of the canines and first molars. For the inter-canine width, the measurement was made from the cusp tip to cusp tip. For the first molars, the

measurement was made from the mesiolingual groove at the gingival margin to the contralateral tooth [15] (Figure 1).

2.3.2. Arch Perimeter. Arch perimeter was measured in three segments per quadrant, starting from the mesial surface of first molars to the mesial surface of first premolars, then from the mesial surface of the first premolars to the mesial surface of the canine, and finally from the mesial surface of the canine to the mesial contact point of the central incisors. The arch perimeter was then calculated by adding the measurements of six segments in each arch [16, 17] (Figure 1).

2.3.3. Arch Depth. Arch depth was determined by measuring a perpendicular line constructed from the mesial contact point of the central incisors to a line connecting the mesial aspect of the first molars. The mesial contact point of the central incisors was determined as the midpoint between the mesial points of the central incisors [16, 17] (Figure 1).

2.3.4. Clinical Crown Height. The clinical crown height was determined by measuring the distance from the most occlusal point of the buccal groove to the gingival level directly below the buccal groove. This allows for an indirect measure of buccal gingival attachment change from pretreatment to posttreatment [13] (Figure 2(a)).

2.3.5. Palatal Height. The model was cross-sectioned at the plane of the buccal groove of the first molars. A linear line was then dropped to the palatal level, and the height was measured (Figure 2(b)).

2.3.6. Molar Angulations. Molar angulation was determined by measuring the angle of intersection of the lines drawn tangent to the mesio-facial and mesio-palatal cusp tips of the maxillary first molars. Angulation differences between pre- and posttreatment indicate the extent of molar tipping during treatment [18] (Figure 2(c)).

2.3.7. Palatal Vault Area. The palatal vault area was defined as the area superior to the palatal margin of the maxillary first molars [13, 19]. (Figure 2(D)).

2.4. Statistical Analysis. To analyze the reliability of the measurements and digital analysis used in this investigation, 10 maxillary dental models were selected randomly and measured twice by a single operator (intraoperator reliability) and then by a second operator (interoperator reliability). The investigator was blinded when performing the measurements. Paired *t*-tests were used to determine intraoperator and interoperator systematic error. The data collected was recorded on a Microsoft Excel Sheet and converted for use with SPSS software (version 20; IBM, Armonk, NY) for data analysis.

A Shapiro-Wilk's test showed that the data was normally distributed; therefore, parametric statistical testing was applied. The mean differences between the pretreatment and posttreatment measurements (increment of change) in each group were evaluated for statistical significance using paired *t*-tests. The mean differences between the three groups were evaluated by analysis of variance (ANOVA) in combination with the Scheffe post hoc test. A P value threshold of ≤.05 was accepted as statistically significant.

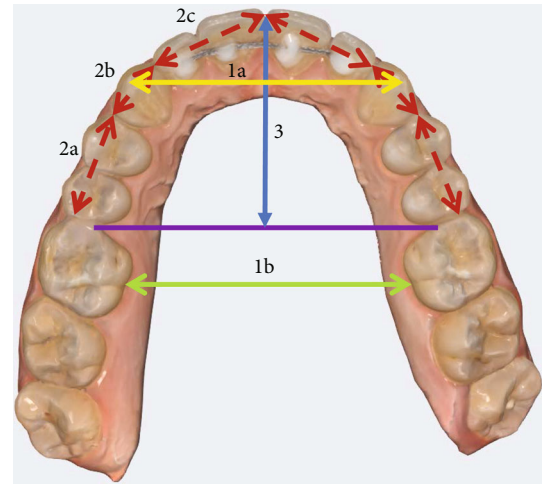

Figure 1: Linear measurements of maxillary dental arch parameters: (1a) inter-canine width from cusp tip to cusp tip; (1b) inter-molar width from mesio-lingual groove at the gingival margin; (2) arch perimeter; and (3) arch depth.

3. Results

The measurement technique used in the study was found to be reliable; repeated measurements on 10 randomly selected study casts demonstrated no significant differences in intra- or interoperator assessments.

At pretreatment, the three groups were heterogeneous for ethnicity, age, and male-female ratios. Mean age of the PAOO (31.7 years) sample was significantly older than the MARPE (20.9 years $P \leq .001$) sample. Active orthodontic treatment time was significantly shorter for PAOO (8.6 months, $P \leq 0.001$) than for MARPE and Damon (24.1 and 16.0 months, respectively). There were also more females in the Damon and PAOO groups (64% and 68%, respectively), compared to the MARPE (32%, $P = 0.19$) sample (Table 1).

Heterogeneous ($P \leq .05$) pretreatment variables were inter-canine width, inter-molar width, and left clinical crown heights. Pretreatment inter-canine width was smaller in PAOO (33.2 mm) compared to Damon (36.1 mm, $P \leq .001$), and inter-molar width was smaller in PAOO (33.3 mm, $P \leq .01$) than Damon (36.5 mm) and MARPE (36.4 mm). The left first molar clinical crown height (CCH) for PAOO (4.8 mm) was smaller than MARPE (5.7 mm, $P \leq .01$) (Table 2). For the three arch parameters that differed significantly at pretreatment, only increments of treatment change were compared among the three study groups. The remaining six arch variables with homogenous pretreatment means were compared at posttreatment in addition to the treatment effect (increments of change) comparisons.

3.1. Intergroup Treatment Effects. For the initial variables that were homogenous at pretreatment, posttreatment arch

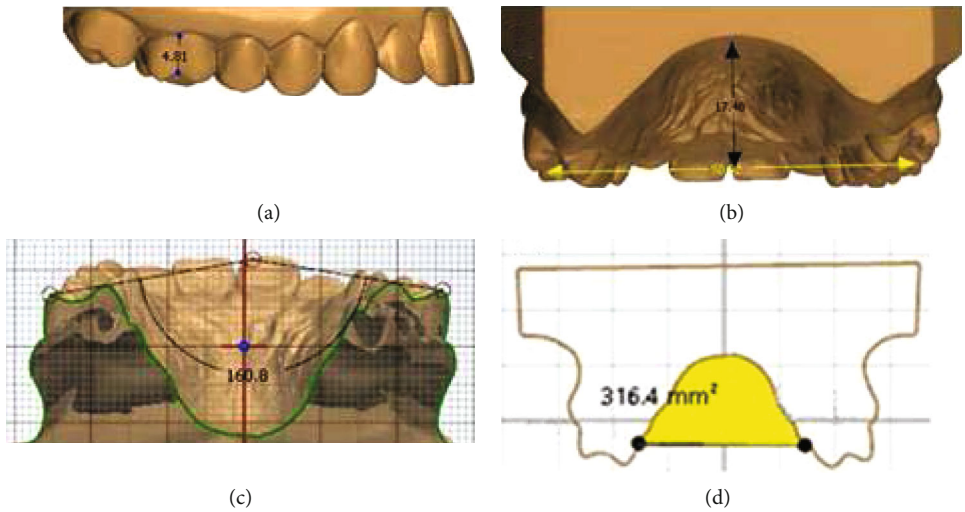

Figure 2: Measurements of maxillary first molar and palate. (a) First molar crown height was determined from the most occlusal point of the buccal groove to the gingival margin below the buccal groove; (b) palatal height was measured at the level of the buccal groove of the first molars with a linear line extended to palate; (c) first molar angulation was determined by measuring the angle of intersection of the lines drawn tangent to the mesio-facial and mesio-palatal cusp tips of the maxillary first molars; and (d) palate vault area measured from the palatal gingival level of the first molars.

Table 1: Demographics representing the three study samples including sample size, mean age (in years), gender (number and percent of sample), and active orthodontic treatment time (in months). Note significant differences ($*P \leq .05$) in PAOO age, male and female ratio for MARPE, and active treatment time for PAOO.

Variable	Damon	MARPE	PAOO
Sample size	23	28	28
Mean age (in years)	25.6	20.9	31.7*
Gender			
Male	8 (35%)	19 (68%)*	9 (32%)
Female	15 (65%)	9 (32%)*	19 (68%)
Active Tx (months)	16.0 ± 2.0	24.1 ± 9.3	8.6 ± 3.2 *

perimeter was significantly greater for MARPE (75.2 mm) at posttreatment than PAOO (72.5 mm, $P \leq .05$). Arch depth was smaller for MARPE (25.7 mm, $P \leq .05$) than both Damon (27.1 mm) and PAOO (27.0 mm). Posttreatment right first molar clinical crown height was increased in the MARPE group in comparison to the PAOO group (5.8 vs 5.0 mm, $P = .01$). Palatal vault area was significantly smaller for PAOO (287.6, $P \leq .05$) than Damon and MARPE (335.5 and 343.1, respectively). There were no significant differences for palatal vault height and molar angulations between the groups (Table 3).

3.2. Intergroup Treatment Effects (Increment of Change). For the initial variables that were heterogeneous at pretreatment, posttreatment inter-canine arch width change was significantly less in Damon (1.4 mm) compared to MARPE (2.3 mm, $P = .04$) and PAOO (3.0 mm, $P \leq .001$). Intermolar width increase was larger for MARPE (4.2 mm) than PAOO and Damon (1 and 0.5 mm, respectively, $P \leq .001$). (Table 4).

3.3. Intragroup Treatment Effects. Inter-canine and intermolar arch widths were significantly increased for all groups posttreatment ($P \leq .001$). Arch perimeter increased significantly in only the MARPE and PAOO groups ($P \leq .001$). Clinical crown height for MARPE increased significantly for the right first molar. Palatal vault height for MARPE significantly decreased, and palatal vault area for MARPE increased significantly. PAOO demonstrated a significant increase in first molar angulations (Table 5).

4. Discussion

The three groups compared were heterogeneous for ethnicity, age, and male-female ratios as well as total treatment time. The MARPE group was considerably younger, with a mean age of 20.9, which seems to be around the ideal age to attempt MARPE, i.e., after sutural closure, but prior to maturation [20]. Treatment using PAOO was completed within 9 months, which is purported to be due to the Regional Acceleratory Phenomenon (RAP) [8, 10, 21, 22]. Damon showed a swift 16-month treatment time, while patients treated with MARPE completed the treatment in a slower 24-month period. Treatment time using MARPE could have been slower due to the dual phase nature of the treatment, in which the first stage utilized the MARPE appliance itself and the second phase utilized the conventional fixed appliance. The treatment of the MARPE group also took place in an academic setting, unlike the former which were treated privately, thereby perhaps extending the treatment time as well. Therefore, not too much can be read into these differences due to the heterogonous collection of the sample, and the differing protocols by the various

Table 2: Heterogeneous pretreatment maxillary dental arch variables among the three study samples. Note that the PAOO sample had significantly (∗) smaller ($P \leq .006$) mean pretreatment dimensions for inter-canine and inter-molar widths as well as left first molar clinical crown height (CCH).

	Initial mean			P sig.		
	Damon	MARPE	PAOO	D-M	D-P	M-P
Inter-canine width	36.1	34.6	33.2	NS	≤.001∗	NS
Inter-molar width	36.5	36.4	33.3	NS	≤.01∗	≤.01∗
Left CCH	5.2	5.7	4.8	NS	NS	≤.01∗

Table 3: A comparison among the three study samples of posttreatment variables that were homogeneous at pretreatment.

	Post Tx mean			P sig.		
	Damon	MARPE	PAOO	D-M	D-P	M-P
Arch perimeter	74.5	75.2	72,5	NS	NS	≤.05∗
Arch depth	27.1	25.7	27	≤.05∗	NS	≤.01∗
Right CCH	5.3	5.8	5	NS	NS	≤.01∗
Palatal vault height	18.6	18.4	17.1	NS	NS	NS
Palatal vault area	335.5	343.1	287.6	NS	≤.05∗	≤.01∗
Molar angulation	158	162	160.4	NS	NS	NS

Table 4: An intergroup comparison of mean increments of treatment change for pretreatment variables that were heterogeneous.

	Mean change from pre- to posttreatment								
	Damon	MARPE	PAOO	D-M		D-P		M-P	
				Mean dif.	P sig.	Mean dif.	P sig.	Mean dif.	P sig.
Inter-canine width	1.4	2.3	2.8	-0.9	≤0.05	-1.4	≤0.01	-0.5	NS
Inter-molar width	0.5	4.2	1.0	-3.6	≤0.01	-0.5	NS	3.2	≤0.01

Table 5: Paired *t*-tests demonstrated pre- to posttreatment intragroup treatment changes.

Variable	Damon group $n = 23$ (8 M; 15F)			MARPE group $n = 28$ (19 M; 9F)			PAOO group $n = 28$ (9 M; 19F)		
	Mean change	SD	*P* signif	Mean change	SD	*P* signif	Mean change	SD	*P* signif
Inter-canine width	1.4	1.66	≤.001∗	2.3	1.21	≤.001∗	3.0	0.76	≤.001∗
Inter-molar width	0.5	1.21	.048∗	4.2	1.87	≤.001∗	1.0	0.72	≤.001∗
Arch perimeter	1.6	4.38	NS	2.5	2.55	≤.001∗	1.2	1.53	≤.001∗
Arch depth	0.4	2.16	NS	-0.1	2.05	NS	0.3	2.25	NS
Right clinical crown height	0.2	0.60	NS	0.3	0.51	.003∗	-0.1	0.90	NS
Left clinical crown height	0.0	0.49	NS	0.2	0.43	NS	-0.1	0.63	NS
Palatal vault height	0.4	1.20	NS	-0.5	1.18	.025∗	-0.2	-0.91	NS
Palatal vault area	12.9	30.6	NS	19.8	35.36	.006∗	-6.8	18.26	NS
Molar angulations	-3.9	9.34	NS	-1.9	8.97	NS	2.5	6.14	.040∗

practitioners. Three pretreatment dental arch parameters also differed, i.e., left clinical crown height and arch widths at the inter-canine and inter-molar levels. In treatment effect studies, a study design with statistically homogeneous initial means is optimal. Because three arch parameters differed significantly at pretreatment, intergroup posttreatment means were not compared for these three study variables. However, statistical comparisons were made among the three samples for the remaining six maxillary dental arch variables.

Posttreatment, MARPE therapy had a greater impact on arch perimeter than PAOO resulting in 2.7 mm greater arch-perimeter than PAOO-treated patients. However, the post-treatment arch depth was smaller for MARPE (25.7 mm)

than both Damon (27.1 mm) and PAOO (27.0 mm). The likely explanation for these two results is that the 4.5 mm average inter-molar width increase with MARPE caused the initial long, narrow arches to expand significantly, thus normalizing the arch form and reducing the arch depth after space closure. In the Damon and PAOO groups, the expansion would seem to be inadequate to cause a significant change in arch form and hence arch depth.

The palatal vault area was significantly smaller at posttreatment for PAOO (287.6) than Damon and MARPE (335.5 and 343.1, respectively). This result is explained by the surgical addition of the bone graft placed palatally in the PAOO group during the procedure, thereby reducing palatal area at the first molar level. Posttreatment right first molar clinical crown height was greater for MARPE than PAOO (5.8 vs 5.0 mm). The MARPE design in this study utilized bands on the upper first molars; therefore, some force was placed on the dentition during the expansion. This force on the upper first molars may have caused some detrimental effects on the periodontium. PAOO, on the other hand, had reduced clinical crown height perhaps due to the alveolar bone graft placed labially resulting in a more robust periodontium.

The increments of change of initially heterogeneous variables showed that the inter-canine expansion obtained was significantly less in the Damon (1.4 mm) treatment system compared to MARPE (2.3 mm) and PAOO (2.8 mm) and also confirms the results of a previous study comparing conventional RME and Damon [23]. Similarly, inter-molar expansion with MARPE (4.3 mm) dramatically exceeded Damon (0.5 mm) and PAOO (1.0 mm), i.e., inter-molar expansion with MARPE was over 8-times greater than Damon and over 4-times greater than PAOO. The inter-molar changes clearly demonstrate the superiority of skeletal expansion caused by sutural separation from the MARPE appliance compared to the limited dental arch wire expansion from both the Damon and PAOO group. Arch wire expansion seems to expand the inter-canine width much more than the inter-molar area, which may result in reduced long-term stability. Surprisingly, the PAOO group showed slightly greater expansion in the canine area compared to the MARPE group.

Intragroup results show that arch depth and left clinical crown height did not significant change within any of the three study groups. All three study groups demonstrated significant inter-molar and inter-canine expansion. In the Damon group, none of the seven remaining arch variables changed significantly during treatment. Within the MARPE group, arch perimeter increased (2.5 mm), palatal height decreased significantly (-0.5 mm), but palatal vault area increased (19.8). The use of miniscrews likely prevented the maxillary first molars from extruding, and the 4.5 mm expansion would explain the increase in palatal vault area in the maxillary first molar region. The arch perimeter also increased within the PAOO (1.2 mm) group, and the 2.5 degree increase in molar angulation would suggest that molar expansion with arch wires resulted in some buccal tipping of the crowns of the first molars. All intragroup statistically significant changes also exceeded clinically significant guidelines except for the inter first molar expansion using the Damon bracket system treatment which was only marginally clinically significant, i.e., 0.5 mm.

4.1. Limitations. The retrospective nature of the study and the heterogeneous groups mean that the results of this study should be construed with some caution. The Damon sample was obtained from Mexico, the MARPE sample was from South Korea, and the PAOO sample was obtained from the USA. All patients treated by expansion were followed by straight wire treatment mechanics, with various finishing wires and arch forms that may have impacted some results. Moreover, impressions were taken immediately posttreatment, and gingival inflammation and/or gingiva compression during alginate impression may have affected the STL models. This study was based only on model evaluation, and CBCT was not performed, and thus skeletal changes could not be investigated.

5. Conclusions

(i) All groups showed significant width increase in the canine and molar area

(ii) MARPE obtained significantly greater amount of posterior expansion (4.2 mm) compared to PAOO (1 mm) and Damon (0.5 mm)

(iii) MARPE and PAOO showed significantly greater expansion in the canine area (2.3 mm and 3 mm, respectively) compared to Damon (1.4 mm)

(iv) MARPE was the only group to show a significant increase in palatal vault area

Data Availability

The datasets used and/or analyzed during the current study are available from the corresponding author on reasonable request.

Conflicts of Interest

The authors declare that they have no conflicts of interest.

References

[1] J. A. Brunelle, M. Bhat, and J. A. Lipton, "Prevalence and distribution of selected occlusal characteristics in the US population, 1988-1991," *Journal of Dental Research*, vol. 75, 2_suppl, pp. 706–713, 1996.

[2] J. A. McNamara, "Maxillary transverse deficiency," *American Journal of Orthodontics and Dentofacial Orthopedics*, vol. 117, no. 5, pp. 567–570, 2000.

[3] A. J. Haas, "Palatal expansion: just the beginning of dentofacial orthopedics," *American Journal of Orthodontics*, vol. 57, no. 3, pp. 219–255, 1970.

[4] M. J. Koudstaal, L. J. Poort, K. G. van der Wal, E. B. Wolvius, B. Prahl-Andersen, and A. J. Schulten, "Surgically assisted rapid maxillary expansion (SARME): a review of the literature," *International Journal of Oral and Maxillofacial Surgery*, vol. 34, no. 7, pp. 709–714, 2005.

[5] C. Carlson, J. Sung, R. W. McComb, A. W. Machado, and W. Moon, "Microimplant-assisted rapid palatal expansion appliance to orthopedically correct transverse maxillary deficiency in an adult," *American Journal of Orthodontics and Dentofacial Orthopedics*, vol. 149, no. 5, pp. 716–728, 2016.

[6] W. M. Wilcko and M. T. Wilcko, "Accelerating tooth movement: the case for corticotomy-induced orthodontics," *American Journal of Orthodontics and Dentofacial Orthopedics*, vol. 144, no. 1, pp. 4–12, 2013.

[7] K. J. Lee, Y. C. Park, J. Y. Park, and W. S. Hwang, "Miniscrew assisted nonsurgical palatal expansion before orthognathic surgery for a patient with severe mandibular prognathism," *American Journal of Orthodontics and Dentofacial Orthopedics*, vol. 137, no. 6, pp. 830–839, 2010.

[8] L. V. de Miranda, L. Capelozza-Filho, R. R. Almeida-Pedrin, F. P. Guedes, C. M. de Almeida, and A. C. de Castro Ferreira Conti, "Tomographic evaluation of the maturation stage of the midpalatal suture in postadolescents," *American Journal of Orthodontics and Dentofacial Orthopedics*, vol. 153, no. 6, pp. 818–824, 2018.

[9] W. M. Wilcko, M. T. Wilcko, J. E. Bouquot, and D. J. Ferguson, "Rapid orthodontics with alveolar reshaping: two case reports of decrowding," *The International Journal of Periodontics & Restorative Dentistry*, vol. 21, no. 1, pp. 9–19, 2001.

[10] D. J. Ferguson, M. T. Wilcko, W. M. Wilcko, and L. Makki, "Scope of treatment with periodontally accelerated osteogenic orthodontics therapy," *Seminars in Orthodontics*, vol. 21, no. 3, pp. 176–186, 2015.

[11] G. Swennen, H. Schliephake, R. Dempf, H. Schierle, and C. Malevez, "Craniofacial distraction osteogenesis: a review of the literature. Part I: clinical studies," *International Journal of Oral and Maxillofacial Surgery*, vol. 30, no. 2, pp. 89–103, 2001.

[12] D. Birnie, "The Damon passive self-ligating appliance system," *Seminars in Orthodontics*, vol. 14, no. 1, pp. 19–35, 2008.

[13] C. S. Handelman, L. Wang, E. A. BeGole, and A. J. Haas, "Nonsurgical rapid maxillary expansion in adults: report on 47 cases using the Haas expander," *The Angle Orthodontist*, vol. 70, no. 2, pp. 129–144, 2000.

[14] L. S. Lemos, M. C. R. Rebello, C. J. Vogel, and M. C. Barbosa, "Reliability of measurements made on scanned cast models using the 3Shape R700 scanner," *Dento Maxillo Facial Radiology*, vol. 44, no. 6, p. 20140337, 2015.

[15] E. W. Brust and J. A. McNamara, "Arch dimensional changes concurrent with expansion in mixed dentition patients," in *Orthodontic Treatment: Outcome and Effectiveness*, C. A. Trotman and J. A. McNamara Jr., Eds., vol. 30 of Craniofacial Growth Series, Center for Human Growth and Development, University of Michigan, Ann Arbor, 1995.

[16] J. A. McNamara Jr., T. Baccetti, L. Franchi, and T. A. Herberger, "Rapid maxillary expansion followed by fixed appliances: a long-term evaluation of changes in arch dimensions," *The Angle Orthodontist*, vol. 73, no. 4, pp. 344–353, 2003.

[17] G. A. Carter and J. A. J. McNamara, "Longitudinal dental arch changes in adults," *American Journal of Orthodontics and Dentofacial Orthopedics*, vol. 114, no. 1, pp. 88–99, 1998.

[18] R. G. Geran, J. A. McNamara, T. Baccetti, L. Franchi, and L. M. Shapiro, "A prospective long-term study on the effects of rapid maxillary expansion in the early mixed dentition," *American Journal of Orthodontics and Dentofacial Orthopedics*, vol. 129, no. 5, pp. 631–640, 2006.

[19] M. Bizzarro, C. Generali, S. Maietta et al., "Association between 3D palatal morphology and upper arch dimensions in buccally displaced maxillary canines early in mixed dentition," *European Journal of Orthodontics*, vol. 40, no. 6, pp. 592–596, 2018.

[20] J. J. Park, Y. C. Park, K. J. Lee, J. Y. Cha, J. H. Tahk, and Y. J. Choi, "Skeletal and dentoalveolar changes after miniscrew-assisted rapid palatal expansion in young adults: a cone-beam computed tomography study," *Korean Journal of Orthodontics*, vol. 47, no. 2, pp. 77–86, 2017.

[21] M. T. Wilcko, W. M. Wilcko, and N. F. Bissada, "An evidence-based analysis of periodontally accelerated orthodontic and osteogenic techniques: a synthesis of scientific perspectives," *Seminars in Orthodontics*, vol. 14, no. 4, pp. 305–316, 2008.

[22] D. Ferguson, A. Nazarov, L. Makki, M. Wilcko, and W. Wilcko, "Posttreatment and retention outcomes with and without periodontally accelerated osteogenic orthodontics assessed using ABO objective grading system," *APOS Trends in Orthodontics*, vol. 6, no. 4, p. 194, 2016.

[23] Y. L. Yu, G. H. Tang, F. F. Gong, L. L. Chen, and Y. F. Qian, "A comparison of rapid palatal expansion and Damon appliance on non-extraction correction of dental crowding," *Shanghai Kou Qiang Yi Xue*, vol. 17, no. 3, pp. 237–242, 2008.

Hindawi
BioMed Research International
Volume 2022, Article ID 7031269, 9 pages
https://doi.org/10.1155/2022/7031269

Research Article

The Effects of Additional Filtration on Image Quality and Radiation Dose in Cone Beam CT: An In Vivo Preliminary Investigation

Jan Houfrar,[1] **Bjorn Ludwig**,[1] **Dirk Bister**,[2] **Manuel Nienkemper**,[3] **Ciamak Abkai**,[4] **and Adith Venugopal**[5,6]

[1]*Department of Orthodontics, Saarland University, Homburg/Saar, Germany*
[2]*Department of Orthodontics, Guy's and St Thomas' NHS Foundation Trust and King's College Dental Institute, London, UK*
[3]*Department of Orthodontics, Heinrich-Heine-University, Düsseldorf, Germany*
[4]*Private Practice, Traben-Trarbach, Germany*
[5]*Department of Orthodontics, Saveetha Dental College, Saveetha Institute of Medical and Technical Sciences, Saveetha University, Chennai, India*
[6]*Department of Orthodontics, University of Puthisastra, Phnom Penh, Cambodia*

Correspondence should be addressed to Adith Venugopal; avenugopal@puthisastra.edu.kh

Received 22 November 2021; Accepted 3 February 2022; Published 2 March 2022

Academic Editor: Shivam Mehta

Purpose. The aim of this study was to investigate the effect of reduced radiation doses on the image quality of cone-beam computed tomography scans and the suitability of such imaging for orthodontics, oral surgery, dental implantology, periodontology, and endodontology. *Materials and Methods*. Cone-beam computed tomography scans of a live patient were performed using seven attenuation filters with increased thickness to decrease the effective radiation dose from 22.4 to 1.8 μSv, and the effects of different radiation doses on image quality were further analysed. Quantitative image quality was calculated using dedicated measures, such as signal and contrast-to-noise ratio and sharpness. A panel of five certified raters assessed the cone-beam computed tomography scans qualitatively. Nine anatomical structures relevant to dentistry were identified, and the overall acceptance was assessed. *Results*. Linear reduction of the effective radiation dose had a nonlinear effect on image quality. A 5-fold reduction in the effective dose led to acceptable quantitative and qualitative image quality measures, and the identification rate of dental anatomical structures was 80% or greater. The use of less than 40% of the reference dose was unacceptable for all dental specialties. *Conclusions*. The ideal radiation dose for specific diagnostic requirements remains a patient-related and specialty-related decision that must be made on an individual basis. Based on the results of this study, it is possible to reduce exposure in selected patients, and at the same time obtain sufficient quality of images for clinical purposes.

1. Introduction

Cone-beam computed tomography (CBCT) was introduced in 1998 [1] and has since been used in all dental disciplines [2, 3], and specific indications have been identified in orthodontics [4], oral surgery [5], dental implantology [6], periodontology [7, 8], and endodontics [9, 10]. CBCT provides three-dimensional (3D) images, which are represented two-dimensionally, and can add valuable diagnostic information [11, 12]; however, the effective radiation dose increases with image quality [13], and clinicians are advised to use ionizing radiation with the lowest achievable radiation dose for safety purposes [14].

During CBCT scans, patients are exposed to radiation doses between 11 and 374 microsievert (μSv) [15, 16] that are significantly higher than those in dental panoramic tomography (DPT) or other routinely used imaging modalities in the maxillofacial area (5–15 μSv) [17–19]. The applied dose depends on the physical process of radiation production, the irradiated area, and the sensitivity of the

radiation-detecting equipment. However, the diagnostic value of an image not only is determined by the radiation dose but also depends on the equipment on which the image is visualized, as well as the person who assesses the image [20–23].

Physical parameters, such as beam quality and dose, determine the image quality of radiographs [14, 24–28]. Some image quality parameters, such as signal-to-noise ratio (SNR), contrast-to-noise ratio (CNR), and sharpness, can be objectively measured; thus, subjective image quality is of essential importance and may have a critical impact on diagnosis and treatment planning. A number of studies have often used dry skull phantoms to determine subjective image quality [20, 21, 23, 24]. However, images obtained from dry skulls differ considerably from live patient images because of the absence of soft tissues; therefore, a dry skull model is poorly appropriate for clinical settings [24]. Hence, this study aimed to acquire CBCT images from a live patient using interchangeable filters and to reduce the effective radiation dose. In addition, we also attempted to determine the effect of radiation doses on subjective image quality and assess the ability of such imaging to identify anatomical structures. The images used for this study were acquired with a commercially available CBCT machine that had been modified using seven copper filters.

2. Methods

2.1. Ethical Approval. The study was performed on a live individual who is one of the authors of this study. He had a skiing accident that resulted in a fractured #21 and warrented a CBCT scan as a part of his clinical care. The subject was assessed by a psychiatrist and found to be competent to evaluate the risks and benefits and to accept full responsibility for the conduct of the experiment. The Declaration of Helsinki does not comment on self-experimentation. The requirement for ethics approval therefore does not apply. Nevertheless, approval for the series of radiographs was obtained from the Trier District Dental Association Public corporation Loebstrasse 18, 54292 Trier. Since the author was also the subject, the requirement for informed consent does not apply. But for the purpose of publication of data, the patient provided an explicit informed consent to participate in the study.

2.2. Imaging. A fully dentate live patient was included in this study. No artefacts due to metal objects were visible on CBCT images.

2.3. CBCT Unit Preparation and Acquisition of Data Sets. Orthophos® XG 3D (Sirona, Bensheim, Germany) was used for imaging. For dose reduction, a series of seven copper (Cu) filters (F1-F7) (10 mm × 10 mm in size) with different thicknesses (Table 1) were used to attenuate the radiation beam; they were mounted as close as possible to the radiation source. The effective radiation dose for F0 (no filter) was 36 μSv (Ludlow et al. [29]) and was used to calculate the interpolated effective dose values by linear regression, which was performed based on air kinetic energy released per unit mass measured using a PTW Nomex® ionization chamber (PTW, Freiburg, Germany) in the central line of the beam at the detector's iso-center. The same instrument parameters (7 mA and 85 kV) were used for all imaging experiments.

Table 1: Filter settings and effective and relative radiation doses.

Filters	Cu-filter thickness (mm)	Air kerma (μGy)	Relative absorbed dose (%)	Interpolated effective dose∗ (μSv)
F0	0 (no filter/ reference)	1255	100	36†
F1	0.2	779	62	22.4
F2	0.4	480	38	13.8
F3	0.7	328	26	9.4
F4	1.0	202	16	5.8
F5	1.3	134	11	3.8
F6	1.5	104	8	3.0
F7	2.0	63	5	1.8

F0 (no filter) was used as the reference dose. Relative absorbed doses were assessed based on ion chamber dosimetric (air kerma) measurements with a repeatability error of <0.03-1%. Interpolated effective doses were calculated as linear interpolation in relation to F0. †Taken from Ludlow et al. [29]. ∗Interpolation was calculated based on relative absorbed dose measurements and a real effective dose reference value.

The field of view was 8 cm × 8 cm with a voxel size of 0.160 mm^3. Eight different 3D data sets were obtained and stored in Digital Imaging and Communications in Medicine (DICOM) format (one for each filter setting) [30]. All the scans were done in under 10 minutes without changing the setups for each scan. Furthermore, the minor head movements were controlled with the support of the headrest.

2.4. Materials Used for Rating. DICOM data was used throughout the study without any image modification/processing. To standardize the images for the ratings, three image sections (A, coronal view section of the lower first molar; B, mandibular axial; and C, maxillary axial) were prepared from each volume dataset. These sections were chosen because they represented the same anatomical location and orientation, as demonstrated in other investigations [20]. The three specific sections depict relevant anatomy for different dental specialties considered in our study. A total of 24 slices were used.

An overview of the 24 slices with relevant filtration settings (F0-F7) for the patient is presented in Figure 1. Images were used without enhancement to achieve a standardized rating environment. Three slices (A, B, and C) were arranged next to each other for every filtration setting. The slides of different attenuations were randomly distributed for blind assessment to prevent preconditioning during the evaluation phase. The contrast and brightness settings were kept constant.

2.5. Qualitative Evaluation. Five CBCT-certified senior dentists at the Dental University Hospital undertook a qualitative analysis of images. The assessors were given verbal

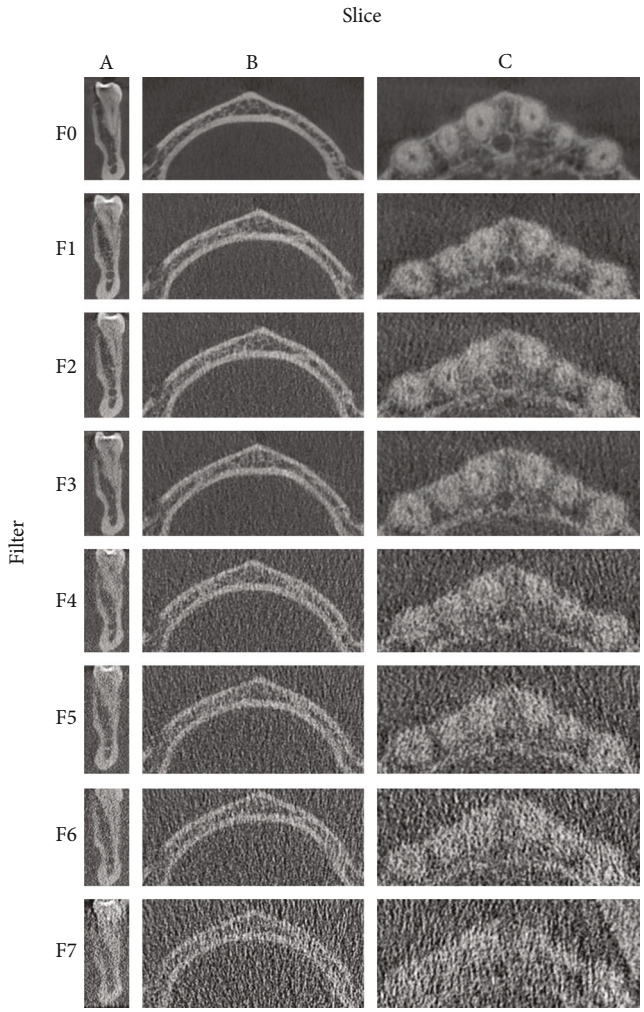

Figure 1: Overview of the 3 slices from 3D CBCT using filters F0-F7. Slice A, coronal view of the lower first molar; slice B, mandibular axial; slice C, maxillary axial.

and written instructions on how to view and assess/rate the images using custom questionnaires. The images were presented in a randomized order, no time limit was set, and a calibrated and certified diagnostic monitor (terra® LCD 2430W, Wortmann AG, Hüllhorst, Germany) was used under standardized conditions.

Based on the questionnaire, subjective image quality was scored using a five-point rating scale (Q1-Q5) (Liang et al. [20]): 1 = excellent, 2 = good, 3 = acceptable, 4 = poor, and 5 = very poor. Evaluators were asked to identify the following nine dental and anatomical structures (A1-A9): A1, mental foramen; A2, mandibular canal; A3, cortical bone; A4, dental pulp; A5, dentin, A6, incisal canal; A7, enamel; A8, periodontal ligament; and A9, cancellous bone. Identification of anatomical structures A1-A9 was scored as "yes" or "no." All examiners were asked to assess whether these images were appropriate for the following specialties: S1, orthodontics; S2, oral surgery; S3, dental implantology; S4, periodontology; and S5, endodontology.

Figure 2: Example of areas used for quantitative image analysis. (a) Background noise; (b) signal bone; (c) signal dentine; (d) the bone soft-tissue edge for sharpness analysis.

2.6. Objective Image Quality. Objective image quality was analysed based on three tissues (bone, dentin, and soft tissue) on the anatomical sections (Figure 2). The following three key metrics were analysed.

(1) *SNR.* The SNR was calculated as shown below (equation (1)). The mean value of the signal (μ_{signal}) was measured from the bone, and the standard deviation of the background noise ($\sigma_{\text{background}}$) was calculated from the soft tissue

$$\text{SNR} = \frac{\mu_{\text{signal}}}{\sigma_{\text{background}}}. \quad (1)$$

(2) *Contrast-to-Noise Ratio (CNR).* The CNR was calculated as shown in equation (2). The mean signal values were measured for the dentine (μ_A) and bone (μ_B); the background noise ($\sigma_{\text{background}}$) was measured from the soft tissue

$$\text{CNR} = \frac{|\mu_A - \mu_B|}{\sigma_{\text{background}}}. \quad (2)$$

(3) The sharpness and edge visibility were calculated as shown in equation (3) on a hard bone-soft tissue edge based on the variation of the 2D line spread function, which is expressed by the 2D gradient of the image ($\nabla f(x)$)

$$\text{sharpness} = \frac{\sigma(|\nabla f(x)|)}{\sigma_{\text{background}}}. \quad (3)$$

2.7. Statistical Analysis. Intra- and interexaminer reliabilities were calculated using the intraclass correlation coefficient based on two separate measurements taken four weeks apart: they were 0.80 and 0.77, respectively. Nonlinear regression was used to calculate the association between the mean detection rate and subjective image quality. Qualitative measures from observer ratings are presented as means and

Table 2: Image quality rating of anatomical structures A1-A9 for filter settings F0-F7.

	F0	F1	F2	F3	F4	F5	F6	F7
Anatomical structures	M ± SD	M ± SD	M ± SD	M ± SD	M ± SD	M ± SD	M ± SD	M ± SD
A1	1.4 ± 0.9	3.2 ± 2.0	3.0 ± 1.6	2.8 ± 1.8	3.6 ± 1.7	4.2 ± 1.8	3.0 ± 2.0	3.4 ± 2.2
A2	2.8 ± 1.3	2.6 ± 1.1	3.2 ± 1.3	4.0 ± 1.2	4.6 ± 0.9	4.6 ± 0.5	4.8 ± 0.4	4.8 ± 0.4
A3	1.6 ± 0.5	2.2 ± 1.8	2.6 ± 1.1	2.8 ± 1.6	3.0 ± 1.6	3.2 ± 2.0	3.4 ± 1.8	3.2 ± 1.8
A4	3.0 ± 1.0	3.4 ± 1.3	3.6 ± 1.3	3.0 ± 1.0	4.0 ± 1.4	4.0 ± 1.2	4.4 ± 0.9	4.0 ± 1.0
A5	2.0 ± 0.7	3.4 ± 1.3	3.4 ± 1.5	3.4 ± 1.1	3.4 ± 1.5	3.8 ± 1.3	4.4 ± 0.9	4.2 ± 0.8
A6	1.4 ± 0.5	1.8 ± 0.8	2.8 ± 1.3	2.6 ± 1.1	3.4 ± 1.5	3.2 ± 2.0	3.6 ± 1.9	3.4 ± 1.7
A7	1.8 ± 0.8	3.0 ± 1.4	3.0 ± 1.6	3.2 ± 1.3	3.0 ± 1.6	3.8 ± 1.3	4.2 ± 1.1	3.8 ± 1.1
A8	3.0 ± 1.2	3.8 ± 1.6	3.6 ± 1.3	4.0 ± 1.0	4.2 ± 1.1	4.4 ± 0.9	4.4 ± 0.9	4.2 ± 0.8
A9	1.4 ± 0.5	3.6 ± 1.3	3.4 ± 1.3	3.4 ± 1.1	3.8 ± 1.6	4.4 ± 0.9	4.2 ± 1.1	4.0 ± 1.0

A1: foramen mentale, A2: mandibular canal, A3: cortical bone, A4: dental pulp, A5: dentine, A6: incisal canal, A7: enamel, A8: periodontal ligament, and A9: cancellous bone. All assessors' ($n = 5$) quality ratings are presented as means (M) and standard deviations (SD).

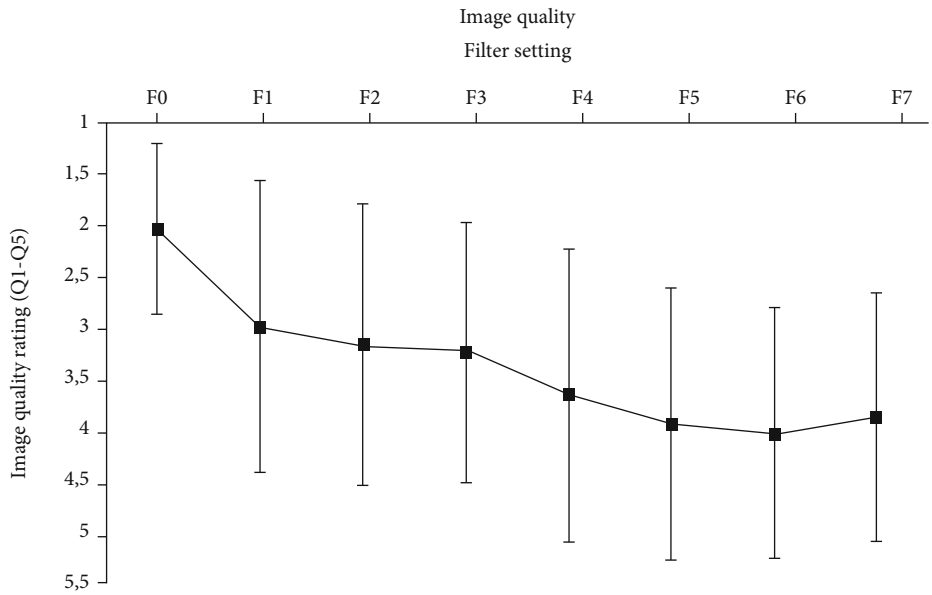

Figure 3: Image quality ratings for all anatomical structures (Q1 to Q5).

standard deviations. Statistical analyses were performed using SPSS® for Windows, version 22.0 (IBM Corp., Armonk, New York, USA). Statistical significance was set at $p < 0.05$.

3. Results

A detailed data analysis of image quality for anatomical structures is shown in Table 2. The cortical bone (A3) and the incisal canal (A6) had the best image quality, whereas the periodontal ligament (A8) had generally poor image quality. Figure 3 shows the mean image quality ratings for all anatomical structures.

Figure 4 shows objective image quality. Image noise was more pronounced for filters higher than F4; SNR and CNR markedly decreased for doses less than 10% of the reference dose. However, it became difficult to measure sharpness when image noise was high, so differentiation between filters F4-F7 was not performed. For filter settings F0-F3, the identification rates were between 80% and 100% (Figure 5).

The perceived usefulness for different dental specialties (S1-S5) is shown in Table 3. CBCT data acquired in this study were most suitable for orthodontics (S1) but were least suitable for endodontics (S5). Filter settings F3-F7 were rated as inappropriate for all specialties.

The relationship between the identification rate of anatomy and image quality (A1-A9) is shown in Figure 6. Notably, the plots followed a polynomial function of the second order; in other words, the relationship was not linear.

4. Discussion

This investigation assessed the subjective image quality of attenuated CBCT images and their ability to identify

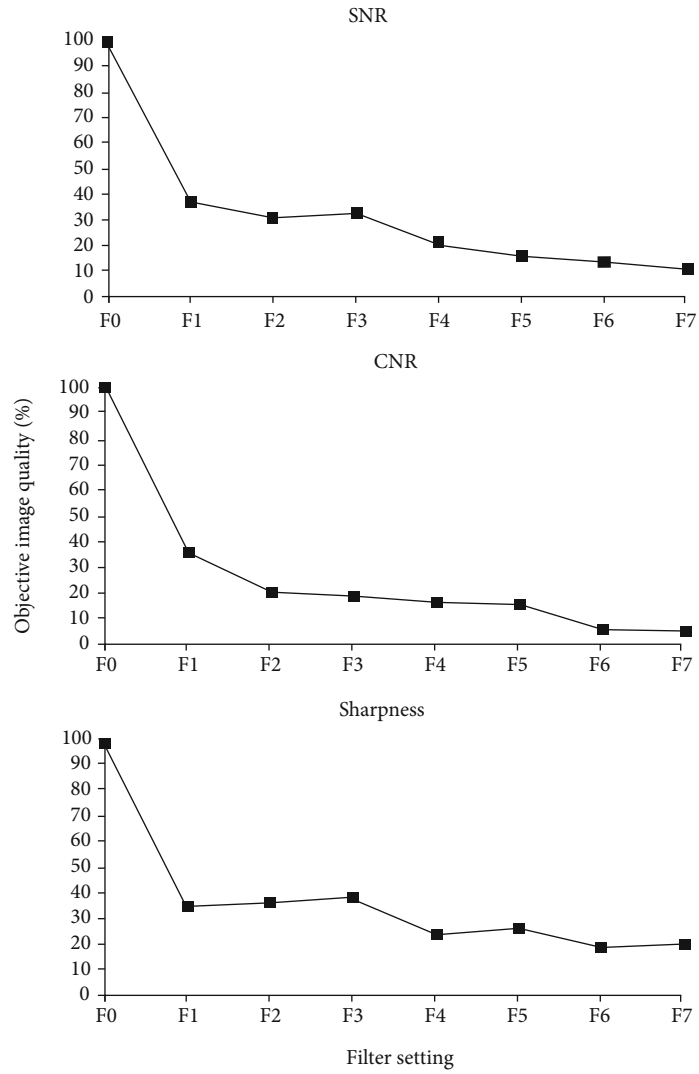

Figure 4: Overall subjective image quality ratings. All assessors' quality ratings (Q1-Q5) for the anatomical structures (A1-A9) investigated are presented as means and standard deviations.

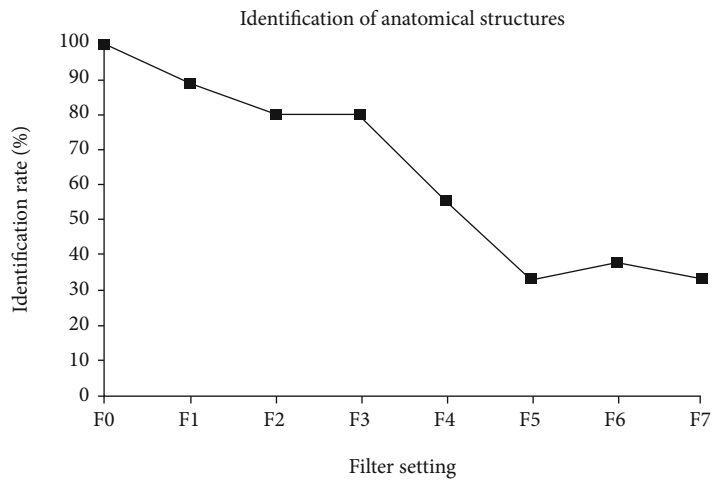

Figure 5: Identification of anatomy. The identification rates of anatomy and all anatomical structures (A1-A9) are shown.

Table 3: Perceived usefulness ratings.

	Perceived usefulness ratings (%)							
	F0	F1	F2	F3	F4	F5	F6	F7
S1	100	40	40	0	0	0	0	0
S2	100	40	20	0	0	0	0	0
S3	80	20	40	0	0	0	0	0
S4	60	0	40	0	0	0	0	0
S5	60	0	0	0	0	0	0	0

Perceived usefulness ratings (%) and different dental specialties depended on filter settings F0-F7. S1: orthodontics; S2: oral surgery; S3: dental implantology; S4: periodontology; S5: endodontics.

anatomical structures. We attempted to determine if CBCT radiographs with reduced effective radiation doses were still able yet maintain the image quality and identify anatomical structures. To the best of our knowledge, this study is the first to analyse the relationship between the identification rate of anatomy and image quality of the attenuated CBCT on a live dentate patient.

For the purpose of this study, we had specifically chosen regions that represented the most relevant structures in different dental disciplines, for example, cortical bone, cancellous bone, root, crowns, enamel, foramina, and other structures of diagnostic interest.

The patient received a combined effective radiation dose of 96 μSv for all images (F0-F7, exposures range from 1.8 to 36 μSv based on interpolation). The radiation burden to the patient in this study was lower than that of other commercially available equipment that could expose the patient to 674 μSv [15]. The copper filters F1-F3 used in our investigation led to effective radiation doses of 22.4, 13.8, and 9.4 μSv, respectively. Notably, the effective radiation dose for a digital full-size DPT and the cephalometric view is approximately 15 μSv [17, 19], and the effective radiation dose of an intraoral radiograph is approximately 5 μSv [18].

4.1. Image Quality and Identification of Anatomy. In our investigation, subjective and objective image quality measures decreased with increased thickness of the copper filters (i.e., reduced radiation dose); the findings further confirm that an increase in the radiation dose improves the image quality [13]. However, ratings on subjective image quality showed considerable variations (Figure 3). These variations may have been due to the random order of presentation of the images. The mean identification rate of anatomy (Figure 5) for filter settings F1-F3 was high. The raters were able to identify 80% of anatomy structures (A1-A9). Objective image quality (SNR, CNR, and sharpness) and subjective image quality were similar for filters F1-F3 (Figure 4). The modulation transfer function (MTF) was not used because it has been shown to be less robust for background noise [31]. These results highlight that the use of filters F1-F3, which correspond to 62%, 38%, and 26% of the reference dose, respectively, did not lead to a linear decrease in image quality; the image quality was consistent with all criteria (SNR, CNR, sharpness, subjective image quality, and mean identification). However, the use of filters F4-F7 led to a remarkable decrease in image quality, indicating a limited clinical availability of filters F4-F7. Notably, additional scattering effects caused by the filters were unlikely to influence our present results since the copper plates were very thin [32].

4.2. Applicability in Dental Specialties. Accumulating evidence indicates that CBCT is a very valuable imaging modality for endodontics and has been considered to have a significant impact on diagnosis and treatment planning. However, CBCT is currently only recommended for a small group of patients with complex endodontic problems [9]. Differences between different anatomical sites (mandibular vs. maxillary, anterior vs. posterior, etc.) needs related to the patient, and the specific clinical situation may have different implications on the outcome and the usefulness of the images in dentistry.

In our study, the assessors found that CBCT images obtained from filters F1-F3 were best suited for orthodontics, oral surgery, and dental implantology, in a descending order. Since periodontology, and endodontics dealt with very small anatomical structures, the images from the filters were deemed inappropriate. However, the assessors rated the data sets obtained from filters F3-F7 as inappropriate for any of the dental specialties (S1-S5) considered in our study. This finding suggests that the attenuated CBCT imaging technique is unlikely to be clinically used in dental specialties relying on the identification of small (micro) structures, such as the periodontal ligament and the root canal system.

4.3. Correlation of the Identification Rate of Anatomy with Image Quality. The nonlinear regression showed a good correlation between identification of anatomy and image quality ($R^2 = 0.92$, $p < 0.001$). These findings demonstrate the usefulness of the attenuated CBCT imaging technique, despite the relatively small number of evaluators. Despite the overall poor median image quality measures, F0 settings exhibited good identification, except for small anatomical structures A4 (dental pulp) and A8 (periodontal ligament). The usefulness of the images for endodontics (S5) and periodontology (S4) was rated lowest.

4.4. Strengths and Limitations of the Study. The CBCT technique in this study was designed to standardize the testing conditions. However, the slides presented to the evaluators were not necessarily relevant to the dental subspecialties. Indeed, scrolling through all the CBCT images leads to a better representation of 3-dimensional structures on a 2-dimensional monitor and allows for changes in brightness, contrast, and different settings of the Hounsfield units (HU).

Although the assessors were certified CBCT image raters, our present results only reflect their subjective impressions of image availability for different dental specialties. Whether an image is considered acceptable for clinical use often depends on the subjective evaluation of clinicians [20–23], regardless of whether an image can be modified for viewing. Our findings confirm that the reduced CBCT radiation dose may still allow reliable assessment of the

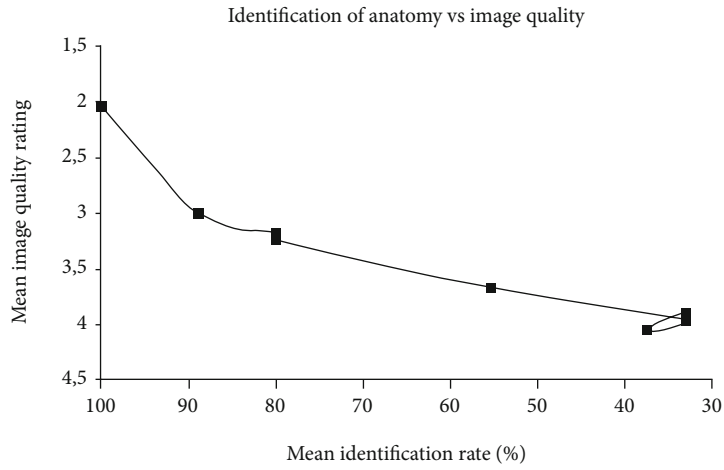

Figure 6: Correlation between the identification rate of anatomy and subjective image quality (F0-F7).

anatomy [23, 33, 34] as long as it is well indicated for a particular specialty.

The assessors considered 25% of CBCT images as inappropriate. The findings are not consistent with those in some current studies, which suggest that CBCT-derived cephalometry is generally comparable, despite not being more reliable [35–41]. Our investigation did not determine the accuracy of amalgamated CBCT images compared with conventional cephalometry. We assessed noncephalometric landmarks on CBCT images using modified equipment with reduced radiation burden. With the equipment used in our study, the radiation burden of CBCT was roughly equivalent to that of combined conventional DPT and cephalometric radiograph [17–19]. This finding suggests that the combined conventional DPT and cephalometric radiograph, which have often been used as part of the initial standard diagnostics [42], could be replaced by CBCT. However, this assumption is only correct if all images are of diagnostic quality. Further studies are needed to determine the reliability of CBCT images acquired by the modified equipment used in our study. Furthermore, different types of filters may have varying effects on the reduction of the subject's radiation exposure as well as the quality of the images obtained. This could be a possible evaluation for further studies. Using filters F1-F3, which were comparable to 62–26 percent of the reference dose, was possible and resulted in reliable anatomical structure identification. As a result, a further dose reduction within this range could be intriguing for future research.

5. Conclusion

Higher radiation doses led to better objective and subjective image quality and identification ratings. However, the relationship between the applied radiation dose and image quality measures was nonlinear. In addition, the use of filters F1-F3, which were equivalent to 62–26% of the reference dose, was feasible and still resulted in reliable identification of anatomical structures. However, image quality decreased markedly for filter settings where less than 11% of the reference dose was used. Moreover, attenuated CBCT was considered acceptable for orthodontics, oral surgery, and dental implantology, but not for periodontology and endodontics. While the loss of image quality may be acceptable for some indications, such imaging approaches cannot be recommended for imaging small anatomical structures, such as the periodontal ligament and the root canal system. Our findings suggest that the best radiation dose for specific diagnostic requirements remains a specialist-patient related decision, which has to be made on an individual basis, and it is possible to reduce exposure in selected patients, and at the same time obtain sufficient quality of images for clinical purposes.

Data Availability

The data used to support the findings of this study are available from the corresponding author upon request.

Conflicts of Interest

Dr. Ciamak Abkai was associated with Dentsply Sirona at the time of the study. There are no other conflicts to declare.

References

[1] P. Mozzo, C. Procacci, A. Tacconi, P. T. Martini, and I. A. Andreis, "A new volumetric CT machine for dental imaging based on the cone-beam technique: preliminary results," *European Radiology*, vol. 8, no. 9, pp. 1558–1564, 1998.

[2] H. M. Alamri, M. Sadrameli, M. A. Alshalhoob, and M. A. Alshehri, "Applications of CBCT in dental practice: a review of the literature," *General Dentistry*, vol. 60, no. 5, pp. 390–400, 2012.

[3] D. C. Hatcher, "Operational principles for cone-beam computed tomography," *Journal of the American Dental Association (1939)*, vol. 141, pp. 3S–6S, 2010.

[4] S. Kapila, R. S. Conley, and W. E. Harrell Jr., "The current status of cone beam computed tomography imaging in orthodontics," *Dento Maxillo Facial Radiology*, vol. 40, no. 1, pp. 24–34, 2011.

[5] W. De Vos, J. Casselman, and G. R. Swennen, "Cone-beam computerized tomography (CBCT) imaging of the oral and

maxillofacial region: a systematic review of the literature," *International Journal of Oral and Maxillofacial Surgery*, vol. 38, no. 6, pp. 609–625, 2009.

[6] M. M. Bornstein, W. C. Scarfe, V. M. Vaughn, and R. Jacobs, "Cone beam computed tomography in implant dentistry: a systematic review focusing on guidelines, indications, and radiation dose risks," *The International Journal of Oral & Maxillofacial Implants*, vol. 29, Supplement, pp. 55–77, 2014.

[7] X. Braun, L. Ritter, P. M. Jervoe-Storm, and M. Frentzen, "Diagnostic accuracy of CBCT for periodontal lesions," *Clinical Oral Investigations*, vol. 18, no. 4, pp. 1229–1236, 2014.

[8] Y. A. Aljehani, "Diagnostic applications of cone-beam ct for periodontal diseases," *Int J Dent*, vol. 2014, pp. 1–5, 2014.

[9] F. J. Mota de Almeida, K. Knutsson, and L. Flygare, "The effect of cone beam CT (CBCT) on therapeutic decision-making in endodontics," *Dento Maxillo Facial Radiology*, vol. 43, no. 4, p. 20130137, 2014.

[10] S. Patel, C. Durack, F. Abella et al., "European Society of Endodontology position statement: the use of CBCT in endodontics," *International Endodontic Journal*, vol. 47, no. 6, pp. 502–504, 2014.

[11] W. C. Scarfe and A. G. Farman, "What is cone-beam CT and how does it work?," *Dental Clinics of North America*, vol. 52, no. 4, pp. 707–730, 2008.

[12] W. C. Scarfe, A. G. Farman, and P. Sukovic, "Clinical applications of cone-beam computed tomography in dental practice," *Journal of the Canadian Dental Association*, vol. 72, no. 1, pp. 75–80, 2006.

[13] M. Loubele, R. Jacobs, F. Maes et al., "Radiation dose vs. image quality for low-dose CT protocols of the head for maxillofacial surgery and oral implant planning," *Radiation Protection Dosimetry*, vol. 117, no. 1-3, pp. 211–216, 2005.

[14] M. Uffmann and C. Schaefer-Prokop, "Digital radiography: the balance between image quality and required radiation dose," *European Journal of Radiology*, vol. 72, no. 2, pp. 202–208, 2009.

[15] J. B. Ludlow, "A manufacturer's role in reducing the dose of cone beam computed tomography examinations: effect of beam filtration," *Dento Maxillo Facial Radiology*, vol. 40, no. 2, pp. 115–122, 2011.

[16] G. Moze, J. Seehra, T. Fanshawe, J. Davies, F. McDonald, and D. Bister, "In vitro comparison of contemporary radiographic imaging techniques for measurement of tooth length: reliability and radiation dose," *Journal of Orthodontics*, vol. 40, no. 3, pp. 225–233, 2013.

[17] J. B. Ludlow, L. E. Davies-Ludlow, and S. C. White, "Patient risk related to common dental radiographic examinations: the impact of 2007 International Commission on Radiological Protection recommendations regarding dose calculation," *Journal of the American Dental Association (1939)*, vol. 139, no. 9, pp. 1237–1243, 2008.

[18] M. Kitafusa, K. Sato, and T. Yosue, "Patient dose in charge-coupled device-based full-mouth intraoral radiography," *Oral Radiology*, vol. 22, no. 2, pp. 62–68, 2006.

[19] H. K. Looe, F. Eenboom, N. Chofor et al., "Conversion coefficients for the estimation of effective doses in intraoral and panoramic dental radiology from dose-area product values," *Radiation Protection Dosimetry*, vol. 131, no. 3, pp. 365–373, 2008.

[20] X. Liang, R. Jacobs, B. Hassan et al., "A comparative evaluation of cone beam computed tomography (CBCT) and multi- slice CT (MSCT): part I. On subjective image quality," *European Journal of Radiology*, vol. 75, no. 2, pp. 265–269, 2010.

[21] K. Kamburoglu, S. Murat, E. Kolsuz, H. Kurt, S. Yuksel, and C. Paksoy, "Comparative assessment of subjective image quality of cross-sectional cone-beam computed tomography scans," *Journal of Oral Science*, vol. 53, no. 4, pp. 501–508, 2011.

[22] E. Sogur, B. G. Baksi, and H. G. Grondahl, "Imaging of root canal fillings: a comparison of subjective image quality between limited cone-beam CT, storage phosphor and film radiography," *International Endodontic Journal*, vol. 40, no. 3, pp. 179–185, 2007.

[23] S. Lofthag-Hansen, A. Thilander-Klang, and K. Grondahl, "Evaluation of subjective image quality in relation to diagnostic task for cone beam computed tomography with different fields of view," *European Journal of Radiology*, vol. 80, no. 2, pp. 483–488, 2011.

[24] J. W. Choi, S. S. Lee, S. C. Choi et al., "Relationship between physical factors and subjective image quality of cone- beam computed tomography images according to diagnostic task," *Oral Surgery, Oral Medicine, Oral Pathology, Oral Radiology*, vol. 119, no. 3, pp. 357–365, 2015.

[25] H. Yan, L. Cervino, X. Jia, and S. B. Jiang, "A comprehensive study on the relationship between the image quality and imaging dose in low-dose cone beam CT," *Physics in Medicine and Biology*, vol. 57, no. 7, pp. 2063–2080, 2012.

[26] K. Orhan, R. Pauwels, Y. Chen, D. Song, and R. Jacobs, "Estimation of the radiation dose for dental spectral cone-beam CT," *Dento Maxillo Facial Radiology*, vol. 50, no. 5, p. 20200372, 2021.

[27] E. Mah, E. R. Ritenour, and H. Yao, "A review of dental cone-beam CT dose conversion coefficients," *Dento Maxillo Facial Radiology*, vol. 50, no. 3, 2021.

[28] A. Yeung, R. Jacobs, and M. M. Bornstein, "Novel low-dose protocols using cone beam computed tomography in dental medicine: a review focusing on indications, limitations, and future possibilities," *Clinical Oral Investigations*, vol. 23, no. 6, pp. 2573–2581, 2019.

[29] J. B. Ludlow, R. Timothy, C. Walker et al., "Effective dose of dental CBCT-a meta analysis of published data and additional data for nine CBCT units," *Dento Maxillo Facial Radiology*, vol. 44, no. 1, p. 20140197, 2015.

[30] W. D. Bidgood Jr. and S. C. Horii, "Introduction to the ACR-NEMA DICOM standard," *Radiographics*, vol. 12, no. 2, pp. 345–355, 1992.

[31] H. Watanabe, E. Honda, and T. Kurabayashi, "Modulation transfer function evaluation of cone beam computed tomography for dental use with the oversampling method," *Dento Maxillo Facial Radiology*, vol. 39, no. 1, pp. 28–32, 2010.

[32] R. Pauwels, K. Araki, J. H. Siewerdsen, and S. S. Thongvigitmanee, "Technical aspects of dental CBCT: state of the art," *Dento Maxillo Facial Radiology*, vol. 44, no. 1, p. 20140224, 2015.

[33] S. Lofthag-Hansen, "Cone beam computed tomography radiation dose and image quality assessments," *Swedish Dental Journal. Supplement*, vol. 209, pp. 4–55, 2010.

[34] International Commission on Radiological Protection, *Recommendations of the international commission on radiological protection. ICRP Publication 103*, Ann IRCP, 2007.

[35] Z. C. Chang, F. C. Hu, E. Lai, C. C. Yao, M. H. Chen, and Y. J. Chen, "Landmark identification errors on cone-beam computed tomography-derived cephalograms and

conventional digital cephalograms," *American Journal of Orthodontics and Dentofacial Orthopedics*, vol. 140, no. 6, pp. e289–e297, 2011.

[36] V. Kumar, J. Ludlow, L. H. Soares Cevidanes, and A. Mol, "In vivo comparison of conventional and cone beam CT synthesized cephalograms," *The Angle Orthodontist*, vol. 78, no. 5, pp. 873–879, 2008.

[37] V. Kumar, J. B. Ludlow, A. Mol, and L. Cevidanes, "Comparison of conventional and cone beam CT synthesized cephalograms," *Dento Maxillo Facial Radiology*, vol. 36, no. 5, pp. 263–269, 2007.

[38] G. S. Liedke, E. L. Delamare, M. B. Vizzotto et al., "Comparative study between conventional and cone beam CT-synthesized half and total skull cephalograms," *Dento Maxillo Facial Radiology*, vol. 41, no. 2, pp. 136–142, 2012.

[39] M. Moshiri, W. C. Scarfe, M. L. Hilgers, J. P. Scheetz, A. M. Silveira, and A. G. Farman, "Accuracy of linear measurements from imaging plate and lateral cephalometric images derived from cone-beam computed tomography," *American Journal of Orthodontics and Dentofacial Orthopedics*, vol. 132, no. 4, pp. 550–560, 2007.

[40] A. Shokri, S. Khajeh, and A. Khavid, "Evaluation of the accuracy of linear measurements on lateral cephalograms obtained from cone-beam computed tomography scans with digital lateral cephalometric radiography: an in vitro study," *The Journal of Craniofacial Surgery*, vol. 25, no. 5, pp. 1710–1713, 2014.

[41] O. J. van Vlijmen, T. Maal, S. J. Berge, E. M. Bronkhorst, C. Katsaros, and A. M. Kuijpers-Jagtman, "A comparison between 2D and 3D cephalometry on CBCT scans of human skulls," *International Journal of Oral and Maxillofacial Surgery*, vol. 39, no. 2, pp. 156–160, 2010.

[42] W. R. Proffit, H. W. Fields, and D. M. Sarver, *Contemporary Orthodontics*, Elsevier, Oxford, 4th edn edition, 2007.

Hindawi
BioMed Research International
Volume 2022, Article ID 8381436, 23 pages
https://doi.org/10.1155/2022/8381436

Research Article

Buccolingual and Mesiodistal Dimensions of the Permanent Teeth, Their Diagnostic Value for Sex Identification, and Bolton Indices

Vahid Rakhshan,[1] **Fataneh Ghorbanyjavadpour**,[2] **and Negin Ashoori**[3]

[1]*Department of Anatomy, Dental School, Azad University of Medical Sciences, Tehran, Iran*
[2]*Department of Orthodontics, School of Dentistry, Ahvaz Jundishapur University of Medical Sciences, Ahvaz, Iran*
[3]*School of Dentistry, Ahvaz Jundishapur University of Medical Sciences, Ahvaz, Iran*

Correspondence should be addressed to Fataneh Ghorbanyjavadpour; fa.ghorbanyjavad@gmail.com

Received 10 November 2021; Accepted 18 January 2022; Published 10 February 2022

Academic Editor: Nafij Jamayet

Introduction. We aimed (1) to measure the mesiodistal and buccolingual widths of the permanent dentition in Iranian orthodontic patients, (2) to determine cut-off points for sex identification based on the mesiodistal and buccolingual diameters, and (3) to calculate Bolton indices. *Methods*. The mesiodistal and buccolingual dimensions of 28 maxillary and mandibular permanent teeth in 331 Iranian nonsyndromic orthodontic patients (dental casts and radiographs) aged 12 to 35 years old with fully erupted permanent dentitions (except the third molars and some sporadic cases of a few teeth missing or excluded) were measured. The anterior, posterior, and overall Bolton ratios were calculated in cases with no missing teeth in the 6-to-6 range. Potentially associated factors (the skeletal Angle classes, crowding, sex, jaws, sides, and age), as well as the value of these measurements for sex determination and cut-off points for sex identification based on these measurements were assessed using receiver-operator characteristic (ROC) curves, analysis of variance (ANOVA), Tukey, unpaired t-test, partial and Pearson correlation coefficients, and multiple linear regression ($\alpha = 0.05$). *Results*. Sex dimorphism was very frequent ($P \leq 0.05$ in 41 out of 56 measurements). Only the buccolingual widths of the maxillary lateral and the mandibular central and lateral differed across the Angle classes (ANOVA/Tukey, $P < 0.05$). Cut-off points were estimated for 38 dental measurements, which were proper for sex identification ($P < 0.05$), with 8 (2 maxillary and 6 mandibular) measurements being highly appropriate (having areas under ROC curves ≥ 64%, $P < 0.05$). Both the mandibular canines were the only teeth with all four measurements highly appropriate for this purpose. Controlling for the role of sex, aging was associated negatively with several crown dimensions (the buccolingual widths of the maxillary first and second premolar and mandibular second premolar and first molar; the mesiodistal diameters of the maxillary central, canine, first premolar, and first molar, mandibular central, lateral, first premolar, and first molar, $P \leq 0.05$, partial correlation coefficient). There were significant correlations among crown sizes. All the 28 (right/left-averaged) measurements were smaller in microdontia cases ($P \leq 0.002$). The anterior, posterior, and overall Bolton indices were 78.05, 105.42, and 91.87, respectively. There were correlations between the overall Bolton ratio with the other two Bolton ratios (Pearson $R = 0.696$, $R = 0.740$, $P < 0.0005$) but not between the anterior and posterior Bolton ratios ($R = 0.045$, $P = 0.459$). The skeletal Angle classes might not be associated with the overall and anterior Bolton ratios (ANOVA, regression, Pearson, $P > 0.05$). However, the posterior Bolton ratio was smaller in class II cases compared to classes I or III (Tukey, $P \leq 0.045$). In the whole sample, there was no sex dimorphism in Bolton ratios (t-test, $P > 0.05$). However, in Angle class II patients, the anterior Bolton ratio was greater in men than in women ($P = 0.014$). *Conclusions*. Sex dimorphism might be very common in the dentition of Iranians, with aging significantly reducing some measurements. The buccolingual widths of some incisors might differ across the skeletal Angle classes. Mandibular canines are the most appropriate teeth for sex identification. The Angle classes might not be associated with the anterior and overall Bolton ratios; nevertheless, the posterior Bolton ratio might be smaller in class II cases compared to others. In general, sex might not affect Bolton ratios; however, in class II patients, the anterior Bolton ratios might be larger in men.

1. Introduction

An important issue in dentistry is metric dental traits or mesiodistal and buccolingual crown sizes [1]. Tooth sizes are important in orthodontics, prosthodontics, restorative dentistry, anatomy, and even anthropological and forensic studies. One of the functions of orthodontists is to correct problems caused by dental size discrepancies in order to improve the mastication efficiency, the beauty of the face, and the orderliness of the dental arch [2]. Knowing the size of the teeth in populations and individuals is critical for proper diagnosis, planning an appropriate treatment, and predicting the results of orthodontic treatment [2–4]. The buccolingual dimension of the teeth is clinically important as one of the determining factors of the width of the upper and lower jaws, the width of the palate, and the space of the tongue. Therefore, the buccolingual dimensions of the teeth are related to the correct arrangement of the posterior teeth [5]. The mesiodistal dimension of the teeth has crucial orthodontic implications: to obtain an optimal occlusion, the mesiodistal measurements of the mandibular and maxillary teeth should relate to each other [6, 7]. Considerable intermaxillary mesiodistal size discrepancies—which are not uncommon—disallow aligning the teeth into an optimal occlusion [7–9]. To account for such intermaxillary relationships, Bolton [10] devised the concept of anterior and overall intermaxillary mesiodistal tooth size ratios (Bolton indices). Later, it was shown that Bolton ratios might be ethnic-specific and therefore should be assessed in different populations [6, 7, 11].

Dental crown dimensions can be used in anthropological studies, evolutionary research, and forensic sciences [3, 12–15]. Gender identification in injured bodies is an essential step and even the first step for forensic purposes [16, 17]. Determining sex through dental traits is a common practice in forensic dentistry and anthropology [18]. The most common measurements used for such purposes are mesiodistal and buccolingual widths which are convenient and reliable [19]. Numerous factors can interfere with tooth size variability, including genetic, epigenetic, or environmental factors [20]. Dental crowns might be larger in men than in women, especially in the case of the canines [13, 21–26]. Therefore, teeth are one of the desirable items for human and sex identification [24, 27, 28]. Dental sizes might also be used to estimate age [29].

Since not many studies have been done on metric dental traits especially large studies or studies in the Iranian population, we aimed to document the metric dental traits (56 mesiodistal and buccolingual crown dimensions of 28 permanent teeth) and then to determine sex dimorphism in each of the dimensions of each permanent tooth. Furthermore, the usefulness of these measurements in identifying the sex was assessed, and the cut-off point for gender determination was estimated. The associations between metric dental traits with the skeletal Angle classification and crowding were examined. Finally, we measured the Bolton intermaxillary mesiodistal tooth size ratios (Bolton indices); we also evaluated the associations between Bolton ratios with the skeletal Angle classes, sex, and age. Besides, we compared the Bolton ratios in this ethnic group with the original ratios measured by Bolton in American Caucasians [10].

2. Materials and Methods

This cross-sectional epidemiological study was performed on 662 maxillary and mandibular dental casts of 331 Iranian orthodontic patients attending the Orthodontic Department and two private orthodontic clinics in Ahvaz, Iran.

For data collection, all the available patients' records and their archival radiographs and casts were subsequently checked and approved/rejected until reaching the desired sample size. The inclusion criteria were being Iranian, 12 to 35 years old, and having a full permanent dentition except for the third molars and with no more than 2 extractions. The exclusion criteria were patients with cleft palates or lips or any systemic diseases or syndromes; patients with any history of previous prosthodontic, surgical, or orthodontic treatments; patients without a complete set of permanent teeth (except cases of hypodontia, cases of single excluded teeth, cases of one or two extracted teeth, and also except the third molars); cases with more than two extracted teeth; patients with more than two partially erupted permanent teeth; cases with poor cast quality; and cases without lateral cephalographs and panoramic radiographs. Additionally, single teeth that were not fully erupted or had (visible or a filed history of) dental caries, crown fractures, restorations, or veneers were excluded. Information on age, sex, and type of the skeletal Angle classification was recorded from the patients' files and their cephalographs. Data collection was performed from 2018 to 2020 [30, 31].

The used casts and radiographs were all archival, and thus, no harm was identified with this study. The protocol ethics were approved by the research committee of the university in accordance with the Helsinki Declaration (ethics code: U-98142).

All the used dental casts had been poured with white dental stone for orthodontic use. All the 56 dental buccolingual and mesiodistal dimensions of the 28 teeth were measured by a trained dentist at the quarter level (for each hemimaxilla or hemimandible of each patient separately): a digital caliper at an accuracy of 0.01 mm was used to measure the buccolingual distance (the largest distance between the buccal and lingual surfaces of the crown perpendicular to the mesiodistal width of that tooth, from the buccal to the lingual height of contours) and mesiodistal dimension (as the maximum distance between the mesial contact point and distal contact point, when the caliper is parallel to the buccal tooth surface); in case the proximal tooth was absent or the tooth was rotated, the anatomically normal contact points of the tooth would be detected by the observer [1, 20]. Microdontia was considered a very small size of a tooth but with a normal shape [32].

Cases with any missing teeth within the tooth range of bimaxillary first 12 teeth (bilateral centrals to the first molars) were identified and excluded. In the remaining 268 patients with no missing teeth in the bimaxillary 6–6 range, the sums of the mesiodistal diameters of the anterior 3 teeth (canine-to-canine) were calculated in the maxilla and also in the mandible. The anterior Bolton ratio was calculated as "100 × the sum of the mesiodistal widths of the 6 mandibular anterior teeth/the sum of the mesiodistal widths of the 6 maxillary anterior teeth" [7–10]. Similarly, in these 268 cases, the sums

Table 1: Descriptive statistics and 95% CIs for the mesiodistal and buccolingual widths (mm) in the right and left sides of the maxilla in males versus females (compared using the *t*-test).

Side	Dimension	Tooth	Sex	*N*	Mean	SD	95% CI		Min	Max	*P*
Right	Buccolingual	1	Female	257	7.369	0.584	7.30	7.44	5.61	9.22	0.044
			Male	73	7.522	0.520	7.40	7.64	6.34	8.88	
			Total	330	7.403	0.573	7.34	7.47	5.61	9.22	
		2	Female	250	6.536	0.644	6.46	6.62	4.47	8.15	0.003
			Male	72	6.812	0.816	6.62	7.00	4.22	9.91	
			Total	322	6.598	0.694	6.52	6.67	4.22	9.91	
		3	Female	253	8.178	0.647	8.10	8.26	5.65	9.65	<0.0005
			Male	73	8.497	0.751	8.32	8.67	6.36	9.88	
			Total	326	8.250	0.683	8.18	8.32	5.65	9.88	
		4	Female	248	9.302	0.642	9.22	9.38	6.62	10.87	0.031
			Male	72	9.488	0.624	9.34	9.63	7.79	10.85	
			Total	320	9.344	0.642	9.27	9.41	6.62	10.87	
		5	Female	254	9.450	0.644	9.37	9.53	6.16	10.94	0.047
			Male	73	9.622	0.657	9.47	9.77	8.29	10.92	
			Total	327	9.489	0.650	9.42	9.56	6.16	10.94	
		6	Female	254	11.373	0.631	11.30	11.45	9.58	12.78	0.008
			Male	72	11.600	0.640	11.45	11.75	10.24	13.11	
			Total	326	11.423	0.639	11.35	11.49	9.58	13.11	
		7	Female	253	11.338	0.798	11.24	11.44	8.75	13.60	0.033
			Male	70	11.570	0.817	11.38	11.76	9.19	13.26	
			Total	323	11.388	0.806	11.30	11.48	8.75	13.60	
	Mesiodistal	1	Female	257	8.626	0.573	8.56	8.70	6.60	10.37	0.031
			Male	73	8.789	0.556	8.66	8.92	7.62	9.98	
			Total	330	8.662	0.572	8.60	8.72	6.60	10.37	
		2	Female	250	6.759	0.708	6.67	6.85	3.90	9.69	0.560
			Male	72	6.812	0.620	6.67	6.96	4.70	8.14	
			Total	322	6.771	0.689	6.70	6.85	3.90	9.69	
		3	Female	255	7.675	0.467	7.62	7.73	6.12	9.15	0.001
			Male	73	7.896	0.509	7.78	8.02	6.93	8.82	
			Total	328	7.724	0.485	7.67	7.78	6.12	9.15	
		4	Female	249	6.946	0.499	6.88	7.01	5.02	9.04	0.187
			Male	72	7.034	0.497	6.92	7.15	5.67	8.16	
			Total	321	6.966	0.499	6.91	7.02	5.02	9.04	
		5	Female	254	6.665	0.499	6.60	6.73	4.93	9.08	0.472
			Male	73	6.713	0.513	6.59	6.83	5.78	8.05	
			Total	327	6.676	0.502	6.62	6.73	4.93	9.08	
		6	Female	254	10.050	0.723	9.96	10.14	6.54	13.16	0.018
			Male	72	10.277	0.691	10.11	10.44	8.52	12.13	
			Total	326	10.100	0.721	10.02	10.18	6.54	13.16	
		7	Female	252	9.780	0.676	9.70	9.86	7.60	11.63	0.001
			Male	70	10.076	0.616	9.93	10.22	8.68	11.45	
			Total	322	9.844	0.674	9.77	9.92	7.60	11.63	

Table 1: Continued.

Side	Dimension	Tooth	Sex	*N*	Mean	SD	95% CI		Min	Max	*P*
	Buccolingual	1	Female	256	7.342	0.620	7.27	7.42	5.79	9.01	0.017
			Male	74	7.536	0.591	7.40	7.67	5.78	9.57	
			Total	330	7.386	0.618	7.32	7.45	5.78	9.57	
		2	Female	252	6.547	0.627	6.47	6.62	4.62	8.41	0.013
			Male	72	6.782	0.931	6.56	7.00	4.80	12.46	
			Total	324	6.599	0.711	6.52	6.68	4.62	12.46	
		3	Female	250	8.172	0.694	8.09	8.26	5.85	9.87	<0.0005
			Male	73	8.500	0.727	8.33	8.67	6.20	10.05	
			Total	323	8.246	0.714	8.17	8.32	5.85	10.05	
		4	Female	250	9.297	0.633	9.22	9.38	6.19	10.91	0.026
			Male	72	9.485	0.616	9.34	9.63	8.27	10.86	
			Total	322	9.339	0.633	9.27	9.41	6.19	10.91	
		5	Female	253	9.406	0.675	9.32	9.49	5.86	10.90	0.040
			Male	74	9.588	0.641	9.44	9.74	8.18	11.05	
			Total	327	9.447	0.670	9.37	9.52	5.86	11.05	
		6	Female	256	11.327	0.629	11.25	11.40	9.53	12.94	0.004
			Male	74	11.568	0.653	11.42	11.72	10.03	13.24	
			Total	330	11.381	0.641	11.31	11.45	9.53	13.24	
		7	Female	253	11.247	0.779	11.15	11.34	8.35	13.14	0.001
			Male	71	11.602	0.727	11.43	11.77	9.61	13.62	
			Total	324	11.325	0.781	11.24	11.41	8.35	13.62	
Left	Mesiodistal	1	Female	256	8.659	0.607	8.58	8.73	6.46	10.61	0.017
			Male	74	8.851	0.601	8.71	8.99	7.52	10.67	
			Total	330	8.702	0.610	8.64	8.77	6.46	10.67	
		2	Female	252	6.788	0.636	6.71	6.87	4.57	8.43	0.685
			Male	72	6.822	0.624	6.68	6.97	4.64	7.96	
			Total	324	6.795	0.633	6.73	6.86	4.57	8.43	
		3	Female	251	7.602	0.478	7.54	7.66	5.02	9.13	0.001
			Male	73	7.814	0.527	7.69	7.94	6.66	9.02	
			Total	324	7.650	0.496	7.60	7.70	5.02	9.13	
		4	Female	250	6.965	0.503	6.90	7.03	4.86	9.02	0.280
			Male	72	7.039	0.543	6.91	7.17	5.49	8.38	
			Total	322	6.981	0.512	6.93	7.04	4.86	9.02	
		5	Female	253	6.642	0.575	6.57	6.71	5.01	9.73	0.037
			Male	74	6.805	0.646	6.66	6.95	5.61	9.96	
			Total	327	6.679	0.595	6.61	6.74	5.01	9.96	
		6	Female	256	10.059	0.632	9.98	10.14	8.26	11.53	0.005
			Male	74	10.297	0.642	10.15	10.45	8.96	11.65	
			Total	330	10.113	0.641	10.04	10.18	8.26	11.65	
		7	Female	253	9.845	0.648	9.77	9.93	8.20	11.66	0.002
			Male	71	10.115	0.561	9.98	10.25	8.95	11.43	
			Total	324	9.904	0.639	9.83	9.97	8.20	11.66	

Tooth numbers 1 to 7 denote the most anterior (the central) to the most posterior (the second molar) teeth. SD: standard deviation; CI: confidence interval; Min: minimum; Max: maximum.

Table 2: Descriptive statistics and 95% CIs for crown measurements (mm) in the mandible, compared between the sexes (using the *t*-test).

Side	Dimension	Tooth	Sex	*N*	Mean	SD	95% CI		Min	Max	*P*
Right	Buccolingual	1	Female	255	6.243	0.489	6.18	6.30	4.50	8.02	0.104
			Male	73	6.352	0.546	6.22	6.48	4.95	7.63	
			Total	328	6.267	0.503	6.21	6.32	4.50	8.02	
		2	Female	255	6.511	0.487	6.45	6.57	5.26	8.33	0.078
			Male	74	6.634	0.651	6.48	6.78	4.79	7.89	
			Total	329	6.539	0.530	6.48	6.60	4.79	8.33	
		3	Female	256	7.398	0.589	7.33	7.47	5.63	8.75	<0.0005
			Male	73	7.783	0.799	7.60	7.97	5.80	9.65	
			Total	329	7.483	0.660	7.41	7.55	5.63	9.65	
		4	Female	253	7.956	0.587	7.88	8.03	6.00	9.50	<0.0005
			Male	73	8.258	0.660	8.10	8.41	7.05	9.97	
			Total	326	8.024	0.616	7.96	8.09	6.00	9.97	
		5	Female	250	8.700	0.585	8.63	8.77	6.44	11.18	0.085
			Male	69	8.841	0.651	8.68	9.00	7.60	9.96	
			Total	319	8.731	0.601	8.66	8.80	6.44	11.18	
		6	Female	254	10.704	0.530	10.64	10.77	8.80	12.22	0.002
			Male	72	10.928	0.610	10.78	11.07	9.74	12.56	
			Total	326	10.753	0.556	10.69	10.81	8.80	12.56	
		7	Female	255	10.509	0.635	10.43	10.59	8.56	12.29	<0.0005
			Male	71	10.822	0.608	10.68	10.97	9.36	12.19	
			Total	326	10.577	0.641	10.51	10.65	8.56	12.29	
	Mesiodistal	1	Female	257	5.380	0.445	5.33	5.43	4.08	6.80	0.377
			Male	73	5.431	0.391	5.34	5.52	4.51	6.32	
			Total	330	5.391	0.433	5.34	5.44	4.08	6.80	
		2	Female	255	5.913	0.424	5.86	5.96	4.62	7.22	0.023
			Male	74	6.041	0.430	5.94	6.14	5.33	7.18	
			Total	329	5.941	0.428	5.90	5.99	4.62	7.22	
		3	Female	257	6.599	0.476	6.54	6.66	5.17	8.78	<0.0005
			Male	73	6.941	0.458	6.83	7.05	5.74	8.02	
			Total	330	6.674	0.493	6.62	6.73	5.17	8.78	
		4	Female	253	7.038	0.497	6.98	7.10	5.32	8.87	0.106
			Male	73	7.144	0.482	7.03	7.26	5.73	8.26	
			Total	326	7.061	0.495	7.01	7.12	5.32	8.87	
		5	Female	250	7.051	0.550	6.98	7.12	5.86	9.40	0.078
			Male	69	7.184	0.557	7.05	7.32	5.86	8.38	
			Total	319	7.080	0.553	7.02	7.14	5.86	9.40	
		6	Female	254	10.782	0.699	10.70	10.87	8.60	12.82	0.017
			Male	72	11.009	0.747	10.83	11.18	9.13	13.05	
			Total	326	10.832	0.715	10.75	10.91	8.60	13.05	
		7	Female	255	10.226	0.676	10.14	10.31	8.20	12.42	<0.0005
			Male	71	10.554	0.697	10.39	10.72	8.94	12.45	
			Total	326	10.297	0.693	10.22	10.37	8.20	12.45	

Table 2: Continued.

Side	Dimension	Tooth	Sex	*N*	Mean	SD	95% CI		Min	Max	*P*
	Buccolingual	1	Female	255	6.224	0.491	6.16	6.28	4.83	7.77	0.036
			Male	74	6.364	0.548	6.24	6.49	4.57	7.70	
			Total	329	6.256	0.507	6.20	6.31	4.57	7.77	
		2	Female	256	6.487	0.544	6.42	6.55	4.88	8.20	0.081
			Male	74	6.611	0.501	6.49	6.73	5.29	8.04	
			Total	330	6.515	0.536	6.46	6.57	4.88	8.20	
		3	Female	257	7.424	0.604	7.35	7.50	5.53	9.10	<0.0005
			Male	74	7.795	0.760	7.62	7.97	6.15	9.20	
			Total	331	7.507	0.659	7.44	7.58	5.53	9.20	
		4	Female	254	7.972	0.573	7.90	8.04	6.16	9.48	<0.0005
			Male	73	8.274	0.652	8.12	8.43	6.56	9.62	
			Total	327	8.040	0.604	7.97	8.11	6.16	9.62	
		5	Female	250	8.699	0.575	8.63	8.77	6.56	10.78	0.048
			Male	71	8.860	0.682	8.70	9.02	6.73	9.96	
			Total	321	8.735	0.603	8.67	8.80	6.56	10.78	
		6	Female	250	10.707	0.558	10.64	10.78	8.83	12.23	0.020
			Male	73	10.887	0.643	10.74	11.04	9.74	12.67	
			Total	323	10.748	0.582	10.68	10.81	8.83	12.67	
		7	Female	255	10.492	0.625	10.41	10.57	8.56	12.05	0.004
			Male	70	10.735	0.627	10.59	10.88	9.31	12.17	
			Total	325	10.544	0.632	10.48	10.61	8.56	12.17	
Left	Mesiodistal	1	Female	257	5.397	0.425	5.35	5.45	4.09	6.59	0.202
			Male	74	5.468	0.388	5.38	5.56	4.20	6.39	
			Total	331	5.413	0.417	5.37	5.46	4.09	6.59	
		2	Female	256	5.954	0.449	5.90	6.01	4.38	7.21	0.149
			Male	74	6.040	0.465	5.93	6.15	4.87	6.98	
			Total	330	5.973	0.454	5.92	6.02	4.38	7.21	
		3	Female	257	6.651	0.457	6.59	6.71	5.44	9.66	<0.0005
			Male	74	6.901	0.488	6.79	7.01	5.70	7.85	
			Total	331	6.707	0.475	6.66	6.76	5.44	9.66	
		4	Female	254	7.031	0.532	6.96	7.10	5.17	8.88	0.048
			Male	73	7.166	0.443	7.06	7.27	6.15	8.26	
			Total	327	7.061	0.516	7.00	7.12	5.17	8.88	
		5	Female	251	7.130	0.595	7.06	7.20	5.82	10.75	0.185
			Male	72	7.234	0.559	7.10	7.37	6.22	8.96	
			Total	323	7.153	0.588	7.09	7.22	5.82	10.75	
		6	Female	250	10.795	0.704	10.71	10.88	6.84	12.65	0.009
			Male	73	11.040	0.685	10.88	11.20	9.35	12.92	
			Total	323	10.851	0.706	10.77	10.93	6.84	12.92	
		7	Female	255	10.239	0.703	10.15	10.33	8.44	12.28	0.003
			Male	70	10.514	0.608	10.37	10.66	9.02	11.78	
			Total	325	10.298	0.692	10.22	10.37	8.44	12.28	

Tooth numbers 1 to 7 indicate the most anterior to the most posterior teeth. SD: standard deviation; CI: confidence interval; Min: minimum; Max: maximum.

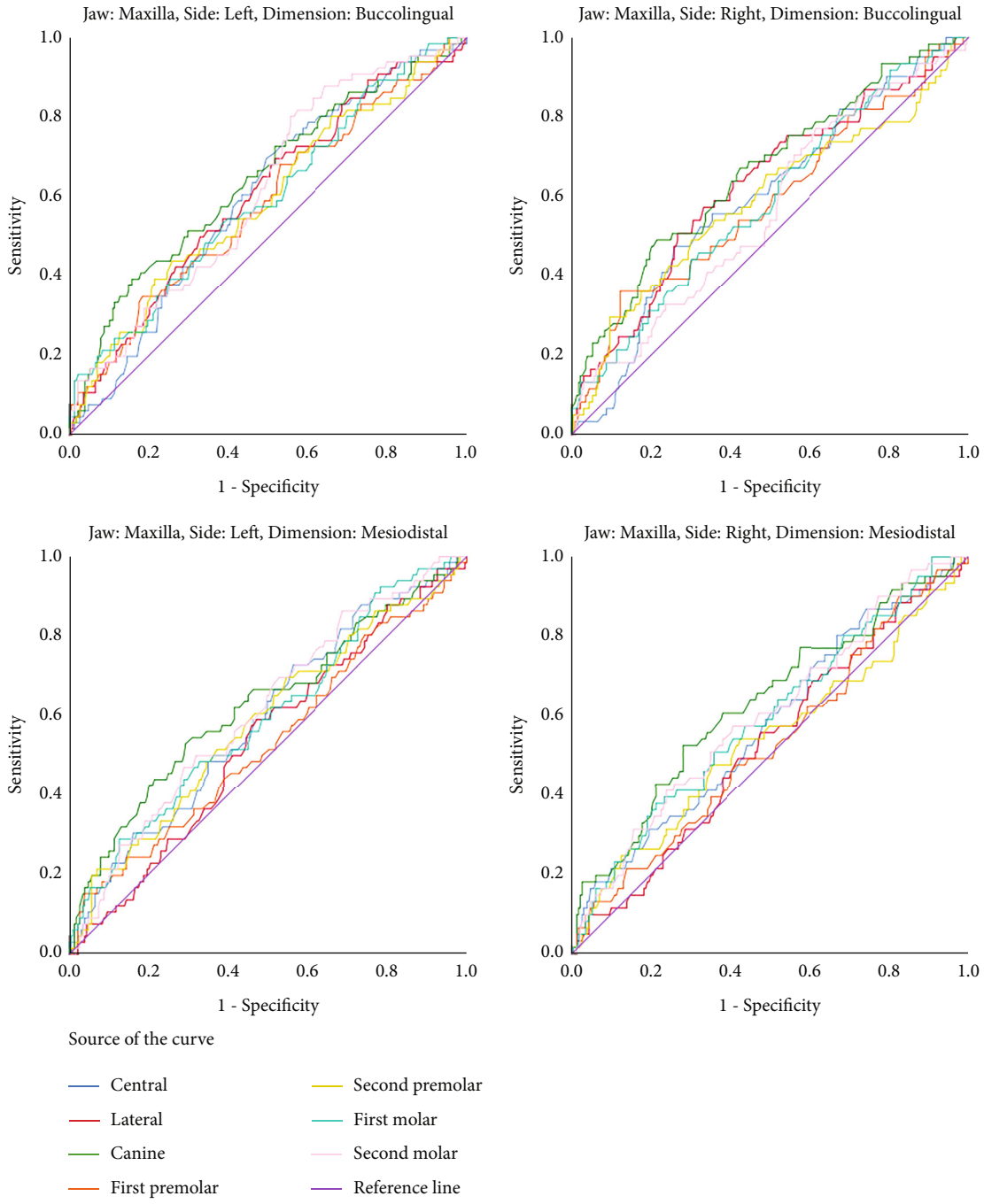

Figure 1: ROC curves of all the assessed mesiodistal and buccolingual dimensions of all the teeth in the left and right sides of the maxilla.

of the mesiodistal widths of the anterior 12 teeth (6–6) in the maxilla and also in the mandible were calculated. The overall Bolton ratio was computed as "100 × the sum of the mesiodistal diameters of the mandibular first 12 teeth (6–6, from the right first molar to the left first molar)/the sum of the mesiodistal dimensions of the maxillary first 12 teeth" [7–10]. The sums of the mesiodistal widths of the bimaxillary bilateral first premolar, second premolar, and first molar were calculated. The posterior Bolton ratio was calculated as "100 × the sum of the mesiodistal measurements of the mandibular premolars and first molars/the sum of the mesiodistal widths of the maxillary premolars and first molars" [33, 34].

2.1. Interexaminer Reproducibility Assessment. A second observer (FG) measured all the buccolingual and mesiodistal dimensions in all teeth of 35 randomly selected patients (4 quadrants, each). The intraclass correlation coefficient (a total of 28 Cronbach alpha values) showed excellent and high interobserver agreements between the two observers in most examinations (12 out of 28 Cronbach alpha values >0.9, 11 other

Table 3: The areas under ROC curves and the cut-off points for sex determination (mm).

Jaw	Side	Dimension	Tooth	Area	SE	*P*	95% CI		Cut-off (mm)
Maxilla	Right	Buccolingual	Central	0.596	0.040	0.021	0.517	0.675	7.715
			Lateral	0.628	0.041	0.002	0.547	0.709	6.950
			Canine	0.662	0.040	<0.0005	0.584	0.741	8.665
			First premolar	0.587	0.043	0.037	0.502	0.672	9.915
			Second premolar	0.590	0.045	0.031	0.502	0.677	10.175
			First molar	0.589	0.041	0.032	0.509	0.670	11.715
			Second molar	0.567	0.041	0.107	0.487	0.648	—
		Mesiodistal	Central	0.575	0.041	0.072	0.494	0.656	—
			Lateral	0.526	0.041	0.527	0.446	0.606	—
			Canine	0.628	0.041	0.002	0.547	0.710	7.930
			First premolar	0.526	0.042	0.528	0.444	0.609	—
			Second premolar	0.536	0.044	0.383	0.449	0.623	—
			First molar	0.590	0.041	0.030	0.509	0.671	10.275
			Second molar	0.598	0.041	0.018	0.518	0.678	10.235
	Left	Buccolingual	Central	0.602	0.038	0.011	0.529	0.676	7.355
			Lateral	0.606	0.039	0.009	0.529	0.683	6.535
			Canine	0.643	0.040	<0.0005	0.566	0.721	8.780
			First premolar	0.583	0.041	0.039	0.503	0.663	9.845
			Second premolar	0.591	0.041	0.024	0.512	0.671	9.865
			First molar	0.596	0.040	0.018	0.518	0.674	11.505
			Second molar	0.616	0.037	0.004	0.543	0.690	11.235
		Mesiodistal	Central	0.591	0.039	0.025	0.513	0.668	8.570
			Lateral	0.537	0.039	0.363	0.460	0.614	—
			Canine	0.627	0.041	0.002	0.546	0.708	7.835
			First premolar	0.532	0.042	0.422	0.450	0.615	—
			Second premolar	0.583	0.041	0.041	0.503	0.663	7.365
			First molar	0.595	0.040	0.019	0.516	0.673	10.815
			Second molar	0.611	0.039	0.006	0.536	0.687	10.155
Mandible	Right	Buccolingual	Central	0.578	0.043	0.056	0.494	0.662	—
			Lateral	0.572	0.043	0.078	0.488	0.655	—
			Canine	0.652	0.043	<0.0005	0.568	0.736	7.905
			First premolar	0.652	0.041	<0.0005	0.572	0.732	8.285
			Second premolar	0.572	0.045	0.078	0.484	0.660	—
			First molar	0.594	0.042	0.021	0.512	0.677	11.455
			Second molar	0.629	0.039	0.002	0.553	0.705	10.755
		Mesiodistal	Central	0.536	0.040	0.372	0.457	0.615	—
			Lateral	0.577	0.041	0.059	0.497	0.656	—
			Canine	0.720	0.036	<0.0005	0.650	0.790	6.835
			First premolar	0.575	0.040	0.066	0.497	0.653	—
			Second premolar	0.563	0.041	0.119	0.483	0.644	—
			First molar	0.605	0.040	0.010	0.526	0.684	10.885
			Second molar	0.620	0.038	0.003	0.545	0.695	10.275
	Left	Buccolingual	Central	0.617	0.039	0.003	0.540	0.695	6.175
			Lateral	0.610	0.039	0.006	0.534	0.686	6.575
			Canine	0.683	0.041	<0.0005	0.604	0.763	7.765
			First premolar	0.673	0.039	<0.0005	0.596	0.749	8.275
			Second premolar	0.606	0.043	0.008	0.522	0.689	9.025
			First molar	0.571	0.042	0.077	0.489	0.652	—

Table 3: Continued.

Jaw	Side	Dimension	Tooth	Area	SE	P	95% CI		Cut-off (mm)
			Second molar	0.603	0.040	0.010	0.526	0.681	10.610
			Central	0.553	0.038	0.183	0.478	0.628	—
			Lateral	0.547	0.042	0.238	0.465	0.629	—
			Canine	0.668	0.041	<0.0005	0.589	0.748	6.960
		Mesiodistal	First premolar	0.585	0.038	0.033	0.511	0.658	6.965
			Second premolar	0.554	0.041	0.172	0.473	0.635	—
			First molar	0.598	0.039	0.014	0.522	0.673	10.910
			Second molar	0.631	0.037	0.001	0.559	0.703	10.275

SE: standard error; CI: confidence interval for the AUC. Measurements below the cut-off points belong to women.

Cronbach alpha values between 0.8 and 0.9, four remaining Cronbach alpha values between 0.75 and 0.8, and one last Cronbach alpha = 0.664, all P values < 0.0005).

2.2. Statistical Analyses. Statistical analysis was performed using SPSS 25 (IBM, Armonk, NY, USA). Descriptive statistics and 95% confidence intervals (CIs) were calculated. Since age might affect some crown dimensions [35], the ages of males and females were compared using an unpaired t -test. Crown dimensions were compared between men and women, using an unpaired t-test. A receiver operating characteristic (ROC) curve was used to estimate the areas under the curve (AUC) and cut-off points for the identification of individuals' sex based on dental measurements. A partial correlation coefficient, controlling for the variable sex, was used to assess correlations between age and crown measurements as well as correlations among dental measurements. In all of these analyses, the analyses for the right and left sides were conducted separately.

2.2.1. Associations between Metric Traits with the Angle Classification and Crowding. The averages were calculated for measurements on the left and right sides. Associations between these average buccolingual or average mesiodistal dimensions with the skeletal Angle classes, crowding, and microdontia were assessed using an independent-sample t -test as well as a one-way analysis of variance (ANOVA) followed by a Tukey post hoc test.

2.2.2. Bolton Anterior, Posterior, and Overall Ratios. An unpaired t-test and a one-way ANOVA followed by a Tukey test were used to compare the Bolton ratios between males and females and among the Angle classes, respectively. The effects of sex and the Angle classes on Bolton ratios were assessed using a multiple linear regression. Correlations between age and Bolton ratios were assessed using a Pearson correlation coefficient. The Bolton ratios were compared with the original ratios reported by Bolton [10] using an unpaired t-test. The level of significance was set at 0.05.

3. Results

There were 74 males and 257 females included in the study. The mean (SD) age of patients was 19.21 ± 4.87 years (range: 12–35). Mean ages of men and women were 18.29 ± 20.49 and 18.55 ± 19.76 years, respectively. The sexes were balanced in terms of age (t-test, $P = 0.716$). Of the patients, 182 (55.7%), 127 (38.8%), and 18 (5.5%) were classes I, II, and III, respectively (the Angle classifications of four patients were not entered). Crowding was observed in 89 out of 331 cases (26.9%).

Numerous teeth had sex dimorphism in terms of buccolingual or mesiodistal measurements (t-test, P values ≤ 0.05, Tables 1 and 2). The few measurements without sex dimorphism in the maxilla were as follows: mesiodistal dimensions of the lateral and both premolars on the right and the lateral and first premolars on the left. In the mandible, the sizes without sex dimorphism were as follows: the buccolingual widths of the central, lateral, and second premolars on the right, and the left lateral, as well as the mesiodistal measurements of the right central and premolars, and the left incisors and second premolar.

The t-test did not show any significant differences between the left versus right sides in any of the teeth of either the maxilla or the mandible (all P values > 0.05).

The statistically significant areas under the ROC curves indicated that numerous teeth can be used for sex determination (Figure 1, Table 3) although AUCs were not considerably large in many of the statistically significant measurements. In each measurement of each quadrant, the canine had the greatest area under the curve among all other teeth. The highest AUC belonged to the mesiodistal dimension of the mandibular canine. The measurements with AUCs ≥ 64% were as follows: the buccolingual size of the right and left maxillary canines and the buccolingual size of the right and left mandibular canines and the right and left mandibular first premolars, as well as the mesiodistal dimension of the right and left mandibular canines (Figures 1 and 2, Table 3). The cut-off points for determining the sex based on the buccolingual and mesiodistal measurements of the maxillary and mandibular permanent teeth are presented in Table 3.

Controlling for the role of sex, age was negatively and weakly correlated with buccolingual widths of the right maxillary first premolar ($r = -0.119$, $P = 0.045$, partial correlation coefficient) and second premolar ($r = -0.121$, $P = 0.040$, Figure 3(a)), the left maxillary first premolar ($r = -0.131$, $P = 0.025$) and second premolar ($r = -0.145$, $P = 0.013$, Figure 3(b)), the right mandibular second premolar ($r = -0.138$, $P = 0.017$) and first molar ($r = -0.155$, $P = 0.007$,

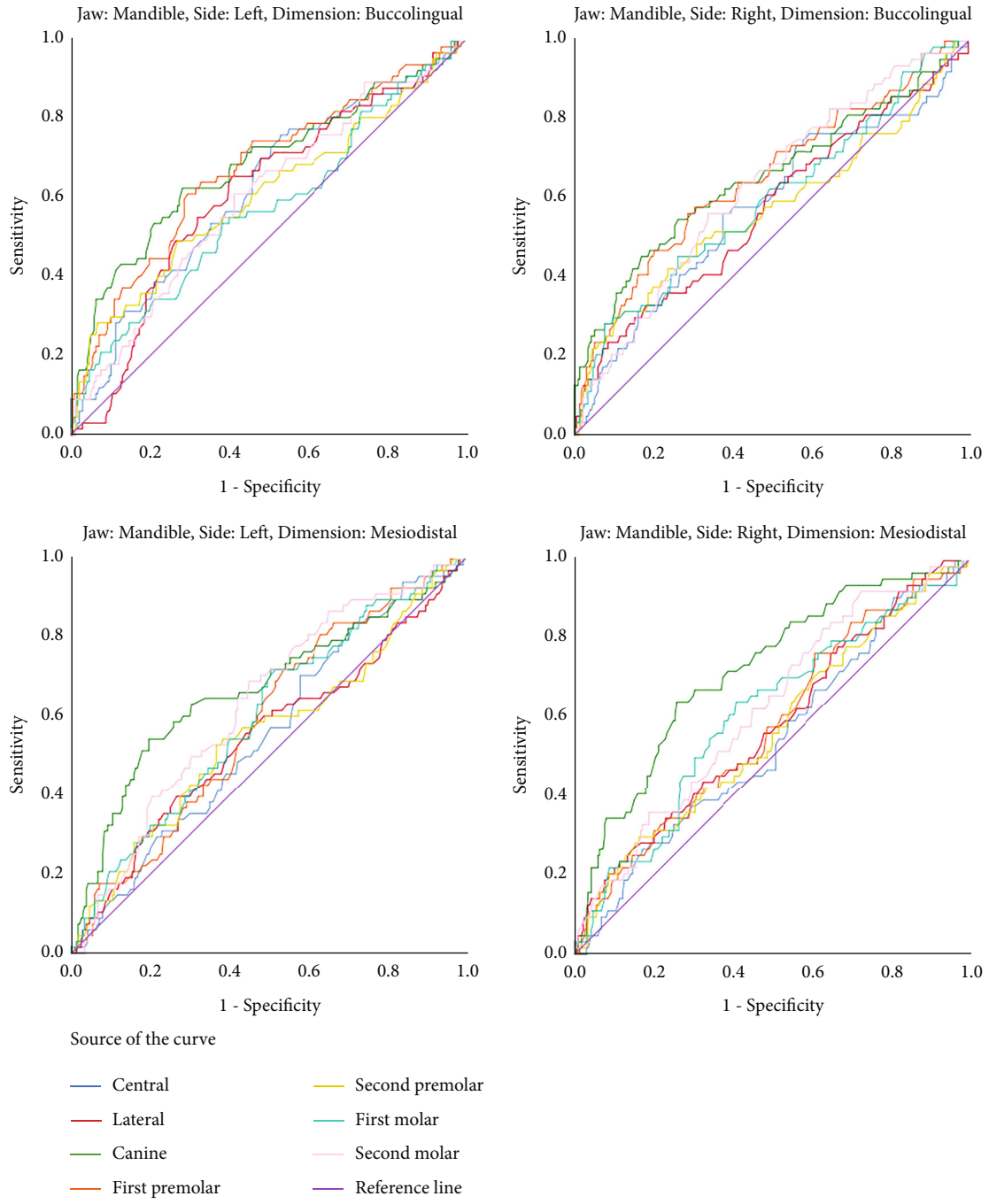

Figure 2: ROC curves of all the assessed mesiodistal and buccolingual dimensions of all the teeth in the left and right sides of the mandible.

Figure 3(c)), and the left mandibular second premolar ($r = -0.131$, $P = 0.023$) and first molar ($r = -0.135$, $P = 0.019$, Figure 3(d), Appendix 1).

Age was also correlated negatively, significantly, and weakly with mesiodistal dimensions of the right maxillary first premolar ($r = -0.124$, $P = 0.034$) and first molar ($r = -0.185$, $P = 0.002$, Figure 4(a)); the left maxillary central ($r = -0.159$, $P = 0.006$), canine ($r = -0.129$, $P = 0.027$), first premolar ($r = -0.133$, $P = 0.023$), and first molar ($r = -0.134$, $P = 0.022$, Figure 4(b)); the right mandibular lateral ($r = -0.177$, $P = 0.002$), first premolar ($r = -0.149$, $P = 0.010$); and first molar ($r = -0.159$, $P = 0.006$, Figure 4(c)); and the left mandibular central ($r = -0.163$, $P = 0.004$), lateral ($r = -0.131$, $P = 0.022$), and first premolar ($r = -0.175$, $P = 0.002$, Figure 4(d), Appendix 1).

3.1. Associations between Metric Traits with the Angle Classification. According to the ANOVA, the teeth that had different sizes in different classes were the maxillary lateral (buccolingual measurement only) and the mandibular central and lateral (buccolingual only, Table 4). According to the Tukey post hoc test, the buccolingual dimension of maxillary

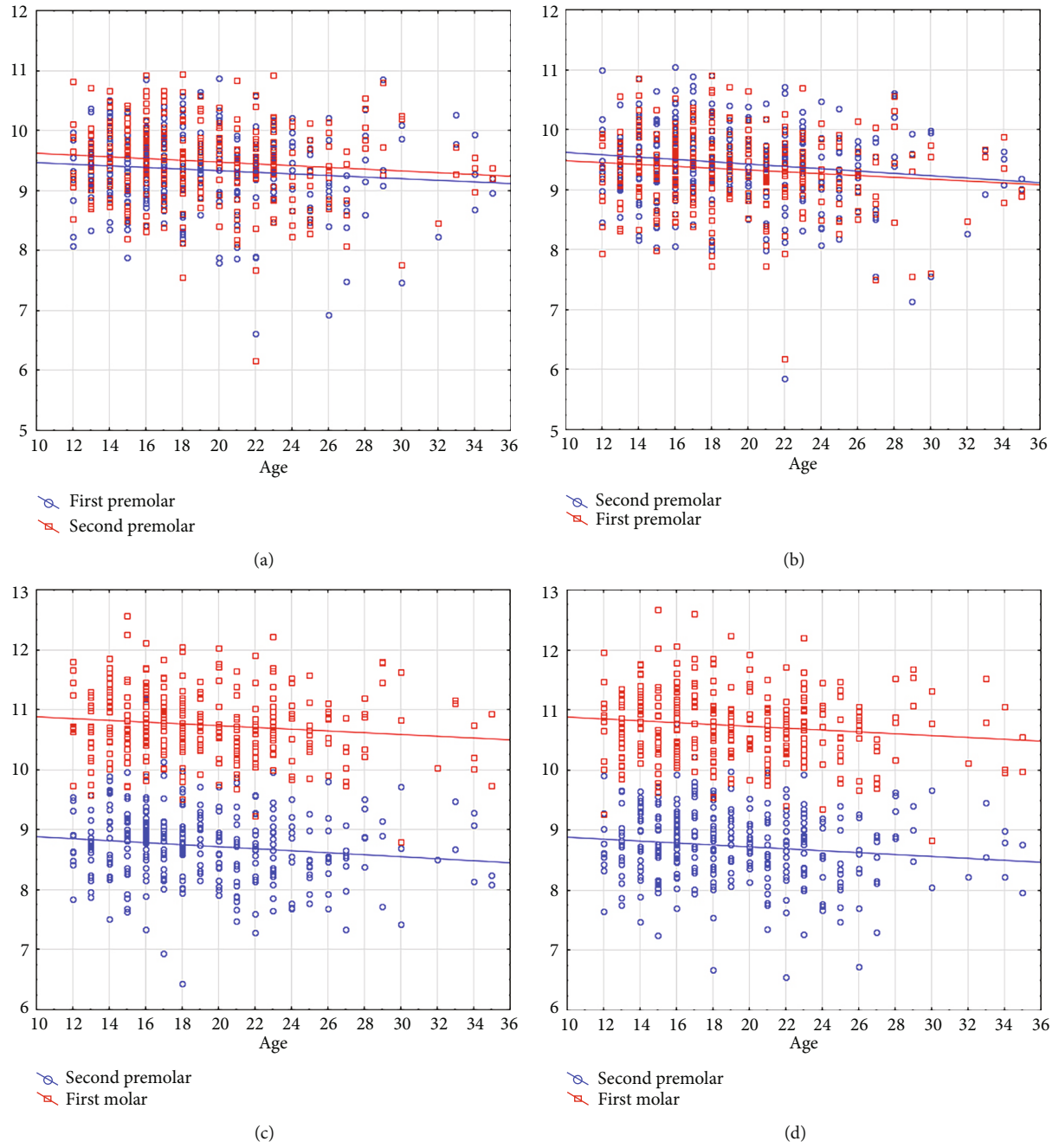

FIGURE 3: Scatterplots showing the significant correlations between age (the X axis, year) and the buccolingual widths (the Y axis, mm), in (a) the right maxillary teeth, (b) the left maxillary teeth, (c) the right mandibular teeth, and (d) the left mandibular teeth.

lateral differed only between classes I and II ($P = 0.030$). Similarly, the buccolingual width of the mandibular central differed only between classes I and II ($P = 0.032$). The buccolingual diameter of the mandibular lateral differed between classes I and II ($P = 0.025$, Table 4).

All dental measurements were similar between cases with and without crowding (t-test, $P > 0.05$, Table 5).

All "left/right-averaged" buccolingual and mesiodistal measurements of all the 14 teeth (the maxillary and mandibular centrals to the second molars, regardless of their right and left sides) differed significantly between the cases with microdontia versus those without it (t-test, $P \leq 0.002$, Table 6).

There were significant positive correlations among all different crown measurements of all the assessed teeth (Appendix 1).

3.2. Bolton Indices. Between men and women, there was no significant difference in terms of Bolton ratios (t-test, Table 7). There was no significant difference among different Angle classes in terms of the overall or anterior Bolton ratios (Table 7).

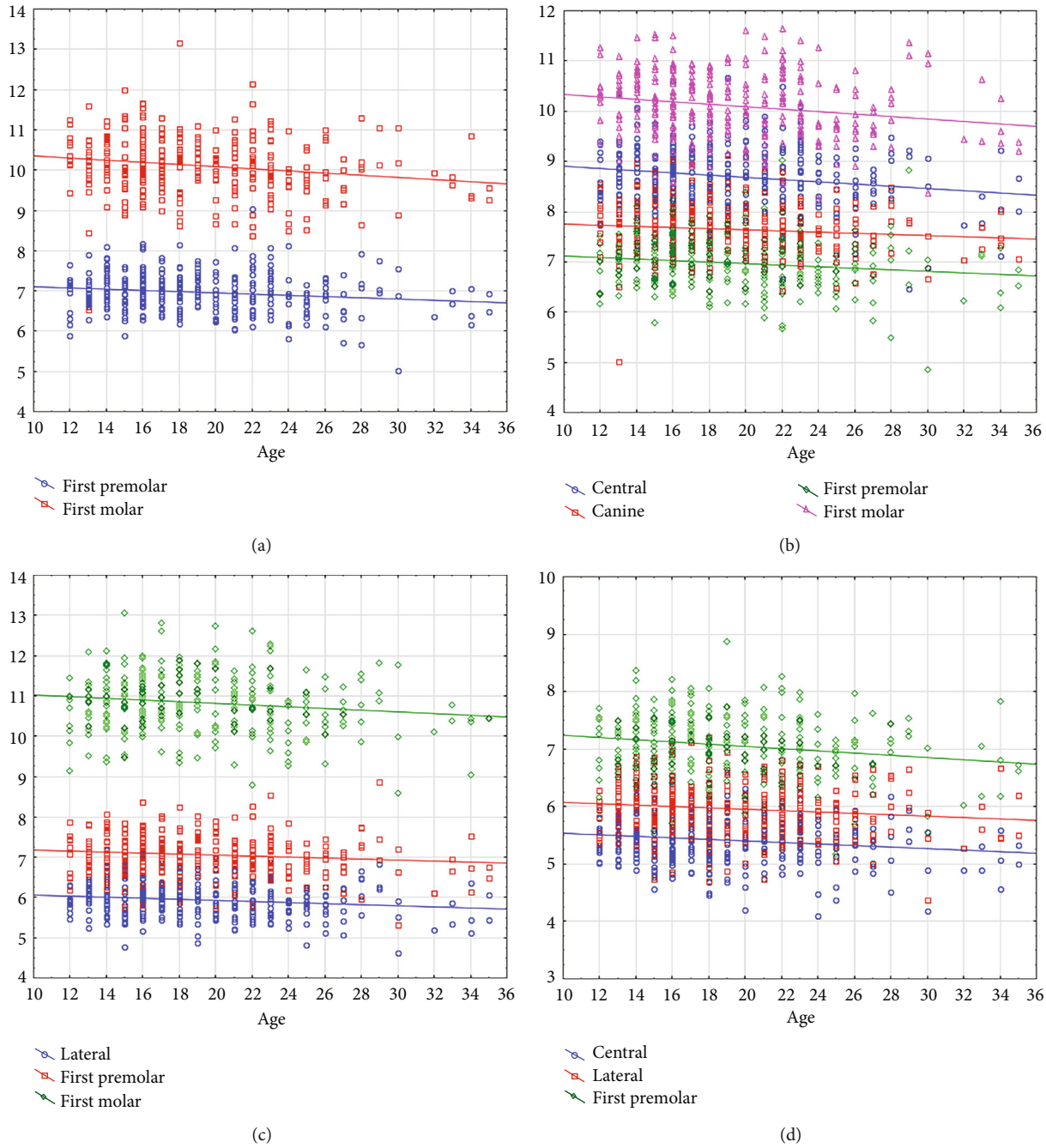

FIGURE 4: Scatterplots illustrating the significant correlations between age (the X axis, year) and the mesiodistal widths (the Y axis, mm), in (a) the right maxillary teeth, (b) the left maxillary teeth, (c) the right mandibular teeth, and (d) the left mandibular teeth.

However, the posterior Bolton ratios differed significantly across the Angle classes (ANOVA, Table 7). The Tukey test showed that the mean posterior Bolton ratio in class II patients was smaller than those in both class I ($P = 0.029$) and class III patients ($P = 0.045$). There was no significant difference between classes I and III ($P = 0.369$, Tukey). The multiple regression did not detect any significant effect of sex ($P \geq 0.080$) or the Angle classification ($P \geq 0.304$) on any Bolton ratios.

There was no correlation between ages with any Bolton ratios (Pearson $R \leq 0.064$, $P \geq 0.297$). The correlations between the overall Bolton index with the anterior Bolton index (Pearson $R = 0.696$, $P < 0.00000005$) and the posterior Bolton index ($R = 0.740$, $P < 0.00000005$) were significant. However, the was no significant correlation between the anterior and posterior Bolton ratios ($R = 0.045$, $P = 0.459$).

The unpaired t-test was used to compare the sexes within each Angle class separately (Table 8). Because of the small number of class III males, no comparisons were done for class III cases. As the only significant comparison, the anterior Bolton ratio of class II men was significantly larger than that of class II women ($P = 0.014$, Table 8).

Table 4: Descriptive statistics and 95% CIs for dental measurements (averages of the right and left sides, mm) in different Angle classes. The classes are compared using the one-way ANOVA.

Jaw	Measurement	Tooth	Class	*N*	Mean	SD	95% CI		Min	Max	*P*
Maxilla	Buccolingual	1	I	182	7.355	0.540	7.28	7.43	5.91	8.68	0.271
			II	127	7.440	0.623	7.33	7.55	5.88	9.04	
			III	18	7.528	0.539	7.26	7.80	6.47	8.45	
		2	I	177	6.516	0.617	6.42	6.61	4.47	8.29	0.039
			II	127	6.706	0.683	6.59	6.83	5.06	10.13	
			III	17	6.635	0.576	6.34	6.93	5.84	7.66	
		3	I	179	8.193	0.657	8.10	8.29	6.24	9.62	0.205
			II	125	8.329	0.689	8.21	8.45	6.18	9.87	
			III	18	8.206	0.571	7.92	8.49	7.10	9.37	
		4	I	177	9.309	0.588	9.22	9.40	6.41	10.74	0.454
			II	125	9.397	0.646	9.28	9.51	7.50	10.69	
			III	17	9.381	0.539	9.10	9.66	8.21	10.12	
		5	I	181	9.425	0.652	9.33	9.52	6.01	10.91	0.360
			II	126	9.522	0.615	9.41	9.63	7.66	10.99	
			III	18	9.549	0.557	9.27	9.83	8.19	10.41	
		6	I	181	11.386	0.575	11.30	11.47	9.73	12.80	0.797
			II	127	11.431	0.657	11.32	11.55	9.81	13.17	
			III	18	11.440	0.689	11.10	11.78	9.96	12.78	
		7	I	178	11.336	0.752	11.23	11.45	8.98	13.04	0.651
			II	125	11.404	0.801	11.26	11.55	9.34	13.32	
			III	18	11.263	0.743	10.89	11.63	9.78	12.80	
	Mesiodistal	1	I	182	8.694	0.545	8.61	8.77	6.64	10.06	0.842
			II	127	8.656	0.580	8.55	8.76	6.84	10.47	
			III	18	8.664	0.673	8.33	9.00	7.14	9.85	
		2	I	177	6.790	0.620	6.70	6.88	3.90	8.10	0.846
			II	127	6.749	0.662	6.63	6.87	4.42	8.04	
			III	17	6.741	0.676	6.39	7.09	5.29	7.70	
		3	I	180	7.697	0.501	7.62	7.77	5.57	9.14	0.558
			II	126	7.689	0.427	7.61	7.76	6.84	8.84	
			III	18	7.572	0.386	7.38	7.76	6.78	8.10	
		4	I	177	6.984	0.488	6.91	7.06	5.58	9.03	0.849
			II	125	6.956	0.491	6.87	7.04	4.94	8.29	
			III	17	7.006	0.385	6.81	7.20	6.38	7.81	
		5	I	181	6.675	0.526	6.60	6.75	5.61	8.96	0.851
			II	126	6.673	0.484	6.59	6.76	4.97	8.09	
			III	18	6.745	0.547	6.47	7.02	5.25	7.52	
		6	I	181	10.080	0.598	9.99	10.17	8.46	11.89	0.161
			II	127	10.185	0.668	10.07	10.30	8.63	11.76	
			III	18	9.932	0.656	9.61	10.26	9.16	11.12	
		7	I	178	9.848	0.592	9.76	9.94	8.26	11.48	0.159
			II	125	9.937	0.631	9.83	10.05	8.23	11.62	
			III	18	9.666	0.688	9.32	10.01	8.77	10.98	

Table 4: Continued.

Jaw	Measurement	Tooth	Class	*N*	Mean	SD	95% CI		Min	Max	*P*
	Buccolingual	1	I	182	6.209	0.457	6.14	6.28	4.78	7.55	0.042
			II	125	6.348	0.491	6.26	6.43	5.20	7.82	
			III	18	6.273	0.477	6.04	6.51	5.25	7.01	
		2	I	182	6.481	0.476	6.41	6.55	5.17	7.66	0.009
			II	127	6.628	0.502	6.54	6.72	5.38	7.97	
			III	18	6.346	0.483	6.11	6.59	5.64	7.23	
		3	I	182	7.442	0.626	7.35	7.53	5.89	8.92	0.235
			II	127	7.565	0.621	7.46	7.67	6.07	9.43	
			III	18	7.480	0.638	7.16	7.80	6.42	8.75	
		4	I	178	8.002	0.572	7.92	8.09	6.11	9.59	0.484
			II	127	8.083	0.603	7.98	8.19	6.11	9.71	
			III	18	8.015	0.558	7.74	8.29	7.05	8.94	
		5	I	180	8.729	0.569	8.65	8.81	6.56	9.95	0.766
			II	124	8.747	0.596	8.64	8.85	6.56	10.18	
			III	18	8.642	0.465	8.41	8.87	7.52	9.29	
		6	I	182	10.734	0.526	10.66	10.81	9.32	12.09	0.908
			II	126	10.752	0.580	10.65	10.85	8.82	12.62	
			III	18	10.787	0.532	10.52	11.05	9.86	11.85	
		7	I	181	10.560	0.616	10.47	10.65	9.26	12.04	0.934
			II	125	10.546	0.612	10.44	10.65	8.56	12.04	
			III	18	10.600	0.546	10.33	10.87	9.56	11.62	
Mandible	Mesiodistal	1	I	182	5.391	0.393	5.33	5.45	4.12	6.41	0.814
			II	127	5.408	0.412	5.34	5.48	4.24	6.45	
			III	18	5.449	0.423	5.24	5.66	4.46	6.00	
		2	I	182	5.962	0.407	5.90	6.02	4.97	7.22	0.554
			II	127	5.959	0.434	5.88	6.04	4.50	7.11	
			III	18	5.850	0.441	5.63	6.07	4.94	6.51	
		3	I	182	6.715	0.426	6.65	6.78	5.48	8.00	0.527
			II	127	6.661	0.481	6.58	6.75	5.39	7.85	
			III	18	6.649	0.394	6.45	6.84	5.80	7.37	
		4	I	178	7.081	0.462	7.01	7.15	5.98	8.30	0.711
			II	127	7.035	0.494	6.95	7.12	5.44	8.26	
			III	18	7.051	0.559	6.77	7.33	5.72	7.57	
		5	I	181	7.127	0.498	7.05	7.20	6.06	8.79	0.656
			II	124	7.090	0.539	6.99	7.19	5.86	8.67	
			III	18	7.199	0.568	6.92	7.48	6.00	8.46	
		6	I	182	10.853	0.676	10.75	10.95	8.95	12.65	0.255
			II	126	10.769	0.723	10.64	10.90	8.17	12.99	
			III	18	11.031	0.514	10.77	11.29	10.14	11.84	
		7	I	181	10.317	0.595	10.23	10.40	8.96	12.01	0.648
			II	125	10.253	0.692	10.13	10.38	8.52	12.31	
			III	18	10.346	0.628	10.03	10.66	9.48	11.78	

Tooth numbers 1 to 7 indicate the central to the second molar teeth. SD: standard deviation; CI: confidence interval; Min: minimum; Max: maximum.

Table 5: Descriptive statistics and 95% CIs for dental measurements (averages of the right and left sides, mm) in crowded versus noncrowded dentitions. The groups are compared using the *t*-test.

Jaw	Measurement	Tooth	Crowding	*N*	Mean	SD	95% CI		Min	Max	*P*
Maxilla	Buccolingual	1	No	242	7.411	0.606	7.33	7.49	5.88	9.04	0.443
			Yes	89	7.356	0.480	7.26	7.46	5.93	8.17	
			Total	331	7.396	0.575	7.33	7.46	5.88	9.04	
		2	No	237	6.622	0.682	6.53	6.71	4.47	10.13	0.191
			Yes	88	6.515	0.569	6.39	6.64	5.27	7.60	
			Total	325	6.593	0.654	6.52	6.66	4.47	10.13	
		3	No	239	8.257	0.660	8.17	8.34	6.24	9.87	0.670
			Yes	87	8.221	0.680	8.08	8.37	6.18	9.55	
			Total	326	8.248	0.664	8.18	8.32	6.18	9.87	
		4	No	239	9.349	0.617	9.27	9.43	6.41	10.74	0.805
			Yes	84	9.330	0.592	9.20	9.46	8.01	10.44	
			Total	323	9.344	0.610	9.28	9.41	6.41	10.74	
		5	No	241	9.454	0.636	9.37	9.53	6.01	10.99	0.512
			Yes	88	9.506	0.627	9.37	9.64	7.90	10.91	
			Total	329	9.468	0.633	9.40	9.54	6.01	10.99	
		6	No	241	11.403	0.611	11.33	11.48	9.73	13.17	0.999
			Yes	89	11.403	0.632	11.27	11.54	9.81	12.76	
			Total	330	11.403	0.616	11.34	11.47	9.73	13.17	
		7	No	236	11.361	0.783	11.26	11.46	8.98	13.32	0.918
			Yes	88	11.351	0.737	11.19	11.51	9.34	13.04	
			Total	324	11.358	0.770	11.27	11.44	8.98	13.32	
	Mesiodistal	1	No	242	8.687	0.602	8.61	8.76	6.64	10.47	0.771
			Yes	89	8.667	0.466	8.57	8.76	7.47	10.13	
			Total	331	8.682	0.568	8.62	8.74	6.64	10.47	
		2	No	237	6.781	0.653	6.70	6.86	3.90	8.07	0.726
			Yes	88	6.753	0.602	6.63	6.88	4.75	8.10	
			Total	325	6.773	0.639	6.70	6.84	3.90	8.10	
		3	No	239	7.701	0.446	7.64	7.76	6.78	9.14	0.375
			Yes	89	7.649	0.521	7.54	7.76	5.57	8.84	
			Total	328	7.687	0.467	7.64	7.74	5.57	9.14	
		4	No	239	6.977	0.480	6.92	7.04	4.94	9.03	0.870
			Yes	84	6.967	0.497	6.86	7.07	5.58	8.08	
			Total	323	6.974	0.484	6.92	7.03	4.94	9.03	
		5	No	241	6.670	0.507	6.61	6.73	4.97	8.96	0.660
			Yes	88	6.698	0.514	6.59	6.81	5.19	8.57	
			Total	329	6.677	0.508	6.62	6.73	4.97	8.96	
		6	No	241	10.090	0.607	10.01	10.17	8.46	11.70	0.424
			Yes	89	10.152	0.694	10.01	10.30	8.47	11.89	
			Total	330	10.106	0.631	10.04	10.17	8.46	11.89	
		7	No	236	9.857	0.595	9.78	9.93	8.26	11.59	0.405
			Yes	88	9.921	0.668	9.78	10.06	8.23	11.62	
			Total	324	9.874	0.616	9.81	9.94	8.23	11.62	

Table 5: Continued.

Jaw	Measurement	Tooth	Crowding	*N*	Mean	SD	95% CI		Min	Max	*P*
	Buccolingual	1	No	241	6.279	0.507	6.21	6.34	4.78	7.82	0.295
			Yes	88	6.216	0.401	6.13	6.30	5.19	7.04	
			Total	329	6.262	0.481	6.21	6.31	4.78	7.82	
		2	No	242	6.559	0.512	6.49	6.62	5.17	7.97	0.052
			Yes	89	6.440	0.439	6.35	6.53	5.46	7.33	
			Total	331	6.527	0.496	6.47	6.58	5.17	7.97	
		3	No	242	7.499	0.632	7.42	7.58	5.89	9.43	0.754
			Yes	89	7.475	0.605	7.35	7.60	6.07	8.65	
			Total	331	7.492	0.624	7.42	7.56	5.89	9.43	
		4	No	241	8.025	0.564	7.95	8.10	6.11	9.32	0.696
			Yes	86	8.054	0.635	7.92	8.19	6.63	9.71	
			Total	327	8.033	0.583	7.97	8.10	6.11	9.71	
		5	No	239	8.730	0.577	8.66	8.80	6.56	9.95	0.955
			Yes	87	8.726	0.574	8.60	8.85	7.33	10.18	
			Total	326	8.729	0.575	8.67	8.79	6.56	10.18	
		6	No	242	10.767	0.551	10.70	10.84	8.82	12.62	0.220
			Yes	88	10.683	0.539	10.57	10.80	9.32	11.88	
			Total	330	10.745	0.548	10.69	10.80	8.82	12.62	
		7	No	238	10.565	0.625	10.48	10.64	8.56	12.04	0.824
			Yes	89	10.548	0.578	10.43	10.67	9.26	11.75	
			Total	327	10.560	0.612	10.49	10.63	8.56	12.04	
Mandible	Mesiodistal	1	No	242	5.412	0.405	5.36	5.46	4.12	6.45	0.510
			Yes	89	5.379	0.393	5.30	5.46	4.47	6.27	
			Total	331	5.403	0.402	5.36	5.45	4.12	6.45	
		2	No	242	5.969	0.414	5.92	6.02	4.50	7.22	0.387
			Yes	89	5.924	0.430	5.83	6.01	4.75	6.98	
			Total	331	5.957	0.418	5.91	6.00	4.50	7.22	
		3	No	242	6.695	0.442	6.64	6.75	5.39	7.98	0.785
			Yes	89	6.680	0.464	6.58	6.78	5.45	8.00	
			Total	331	6.691	0.447	6.64	6.74	5.39	8.00	
		4	No	241	7.067	0.462	7.01	7.13	5.44	8.30	0.703
			Yes	86	7.044	0.526	6.93	7.16	5.67	8.26	
			Total	327	7.061	0.479	7.01	7.11	5.44	8.30	
		5	No	239	7.121	0.522	7.05	7.19	5.86	8.79	0.984
			Yes	88	7.120	0.523	7.01	7.23	6.09	8.62	
			Total	327	7.121	0.521	7.06	7.18	5.86	8.79	
		6	No	242	10.848	0.673	10.76	10.93	8.78	12.99	0.515
			Yes	88	10.792	0.733	10.64	10.95	8.17	12.65	
			Total	330	10.833	0.689	10.76	10.91	8.17	12.99	
		7	No	238	10.278	0.640	10.20	10.36	8.52	12.31	0.397
			Yes	89	10.345	0.625	10.21	10.48	8.95	11.84	
			Total	327	10.297	0.635	10.23	10.37	8.52	12.31	

Tooth numbers 1 to 7 indicate the central to the second molar teeth. SD: standard deviation; CI: confidence interval; Min: minimum; Max: maximum.

Table 6: Descriptive statistics and 95% CIs for dental sizes (averages of the right and left sides, mm) in cases with and without microdontia. The groups are compared using the *t*-test.

Jaw	Measurement	Tooth	Microdontia	*N*	Mean	SD	95% CI		Min	Max	*P*
Maxilla	Buccolingual	1	No	203	7.489	0.550	7.41	7.56	5.91	9.04	<0.0005
			Yes	128	7.250	0.584	7.15	7.35	5.88	8.52	
			Total	331	7.396	0.575	7.33	7.46	5.88	9.04	
		2	No	199	6.681	0.650	6.59	6.77	4.51	10.13	0.002
			Yes	126	6.454	0.639	6.34	6.57	4.47	8.19	
			Total	325	6.593	0.654	6.52	6.66	4.47	10.13	
		3	No	200	8.370	0.659	8.28	8.46	6.18	9.87	<0.0005
			Yes	126	8.054	0.628	7.94	8.16	6.24	9.54	
			Total	326	8.248	0.664	8.18	8.32	6.18	9.87	
		4	No	196	9.483	0.525	9.41	9.56	8.01	10.74	<0.0005
			Yes	127	9.129	0.668	9.01	9.25	6.41	10.68	
			Total	323	9.344	0.610	9.28	9.41	6.41	10.74	
		5	No	202	9.663	0.508	9.59	9.73	8.36	10.99	<0.0005
			Yes	127	9.156	0.689	9.04	9.28	6.01	10.78	
			Total	329	9.468	0.633	9.40	9.54	6.01	10.99	
		6	No	202	11.584	0.558	11.51	11.66	10.11	13.17	<0.0005
			Yes	128	11.117	0.595	11.01	11.22	9.73	12.47	
			Total	330	11.403	0.616	11.34	11.47	9.73	13.17	
		7	No	197	11.609	0.678	11.51	11.70	9.54	13.32	<0.0005
			Yes	127	10.969	0.743	10.84	11.10	8.98	12.89	
			Total	324	11.358	0.770	11.27	11.44	8.98	13.32	
	Mesiodistal	1	No	203	8.834	0.514	8.76	8.91	7.63	10.47	<0.0005
			Yes	128	8.440	0.567	8.34	8.54	6.64	10.33	
			Total	331	8.682	0.568	8.62	8.74	6.64	10.47	
		2	No	199	6.977	0.513	6.91	7.05	4.74	8.10	<0.0005
			Yes	126	6.451	0.685	6.33	6.57	3.90	7.70	
			Total	325	6.773	0.639	6.70	6.84	3.90	8.10	
		3	No	201	7.826	0.444	7.76	7.89	6.84	9.14	<0.0005
			Yes	127	7.467	0.416	7.39	7.54	5.57	8.47	
			Total	328	7.687	0.467	7.64	7.74	5.57	9.14	
		4	No	196	7.107	0.430	7.05	7.17	5.58	8.29	<0.0005
			Yes	127	6.770	0.492	6.68	6.86	4.94	9.03	
			Total	323	6.974	0.484	6.92	7.03	4.94	9.03	
		5	No	202	6.817	0.469	6.75	6.88	5.70	8.57	<0.0005
			Yes	127	6.455	0.490	6.37	6.54	4.97	8.96	
			Total	329	6.677	0.508	6.62	6.73	4.97	8.96	
		6	No	202	10.318	0.588	10.24	10.40	8.74	11.89	<0.0005
			Yes	128	9.773	0.549	9.68	9.87	8.46	11.12	
			Total	330	10.106	0.631	10.04	10.17	8.46	11.89	
		7	No	197	10.100	0.568	10.02	10.18	8.59	11.62	<0.0005
			Yes	127	9.524	0.517	9.43	9.61	8.23	11.05	
			Total	324	9.874	0.616	9.81	9.94	8.23	11.62	

Table 6: Continued.

Jaw	Measurement	Tooth	Microdontia	*N*	Mean	SD	95% CI		Min	Max	*P*
	Buccolingual	1	No	201	6.329	0.470	6.26	6.39	4.78	7.82	0.001
			Yes	128	6.157	0.481	6.07	6.24	4.83	7.37	
			Total	329	6.262	0.481	6.21	6.31	4.78	7.82	
		2	No	203	6.598	0.472	6.53	6.66	5.21	7.97	0.001
			Yes	128	6.414	0.513	6.32	6.50	5.17	7.53	
			Total	331	6.527	0.496	6.47	6.58	5.17	7.97	
		3	No	203	7.595	0.650	7.51	7.69	5.89	9.43	<0.0005
			Yes	128	7.329	0.543	7.23	7.42	5.91	8.71	
			Total	331	7.492	0.624	7.42	7.56	5.89	9.43	
		4	No	200	8.169	0.535	8.09	8.24	6.97	9.59	<0.0005
			Yes	127	7.818	0.592	7.71	7.92	6.11	9.71	
			Total	327	8.033	0.583	7.97	8.10	6.11	9.71	
		5	No	198	8.891	0.510	8.82	8.96	7.33	9.95	<0.0005
			Yes	128	8.479	0.581	8.38	8.58	6.56	10.18	
			Total	326	8.729	0.575	8.67	8.79	6.56	10.18	
		6	No	202	10.914	0.501	10.84	10.98	9.82	12.62	<0.0005
			Yes	128	10.477	0.515	10.39	10.57	8.82	11.60	
			Total	330	10.745	0.548	10.69	10.80	8.82	12.62	
		7	No	199	10.732	0.541	10.66	10.81	9.31	12.04	<0.0005
			Yes	128	10.292	0.621	10.18	10.40	8.56	11.88	
			Total	327	10.560	0.612	10.49	10.63	8.56	12.04	
Mandible	Mesiodistal	1	No	203	5.495	0.377	5.44	5.55	4.51	6.45	<0.0005
			Yes	128	5.257	0.397	5.19	5.33	4.12	6.41	
			Total	331	5.403	0.402	5.36	5.45	4.12	6.45	
		2	No	203	6.054	0.387	6.00	6.11	5.18	7.11	<0.0005
			Yes	128	5.803	0.421	5.73	5.88	4.50	7.22	
			Total	331	5.957	0.418	5.91	6.00	4.50	7.22	
		3	No	203	6.811	0.424	6.75	6.87	5.74	7.98	<0.0005
			Yes	128	6.502	0.418	6.43	6.58	5.39	8.00	
			Total	331	6.691	0.447	6.64	6.74	5.39	8.00	
		4	No	200	7.207	0.430	7.15	7.27	6.06	8.30	<0.0005
			Yes	127	6.831	0.462	6.75	6.91	5.44	7.80	
			Total	327	7.061	0.479	7.01	7.11	5.44	8.30	
		5	No	199	7.286	0.500	7.22	7.36	6.19	8.79	<0.0005
			Yes	128	6.864	0.445	6.79	6.94	5.86	8.13	
			Total	327	7.121	0.521	7.06	7.18	5.86	8.79	
		6	No	202	11.066	0.606	10.98	11.15	9.41	12.99	<0.0005
			Yes	128	10.467	0.652	10.35	10.58	8.17	12.15	
			Total	330	10.833	0.689	10.76	10.91	8.17	12.99	
		7	No	199	10.508	0.567	10.43	10.59	9.18	12.31	<0.0005
			Yes	128	9.968	0.597	9.86	10.07	8.52	11.84	
			Total	327	10.297	0.635	10.23	10.37	8.52	12.31	

Tooth numbers 1 to 7 denote the central to the second molar teeth. SD: standard deviation; CI: confidence interval; Min: minimum; Max: maximum.

Table 7: The Bolton ratios in men, women, and different Angle classes.

Bolton ratio	Variables	*N*	Mean	SD	95% CI		Min	Max	*P*
Overall	Female	210	91.78	2.48	91.44	92.12	83.97	99.09	0.229
	Male	58	92.22	2.42	91.58	92.85	86.32	99.87	
	Total	268	91.87	2.47	91.58	92.17	83.97	99.87	
Anterior	Female	210	77.86	3.11	77.44	78.29	69.00	89.43	0.059
	Male	58	78.74	3.02	77.94	79.53	71.45	87.61	
	Total	268	78.05	3.11	77.68	78.43	69.00	89.43	
Posterior	Female	210	105.42	3.77	104.91	105.93	96.20	114.43	0.995
	Male	58	105.41	3.83	104.41	106.42	97.14	115.59	
	Total	268	105.42	3.77	104.96	105.87	96.20	115.59	
Overall	Class I	142	91.96	2.43	91.56	92.37	86.32	99.09	0.083
	Class II	110	91.55	2.41	91.10	92.01	83.97	99.87	
	Class III	13	93.03	2.50	91.52	94.54	88.94	97.73	
Anterior	Class I	142	77.90	2.98	77.41	78.40	71.45	86.06	0.667
	Class II	110	78.16	3.30	77.54	78.79	69.00	89.43	
	Class III	13	78.56	2.96	76.77	80.35	74.48	85.40	
Posterior	Class I	142	105.80	3.64	105.19	106.40	96.78	112.49	0.008
	Class II	110	104.60	3.69	103.90	105.30	96.20	115.59	
	Class III	13	107.19	4.16	104.67	109.70	100.42	112.31	

SD: standard deviation; CI: confidence interval; Min: minimum; Max: maximum. The *P* values for comparisons between men and women are calculated using the unpaired *t*-test. The *P* values for comparisons across Angle classes are calculated using the one-way ANOVA.

Table 8: The Bolton indices in men versus women within different Angle classes.

Angle classes	Bolton ratio	Sex	*N*	Mean	SD	95% CI		Min	Max	*P*
Class I	Overall	Female	115	91.91	2.48	91.45	92.37	86.40	99.09	0.586
		Male	27	92.19	2.22	91.32	93.07	86.32	95.72	
	Anterior	Female	115	77.89	2.97	77.34	78.44	72.16	86.06	0.909
		Male	27	77.96	3.09	76.74	79.18	71.45	86.02	
	Posterior	Female	115	105.69	3.72	105.00	106.38	96.78	112.37	0.472
		Male	27	106.25	3.28	104.96	107.55	99.47	112.49	
Class II	Overall	Female	82	91.35	2.35	90.83	91.86	83.97	97.67	0.121
		Male	28	92.17	2.53	91.19	93.15	87.72	99.87	
	Anterior	Female	82	77.72	3.33	76.99	78.45	69.00	89.43	0.014
		Male	28	79.48	2.92	78.35	80.61	74.52	87.61	
	Posterior	Female	82	104.64	3.60	103.85	105.43	96.20	114.43	0.841
		Male	28	104.48	4.01	102.92	106.03	97.14	115.59	
Class III	Overall	Female	11	93.46	2.48	91.79	95.13	88.94	97.73	—
		Male	2	90.69	0.57	—	—	90.28	91.09	
	Anterior	Female	11	78.72	3.15	76.60	80.83	74.48	85.40	—
		Male	2	77.68	2.09	—	—	76.20	79.15	
	Posterior	Female	11	107.94	4.09	105.20	110.69	100.42	112.31	—
		Male	2	103.03	0.46	—	—	102.71	103.36	

SD: standard deviation; CI: confidence interval; Min: minimum; Max: maximum. The *P* values are calculated using the unpaired *t*-test.

The comparison of the overall Bolton ratio of this sample (Table 7) with the original overall Bolton ratio (mean: 91.3, SD: 1.91, $n = 55$) [10] did not show a significant difference (unpaired t-test, $P = 0.107$). However, the anterior Bolton ratio of this sample was significantly greater (t-test, $P = 0.0498$, Table 7) than the original anterior Bolton ratio (mean: 77.2, SD: 1.65, $n = 55$) [10].

4. Discussion

Tooth size variation is influenced by environmental and genetic factors including race, sex, heredity, cellular changes, and bilateral asymmetry [4, 20, 36]. Environmental factors include nutrition, disease, and climate, which might affect the prenatal dental system and seem to make little change to the normal dental system [37]. The strong contribution of genetic factors to the differences in dental measurements has been shown, but the influence of environmental factors seems plausible as well. Both environmental and genetic factors play a role in the etiology of supernumerary teeth, hypodontia, megadontia, and microdontia [38]. Sizes of teeth might vary in different populations [1, 20, 39]. Sex dimorphism has been reported as ranging between 0.82% and 5.97% for all teeth [4]. An example of a sex difference is the tendency of men to have larger teeth than women, which reflects the relationship between the X chromosome and the Y chromosome. For example, men who are XXY and XYY have teeth larger than XY men [1]. Our results were in line with these suggestions.

Keiser and Julius examined mesiodistal and buccolingual tooth sizes and concluded that they could be used to determine sex [40]. Using the dental dimensions of one ethnic group might be used in other ethnicities as well [41]. One of the preferred methods is to use the canine index, which uses the mesiodistal size of the mandibular canine together with intercanine width [42–44]. But the most widely used method is the mesiodistal and buccolingual dimensions [13, 22, 23]. The mandibular canine seems to have the greatest sex dimorphism among all teeth while incisors might have the least sexual dimorphism [24–26]. A recent meta-analysis suggested that the canine might have the most sex dimorphism among all teeth, which might be due to the longer duration of amelogenesis of this tooth in men compared to women [4]. This is in agreement with our findings of the possibility of the use of mandibular canines in predicting gender. Some researchers have shown that when the mesiodistal size of the canine tooth is larger than 7.0 to 7.2 mm, there is a very high probability that the person is male [16, 24, 45], and this was in line with our results pertaining to the mandibular canine. Some authors have suggested that both the mesiodistal and buccolingual dimensions are needed together for sex determination [46]. In our study, many molar teeth could be used for sex identification. In earlier research, this tooth was sometimes useful, and in some studies, it was useful merely alongside other teeth for sex determination, indicating the role of ethnicity in sex dimorphism [47–51].

Our findings indicated that aging might reduce the mesiodistal and buccolingual dimensions of certain teeth. In archaeological studies, the pattern of increased wear appears to be age-dependent, while in modern populations, men are more prone to tooth wear than women [35]. Such wear might affect both epidemiological and clinical outcomes and should be taken into account in such examinations.

The Bolton ratios found in this study were within the range reported earlier [6, 7, 11, 33, 34]. In comparison to the original Bolton ratios, our sample's anterior Bolton ratio was larger. This should be considered when practicing on Iranian patients; still, it should be noted that such results are not definitive, and sometimes, even studies conducted within the same ethnicity and country yield different results [6, 11]. The Angle classes were not associated with the anterior and posterior Bolton ratios in this sample. This finding was similar to some previous studies [8, 52–54] but in contrast to some others [33, 55]. It was found, however, that the posterior Bolton ratio might be smaller in class II patients, compared to classes I and III. In terms of sex dimorphism in Bolton ratios, when our whole sample was assessed, no sexual dimorphism was observed in this study. This finding was in line with most previous studies as well as the conclusion of a recent meta-analysis on Bolton ratios [6, 7, 53–55]. However, when sex dimorphism was examined separately within each of the Angle classes I or II, it was found that in class II patients, the anterior Bolton ratio might be greater in men than in women. We observed a 70% positive correlation between the anterior and overall Bolton indices. This was greater than the studies of Bolton (50% correlation) [10] or White (-12% correlation) [56] but slightly smaller than a study on Sudanese people (79% correlation) [7]. The controversies might be attributable to real ethnic differences as well as methodological variations such as eligibility criteria or sample sizes. The concept of the posterior Bolton ratio is introduced and assessed in merely two studies [33, 34]. We observed a 74% correlation between the posterior and overall Bolton ratios and almost no correlation between the anterior and posterior Bolton ratios. More studies are needed on the posterior Bolton ratio.

This study was limited by some factors. The number of females was much greater than males, although both seemed to be adequate. Moreover, the sample size pertaining to the Bolton ratios of class III men was very small. Hence, we did not perform inferential statistics on this subgroup. The generalizability of some aspects of this research was limited to the target population (Iranian orthodontic patients).

5. Conclusions

Within the limitations of this study, the following key points can be summarized:

(1) Sex dimorphism existed in most dental measurements. ROC curve analyses indicated that (A) the mandibular teeth mostly seemed better than the maxillary ones for sex identification; (B) the most appropriate dental measurements for sex determination were the buccolingual dimension of the right and left maxillary canines, the buccolingual measurement of the right and left mandibular canines and the right and left mandibular first premolars,

as well as (C) the mesiodistal dimension of the right and left mandibular canines

(2) Cut-off points for sex identification based on proper dental measurements were calculated for 38 teeth. In the maxilla, the buccolingual cut-off points ranged from 7.715 mm for the central to 11.715 mm for the first molar; the mesiodistal cut-offs ranged from 8.750 mm for the central to 10.815 mm for the first molar. In the mandible, the range of buccolingual cut-off points was 6.175 mm to 11.455 mm (the central to the first molar), while the range of mesiodistal cut-off points was 6.835 mm to 10.910 mm (the canine to the first molar).

(3) (A) Aging might slightly reduce the buccolingual crown dimension in a few posterior teeth: the right and left maxillary first premolar and second premolar and right and left mandibular second premolar and first molar. (B) It might also slightly reduce the mesiodistal widths of certain anterior and posterior teeth: the right maxillary first premolar and first molar, the left maxillary central, canine, first premolar, first molar, the right mandibular lateral, first premolar, and first molar, and the left mandibular central, lateral, and first premolar

(4) (A) The only measurements differing among the skeletal Angle classes were the buccolingual widths of the maxillary lateral, the mandibular central, and the mandibular lateral. These differed mainly between classes I and II. (B) Dental measurements might not differ between crowded and noncrowded dentitions. (C) All crown sizes might be smaller in microdontia cases compared to cases without this anomaly

(5) The anterior, posterior, and overall Bolton indices were 78.05, 105.42, and 91.87, respectively. The skeletal Angle classification might not be associated with the anterior and overall Bolton ratios. However, class II patients might have smaller posterior Bolton ratios compared to class I or III patients. Aging might not affect Bolton indices. In the whole sample, there was no sexual dimorphism in either of these indices. However, in class II patients, the anterior Bolton ratio was greater in men than in women. There were 69.6% and 74.0% correlations between the overall Bolton indexes with the anterior and posterior Bolton indices, respectively. The anterior and posterior Bolton indices might not be correlated. The overall Bolton ratio in this population might not differ much from the original overall Bolton ratio. Nonetheless, this population's anterior Bolton ratio might be greater than Bolton's original anterior ratio

Data Availability

The raw data are available from the authors upon reasonable request.

Ethical Approval

Protocol ethics were approved by the Research Committee of the University in accordance with the Helsinki Declaration.

Conflicts of Interest

The authors declare that they have no conflict of interest.

Authors' Contributions

Negin Ashoori collected the data and wrote the thesis. Fataneh Ghorbanyjavadpour collected the data and mentored the thesis. Vahid Rakhshan conceived the study and all the ideas and hypotheses, designed the study, validated the data and fully analyzed it, mentored the thesis, interpreted the findings, drafted and revised the manuscript, and created the Tables/Appendix/Figures.

Supplementary Materials

Supplementary file: Appendix 1. Online supplementary spreadsheet showing partial correlation coefficients (controlling for the role of sex) across tooth sizes and between age and tooth sizes. *(Supplementary Materials)*

References

[1] V. Deepak, S. Goryawala, Y. Reddy, and R. Chhabra, "Assessment of ethnicity in Indian population using tooth crown metric dental traits," *Journal of International Oral Health: JIOH*, vol. 7, no. 9, pp. 83–87, 2015.

[2] R. Togoo, W. Alqahtani, E. Abdullah et al., "Comparison of mesiodistal tooth width in individuals from three ethnic groups in southern Saudi Arabia," *Nigerian Journal of Clinical Practice*, vol. 22, no. 4, p. 553, 2019.

[3] A. I. Shaweesh, "Mesiodistal and faciolingual diameters of the permanent teeth in a Jordanian population," *Archives of Oral Biology*, vol. 73, pp. 253–258, 2017.

[4] P. R. da Silva, M. C. Lopes, I. E. Martins-Filho, M. G. H. Biazevic, and E. Michel-Crosato, "Tooth crown mesiodistal measurements for the determination of sexual dimorphism across a range of populations: a systematic review and meta-analysis," *The Journal of Forensic Odonto-Stomatology*, vol. 37, no. 1, pp. 2–19, 2019.

[5] M. K. Agenter, E. F. Harris, and R. N. Blair, "Influence of tooth crown size on malocclusion," *American Journal of Orthodontics and Dentofacial Orthopedics*, vol. 136, pp. 795–804, 2009.

[6] V. Machado, J. Botelho, P. Mascarenhas, J. J. Mendes, and A. Delgado, "A systematic review and meta-analysis on Bolton's ratios: normal occlusion and malocclusion," *Journal of Orthodontics*, vol. 47, pp. 7–29, 2020.

[7] A. H. AaH, A.-H. M. Eldin, and H. A. Hashim, "Bolton tooth size ratio among Sudanese population sample: a preliminary study," *Journal of Orthodontic Science*, vol. 4, no. 3, pp. 77–82, 2015.

[8] D. R. Crosby and C. G. Alexander, "The occurrence of tooth size discrepancies among different malocclusion groups," *American Journal of Orthodontics and Dentofacial Orthopedics*, vol. 95, pp. 457–461, 1989.

[9] J. E. Freeman, A. J. Maskeroni, and L. Lorton, "Frequency of Bolton tooth-size discrepancies among orthodontic patients," *American Journal of Orthodontics and Dentofacial Orthopedics*, vol. 110, pp. 24–27, 1996.

[10] W. A. Bolton, "Disharmony in tooth size and its relation to the analysis and treatment of malocclusion," *The Angle Orthodontist*, vol. 28, pp. 113–130, 1958.

[11] M. Kachoei, M. H. Ahangar-Atashi, and S. Pourkhamneh, "Bolton's intermaxillary tooth size ratios among Iranian schoolchildren," *Medicina Oral, Patología Oral y Cirugía Bucal*, vol. 16, pp. e568–e572, 2011.

[12] T. Brown, B. Margetts, and G. Townsend, "Comparison of mesiodistal crown diameters of the deciduous and permanent teeth in Australian Aboriginals," *Australian Dental Journal*, vol. 25, pp. 28–33, 1980.

[13] C. F. Moorrees, S. Ø. Thomsen, E. Jensen, and P. K.-J. Yen, "Mesiodistal crown diameters of the deciduous and permanent teeth in individuals," *Journal of Dental Research*, vol. 36, pp. 39–47, 1957.

[14] T. Yonezu, J. J. Warren, S. E. Bishara, and K. L. Steinbock, "Comparison of tooth size and dental arch widths in contemporary Japanese and American preschool children," *World Journal of Orthodontics*, vol. 2, 2001.

[15] H.-I. Yoo, D.-W. Yang, M.-Y. Lee, M.-S. Kim, and S.-H. Kim, "Morphological analysis of the occlusal surface of maxillary molars in Koreans," *Archives of Oral Biology*, vol. 67, pp. 15–21, 2016.

[16] P. Srivastava, "Correlation of odontometric measures in sex determination," *Journal of Indian Academy of Forensic Medicine*, vol. 32, pp. 56–61, 2010.

[17] R. Thapar, P. V. Angadi, S. Hallikerimath, and A. D. Kale, "Sex assessment using odontometry and cranial anthropometry: evaluation in an Indian sample," *Forensic Science, Medicine, and Pathology*, vol. 8, pp. 94–100, 2012.

[18] S. A. Mackinejad, R. Kaviani, V. Rakhshan, and F. Khabir, "Assessment of the cut-off point of mesiodistal and buccolingual widths of permanent teeth for determination of sex," *Isfahan Dental Journal*, vol. 11, pp. 153–162, 2015.

[19] S. S. Babu, S. S. Nair, D. Gopakumar, N. Kurian, A. Parameswar, and T. K. Baby, "Linear odontometric analysis of permanent dentition as a forensic aid: a retrospective study," *Journal of Clinical and Diagnostic Research: JCDR*, vol. 10, p. ZC24, 2016.

[20] A. Brook, R. Griffin, G. Townsend, Y. Levisianos, J. Russell, and R. Smith, "Variability and patterning in permanent tooth size of four human ethnic groups," *Archives of Oral Biology*, vol. 54, pp. S79–S85, 2009.

[21] F. Hattab, S. Al-Khateeb, and I. Sultan, "Mesiodistal crown diameters of permanent teeth in Jordanians," *Archives of Oral Biology*, vol. 41, pp. 641–645, 1996.

[22] S. Garn, A. Lewis, and A. Walenga, "Maximum-confidence values for the human mesiodistal crown dimension of human teeth," *Archives of Oral Biology*, vol. 13, pp. 841–844, 1968.

[23] S. M. Garn, P. Cole, R. Wainwright, and K. Guire, "Sex discriminatory effectiveness using combinations of permanent teeth," *Journal of Dental Research*, vol. 56, no. 6, pp. 697–697, 1977.

[24] S. Kaushal, V. Patnaik, and G. Agnihotri, "Mandibular canines in sex determination," *Journal of the Anatomical Society of India*, vol. 52, pp. 119–124, 2003.

[25] S. M. Garn, A. B. Lewis, D. R. Swindler, and R. S. Kerewsky, "Genetic control of sexual dimorphism in tooth size," *Journal of Dental Research*, vol. 46, pp. 963–972, 1967.

[26] J. W. Hsu, P. L. Tsai, T. H. Hsiao, H. P. Chang, L. M. Liu, K. M. Liu et al., "Ethnic dental analysis of shovel and Carabelli's traits in a Chinese population," *Australian Dental Journal*, vol. 44, pp. 40–45, 1999.

[27] D. L. Anderson and G. W. Thompson, "Interrelationships and sex differences of dental and skeletal measurements," *Journal of Dental Research*, vol. 52, pp. 431–438, 1973.

[28] K. Petersen and S. Kogon, "Dental identification in the Woodbridge disaster," *Journal of the Canadian Dental Association*, vol. 37, pp. 275–279, 1971.

[29] N. H. Felemban and B. S. Manjunatha, "Prevalence of the number of cusps and occlusal groove patterns of the mandibular molars in a Saudi Arabian population," *Journal of Forensic and Legal Medicine*, vol. 49, pp. 54–58, 2017.

[30] T. K. Baby, S. Sunil, and S. S. Babu, "Nonmetric traits of permanent posterior teeth in Kerala population: a forensic overview," *Journal of oral and maxillofacial pathology: JOMFP*, vol. 21, p. 301, 2017.

[31] F. Ghorbanijavadpour, V. Rakhshan, and N. Ashoori, "Evaluation of prevalence of hypodontia based on sex, dental and skeletal relationship in patients admitted to Ahvaz Dental School," *Journal of Isfahan Dental School*, vol. 17, pp. 56–63, 2021.

[32] R. C. Scheid and G. Weiss, *Woelfel's dental anatomy*, Jones & Bartlett Publishers, 2020.

[33] H. R. Fattahi, H. R. Pakshir, and Z. Hedayati, "Comparison of tooth size discrepancies among different malocclusion groups," *European Journal of Orthodontics*, vol. 28, pp. 491–495, 2006.

[34] A. Laino, G. Quaremba, S. Paduano, and S. Stanzione, "Prevalence of tooth-size discrepancy among different malocclusion groups," *Progress in Orthodontics*, vol. 4, pp. 37–44, 2003.

[35] A. Brook, C. Underhill, L. Foo, and M. Hector, "Approximal attrition and permanent tooth crown size in a Romano-British population," *Dental Anthropology Journal*, vol. 19, pp. 23–28, 2006.

[36] S. E. Bishara, J. R. Jakobsen, E. M. Abdallah, and A. F. Garcia, "Comparisons of mesiodistal and bnccolingnal crown dimensions of the permanent teeth in three populations from Egypt, Mexico, and the United States," *American Journal of Orthodontics and Dentofacial Orthopedics*, vol. 96, pp. 416–422, 1989.

[37] H. Bailit, "Dental variation among populations. An anthropologic view," *Dental Clinics of North America*, vol. 19, pp. 125–139, 1975.

[38] A. Brook, "A unifying aetiological explanation for anomalies of human tooth number and size," *Archives of Oral Biology*, vol. 29, pp. 373–378, 1984.

[39] T. Hanihara and H. Ishida, "Metric dental variation of major human populations," *American Journal of Physical Anthropology: The Official Publication of the American Association of Physical Anthropologists*, vol. 128, pp. 287–298, 2005.

[40] J. A. Kieser and K. Julius, *Human Adult Odontometrics: the Study of Variation in Adult Tooth Size*, Cambridge University Press, 1990.

[41] J. Verhoeven, J. Van Aken, and G. Van Der Weerdt, "The length of teeth: a statistical analysis of the differences in length

of human teeth for radiologic purposes," *Oral Surgery, Oral Medicine, Oral Pathology*, vol. 47, pp. 193–199, 1979.

[42] N. G. Rao, N. N. Rao, M. L. Pai, and M. S. Kotian, "Mandibular canine index—a clue for establishing sex identity," *Forensic Science International*, vol. 42, pp. 249–254, 1989.

[43] H. Sherfudhin, M. Abdullah, and N. Khan, "A cross-sectional study of canine dimorphism in establishing sex identity: comparison of two statistical methods," *Journal of Oral Rehabilitation*, vol. 23, pp. 627–631, 1996.

[44] M. Muller, L. Lupi-Pegurier, G. Quatrehomme, and M. Bolla, "Odontometrical method useful in determining gender and dental alignment," *Forensic Science International*, vol. 121, pp. 194–197, 2001.

[45] B. Rai, S. Dhattarwal, S. Anand, and D. Bhardwaj, "Mesio-distal diameter of mandibular canine as a sex and intercanine distance as the age determinant," *Indian Internet Journal of Forensic Medicine & Toxicology*, vol. 6, pp. 44–47, 2008.

[46] A. B. Acharya and S. Mainali, "Sex discrimination potential of buccolingual and mesiodistal tooth dimensions," *Journal of Forensic Sciences*, vol. 53, pp. 790–792, 2008.

[47] R. Shrestha, "Measurement of mesio-distal tooth diameter of Nepalese permanent dentition," *Journal of Nepal Dental Association*, vol. 7, pp. 55–63, 2005.

[48] M. Y. İşcan and P. S. Kedici, "Sexual variation in bucco-lingual dimensions in Turkish dentition," *Forensic Science International*, vol. 137, pp. 160–164, 2003.

[49] G. Townsend, "Tooth size characteristics of Australian Aborigines," *Occasional Papers in Human Biology*, vol. 1, pp. 17–38, 1979.

[50] L. J. Ghose and V. S. Baghdady, "Analysis of the Iraqi dentition: mesiodistal crown diameters of permanent teeth," *Journal of Dental Research*, vol. 58, pp. 1047–1054, 1979.

[51] E. F. Harris and M. T. Nweeia, "Tooth size of Ticuna Indians, Colombia, with phenetic comparisons to other Amerindian," *American Journal of Physical Anthropology*, vol. 53, pp. 81–91, 1980.

[52] H. A. Hashim and B. Zuhair Murshid, "Mesiodistal tooth width in a Saudi population: a preliminary report," *Saudi Dental Journal*, vol. 5, pp. 68–72, 1992.

[53] G. Basaran, M. Selek, O. Hamamci, and Z. Akkuş, "Intermaxillary Bolton tooth size discrepancies among different malocclusion groups," *The Angle Orthodontist*, vol. 76, pp. 26–30, 2006.

[54] T. Uysal, Z. Sari, F. A. Basciftci, and B. Memili, "Intermaxillary tooth size discrepancy and malocclusion: is there a relation?," *The Angle Orthodontist*, vol. 75, pp. 208–213, 2005.

[55] Q. Nie and J. Lin, "Comparison of intermaxillary tooth size discrepancies among different malocclusion groups," *American Journal of Orthodontics and Dentofacial Orthopedics*, vol. 116, pp. 539–544, 1999.

[56] L. W. White, "The clinical use of occlusograms," *Journal of Clinical Orthodontics*, vol. 16, pp. 92–103, 1982.

Hindawi
BioMed Research International
Volume 2022, Article ID 4695193, 10 pages
https://doi.org/10.1155/2022/4695193

Research Article

An Analysis of Maxillary Anterior Teeth Crown Width-Height Ratios: A Photographic, Three-Dimensional, and Standardized Plaster Model's Study

Naseer Ahmed,[1,2] **Mohamad Syahrizal Halim**,[3] **Ayesha Aslam**,[4] **Zuryati Ab Ghani**,[5] **Jawad Safdar**,[6] **and Mohammad Khursheed Alam**[7,8,9]

[1]*Prosthodontics Unit, School of Dental Sciences, Health Campus, Universiti Sains Malaysia, Kubang Kerian, 16150 Kota Bharu, Kelantan, Malaysia*
[2]*Department of Prosthodontics, Altamash Institute of Dental Medicine, Karachi 75500, Pakistan*
[3]*Conservative Dentistry Unit, School of Dental Sciences, Health Campus, Universiti Sains Malaysia, Kubang Kerian, 16150 Kota Bharu, Kelantan, Malaysia*
[4]*Department of Prosthodontics, Army Medical College/Armed Forces Institute of Dentistry, National University of Medical Sciences, Islamabad, Pakistan*
[5]*Prosthodontics Unit, School of Dental Sciences, Health Campus, Universiti Sains, Kubang Kerian, 16150 Kota Bharu, Kelantan, Malaysia*
[6]*Department of Oral and Maxillofacial Surgery. Dow Dental College, Dow University of Health Sciences, Karachi, Pakistan*
[7]*Department of Preventive Dentistry, College of Dentistry, Jouf University, Sakaka, Al Jouf 72345, Saudi Arabia*
[8]*Centre for Transdisciplinary Research (CFTR), Saveetha Dental College, Saveetha Institute of Medical and Technical Sciences, Saveetha University, Chennai 600077, India*
[9]*Department of Public Health, Faculty of Allied Health Sciences, Daffodil International University, Dhaka 1207, Bangladesh*

Correspondence should be addressed to Mohamad Syahrizal Halim; drsyah@usm.my
and Mohammad Khursheed Alam; mkalam@ju.edu.sa

Received 13 October 2021; Accepted 25 January 2022; Published 7 February 2022

Academic Editor: Iole Vozza

Objective. To analyze the width and height ratios of maxillary anterior teeth at different crown levels through photographs, 3D, and plaster dental model techniques in a subset of the Pakistani population. *Material and Methods*. This clinical study consisted of 230 participants. The maxillary impression, standardized photographs, and models were constructed for crown width and height analysis. The SPSS version 25 was used for statistical analysis. Descriptive statistics were carried out for mean, standard deviation, and percentage calculation of teeth width and height, gender, and age of participants. Paired *t*-test analysis was carried out to compare the dependent variables (teeth size, width, and height ratios) with independent variables (techniques applied, side disparity). A p value of ≤ 0.05 was considered statistically significant. *Results*. The mean width and height of maxillary anterior teeth obtained through photographs, 3D, and plater models were statistically different. The 3D dental model analysis showed reliable and accurate results. The mean width and height ratio of teeth were different on both sides of the arch. There was a significant difference ($p = 0.001$) in crown width-height ratios at different crown levels. *Conclusion*. The width and height ratios in the studied population were different at various crown levels. The dimensions of teeth varied from the incisal to the cervical part of the crown. Hence, rather than relying on a single, fixed ratio of 78% to 80% suggested by researchers for anterior teeth, the clinician should adopt different crown width-height ratios to restore teeth with the optimum esthetic outcome.

1. Introduction

Esthetic restoration of smiles is a complicated process mandating a multidisciplinary approach [1]. The major concern for patients seeking esthetic dental treatment is the appearance of anterior teeth [2]. Among other parameters, the dimensions of maxillary anterior teeth are the most significant factors in achieving harmonious and esthetic outcomes [3]. However, defining ideal tooth dimensions is rather difficult owing to individual variations and proximal tooth wear [4].

Maxillary anterior teeth, being the most prominent ones, are paramount to the restoration of anterior dental esthetics as well as overall facial esthetics [5]. Selection of appropriate crown length and width is essential to creating esthetically pleasing smiles. Crown width to length ratio is considered as the most stable parameter, essential to achieve a harmony between dental esthetics and facial contours [6]. For maxillary anterior teeth, several theories exist suggesting the ideal proportions that may result in esthetic results such as golden proportion, golden percentage, and recurring esthetic dental proportion [7].

The ratio between height and width of maxillary anterior has been assessed using several methods. Sterret et al. [8] employed dental casts to assess the crown width to height ratio (CWHR) of maxillary anterior teeth. They reported a CWHR of 85%, 76%, and 77% for males and 86%, 79%, and 81% for females for maxillary central incisors, lateral incisors, and canines, respectively. Magne et al., in contrast, utilized extracted teeth to measure CWHR and observed mean ratios of 78% for central incisors and 73% each for lateral incisors and canines [9]. While Chu [10] reported a CWHR of 78% for all maxillary anterior teeth using "Chu's esthetic proportion gauge," Shahid et al. [11] and Yuan et al. [5] utilized digital calipers to measure the dimensions of maxillary teeth and reported significant differences only in terms of crown widths and height between males and females and not in CWHR. With advancements in digital dentistry, 3D digital models and software are now being used for easier and faster measurements of dental clinical parameters [7, 12].

As previously stated, knowledge about crown width and height (W/H) ratio is critical for optimal restoration of maxillary anterior teeth. A study presenting crown width-height ratio of maxillary anterior teeth at different crown levels is lacking. The present study, therefore, is aimed at determining the crown width-height ratio of maxillary anterior teeth at different clinical crown levels utilizing 2D photographs, plaster, and 3D digital dental models. Specific objectives of the study included the following:

(i) To evaluate the mean mesiodistal widths and incisocervical lengths of maxillary anterior teeth using 2D photographs, 3D models, and standard plaster models

(ii) To evaluate the mesiodistal widths and incisocervical lengths of maxillary anterior teeth using 2D photographs, 3D models, and standard plaster models at different crown levels

(iii) To evaluate the width-height ratios of maxillary anterior teeth at different crown levels

(iv) To compare the mean width-height ratios of maxillary anterior teeth at different crown levels

2. Materials and Methods

2.1. Study Setting and Sample Size. This analytical study was carried out at the Altamash Institute of Dental Medicine, Pakistan. A total of 230 subjects participated in this study. The age range of participants was 18 to 30 years. A nonprobability convenience sampling technique was used to recruit participants in this study. The flow diagram of the stepwise methodological approach adopted in this study is described in Figure 1. The sample size was calculated with public service of creative research systems survey software (creative research systems, version 9, Petaluma, California, United States). Considering the width and height ratio of 85.55% for central incisor [13], the estimated sample size at 5% margin of error with 95% confidence interval, 230 individuals with intact natural maxillary anterior teeth were invited to participate in this study, considering the 10,000,000 population.

2.2. Participant Recruitment and Ethical Consideration. The ethical permission was obtained from the ethical review board of AIDM number AIDM/EC/06/2019/06 and Universiti Sains Malaysia number USM/JEPeM/19060380. The participants were interviewed. The informed consent for voluntary participation and refusal at any time from the study was carried out for each participant. The form number, nationality, age, gender, height, weight of participants, and contact details were noted. The intraoral and extraoral examination was carried out to eliminate facial malformation, asymmetry, deviation of temporomandibular joint, and difficulty in mouth opening. The participants were also screened for dental caries, any restoration in anterior teeth, malalignment of teeth, gingival inflammation, and history of orthodontic treatment. Two hundred and fifty participants were initially screened to be included in the study. Later, 20 participants were excluded based on malalignment of teeth, facial asymmetry, restored teeth, i.e., composite restoration, crown, and bridgework, subjects with blur/unclear photographs, impression making errors, and broken or destroyed dental casts in the process of fabrication.

2.3. Capturing Retracted Smile Intraoral Photograph. A digital camera (Canon EOS, DSLR Camera, CMOS, 18 MP,1920 X 1080 p/30 fps) was used to capture crisp clear images. The camera was equipped with a built-in magnification lens of (18 – 55 mm + 75 – 300 mm) to capture reproducible images. The 1 : 1 macro setting was used for close-up photography of teeth and generally included 4 four maxillary incisors and canine teeth on the sensor. The 1 : 1 setting was used for capturing anterior teeth images with a focus set on subject's central incisor tooth. The camera was set at the 12 o'clock position, mounted on a tripod with a standardized focus and distance of 1.5 meters from the participants to ensure distortion-free images. The surrounding lighting remained

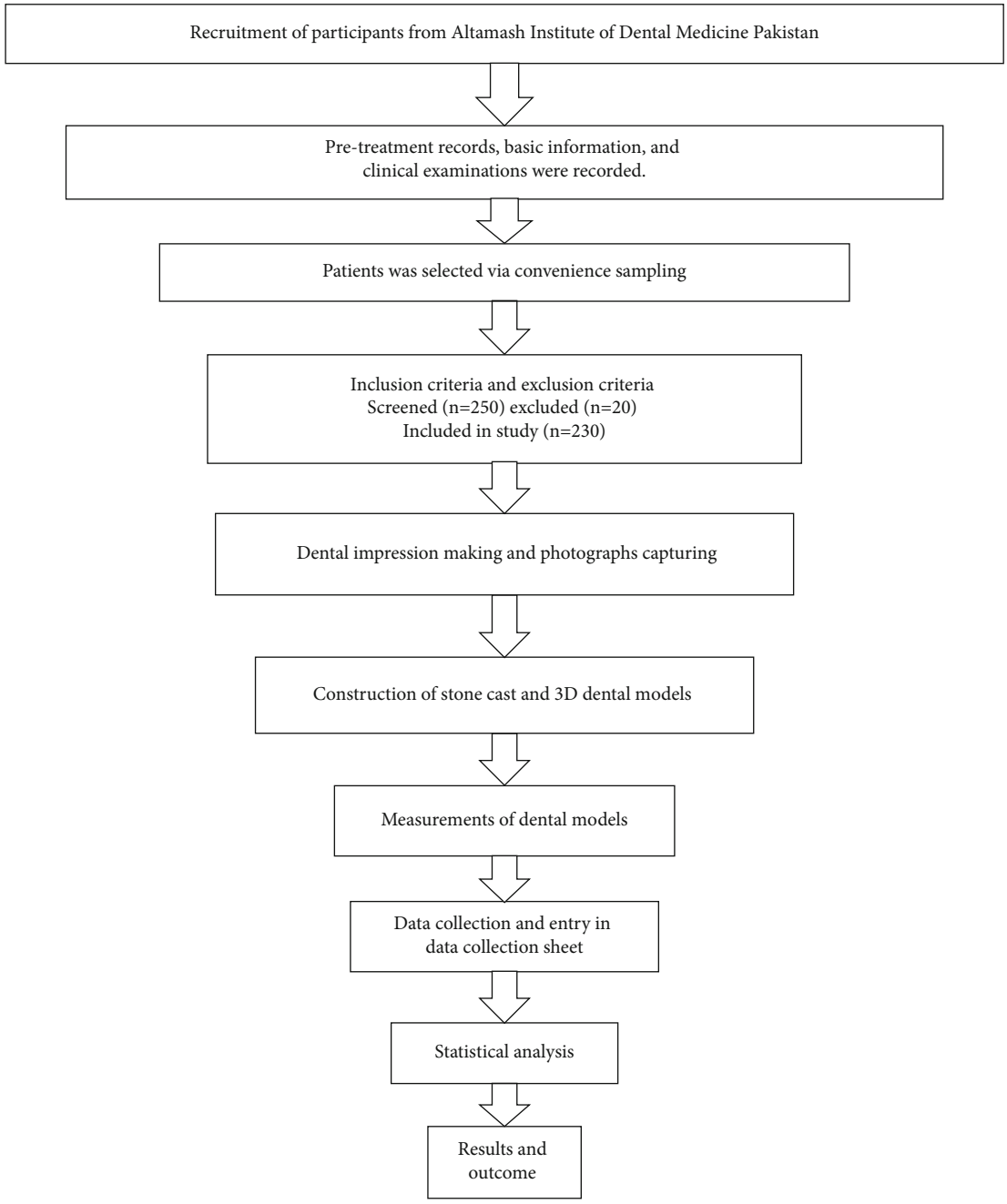

Figure 1: Flow diagram of the study methodology.

the same for all the photographs. A ring flashlight source system (LED-FD,480II, Medike Photo and Video Co., Ltd. Yidoblo, Guangdong, China) was used, and its configuration consisted of a light unit that was mounted next to the camera lens. The design was of a movable type which consisted of a light (fluorescent) that was mounted further from the lens placed in variable custom positions around a circular mounting bracket. A photograph of anterior teeth for assessment of study subjects was taken from the front, with the subject in a seated position. The head position was guided by the investigator to assist the participants in assuming their natural head position. The height of the lens of the camera was adjusted on the tripod to match the level of the incisors for retracted smile image capture. The participants were seated upright with shoulders and head held straight and facing forward, looking straight ahead at the lens of the camera; the natural head position was standardized along both horizontal and vertical axes. In all intraoral photos, the upper and lower lips were retracted to display the maxillary anterior teeth. This procedure was like the protocol described by Bidra et al. [14] (Figure 2).

2.4. Maxillary Impression and Dental Cast Making. For the fabrication of the maxillary cast, the perforated type of stainless-steel maxillary impression tray was carefully selected; the tray must cover the hamular notches and fovea

Figure 2: Pictorial illustration showing methodology of obtaining standard digital images with subject in natural head position.

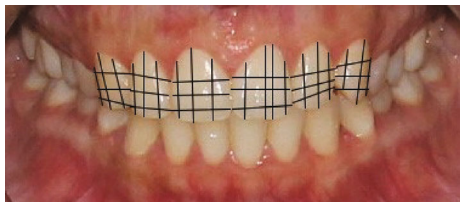

Figure 3: Demonstrating the method applied to measure maxillary anterior teeth width and height.

palatine and also provide adequate space for 3-4 millimeters for the impression material uniformly. The borders of the tray were extended up to the functional sulcus depth without causing physical discomfort to the participants.

The impressions of the maxillary arch were made of all subjects using irreversible hydrocolloid material (fast setting alginate hydrogum; Zharmack Spa). It was manipulated according to manufacturer's instructions. The errorless impressions after making were washed under running tap water for 10 seconds to remove debris and salivary pellicle. Every impression was immersed in dimethyl ammonium chloride solution (BODE) for 10 minutes to achieve disinfection. After disinfection, a serial number was allotted to each impression for identification purposes. The impressions were poured with type IV dental stone (ISO Type 3, Elite Rock Zharmack Spa). The dental cast was removed from the impression after 30 minutes to avoid errors like dimensional changes and desiccation of the cast by the set impression material. After removal, the cast was coded with a serial number of subjects using a permanent marker. The bases of casts were made with soft plaster using standardized base formers. To obtain a 3D model, the cast was scanned by UP3D Dental Laboratory Scanner (UP360+, $300 \times 300 \times 400$ mm, 3D scanner, Shenzhen, China). The scanner was equipped with 2.0 MP cameras that can scan with high precision up to 6 μm. The full-arch 3D scan was obtained in 20 seconds. The scanned images were displayed on a compatible dental design software (UPCAD, UP3D, Shenzhen, China), then transferred via USB to store in a personal computer.

2.5. Plaster, Photographic, and 3D Dental Cast Teeth Width Measurement. The photographic and 3D dental cast mesiodistal width of the maxillary anterior teeth was recorded with a measuring tool in millimeters setting through Photoshop software (Adobe, version 21.0.2, San Jose, California, United States). The plaster dental cast widths were calculated with a sharp-tipped digital Vernier calliper (Neiko 01407A Electronic Digital Calliper), read to the nearest 0.02 mm. The mesiodistal widths of central incisors, lateral incisors, and canines were measured from the facial side.

The width of the maxillary anterior teeth crown was measured at the incisal third, middle third, and cervical third of the crown from the labial aspect. The height of the crown was measured from 3 aspects; the mesial third of the crown from incisal edge to base of interdental papilla similarly at the distal third the crown length was measured in millimeters and recorded. The crown height was also measured at the middle one-third from the incisal edge to the deepest point in the cervical third of the crown (Figure 3). The information regarding teeth measurements obtained from all three sources was recorded and transferred to a computer spreadsheet.

2.6. Calculation of Crown Width and Height Ratios. To calculate the crown width and height (W/H) ratios, the incisal third width was divided by mesial third height, middle third width was divided by middle third crown height, and cervical third width was divided by distal third crown height. This way, the width and height ratio of each tooth was calculated at three different crown levels.

2.7. Validity and Reliability Assessment. The data methods and collection were performed by a single operator (N.A.). Initially, for interoperator assessment, the data collection was performed by a senior colleague (J.S.). The data was then subjected to correlation analysis; a strong correlation value of (0.739) was noted between the operator measurements.

To minimize intraoperator errors, each measurement was performed thrice; a constant or mean value of variables was then noted in proforma. Furthermore, 20% of photographs and dental models were assessed after 2 weeks by the same operator. The data was analyzed later by the Dahlberg formula to detect intraoperator reliability through correlation statistics.

For validity purposes, 20% of dental cast measurements that were carried out with a Vernier calliper were compared with 3D dental cast measurements through adobe photoshop software (Adobe, version 21.0.2, San Jose, California, United States). The intraclass correlation coefficient test (ICC) was carried to obtain an association between the two sets of measurements. A strong correlation value of (0.816) was found because of the analysis.

To minimize the photographic error, the actual width of maxillary anterior teeth obtained from the dental cast was divided by perceived width from photographs to obtain a conversion factor [15]. The perceived teeth widths were then multiplied by the conversion factor, to overcome magnification error and achieve the true width captured in the photograph.

Table 1: Distribution of mean maxillary anterior teeth widths obtained from 2D images and 3D and plaster dental models ($n = 230$).

Maxillary teeth	2D photographic width		3D digital model width		Plaster dental cast width	
	Mean	Standard deviation	Mean	Standard deviation	Mean	Standard deviation
Right central incisor	16.114	2.366	8.397	0.540	8.627	0.453
Right lateral incisor	13.888	5.156	7.735	0.554	7.371	0.539
Right canine	11.079	3.093	8.042	0.390	7.864	0.457
Left central incisor	16.366	5.655	8.788	0.426	8.723	0.479
Left lateral incisor	13.308	1.318	7.847	0.620	7.623	0.637
Left canine	10.937	0.803	8.157	0.464	7.959	0.482
Combine six teeth width	81.722	9.924	48.969	1.508	48.170	1.551

2D: two-dimensional; 3D: three-dimensional.

Table 2: Comparison of mean maxillary anterior teeth widths obtained from 2D images and clean width obtained after photographic error assessment ($n = 230$).

Maxillary teeth	2D photographic width		Clean width	
	Mean	Standard deviation	Mean	Standard deviation
Right central incisor	16.114	2.366	8.130	0.717
Right lateral incisor	13.888	5.156	6.241	0.903
Right canine	11.079	3.093	6.619	1.319
Left central incisor	16.366	5.655	7.965	0.848
Left lateral incisor	13.308	1.318	5.983	0.937
Left canine	10.937	0.803	6.384	1.320
Combine six teeth width	81.722	9.924	40.788	4.090

Clean width: mesiodistal teeth dimension obtained after photographic error estimation assessment; 2D: two-dimensional ($p < 0.05$).

Table 3: Comparison of different combined mesiodistal widths of six maxillary anterior teeth ($n = 230$).

Variables	Mean	Standard deviation
2D photographic	81.722	9.924
3D digital model	48.969	1.508
Clean mesiodistal teeth width	40.788	4.090
Plaster dental cast	48.170	1.551

2.8. Statistical Analysis. The data were analyzed with Statistical Package for the Social Sciences Software (IBM, SPSS Statistics, version 25, Chicago, Illinois, United States). The distribution of data was analysed with normality plots and testing (Shapiro-Wilk and Kolmogorov-Smirnov). Descriptive analysis of categorical (gender) and continuous (age, teeth width, height, and ratios) variables was performed, to calculate frequency, percentage, mean, and standard deviation. Moreover, mean values of dependent variables (width and height ratios of maxillary anterior teeth) were compared using paired t-test to detect the mean differences and side disparity. A p value ≤ 0.05 was taken as statistically significant.

3. Results

The dropout rate of participants in this study was 0.08%. The mean age of the participants was 24.210 ± 3.541. There were 112 (48.7%) male and 118 (51.3%) female participants in this study.

The mean width of maxillary anterior teeth obtained through 2D dental images was recorded 16.114 ± 2.366 for right central incisor, 13.888 ± 5.156 for right lateral incisors, and 11.079 ± 3.093 for a canine tooth. The mean width of the left central incisor was 16.366 ± 5.655, 13.308 ± 1318 lateral incisor, and 10.937 ± 0.803 for a canine tooth.

The mean width of maxillary anterior teeth obtained through 3D dental images was 8.397 ± 0.540 in the right central incisor, 7.735 ± 0.554 right lateral incisor, and 8.042 ± 0.390 for a canine tooth. The mean width of the left central incisor was 8.788 ± 0.426, 7.847 ± 0.620 lateral incisors, and 8.157 ± 0.464 in the canine tooth.

The mean width of maxillary anterior teeth obtained through plaster dental cast was 8.627 ± 0.453 in the right central incisor, 7.371 ± 0.539 in the right lateral incisor, and 7.864 ± 0.457 for a canine tooth. The mean width of the left central incisor was 8.723 ± 0.479, while 7.623 ± 0.637 in the lateral incisor and 7.959 ± 0.482 in the canine tooth (Table 1).

The clean width of maxillary anterior teeth in this study was 8.130 ± 0717 in the right central incisor, while for the lateral incisor, it was 6.241 ± 0.903, and 6.619 ± 1.319 in the canine tooth, whereas in left central incisor 7.965 ± 0.848, lateral incisor 5.983 ± 0.937, and 6.384 ± 1.320 in the canine tooth. There was a significant difference ($p < 0.05$) between the mean values of photographic and clean widths of maxillary anterior teeth (Table 2).

The combined width of maxillary anterior teeth analyzed through 2D photographs were 81.722 ± 9.924, 3D digital models were 48.969 ± 1.508, clean mesiodistal width was 40.788 ± 4.090, and plaster dental cast was 48.170 ± 1.551 (Table 3).

The mean mesiodistal widths of the right central incisor at incisal one-third of the crown was 8.912 ± 0.476, middle third 8.623 ± 0.444, and cervical third 8.354 ± 0.487. The lateral incisor incisal one-third width was 7.826 ± 0.602, the middle third width was 8.623 ± 0.444, and the width at cervical third was 8.354 ± 0.487. Canine tooth incisal one-third width was 8.364 ± 0.457, middle one-third width was

Table 4: Characteristics of mesiodistal widths of maxillary anterior teeth different crown level ($n = 230$).

Variables	Incisal third width	Middle third width	Cervical third width
Right central incisor	8.912 ± 0.476	8.623 ± 0.444	8.354 ± 0.487
Right lateral incisor	7.826 ± 0.602	7.371 ± 0.539	6.366 ± 0.543
Right canine	8.364 ± 0.457	7.864 ± 0.457	6.864 ± 0.457
Left central incisor	9.219 ± 0.506	8.723 ± 0.479	7.765 ± 0.526
Left lateral incisor	8.123 ± 0.637	7.623 ± 0.637	6.623 ± 0.637
Left canine	8.455 ± 0.475	7.959 ± 0.482	6.984 ± 0.489

Table 5: Characteristics of incisocervical length of maxillary anterior teeth at different crown levels ($n = 230$).

Variables	Mesial third length	Middle third length	Distal third length
Right central incisor	8.023 ± 0.908	9.990 ± 0.883	7.059 ± 0.921
Right lateral incisor	7.611 ± 0.603	9.093 ± 0.642	6.608 ± 0.613
Right canine	7.305 ± 0.638	8.805 ± 0.638	7.235 ± 0.635
Left central incisor	7.435 ± 0.558	8.929 ± 0.520	7.059 ± 0.623
Left lateral incisor	7.196 ± 0.670	8.485 ± 0.691	7.456 ± 0.713
Left canine	7.281 ± 0.665	8.839 ± 0.884	6.766 ± 0.775

7.864 ± 0.457, while the mean cervical third width was 6.864 ± 0.457.

Similarly, on the left side of the arch, the mean incisal one-third width of the central incisor tooth was 9.219 ± 0.506, middle third width recorded 8.723 ± 0.479, and cervical third 7.765 ± 0.526; as far as the lateral incisor is concerned, the mean incisal one-third width was 8.123 ± 0.637 , middle one-third 7.623 ± 0.637, and cervical one-third was 6.623 ± 0.637. Whereas the mean width of the canine tooth at incisal one-third was 8.455 ± 0.475, the middle third was 7.959 ± 0.482, and at the cervical one-third, it was 6.984 ± 0.489 (Table 4).

Furthermore, the mean length of maxillary anterior teeth at different crown levels was the following. The mesial one-third length of the right central incisor was 8.023 ± 0.908, the middle third length was 9.990 ± 0.883, and the distal third length was 7.059 ± 0.921, whereas in lateral incisor, mesial third length was 7.611 ± 0.603, middle third length was 9.093 ± 0.642, while the distal third length was recorded as 6.608 ± 0.613. The mesial third length of the canine tooth was 7.305 ± 0.638, the middle third length was 8.805 ± 0.638 , and the cervical third was 7.235 ± 0.635.

However, on the left side of the arch, the mean mesial one-third length of the central incisor tooth was 7.435 ± 0.558, middle third length 8.929 ± 0.520, and the distal third was 7.059 ± 0.623. As far as the lateral incisor is concerned, the mean mesial one-third length was 7.196 ± 0.670, middle one-third length 8.485 ± 0.691, and distal one-third was 7.456 ± 0.713, whereas the mean length of the canine tooth at mesial one-third was 7.281 ± 0.665, middle third 8.839 ± 0.884, and at the distal one-third, it was 6.766 ± 0.775 (Table 5).

The W/H ratios of maxillary anterior teeth at different crown levels revealed a value of 112.245 ± 13.443 at incisal one-third in the right central incisor, while 87.271 ± 8.798 at the middle third of the crown, and 120.286 ± 16.753 at a cervical third of the crown. Similarly, the width to height ratio at incisal one-third of the right lateral incisor was 99.738 ± 13.479, the middle one-third ratio was 98.965 ± 14.596, whereas at the cervical third, the ratio obtained was 97.143 ± 13.315. The incisal one-third width and height ratio of the right canine was 113.773 ± 17.642, the middle third ratio was 88.651 ± 12.509, and the cervical third was 95.682 ± 14.268.

Moreover, the width to height ratio of maxillary anterior teeth at the left side of the arch revealed a ratio of 124.178 ± 10.436 at incisal one-third in the left central incisor, 98.202 ± 6.781 at the middle third of the crown, while 110.570 ± 9.846 for the cervical third of the crown. Additionally, the width to height ratio at incisal one-third of left lateral incisor was 113.226 ± 15.983, the middle one-third ratio was 89.830 ± 11.437, whereas at the cervical third, the ratio of 89.527 ± 12.697 was found. The incisal one-third width and height ratio of the left canine was 114.978 ± 17.024, the middle third was 96.446 ± 111.824, and the cervical third was 102.848 ± 15.729 (Table 6).

Table 7 is presenting paired t-test analysis of crown W/H ratios at different crown levels. There was a significant difference ($p = 0.001$) between width and height ratio of central incisor at incisal third, supported by a greater t-value of -11.932 indicating a large difference between the mean values. The width-height ratio at the middle third was also significant ($p = 0.001$), shown by a large t-value (-16.034). Similarly, the cervical third width and height ratios were also statistically significant ($p = 0.001$), and a large t-value was noted (7.895).

Furthermore, the comparison of side disparity in maxillary anterior teeth revealed a significant difference ($p = 0.001$) between the width and height ratio of lateral incisor at incisal third, aided by a greater t-value of (12.033) indicating a large difference between the mean values. The width-height ratio at the middle third showed a significant difference ($p = 0.001$), supported by a large t-value (9.568). Likewise, the cervical third width and height ratio was also statistically significant ($p = 0.001$), endorsed by a large t-value (8.092).

However, no significant difference ($p = 0.296$) was found between the width and height ratio of the canine tooth at incisal third level, supported by a small t-value of -1.048 indicating no variation between the mean values. The width-height ratio at the middle third was also statistically significant ($p = 0.001$); this finding was supported by a t -value (-3.404). Likewise, the cervical third level width and height ratios showed a significant difference ($p = 0.001$) in mean values, indicated by a large t-value (-17.145).

Table 6: Distribution of width-height ratios of maxillary anterior teeth at different crown levels ($n = 230$).

Variables	Incisal third width and height ratio % SD	Middle third width and height ratio % SD	Cervical third width and height ratio % SD
Right central incisor	112.245 ± 13.443	87.271 ± 8.798	120.286 ± 16.753
Right lateral incisor	99.738 ± 13.479	98.965 ± 14.596	97.143 ± 13.315
Right canine	113.773 ± 17.642	88.651 ± 12.509	95.682 ± 14.268
Left central incisor	124.178 ± 10.436	98.202 ± 6.781	110.570 ± 9.846
Left lateral incisor	113.226 ± 15.983	89.830 ± 11.437	89.527 ± 12.697
Left canine	114.978 ± 17.024	96.446 ± 111.824	102.848 ± 15.729

%: percentage; SD: standard deviation.

4. Discussion

The present study is aimed at evaluating the crown width-height ratio of maxillary anterior teeth at different clinical crown levels utilizing 2D photographs and 3D digital dental models. The mean combined mesiodistal widths of maxillary anterior teeth were 81.722 ± 9.924 for 2D photographs, 48.969 ± 1.508 using 3D digital models, 40.788 ± 4.090 clean width after error correction for 2D photographs, and 48.170 ± 1.551 using plaster models. A statistically significant difference ($p < 0.05$) between the mean values of photographic and clean widths of maxillary anterior teeth was seen. The values of photographic width were drastically different form clean width of anterior teeth; the reason is lack of minimizing the photographic error during capture. The images get distorted and enlarged due to difference in a camera focal length, shutter speed, and macro settings; hence, it effects a photograph accuracy and reproducibility. The current study overcomes the distortion effect by adopting the "conversion factor" method proposed by Ward [15] to obtain an accurate and reproducible dental images. The use of such photographic error assessment techniques was also recommended in other studies carried out by Kois [16] and Pitel et al. [17].

In this study, a statistically significant difference ($p = 0.001$) was observed between the width and height ratio of all right and left side anterior teeth at incisal, middle, and cervical thirds except for maxillary canine where the width-height ratio at incisal third was not statistically significant ($p = 0.296$). The crown width and height ratios were measured at different anatomical levels in this study; therefore, a single value of W/H ratio (73 to 95%) like proposed by Shahid et al. [11] in both sexes that was concluded, based on the middle third width and height of the teeth, and further compared with arch form, arch perimetry and width cannot be compared with our study due to difference in methodology.

In the present study, for maxillary anterior teeth, the greatest crown dimensions were observed for maxillary central incisors, followed by maxillary canines and maxillary lateral incisors. This is by the findings of Alqahtani et al. [2], Sitthiphan et al. [6], Sah et al. [18], Orozco-Varo et al. [19], and Aldegheishem et al. [20]. In the current study, the mean width-height ratio for the right central incisor at the incisal, middle, and cervical thirds of the crown was 112.24%, 87.27%, and 120.286%, respectively (mean: 106.59%), while for the left central incisor, these ratios were 124.17%, 98.2%, and 110.57%, respectively (mean: 110.98%). Likewise, for the right lateral incisor, mean width-height ratios were 99.7%, 98.9%, and 97.1% (mean: 98.56%), and for the left lateral incisor, mean width-height ratios were 113.22%, 89.8%, and 89.52% (mean: 97.5%). For the right canine, mean width-height ratios were 113.77%, 88.65%, and 95.68% (mean: 99.36%), while for the left canine, ratios were 114.97%, 96.44%, and 102.84% (mean: 104.75%). Song et al. [21] in their study carried out similar work but measured the crown width-height ratios at two levels only, namely, mesiodistal width to length (MDW/L) ratio and the cervical width to length (CW/L) ratio. They reported a mean MDW/L of 86% and CW/L of 73% for the central incisors, 84% MDW/L and 67% CW/L for lateral incisors, and 87% MDW/L and 71% CW/L ratio for maxillary canines in the Korean population indicating an increased length of teeth in the said population. These differences can be attributed to differences in ethnicity that have been suggested to affect tooth dimensions among populations [22].

In the present study, the mean width and height of central incisors were 8.59 mm and 8.08 mm, respectively. For lateral incisors, the mean width and length were 7.32 mm and 7.74 mm, while for canine, respective values were 7.75 mm and 7.71 mm. These findings are comparable to those reported by Melo et al. [23] who implied that the findings are not by the "ideal tooth dimensions." We failed to find any study that evaluated widths and lengths of maxillary anterior teeth at various crown levels, and hence, it was difficult to draw comparisons.

Attempts have been made to curtail possible sources of error and bias in the present study. The main limitation of the study is perhaps its relatively smaller sample size. Future studies with a larger and more diverse sample may reveal interesting results. To limit human error in data collection, all procedures have been carried out by a single operator, where equipment has been used such as cameras and intraoral scanners; the inherent margin of error of the said equipment may have been incorporated, but as such, it does not appear to affect the study results.

In the context of external validity, the results of the present study are generalizable to the Pakistani population in particular and the Southeast Asian population in general. The subjects for this study have been selected from the general population presenting to institute's OPD. Since it is a purely observational study, the effect of any intended

Table 7: Comparison of mean width height W/H ratios of maxillary anterior teeth at different crown levels, paired T-test analysis ($n = 230$).

Variables	Incisal third width and height ratio % SD	p value	Middle third width and height ratio % SD	p value	Cervical third width and height ratio % SD	p value
Right central incisor	112.245 ± 13.443	0.001*	87.271 ± 8.798	0.001*	120.286 ± 16.753	0.001*
Left central incisor	124.178 ± 10.436		98.202 ± 6.781		110.570 ± 9.846	
Right lateral incisor	99.738 ± 13.479	0.001*	98.965 ± 14.596	0.001*	97.143 ± 13.315	0.001*
Left lateral incisor	113.226 ± 15.983		89.830 ± 11.437		89.527 ± 12.697	
Right canine	113.773 ± 17.642	0.296	88.651 ± 12.509	0.001*	95.682 ± 14.268	0.001*
Left canine	114.978 ± 17.024		96.446 ± 111.824		102.848 ± 15.729	

*p value less than 0.001; t-value: it measures the size of the difference relative to the variation in sample data. The smaller the t-value, the more similarity exists between the two sample sets, while a large t-score indicates that the groups are different. SD: standard deviation.

interventions and their subsequent outcomes is ruled out by default. If the study were to be repeated in the same population with a different sample, it should yield similar results. However, if subjects from different ethnic backgrounds are selected, results may vary.

5. Conclusions

The results of this revealed the following outcome.

(1) There was a significant difference when the mean mesiodistal widths and incisocervical lengths of maxillary anterior teeth obtained through 2D photographs were compared with 3D models and standard plaster models, whereas no difference was found between maxillary anterior teeth width of 3D and plaster models. The 3D dental model analysis is accurate and reliable

(2) The width and height ratios in the studied population were different at various crown levels. The dimensions of teeth varied from the incisal to the cervical part of the crown. In the current study, the width-height ratio for the right central incisor was 112.24% at incisal, 87.27% middle, and 120.286% at the cervical level of the crown, respectively. The mean W/H ratio was 106.59%. In the left central incisor, these ratios were 124.17%, 98.2%, and 110.57%, respectively, with a mean ratio of 110.98%

(3) Likewise, for the right lateral incisor, width-height ratios were 99.7%, 98.9%, and 97.1%, while the mean ratio was 98.56%. In the left lateral incisor, mean width-height ratios were 113.22%, 89.8%, and 89.52% whereas, the mean ratio was 97.5%

(4) The width-height ratios in right canine tooth were 113.77%, 88.65%, and 95.68% (mean: 99.36%), while for the left canine, the ratios were 114.97%, 96.44%, and 102.84% (mean: 104.75%)

(5) Hence, rather than relying on a fixed and single ratio of 78% to 80%, the clinician should adopt different width-height ratios to restore teeth with the optimum esthetic outcome

Data Availability

The raw data used to support the findings of this study are included within the article.

Conflicts of Interest

The authors declare no conflict of interest.

Authors' Contributions

N.A, M.S.H, and Z.A.G planned and designed the present work, and N. A, M.S.H, and J. S were responsible for realizing the work. N. A, A. A, and J. S were responsible for the data acquisition and analysis. N. A, M.S.H, A.A., and M.K.A drafted and revised the manuscript. NA, MKA, M.S.H, and Z.A.G approved the final version of the manuscript. All authors read and approved the final manuscript. M.S.H and M.K.A contributed equally to this work and are corresponding authors.

Acknowledgments

The authors thank all participants, the School of Dental Sciences, Health Campus, Universiti Sains Malaysia, and Altamash Institute of Dental Medicine, Pakistan, for the support and facilitation in this study.

References

[1] A. Al Taki, A. M. Hamdan, Z. Mustafa, M. Hassan, and S. Abu-Alhuda, "Smile esthetics: impact of variations in the vertical and horizontal dimensions of the maxillary lateral incisors," *Eur J Dent*, vol. 11, no. 4, pp. 514–520, 2017.

[2] A. S. Alqahtani, S. R. Habib, M. Ali, A. S. Alshahrani, N. M. Alotaibi, and F. A. Alahaidib, "Maxillary anterior teeth dimension and relative width proportion in a Saudi subpopulation," *Journal of Taibah University Medical Sciences*, vol. 16, no. 2, pp. 209–216, 2021.

[3] N. Sandeep, P. Satwalekar, S. Srinivas, C. S. Reddy, G. R. Reddy, and B. A. Reddy, "An analysis of maxillary anterior teeth dimensions for the existence of golden proportion: clinical study," *Journal of International Oral Health: JIOH*, vol. 7, no. 9, pp. 18–21, 2015.

[4] M. Khan, M. A. Khan, and U. Hussain, "Clinical crown length, width and the width/length ratio in the maxillary anterior region in a sample of Mardan population," *Pakistan Oral & Dental Journal*, vol. 35, no. 4, pp. 738–741, 2021.

[5] P. H. Yuan, I. A. Evangelina, and G. Gayatri, "Comparison of crown width, length, width/length ratio of maxillary anterior teeth between male and female dental students," *Padjadjaran Journal of Dentistry*, vol. 30, no. 3, pp. 170–177, 2018.

[6] P. Sitthiphan, N. Viwattanatipa, P. Amornvit, B. Shrestha, M. L. T. Srithavaj, and M. K. Alam, "Comparison of maxillary anterior teeth crown ratio (width/length) between gender in Laotian population," *International Medical Journal*, vol. 22, no. 3, pp. 199–205, 2015.

[7] N. Ahmed, M. S. B. Halim, Z. A. Ghani et al., "A 2D photographic and 3D digital dental model analysis of golden percentage in maxillary anterior teeth," *BioMed Research International*, vol. 2021, Article ID 6674400, 7 pages, 2021.

[8] J. D. Sterrett, T. Oliver, F. Robinson, W. Fortson, B. Knaak, and C. M. Russell, "Width/length ratios of normal clinical crowns of the maxillary anterior dentition in man," *Journal of Clinical Periodontology*, vol. 26, no. 3, pp. 153–157, 1999.

[9] P. Magne, G. O. Gallucci, and U. C. Belser, "Anatomic crown width/length ratios of unworn and worn maxillary teeth in white subjects," *The Journal of Prosthetic Dentistry*, vol. 89, no. 5, pp. 453–461, 2003.

[10] S. J. Chu, "Range and mean distribution frequency of individual tooth width of the maxillary anterior dentition," *Practical Procedures and Aesthetic Dentistry*, vol. 19, no. 4, pp. 209–215, 2007.

[11] F. Shahid, M. K. Alam, and M. F. Khamis, "Maxillary and mandibular anterior crown width/height ratio and its relation to various arch perimeters, arch length, and arch width

groups," *European Journal of Dentistry*, vol. 9, no. 4, pp. 490–499, 2015.

[12] X.-J. Yin, B.-Y. Wei, X.-P. Ke et al., "Correlation between clinical parameters of the crown and gingival morphology of anterior teeth and periodontal biotypes," *BMC Oral Health*, vol. 20, no. 1, pp. 1–8, 2020.

[13] S. Jain, M. Reddy, P. Raghav et al., "Assessment of tooth proportions in an aesthetically acceptable smile," *Journal of Clinical and Diagnostic Research*, vol. 9, no. 4, pp. ZC01–ZC04, 2015.

[14] A. S. Bidra, F. Uribe, T. D. Taylor, J. R. Agar, P. Rungruanganunt, and W. P. Neace, "The relationship of facial anatomic landmarks with midlines of the face and mouth," *Journal of Esthetic Dentistry*, vol. 102, no. 2, pp. 94–103, 2009.

[15] D. H. Ward, "Proportional smile design using the recurring esthetic dental (RED) proportion," *Dental Clinics of North America*, vol. 45, no. 1, pp. 143–154, 2001.

[16] J. C. Kois, "Digital smile design meets the dento-facial analyzer: optimizing esthetics while preserving tooth structure," *Compendium of Continuing Education in Dentistry (Jamesburg, NJ: 1995)*, vol. 37, no. 1, pp. 46–50, 2016.

[17] M. L. Pitel, K. M. Raley-Susman, and A. Rubinov, "Preferences of lay persons and dental professionals regarding the recurring esthetic dental proportion," *Journal of Esthetic and Restorative Dentistry*, vol. 28, no. 2, pp. 102–109, 2016.

[18] S. K. Sah, H. D. Zhang, T. Chang et al., "Maxillary anterior teeth dimensions and proportions in a central mainland Chinese population," *The Chinese Journal of Dental Research*, vol. 17, no. 2, pp. 117–124, 2014.

[19] A. Orozco-Varo, G. Arroyo-Cruz, R. Martínez-De-Fuentes, and E. Jiménez-Castellanos, "Biometric analysis of the clinical crown and the width/length ratio in the maxillary anterior region," *The Journal of Prosthetic Dentistry*, vol. 113, no. 6, pp. 565–570.e2, 2015.

[20] A. Aldegheishem, A. Azam, E. Al-Madi, L. Abu-Khalaf, B. Bani Ali, and L. Anweigi, "Golden proportion evaluation in maxillary anterior teeth amongst Saudi population in Riyadh," *The Saudi Dental Journal*, vol. 31, no. 3, pp. 322–329, 2019.

[21] J. W. Song, R. Leesungbok, S. J. Park, S. H. Chang, S. J. Ahn, and S. W. Lee, "Analysis of crown size and morphology, and gingival shape in the maxillary anterior dentition in Korean young adults," *The Journal of Advanced Prosthodontics*, vol. 9, no. 4, pp. 315–320, 2017.

[22] A. R. Al-Khatib, Z. A. Rajion, S. M. Masudi, R. Hassan, P. J. Anderson, and G. C. Townsend, "Tooth size and dental arch dimensions: a stereophotogrammetric study in Southeast Asian Malays," *Orthodontics & Craniofacial Research*, vol. 14, no. 4, pp. 243–253, 2011.

[23] M. Melo, F. Ata-Ali, J. Huertas et al., "Revisiting the maxillary teeth in 384 subjects reveals a deviation from the classical aesthetic dimensions," *Scientific Reports*, vol. 9, no. 1, p. 730, 2019.

Hindawi
BioMed Research International
Volume 2022, Article ID 1473977, 11 pages
https://doi.org/10.1155/2022/1473977

Research Article

Artificial Intelligence for Classifying and Archiving Orthodontic Images

Shihao Li,[1] **Zizhao Guo**,[1] **Jiao Lin**,[2] **and Sancong Ying**[3]

[1]*National Key Laboratory of Fundamental Science on Synthetic Vision, College of Computer Science, Sichuan University, Chengdu, Sichuan 610041, China*
[2]*Sichuan Hospital of Stomatology, Chengdu, Sichuan 610041, China*
[3]*College of Computer Science, Sichuan University, Chengdu, Sichuan 610041, China*

Correspondence should be addressed to Sancong Ying; yingsancong@scu.edu.cn

Received 5 October 2021; Revised 17 December 2021; Accepted 4 January 2022; Published 27 January 2022

Academic Editor: Shivam Mehta

One of the main requirements for orthodontic treatment is continuous image acquisition. However, the conventional system of orthodontic image acquisition, which includes manual classification, archiving, and monitoring, is time-consuming and prone to errors caused by fatigue. This study is aimed at developing an effective artificial intelligence tool for the automated classification and monitoring of orthodontic images. We comprehensively evaluated the ability of a deep learning model based on Deep hidden IDentity (DeepID) features to classify and archive photographs and radiographs. This evaluation was performed using a dataset of >14,000 images encompassing all 14 categories of orthodontic images. Our model automatically classified orthodontic images in an external dataset with an accuracy of 0.994 and macro area under the curve of 1.00 in 0.08 min. This was 236 times faster than a human expert (18.93 min). Furthermore, human experts with deep learning assistance required an average of 8.10 min to classify images in the external dataset, much shorter than 18.93 min. We conclude that deep learning can improve the accuracy, speed, and efficiency of classification, archiving, and monitoring of orthodontic images.

1. Introduction

Image data are fundamental in most medical settings. In dentistry, for example, imaging is useful for diagnosis, treatment planning, monitoring, and doctor-patient communication. Orthodontists use image data for clinical decision-making, tracking teeth, and planning treatment. Traditionally, these images have been indexed (i.e., labeled based on clinical features) and stored manually, but as digital dentistry has advanced, imaging data are increasingly indexed and stored in digital archives or patient management systems, allowing for easy retrieval for further diagnostics, treatment, and monitoring [1]. Therefore, it would be useful to develop a fully automated classification and archiving method to improve the quality of dental work, as well as relieve the workload for orthodontists.

Image indexing is an image classification task that can be automated using artificial intelligence (AI), especially AI based on deep learning [2]. Deep learning is a branch of machine learning that excels in analyzing high-dimensional data such as text and images [3]. Deep learning has completely replaced certain traditional machine learning-based tasks in computer vision, such as classification [4], segmentation [5], and detection [6]. In dentistry, studies have begun applying deep learning to diagnosis, screening, and decision-making [7]. For example, one study [8] used deep learning to assist orthodontists in skeletal classification using a large dataset of lateral cephalograms (5890 images). After training and validating the model, those authors reported that their deep learning model performed vertical and sagittal skeletal classification with sensitivity, specificity, and accuracy of >90%. Another study reported a deep learning method that was able to detect dental caries in near-infrared transillumination imaging with an overall mean intersection-over-union score of 72.7% relative to the performance of professional dentists [9]. Additionally, deep

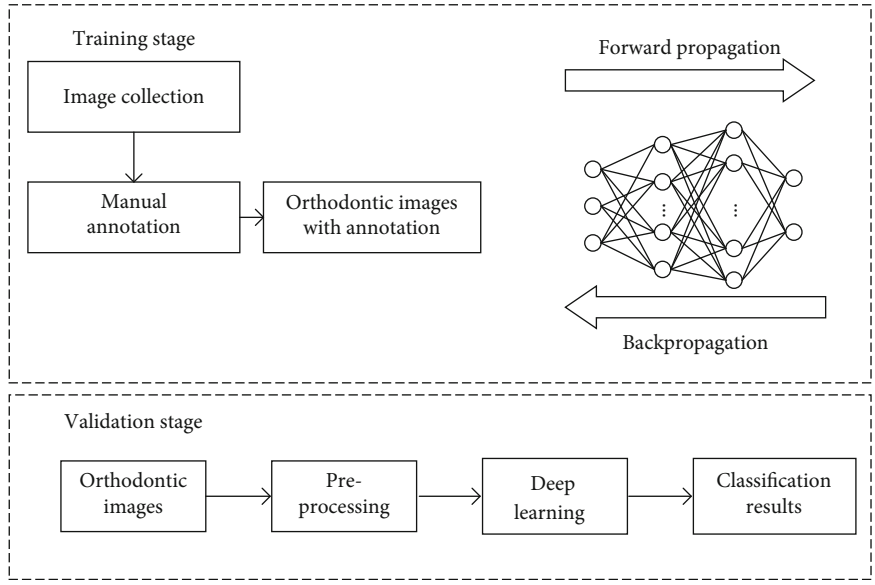

Figure 1: The construction of a deep learning model.

learning can be used to automatically identify landmarks in X-ray images for the analysis of orthodontic treatments [10]. However, the imaging data in that study had to be manually selected from case data, as required in commonly used dental applications such as the Invisalign (Align Technology, Santa Clara, CA, USA) orthodontic system. Therefore, developing an automated classification, archiving, and monitoring method that can work in conjunction with other special analysis algorithms may lead to an end-to-end dental AI application that can improve the quality of clinical practice.

In the present study, we propose an automated deep learning method for the classification and archiving of orthodontic images based on the DeepID model [11], which leverages deep convolutional networks (ConvNets) to extract features and joint Bayesian [12] algorithm for verification. For practical application, this framework is also easy to extend new functions without retraining the model, because the classification result is obtained by comparing DeepID features of sample. Figure 1 depicts a standard flowchart for the construction of deep learning model. A total of 15,819 orthodontic images were collected for model training, validation, and testing. A comprehensive evaluation of our model showed that we were able to accurately classify orthodontic images into six different intraoral photos, six different extraoral photos, and two radiographs. We also conducted experiments to make a comparison of our method and several popular models, such as ResNet-34 [13], GoogLeNet [14], and MobileNetV2 [15]. The results showed that although our model is relatively shallower, we still have achieved an excellent performance of 99.4% accuracy. Furthermore, our model was able to detect repeated or missing images in case data. As far as we know, this is the first report of an AI method to classify and archive orthodontic images. Our findings suggest that deep learning models can reduce tedious and repetitive work as well as improve the quality of orthodontic treatment, making AI a powerful tool for clinical practice.

2. Materials and Methods

2.1. Study Population. We retrospectively examined orthodontic images obtained from 1000 patients who received orthodontic treatment between January and December 2019 in the Sichuan Hospital of Stomatology, the Simai Clinic, and the Yingke Clinic. In order to evaluate our method, orthodontic images from 100 patients at the Haoya Clinic were obtained as an external dataset. Demographic and clinical characteristics of the patients included in the study are shown in Table 1.

2.2. Image Dataset. In this study, orthodontic images were defined as 14 categories: frontal at rest, frontal smile, oblique at rest, oblique smile, profile at rest, profile smile, intraoral right, intraoral front, intraoral left, maxillary occlusal, mandibular occlusal, overjet, lateral cephalogram, and panoramic radiograph. Data collection is shown in Figure 2. Representative examples of orthodontic images obtained from patients are shown in Figure 3.

Using these images, we created two nonoverlapping datasets: one was used as an internal dataset for model training and validation, and another was used as an external dataset to compare and evaluate the efficacy of human experts (orthodontists) versus the deep learning method. In both datasets, all orthodontic images were manually classified by an experienced orthodontist. To avoid mislabeled data and ensure the reliability of the dataset, a more senior orthodontic specialist with 30 years of experience reexamined all the images.

The original image was archived based on the patient list using unlabeled images. We found that half of the patients in

Table 1: Clinical and demographic characteristics of included patients.

Characteristic	Internal dataset (n = 1,000)		External dataset (n = 100)
	Training (n = 900)	Validation (n = 100)	
Age in years	29 (4-62)	27.9 (4-58)	28.7 (4-60)
Sex			
Male	248 (27.6)	30 (30)	32 (32)
Female	652 (72.4)	70 (70)	68 (68)
Photograph classification			
Frontal at rest	950 (7.3)	100 (7.1)	110 (7.7)
Frontal smile	1,012 (7.8)	100 (7.1)	99 (7)
Oblique at rest	896 (6.9)	100 (7.1)	109 (7.7)
Oblique smile	906 (7)	100 (7.1)	123 (8.7)
Profile at rest	1,002 (7.7)	100 (7.1)	87 (6.1)
Profile smile	935 (7.2)	100 (7.1)	90 (6.3)
Intraoral right	976 (7.5)	100 (7.1)	102 (7.2)
Intraoral front	899 (6.9)	100 (7.1)	109 (7.7)
Intraoral left	1,009 (7.7)	100 (7.1)	107 (7.5)
Maxillary occlusal	828 (6.4)	100 (7.1)	98 (6.9)
Mandibular occlusal	932 (7.2)	100 (7.1)	97 (6.8)
Overjet	854 (6.6)	100 (7.1)	89 (6.3)
Radiograph classification			
Lateral cephalogram	900 (6.9)	100 (7.1)	100 (7)
Panoramic radiograph	900 (6.9)	100 (7.1)	100 (7)
Total number of images	12,999	1,400	1,420

Values are n, n (%), or median (range).

the external dataset had repeated and/or missing images (~2 repeated and/or missing images per patient), and the remaining patients had a total of 14 qualified orthodontic images.

2.3. Classification of Orthodontic Images Based on Deep Learning. In this study, we propose a method of orthodontic image classification based on DeepID [11] that comprises three stages: preprocessing, classification, and postprocessing. All RGB images were checked and resized to 450×300 or 300×450 pixels based on their aspect ratio. A flowchart depicting the orthodontic image classification based on DeepID is shown in Figure 4.

The preprocessing stage included three functions: face detection, intraoral image transposition, and grayscale image tagging. The face detector was powered by OpenCV using the single-shot multibox detector (SSD) method [16]. In the case of dental imaging, the lateral cephalogram and the panoramic radiograph are typical grayscale images. Grayscale images are "one-channel", and other images are RGB image with "three-channel". Therefore, the grayscale images can be found easily available because of their "one-channel" characteristic. The final outputs of the preprocessing stage were facial regions, transposed original images, and grayscale images, if included.

In the next stage, the deep learning model processed the facial regions and the transposed photographs to classify each RGB image based on 12 categories. In addition, the grayscale images were examined in terms of their aspect ratio: the aspect ratio (width : height) of the lateral cephalogram was approximately 1.2 : 1, and that of the panoramic radiograph was approximately 2 : 1. Thus, classifying these images was straightforward. The deep learning model was trained using facial regions observed in intraoral photographs corresponding to 12 categories; these images were annotated by an orthodontist based on the guidelines provided by the orthodontic naming rule [17].

We designed our framework based on the concept of DeepID, which are high-level overcomplete features that contain discriminative information for recognition; after DeepID features have been produced, the joint Bayesian model will make classification based on them. The illustration of our DeepID features extraction process is shown in Figure 5.

Our framework is composed of convolutional layers, subsampling layers, ReLU layers, and residual blocks, as shown in Figure 5. In the method, we designed most of the convolutional functions with 3×3 filters; while concerning the images that fed into the network often with a larger size, we adopt 7×7 filters for the input layer. For improving convergence and reducing overfitting, we applied residual shortcuts after the Conv2 layer, Conv3 layer, Conv4 layer, and Conv5 layer, respectively. All residual blocks with the same architecture are illustrated in Figure 6. In the end, DeepID features were obtained based on the output of the Conv6 layer and Conv7 layer with a skip connection.

The residual architecture was proposed to address the issue of vanishing/exploding gradients and degradation that happened in traditional CNNs. After the inference step,

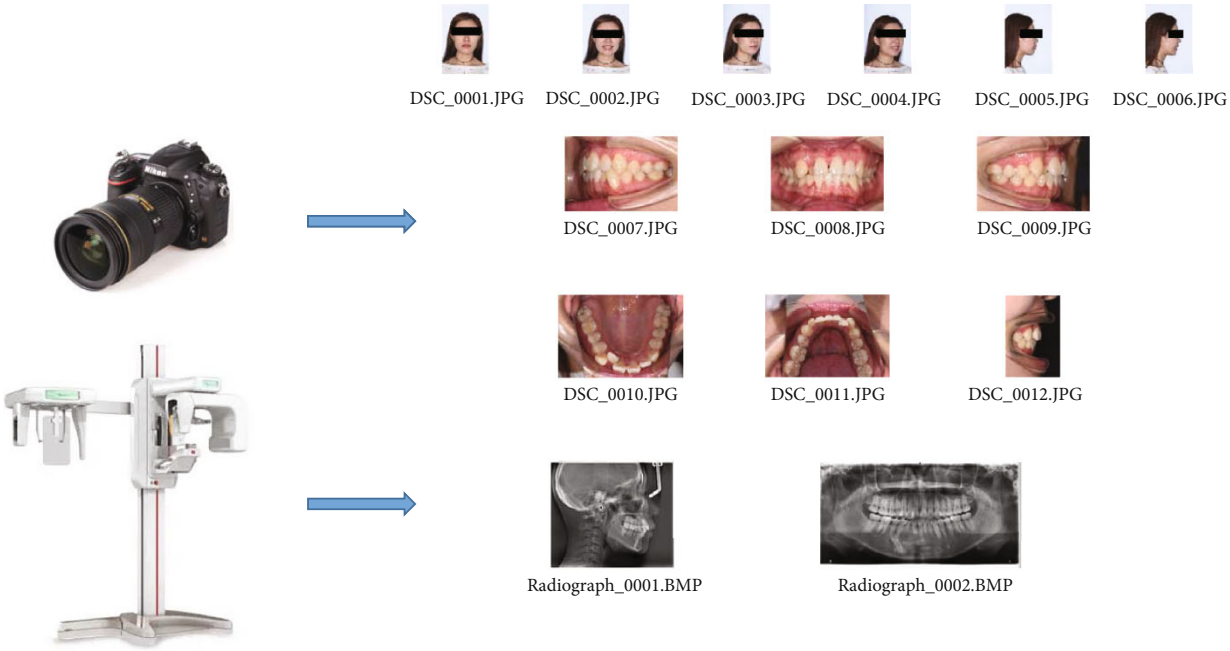

Figure 2: Diagram of data collection.

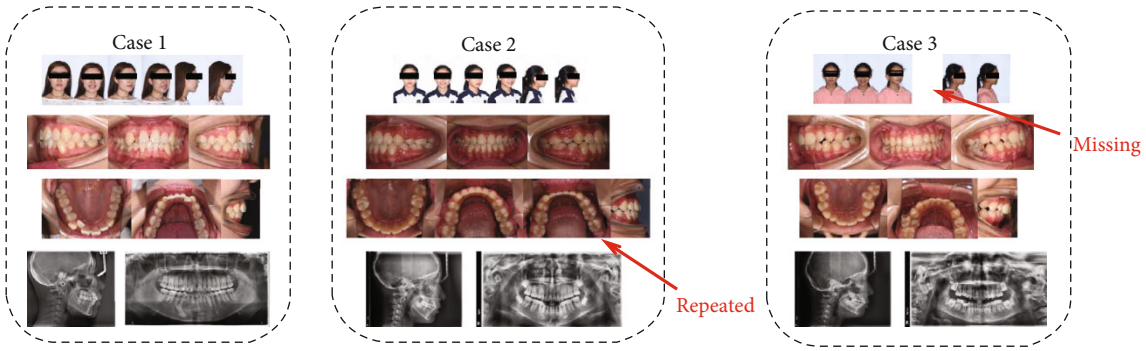

Figure 3: Representative examples of orthodontic images obtained from patients.

produced DeepID features are passed to the joint Bayesian model [12] and yield the final classification results.

During orthodontic treatment, photographs of the maxillary and mandibular occlusal are obtained using an intraoral mirror, and orthodontists have to manually flip these images in order to analyze them further. Missing and repeat orthodontic images also frequently occur, making analysis even more inconvenient. In this study, we performed a mirror flip operation and an integrity check during the postprocessing stage based on the results obtained in the classification stage. Finally, experienced orthodontists confirmed the results of the deep learning model classification and, if necessary, corrected them for later orthodontic analysis.

2.4. Statistical Analysis and Evaluation Criteria. All statistical analyses were performed using SPSS 26.0 (IBM, Chicago, IL, USA) and the Python sklearn library. To evaluate the performance of our method, we used the following metrics: accuracy, macro area under the curve (macro-AUC), time taken to archive, and receiver operating characteristic (ROC) curves. To compare the efficacy of the deep learning method against that of human experts, we compared the classification performance of three orthodontic specialists with more than five years of experience with that of the deep learning model on the same set of orthodontic images from the external dataset. The three specialists had been trained to identify images using orthodontic naming conventions [17]. In our AI system, deep learning generated an archiving spreadsheet that showed predictive classification and hyperlinks for each image (Figure 7), and the orthodontists had to confirm whether the classification generated by the deep learning model was consistent with their interpretation or not. In the case of inconsistencies, they corrected the classification of those particular images. If there were duplicate images in certain categories, the specialists selected one image that

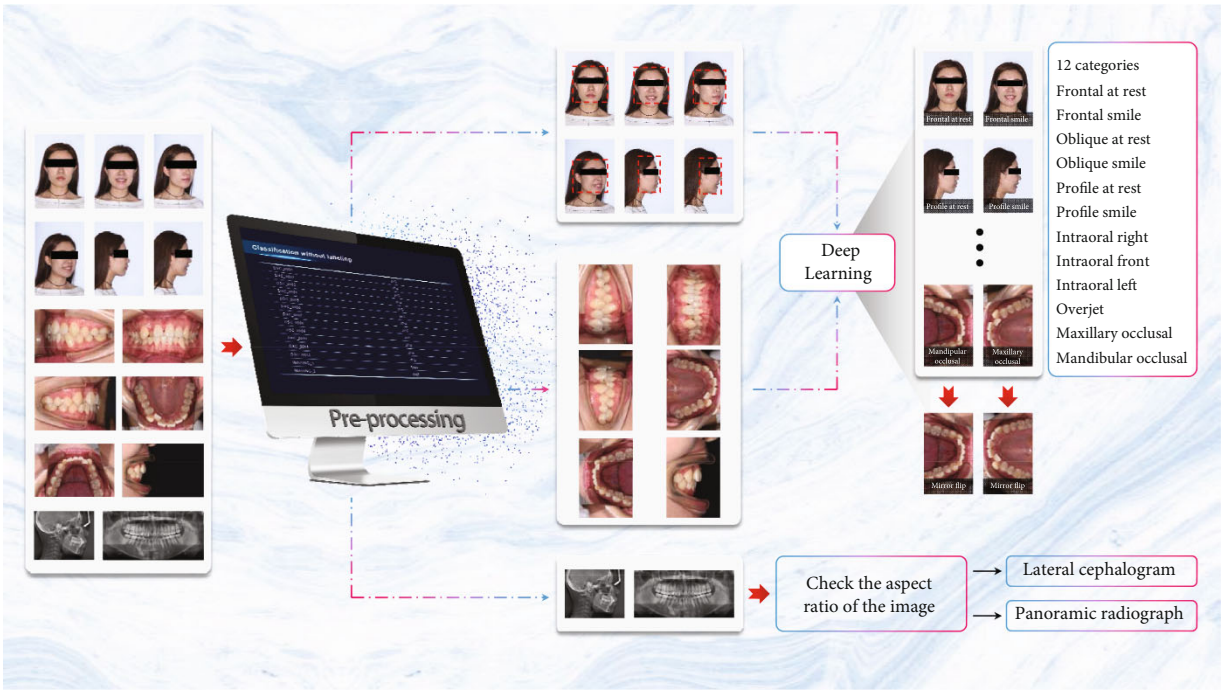

Figure 4: Flowchart depicting classification of orthodontic images using deep learning.

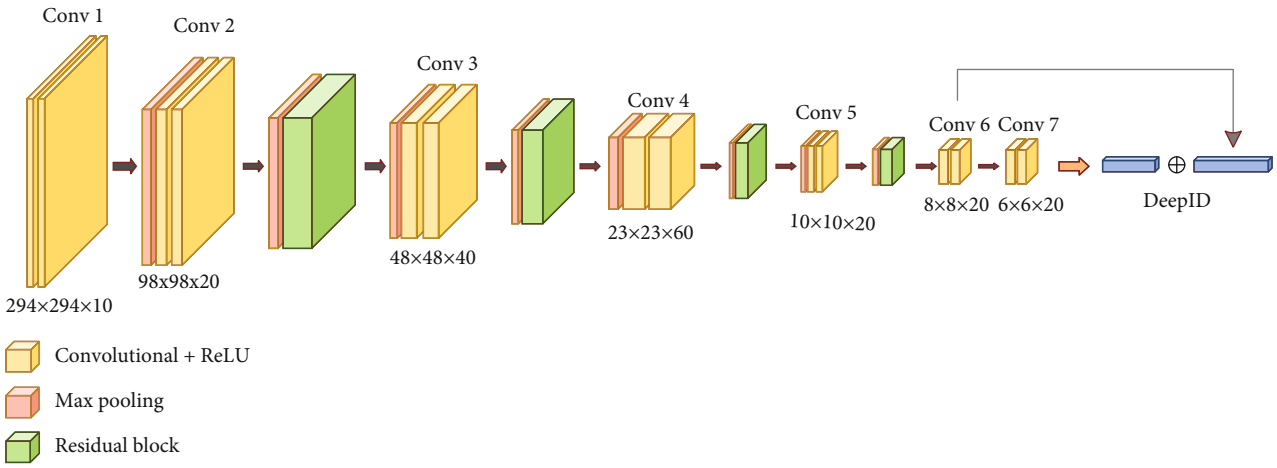

Figure 5: The architecture of the proposed model.

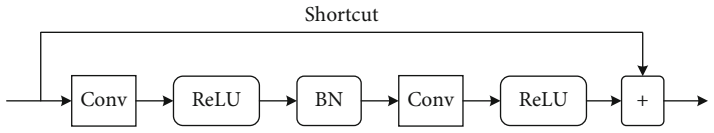

Figure 6: The structure of residual block.

could be retained for that category. In addition, the specialists recorded missing images and categories (Figure 8).

3. Results

3.1. Imaging Dataset. A total of 16,221 orthodontic images were obtained from the included patients. Of these, we excluded blurred images (106) as well as other photographs and radiographs (296) that did not meet the requirements of the American Board of Orthodontists [18]. We included a total of 14,399 orthodontic images in the internal dataset and 1,420 orthodontic images in the external dataset. The internal dataset was then randomly divided into two groups: a training set (12,999 images) and a validation set (1400 images; 100 images corresponding to each of the 14 categories).

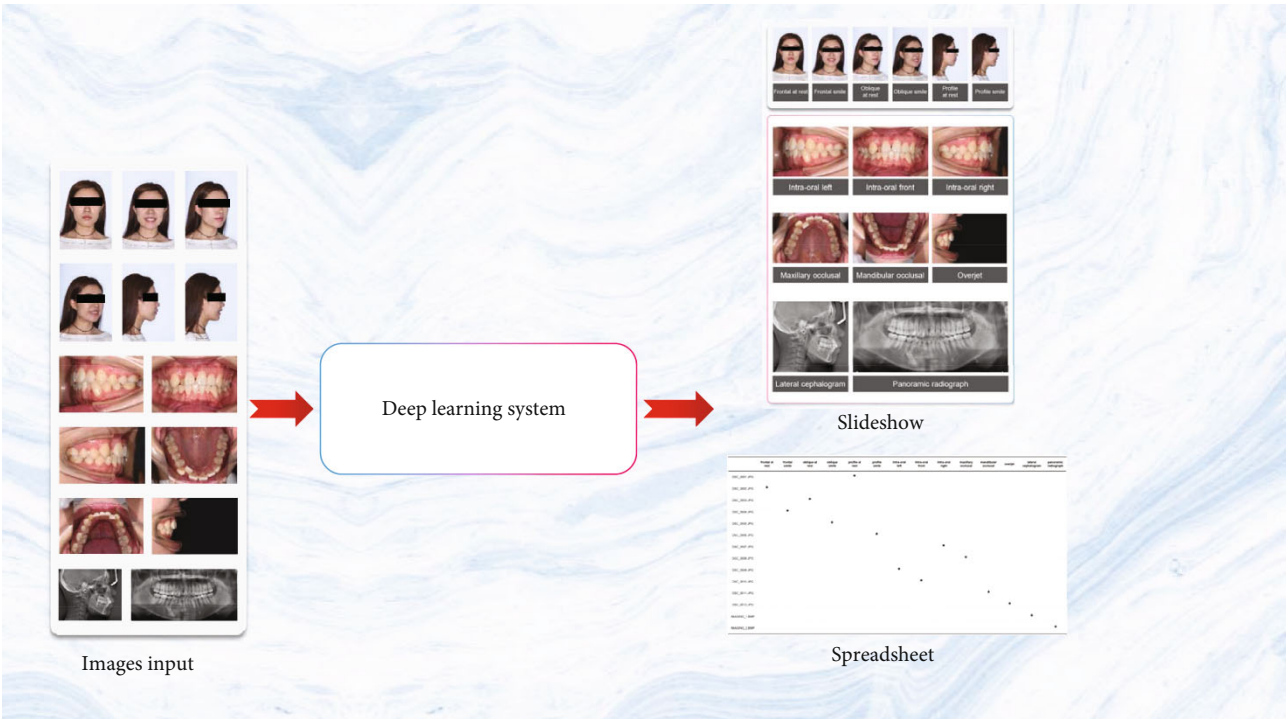

Figure 7: Overview of the classification and monitoring application.

Figure 8: Slideshow examples of classification and monitoring of orthodontic images using deep learning.

3.2. Deep Learning Model. All experiments were performed using Python 3.6 and TensorFlow 1.9 on a single NVIDIA RTX 2080Ti [19]. We proposed a modified model for automated classification, archiving, and monitoring of orthodontic images based on DeepID. In the training phase, we randomly selected 100 patients from the internal dataset as a validation set and performed a cross-validation procedure. Regarding the configuration of the hyperparameter, we used a learning rate of 0.001 and a batch size of 50 in the Adam optimizer. "Cross-Entropy" was chosen as the loss function, and the epoch number was set to 100 for model training. According to the performance of the validation set, the

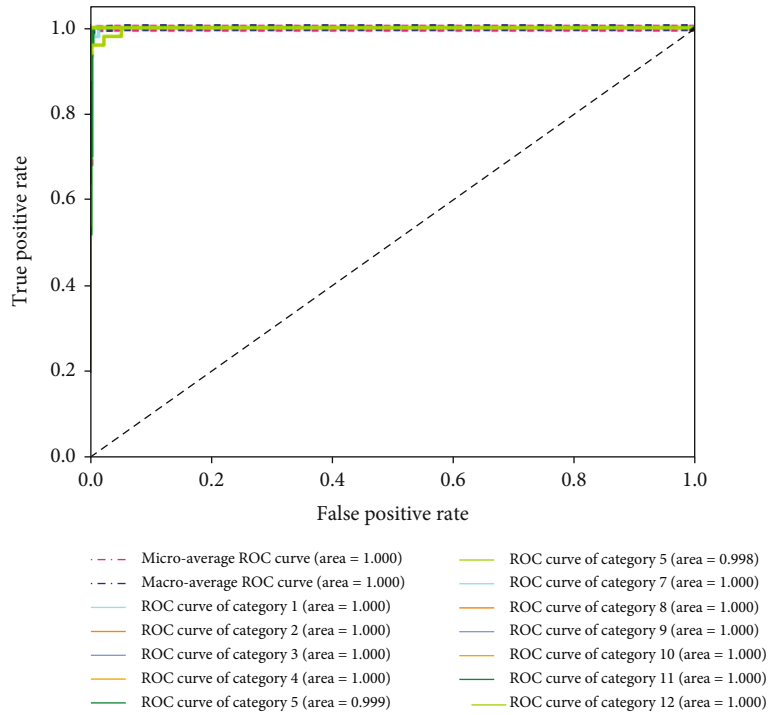

Figure 9: Receiver operating characteristic (ROC) curves associated with the deep learning model. Areas under the curve (AUCs) are provided in parentheses.

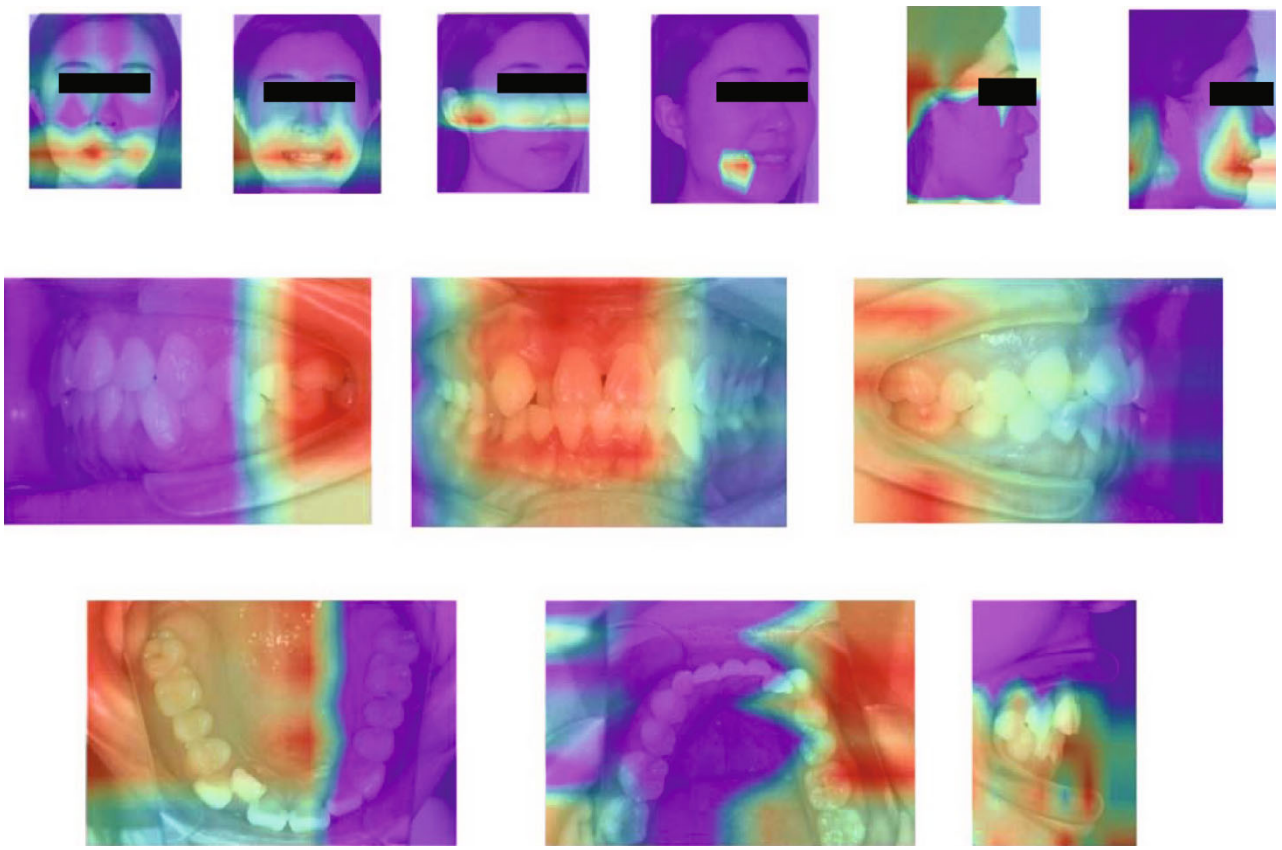

Figure 10: Gradient-weighted class activation maps (heat maps) highlighting regions in orthodontic images that were particularly relevant for classification.

Table 2: Comparison of our algorithm with several popular models.

Method	Parameters (M)	Accuracy (%)	Efficiency (MFLOPs)
AlexNet [21]	57.1	98.2	1198.7
GoogLeNet [14]	5.6	99.4	2589.1
MobileNet V2 [15]	2.2	98.7	587.5
ResNet-34 [13]	21.2	99.2	6849.5
DenseNet-121 [22]	6.9	98.2	4991.4
ShuffleNet V2 [15]	0.35	97.3	**78.6**
Ours	**0.17**	**99.4**	211.9

highest performance with respect to image classification occurred between 45 and 60 epochs. We selected the model based on the validation set with the highest performance for all subsequent work. Figure 8 shows slideshow examples of automated classification for orthodontic images according to the human-reviewed archiving table.

The deep learning model was able to classify images within 0.08 min at an accuracy of 0.994 and a macro-AUC of 1.00. The ROC curves of our model are depicted in Figure 9, including macro- and micro-AUC, as well as ROC curves of all 12 categories. Although deep learning is considered to be a "black box", gradient-weighted class activation mapping (Grad-CAM) can provide an explanation for the way in which deep learning systems make decisions based on their interpretation of the input data [20]. Grad-CAM provided visualizations of the weighted activation maps in the form of heat maps that highlight active regions of an image that were most relevant to the classification results (Figure 10).

3.3. Comparison of Advanced Deep Learning Models. We have conducted experiments on different models as well as other machine learning methods to make the evaluation, as illustrated in Table 2 and Table 3. We compared them by applying the metrics of parameter numbers, classification accuracy, and operation efficiency. For all models, we set input size as $300 \times 300 \times 3$, and the Python package thop is applied to calculate the floating point operations per second (FLOPs). We can easily observe that GoogLeNet and our model achieved the highest accuracy, while our model requires the least parameters. In comprehensive consideration, our model can make precise recognition with less computational resources; it is significant for the application field.

3.4. Comparison of Model-Only and Expert-Only Classification. The deep learning model demonstrated a strong ability to learn from features in the radiographs, as well as from manually annotated intra- and extraoral images. Compared to expert-only classification, our model showed excellent performance and high accuracy for archiving orthodontic images (Table 4). Although the values of accuracy and macro-AUC were similar for the deep learning model and the human experts, we found that the deep learning model required only 0.08 min to archive 100 orthodontic patients (1,420 images), while a human expert required an average of 18.93 min to classify, select, remove, and record the same set of orthodontic images (Table 4). Our results indicate that the fully automated method based on deep learning was 236 times faster than the human expert.

Table 3: Comparison of our model and other machine learning methods.

Method	Accuracy (%)
BCAoMID-F [23]	84.3
CPoAMoTI [24]	77.2
Ours	99.4

3.5. Comparison of Human Experts with or without Deep Learning Assistance. To comprehensively evaluate the applicability of our deep learning model, we compared the efficiency of human-only and human-machine methods to classify, select, remove, and record orthodontic images. Three human experts with deep learning assistance required on average 8.10 min to classify and monitor images from the external dataset (100 patients), which was more efficient than manual classification performed by the human expert (18.93 min). Deep learning assistance also improved the accuracy of classification by 1% and the macro-AUC value by 0.1 (Table 4).

4. Discussion

Since orthodontic treatment requires continuous image acquisition, orthodontists have begun implementing automated classification and monitoring systems based on deep learning algorithms. The average length of orthodontic treatment can last anywhere between 12 and 36 months. All treatment begins with one or two initial consultations with an orthodontist, during which the orthodontist takes radiographs and photographs of patients, discusses the treatment options, and provides a detailed plan. However, during traditional acquisition of photographs and radiographs, missing and repeat orthodontic images frequently occur, making manual data archiving necessary for every patient. In the present study, we propose a practical deep learning-based method for the automated classification, archiving, and monitoring of orthodontic images. Our findings indicate that deep learning models can be used to quickly and effectively classify and monitor orthodontic images with very high accuracy, as well as support decisions about further orthodontic treatment.

Many studies have reported that deep learning methods have an impressive learning capacity and classification accuracy in dental applications, such as skeletal classification, detection of white spot lesions, and detection of dental caries [8, 25, 26]. However, very few studies have examined deep learning in the classification of orthodontic images. In the present study, we found that deep learning models can be

Table 4: Performance of human experts and deep learning during classification of orthodontic images in the external dataset.

Operator	Method	Accuracy	Macro-AUC	Time taken to archive (min)
Deep learning	Automatic	0.994	1.00	0.08
Expert 1	Manual	0.988	0.992	19.19
	Deep learning assistance	0.998	0.997	8.27
Expert 2	Manual	0.987	0.985	18.97
	Deep learning assistance	0.997	0.996	7.92
Expert 3	Manual	0.983	0.983	18.63
	Deep learning assistance	0.996	0.996	8.10

AUC: area under the curve.

used to effectively classify and monitor orthodontic images using a set of annotated photographs; the model tested in our study demonstrated excellent classification, as assessed using ROC curves and macro-AUC values. Additionally, the Grad-CAM heat maps indicated that our deep learning model, working only from image-level annotation, was able to identify differences in features across orthodontic categories. The heat maps in our study highlighted regions in the mouth, ear, and retractor as particularly relevant to classification. In addition, human experts with deep learning assistance classified orthodontic images with higher accuracy and efficiency than experts on their own.

In the present study, images of each orthodontic patient included six intraoral photographs, six extraoral photographs, and two radiographs. A study involving dental radiographs applied deep learning models to classify panoramic, periapical, bitewing, and cephalometric radiographs into four categories for image indexing and storing [27]: they found that deep learning showed superior performance in the classification task, with an accuracy of 99.7%, but they did not monitor the occurrence of repeated or missing images. In contrast to that work, we recommend classifying lateral cephalograms and panoramic radiographs using a computer program and clear classification rules if the aspect ratio is significantly different between lateral cephalogram and panoramic radiograph. However, the aspect ratio of radiographs is based on the radiograph machine so that the aspect ratio does not always exist significant differences. The ratio-based method may be ineffective if the aspect ratio is not significantly different between lateral cephalogram and panoramic radiograph. Under this condition, it is necessary to consider the deep learning method proposed by Cejudo et al. for radiograph classification [27]. Hence, we concluded that ratio-based method is more suitable for the radiographs with significant difference in aspect ratio, but deep learning as the second choice is also considered for the classification if the aspect ratio without significant differences. In addition, other machine learning methods (BCAo-MID-F and CPoAMoTI) were compared to our deep learning model (Table 3). The experimental results demonstrated that traditional machine learning methods cannot accurately distinguish orthodontic images due to their limited capacity of feature extraction.

Our model takes advantage of residual architectures, which successfully prevented the problem that the model does not converge on the learning process due to vanishing/exploding gradients. The proposed model is quite small compared to advanced methods, so we can avoid many problems, like overfitting, the limitation constrained by computational resources [28]. A small model also leads to a fast recognition speed. It helps the real-time application. The model is custom-made for a certain target, and the size and architecture of it balanced the accuracy and speed. Therefore, after plenty of parameters adjust work, it is superior to these advanced models on this kind of orthodontic image recognition task. For the task of fixed-number categories, DeepID-based method does not show superiority relative to other classification models, but concerning the expansibility, the produced DeepID features can directly transfer for other tasks without retraining network; this is significant for practical application.

We are unaware of previous studies using deep learning to classify extraoral images. We speculated that deep learning models cannot effectively learn features from extraoral images if they are trained using images at the original resolution. Indeed, our model also showed unsatisfactory performance when asked to classify extraoral images at their original resolution. Studies on face recognition show that developers prefer to train deep learning models using facial regions within images, rather than the entire images [29]. Differences among facial regions are usually visible in the regions of the mouth, ears, and facial wrinkles. However, the resolution in these regions can be much smaller than the resolution of the original image, so the model may find it difficult to learn the relevant features. In order to overcome this difficulty, we made sure that facial regions were detected and cropped to identify feature constraints; these facial regions were then used for model training and testing for the classification of extraoral photographs. According to our experimental results, deep learning showed high accuracy in the classification of extraoral photographs when the facial region detector was used.

As far as we know, the present work is the first study testing a deep learning model for the classification, archiving, and monitoring of orthodontic images. Many popular orthodontic systems still use manual classification methods for archiving and managing patient data: our proposed method can be effectively integrated into these applications to help orthodontists save time and effort. Our findings show that the differences among orthodontic images are large enough that deep learning can easily classify them. In fact, we were able to identify all 14 categories of orthodontic

images using our model. We also demonstrated that deep learning is a superior and promising method as a useful tool for dental practice. And further validation is still required by using different types of datasets from different sources, different practices, and different regions across the world.

As digital dentistry has advanced, many dental applications have been developed for the automated analysis of dental imaging. As a fundamental yet flexible method, our deep learning approach can help these dental applications quickly find the required data among a massive number of orthodontic images. For example, deep learning can be used to detect and localize malocclusion in intraoral photographs [30], and it can assess facial attractiveness based on extraoral photographs [31]. Deep learning can also extract features from radiographs and then identify landmarks or detect disease in an automated way [7, 10]. In future, it may be possible to apply deep learning to even more complex tasks, such as angle's classifications of malocclusion.

Nevertheless, our study presents several limitations. Firstly, our results must be considered with caution in light of the fact that our method was based on orthodontic-required images. We applied the model only to images that experienced orthodontists had manually reviewed in order to ensure adequate quality and appropriateness. Hence, our model may not achieve enough high accuracy in other datasets which exist significant differences with our dataset. Secondly, the performance of deep learning mainly relies on massive training samples with high-quality annotation. However, the manual annotation is a labor-intensive work, especially in dentistry. Thus, annotation for model training may not carry out in some geographical areas because of the lack of dentists. Finally, deep learning is a data-driven method so that the quality of massive sample is required to be controlled by human experts. Future work should explore automated quality evaluation of images prior to classification, which will be especially important for processing extremely large datasets.

5. Conclusions

In this paper, a deep learning model was developed for classifying and archiving orthodontic images based on DeepID. The performance of the model was comprehensively evaluated by an external testing set and comparison with orthodontists. Our findings show that deep learning methods can be used to automatically classify, archive, and monitor orthodontic images with higher accuracy and speed than manual methods. The modified model based on DeepID used in this study demonstrated an excellent ability to classify orthodontic images. Additionally, deep learning can help make dental follow-up and treatment more efficient, while reducing dentists' workload.

Data Availability

The datasets generated or analyzed during the current study are not publicly available in order to preserve patient confidentiality but are available from the corresponding author on reasonable request.

Conflicts of Interest

The authors declare that there is no conflict of interest regarding the publication of this paper.

Authors' Contributions

Shihao Li and Zizhao Guo contributed equally to this work.

Acknowledgments

The authors disclose the following financial support for the research, authorship, and/or publication of this article. This work was supported by the Major Special Science and Technology Project of Sichuan Province (grant no. 2018GZDZX0024) and the Sichuan Science and Technology Program (grant no. 2020YFG0288).

References

[1] J. Liu, Y. Chen, S. Li, Z. Wu, and Z. Wu, "Machine learning in orthodontics: challenges and perspectives," *Advances in Clinical and Experimental Medicine: Official Organ Wroclaw Medical University*, vol. 30, no. 10, pp. 1065–1074, 2021.

[2] R. Ren, H. Luo, C. Su, Y. Yao, and W. Liao, "Machine learning in dental, oral and craniofacial imaging: a review of recent progress," *PeerJ*, vol. 9, article e11451, 2021.

[3] Y. LeCun, Y. Bengio, and G. Hinton, "Deep learning," *Nature*, vol. 521, no. 7553, pp. 436–444, 2015.

[4] L. Li, L. X. Qin, Z. G. Xu et al., "Using artificial intelligence to detect COVID-19 and community-acquired pneumonia based on pulmonary CT: evaluation of the diagnostic accuracy," *Radiology*, vol. 296, no. 2, pp. E65–E71, 2020.

[5] S. Li, J. Xiao, L. He, X. Peng, and X. Yuan, "The tumor target segmentation of nasopharyngeal cancer in CT images based on deep learning methods," *Technology in Cancer Research & Treatment*, vol. 18, p. 8, 2019.

[6] X. W. Wu, D. Sahoo, and S. C. H. Hoi, "Recent advances in deep learning for object detection," *Neurocomputing*, vol. 396, pp. 39–64, 2020.

[7] J. L. Liu, S. H. Li, Y. M. Cai et al., "Automated radiographic evaluation of adenoid hypertrophy based on VGG-Lite," *Journal of Dental Research*, vol. 100, no. 12, pp. 1337–1343, 2021.

[8] H. J. Yu, S. R. Cho, M. J. Kim, W. H. Kim, J. W. Kim, and J. Choi, "Automated skeletal classification with lateral cephalometry based on artificial intelligence," *Journal of Dental Research*, vol. 99, no. 3, pp. 249–256, 2020.

[9] F. Casalegno, T. Newton, R. Daher et al., "Caries detection with near-infrared transillumination using deep learning," *Journal of Dental Research*, vol. 98, no. 11, pp. 1227–1233, 2019.

[10] J. H. Lee, H. J. Yu, M. J. Kim, J. W. Kim, and J. Choi, "Automated cephalometric landmark detection with confidence regions using Bayesian convolutional neural networks," *BMC Oral Health*, vol. 20, no. 1, p. 270, 2020.

[11] Y. Sun, Z. Wang, H. Liu, and G. Cheng, "Non-convex Statistical Optimization for Sparse Tensor Graphical Model," *Advances in Neural Information Processing Systems*, vol. 28, pp. 1081–1089, 2015.

[12] D. Chen, X. Cao, L. Wang, F. Wen, and J. Sun, "Bayesian face revisited: a joint formulation," in *European conference on computer vision*, vol. 7574, pp. 566–579, Springer, 2012.

[13] K. He, X. Zhang, S. Ren, and J. Sun, "Deep residual learning for image recognition," in *Proceedings of the IEEE Conference on Computer Vision and Pattern Recognition (CVPR)*, pp. 770–778, Las Vegas, NV, USA, 2016.

[14] C. Szegedy, W. Liu, Y. Jia et al., "Going deeper with convolutions," in *2015 IEEE Conference on Computer Vision and Pattern Recognition (CVPR)*, pp. 1–9, Boston, MA, USA, 2015.

[15] M. Sandler, A. Howard, M. Zhu, A. Zhmoginov, and L.-C. Chen, "MobileNetV2: inverted residuals and linear bottlenecks," in *Proceedings of the IEEE conference on computer vision and pattern recognition*, pp. 4510–4520, Salt Lake City, UT, USA, 2018.

[16] W. Liu, D. Anguelov, D. Erhan et al., Part 1, "SSD: single shot multibox detector," in *European Conference on Computer Vision (ECCV)*, vol. 9905, pp. 21–37, Springer, 2016.

[17] A. Nayak, "Clinical photography: A to Z," *Apos Trends in Orthodontics*, vol. 7, no. 1, pp. 19–28, 2017.

[18] C. H. Chung, L. P. Tadlock, N. Barone et al., "American Board of Orthodontics: time for change," *American Journal of Orthodontics and Dentofacial Orthopedics*, vol. 153, no. 3, pp. 321–323, 2018.

[19] M. Abadi, "TensorFlow: learning functions at scale," *ACM SIGPLAN Notices*, vol. 51, no. 9, pp. 1–1, 2016.

[20] R. R. Selvaraju, M. Cogswell, A. Das, R. Vedantam, D. Parikh, and D. Batra, "Grad-CAM: visual explanations from deep networks via gradient-based localization," *International Journal of Computer Vision*, vol. 128, no. 2, pp. 336–359, 2020.

[21] A. Krizhevsky, I. Sutskever, and G. E. Hinton, "ImageNet classification with deep convolutional neural networks," *Communications of the ACM*, vol. 60, no. 6, pp. 84–90, 2017.

[22] G. Huang, Z. Liu, L. Van Der Maaten, and K. Q. Weinberge, "Densely connected convolutional networks," in *Proceedings of the IEEE conference on computer vision and pattern recognition*, pp. 2261–2269, Honolulu, HI, USA, 2017.

[23] A. Glowacz, "Ventilation diagnosis of angle grinder using thermal imaging," *Sensors*, vol. 21, no. 8, p. 2853, 2021.

[24] A. Glowacz, "Thermographic fault diagnosis of ventilation in BLDC motors," *Sensors*, vol. 21, no. 21, p. 7245, 2021.

[25] H. Askar, J. Krois, C. Rohrer et al., "Detecting white spot lesions on dental photography using deep learning: a pilot study," *Journal of Dentistry*, vol. 107, article 103615, 2021.

[26] J. H. Lee, D. H. Kim, S. N. Jeong, and S. H. Choi, "Detection and diagnosis of dental caries using a deep learning-based convolutional neural network algorithm," *Journal of Dentistry*, vol. 77, pp. 106–111, 2018.

[27] J. E. Cejudo, A. Chaurasia, B. Feldberg, J. Krois, and F. Schwendicke, "Classification of dental radiographs using deep learning," *Journal of Clinical Medicine*, vol. 10, no. 7, p. 1496, 2021.

[28] N. Srivastava, G. Hinton, A. Krizhevsky, I. Sutskever, and R. Salakhutdinov, "Dropout: a simple way to prevent neural networks from overfitting," *Journal of Machine Learning Research*, vol. 15, pp. 1929–1958, 2014.

[29] X. D. Sun, P. C. Wu, and S. C. H. Hoi, "Face detection using deep learning: an improved faster RCNN approach," *Neurocomputing*, vol. 299, pp. 42–50, 2018.

[30] S. Talaat, A. Kaboudan, W. Talaat et al., "The validity of an artificial intelligence application for assessment of orthodontic treatment need from clinical images," *Seminars in Orthodontics*, vol. 27, no. 2, pp. 164–171, 2021.

[31] R. Patcas, R. Timofte, A. Volokitin et al., "Facial attractiveness of cleft patients: a direct comparison between artificial-intelligence-based scoring and conventional rater groups," *European Journal of Orthodontics*, vol. 41, no. 4, pp. 428–433, 2019.